UNIVERSIDAD DE CANTABRIA

ESCUELA DE DOCTORADO DE LA UNIVERSIDAD DE CANTABRIA
DOCTORADO EN INGENIERÍA QUÍMICA DE LA ENERGÍA Y DE PROCESOS

Memoria de Tesis Doctoral presentada para optar al título de Doctor

Hydrogen recovery from industrial waste gas streams for fuel cell application

Recuperación de hidrógeno de corrientes gaseosas residuales de origen industrial para su aplicación en pilas de combustible

María Yáñez Díaz

Dirigida por:

Dr. Alfredo Ortiz Sainz de Aja

Prof. Dr. Eugenio Daniel Gorri Cirella

Santander, 2019

AGRADECIMIENTOS

En primeiro lugar, aos meus irmáns e aos meus pais que sempre me apoiaron e débolles o que hoxe son. E por suposto, á miña familia. Grazas, pola vosa confianza e orgullo incondicional, dedícovos esta tese de doutoramento.

A Ander y Alai, gracias por haber aparecido en mi vida y por vuestros consejos diarios.

A mis amigos y compañeros. Vuestro consejo, punto de vista, apoyo y experiencia es algo que ha significado mucho para mí. Gracias por todos vuestros abrazos, sonrisas y conversaciones durante los cafés.

Thanks also to Braulio and Ignacio, even at distance, the experience of working with distinguished researchers is always rewarding and satisfying.

Muito obrigada a Frederico e Adélio, Porto é uma das melhores cidades em que já estive. Estou muito feliz pelo tempo em que eu estive lá aprendendo com os melhores.

Y finalmente, a los directores de esta tesis, Alfredo y Daniel, de quienes he aprendido muchísimo durante estos años. Extiendo este agradecimiento a Inmaculada dado su colaboración y dedicación en esta tesis.

ACKNOWLEDGEMENTS

Programa de Doctorado en Ingeniería Química, de la Energía y de Procesos

(BOE núm. 16, de 19 de enero de 2015. RUCT: 5601000)

The research described in this thesis has been conducted at Advanced Separation Processes (ASP) Research Group of the Chemical and Biomolecular Engineering Department of the University of Cantabria.

This thesis has been co-financed almost entirely by the European Regional Development Fund within the framework of the Interreg SUDOE Programme, through the three-year European project: PEMFC-SUDOE project (SOE1/P1/E0293 - INTERREG SUDOE/FEDER, UE), "Energy Sustainability at the SUDOE Region: Red PEMFC-SUDOE". Likewise, this research was also financially supported by the Spanish Ministry of Economy and Competitiveness and the European Regional Development Fund through the R&D projects: CTQ2015-66078-R (MINECO/FEDER, UE), "Advanced separation applications. Mathematical modeling and proof of concept"; CTQ2016-75158-R (AEI/FEDER, UE), "Selective composite membranes and their incorporation into microfluidic devices"; and RTI2018-093310-B-I00 (MINECO/AEI/FEDER, UE), "High-Performance Microfluidic Separations. Challenges and opportunities".

I would like to thank the University of Porto, for the research stay I carried out there, which was really helpful for the development of this thesis. The three-month research stay (January - April 2019) was conducted at Chemical Engineering Department, University of Porto, Portugal, under the supervision of Prof. Dr. Adélio Miguel Magalhães Mendes. Likewise, I would also like to thank the collaborative work carried out during this thesis with the researchers Braulio Brunaud and Prof. Ignacio E. Grossmann of the Department of Chemical Engineering at the Carnegie Mellon University, Pittsburg, USA.

TABLE OF CONTENTS

SUMMARY

RESUMEN

CHAPTER 1. INTRODUCTION TO HYDROGEN SEPARATION TECHNIQUES

CHAPTER 2. UPCYCLING OF SURPLUS HYDROGEN INTO A HYDROGEN SUPPLY CHAIN

CHAPTER 3. MEMBRANE-BASED PROCESS AS AN ALTERNATIVE FOR HYDROGEN SEPARATION

SUMMARY

THESIS SCOPE AND OUTLINE

i. MOTIVATION

Interest in hydrogen has been growing over the past decade as a way of enabling a full large-scale integration of renewables in response to decarbonize all sectors of the economy and concerns about the global proved fossil-fuel reserves [1]. While much of the hydrogen is currently produced from low-cost natural gas, hydrogen production from carbon-lean and carbon-free energy sources has the potential to serve as a long-term environmentally friendly alternative in a truly sustainable energy system [2]. Once it is produced, hydrogen acts essentially as a fuel gas opening the possibility of maintaining energy stored as long as needed [3]. To provide electricity back to the grid, hydrogen can be fed into a fuel cell or combustion engine where it is burnt. But even when made from non-renewable energy sources, hydrogen still has certain advantages over fossil fuels, because of the high efficiency of such fuel cell systems [4]. Therefore, hydrogen demand for fuel cell applications is expected to grow rapidly in all end-sectors of the economy: industrial, transportation, residential and commercial. Especially, the transport growth makes this a key sector with increasing demand for hydrogen as an attractive alternative to non-renewable fuels [5].

At the same time, hydrogen-rich industrial waste streams are produced in relevant amounts considering both, hydrogen generated due to excess of plant's capacity and by-product hydrogen [6]. With the aim of tackling this wasting of resources, this available surplus hydrogen that in some cases is simply vented or flared to the atmosphere, has also become attractive sources of feedstock for the manufacture of commodity chemicals such as ammonia or methanol, or even to be upgraded to fuel for both transportation and stationary applications. The need to compete against the fluctuations in fuel energy prices and promote the circular economy by upcycling the resources, leads to a great relevance of hydrogen-containing waste gas streams recovery. Depending on the industrial origin, low-quality hydrogen, which could contain different types of contaminants, needs to be purified using gas clean-up technologies [7]. The most promising technologies to purify hydrogen are pressure swing adsorption (PSA) and membrane systems. Each of these separation methods has its unique capabilities and constraints. Developments in hydrogen separation techniques are driven not only by cost and performance, but also by the purity requirements of the final application. In this regard, high-purity hydrogen is beneficial not only to ensure that the impurities do not affect system operation and efficiency, but also to achieve lifetime targets of fuel cell systems to become a competitive alternative against burning off in flare systems [8].

Consequently, especial effort must be made to assess the real potential of industrial surplus hydrogen in terms of technical performance as well as cost. That means that hydrogen upcycled from multicomponent waste gas streams should be measured with a cost, which can competitive with conventional fuels within the automotive industry allowing hydrogen penetration into the market. Therefore, there is still room for assessing the potential of upcycling industrial hydrogen-containing waste gas streams, which has been the motivation of this thesis. This research field is highly pertinent but unusually exploited, and it deserves the scientific community's attention.

ii. OBJECTIVES OF THE THESIS

In view of the above, the overall objective of this thesis is the contribution to the recovery of hydrogen from industrial waste gas mixtures by investigating two different separation technologies: polymeric membranes and PSA processes, in order to obtain high-purity hydrogen. To achieve such general goal, the research has been centered in providing methodological issues to surplus hydrogen recovery; evaluating the performance of commercial hydrogen-selective polymeric membranes using multicomponent gas mixtures; and producing fuel cell grade hydrogen from an industrial waste gas stream via PSA process.

Therefore, the following specific objectives are defined:

- To carry out a state-of-the-art review in industrial hydrogen-containing waste gas streams with great potential to be upcycled.
- To provide the methodology to assess the techno-economic feasibility of various by-product gases to embed sustainability across a hydrogen supply chain.
- To identify the most appropriate hydrogen-selective membranes according to the waste gas streams under selection.
- To study the permeation of pure gases and multicomponent mixtures of H_2, N_2, CH_4, CO, and CO_2 at different operation conditions through dense polymeric membranes.
- To assess in terms of performance as well as cost the production of fuel cell grade hydrogen using four-component mixture of H_2, N_2, CH_4, and Ar, via four-column PSA process.
- General prospects for further research and industrial implementation.

iii. STRUCTURE OF THE THESIS

The content of this dissertation is addressed in five main chapters, driven by the major objectives previously explained.

To introduce, comprehend and study the research trends of waste gas streams upcycling, a detailed introduction is performed in **Chapter 1**. Initially, hydrogen as a unique and versatile energy carrier is explained, focusing in its potential as a future carbon-free road transport fuel. After that, hydrogen-containing effluent gases with major potential for hydrogen recovery are identified. Then, established hydrogen purification techniques are introduced. Special detail is taken while describing polymeric membrane systems and PSA technologies, since there are the ones that exhibit the best cost-effective performance, and thus, the ones studied in this thesis. A detailed description of the fuel quality requirements for fuel cell systems is presented at the end of this chapter.

In **Chapter 2**, surplus gases are proven to be integrated into a hydrogen supply chain as a means of distributed hydrogen generation. This work provides the methodology to assess the techno-economic feasibility of upcycling industrial waste gas streams into the hydrogen supply chain. Using an optimization modelling approach, it contributes to satisfy the growing hydrogen demand for stationary and road transport applications over a 30-year time horizon. It was selected the northern Spain region for the case study to be analyzed. This work has been carried out in collaboration with researchers of the Chemical Engineering Department at the Carnegie Mellon University, Pittsburg, USA.

In **Chapter 3**, membrane-based process as an alternative hydrogen separation technology for the upcycling of waste gases is assessed by means of the real performance. A comparative performance analysis of commercially available polymeric membranes for hydrogen separation is developed, and applied to industrial waste gas mixtures in order to obtain high-purity hydrogen that meets the quality standards to be used in hydrogen-based applications. An experimental gas permeation setup suited for multicomponent waste mixtures is designed and tailored for this purpose. To attest the mixed-gas permeation performance, the influence of the feed gas composition, temperature and pressure over permeability, selectivity and outlet gas purity is studied.

In **Chapter 4**, multicolumn PSA process as an alternative separation technology for upgrading hydrogen is assessed in terms of performance as well as cost using purge gases from ammonia industry, as a promising hydrogen source. The optimal experimental conditions to produce fuel

cell grade hydrogen via cyclic four-column PSA unit using a four-component gas mixture, are studied. This work was carried out in the Chemical Engineering Department at the University of Porto, Portugal, during a research stay between January and April 2019.

Usefully, each of the chapters ends with a brief section dealing primarily with abbreviations and nomenclature, but also with its own bibliography and appendix sections. The conclusion and future work lines of this thesis are presented in **Chapter 5**, and this chapter is also translated into Spanish. Finally, a list of contributions by the author of the thesis is listed in **Appendix I.**

REFERENCES

[1] International Renewable Energy Agency (IRENA), Global Energy Transformation: A Roadmap to 2050, (2018). www.irena.org.

[2] R.S. Cherry, A hydrogen utopia?, Int. J. Hydrogen Energy. 29 (2004) 125–129.

[3] J. Bellosta von Colbe, J.R. Ares, J. Barale, et al., Application of hydrides in hydrogen storage and compression: Achievements, outlook and perspectives, Int. J. Hydrogen Energy. 44 (2019) 7780–7808.

[4] J. Gao, M. Li, Y. Hu, et al., Challenges and developments of automotive fuel cell hybrid power system and control, Sci. China Inf. Sci. 62 (2019) 1–25.

[5] M.R. Rahimpour, A. Asgari, Production of hydrogen from purge gases of ammonia plants in a catalytic hydrogen-permselective membrane reactor, Int. J. Hydrogen Energy. 34 (2009) 5795–5802.

[6] S.C.T. J. Perrin, R. Steinberger-Wilkens, CertifHy project “Overview of the market segmentation for hydrogen across potential customer groups, based on key application areas,” 2015.

[7] M. Ball, M., Wietschel, The Hydrogen Economy: Opportunities and Challenges, Cambridge University Press, New York, 2009.

[8] G.T. F. Blank, M. Klages, S. Mock, DAIMLER: The Importance of Fuel Quality, (2017). www.hycora.eu/workshops.

RESUMEN

DESCRIPCIÓN Y ALCANCE DE LA TESIS

i. MOTIVACIÓN

Durante esta última década, en respuesta a la descarbonización de los sectores finales de la economía y a la preocupación acerca de las reservas de combustibles fósiles en el mundo, el interés por el hidrógeno ha aumentado como una forma de hacer frente a la integración completa de las energías renovables [1]. Mientras que a día de hoy la mayor parte del hidrógeno se obtiene a coste reducido a partir de gas natural, el hidrógeno producido mediante fuentes de energía de baja o nula emisión de carbono se trata de la alternativa ecológica a largo plazo en un sistema energético sostenible [2]. Una vez se produce, el hidrógeno actúa esencialmente como un gas de combustión permitiendo almacenar la energía de forma química y liberarla cuándo y cómo sea necesario [3]. Para suministrar la electricidad de vuelta a la red de distribución, el hidrógeno puede alimentar una pila de combustible o motor de combustión en donde se quema. Pero incluso cuando proviene de fuentes de energía no renovables, el hidrógeno presenta ciertas ventajas competitivas con respecto a los combustibles fósiles y esto es debido a la elevada eficiencia energética de los sistemas basados en pilas de combustible [4]. Por tanto, se espera que la demanda del hidrógeno en aplicaciones de pilas de combustible crezca rápidamente en todos los sectores finales de la económica: industrial, transporte, residencial y comercial. Especialmente, el crecimiento previsto en el transporte hace que éste sea un sector clave con una demanda creciente de hidrógeno como una opción atractiva frente a los combustible no renovables [5].

Al mismo tiempo, corrientes gaseosas residuales que contienen hidrógeno de origen industrial son producidas en elevadas cantidades, considerando tanto el hidrógeno generado en exceso como el producido como subproducto [6]. Con el fin de abordar este desaprovechamiento de recursos, este excedente de hidrógeno que está disponible y que en algunos casos simplemente es quemado o venteado a la atmósfera, resulta ser una fuente de recursos muy atractiva para la producción de productos químicos tales como amoniaco o metanol, o incluso mejorar su grado de pureza para ser usado como fuel en aplicaciones estacionarias o para transporte. La necesidad de competir contra las fluctuaciones de los precios de los combustibles y de la energía, así como promover una economía circular aprovechando los recursos, dan lugar a la importancia de la recuperación de corrientes gaseosas residuales que contengan hidrógeno.

El hidrógeno de baja pureza, el cual puede contener diferentes tipos de contaminantes dependiendo de su origen industrial, requiere ser purificado mediante tecnologías de separación de gases [7]. Las tecnologías más prometedoras para purificar hidrógeno son: la adsorción por cambio de presión (PSA, por sus siglas en inglés) y los sistemas de membranas. Cada uno de estos métodos de separación dispone de capacidades únicas y limitaciones. El desarrollo de las técnicas de separación de hidrógeno no sólo está impulsado por su rendimiento o coste, sino también por los requerimientos de pureza de la aplicación. En este sentido, el hidrógeno de alta pureza es beneficial no solo para asegurar que las impurezas no afecten al sistema y a su eficiencia, sino también para alcanzar los objetivos de durabilidad de los sistemas basados en pilas de combustible y llegar a ser una alternativa competitiva frente a su uso como gas de combustible enviado directamente a sistemas de antorcha [8].

Por ello, debe llevarse a cabo una especial atención a la evaluación del potencial real del excedente hidrógeno industrial en términos de rendimiento y coste. Esto significa que el hidrógeno producido a partir de corrientes gaseosas residuales debe medirse con un coste, el cual pueda ser competitivo con los combustibles convencionales dentro de la industria del automóvil, permitiendo así la penetración de hidrógeno en el mercado. Por tanto, todavía hay margen para la evaluación del potencial de recuperación de corrientes gaseosas residuales con hidrógeno, la cual ha sido la motivación de esta tesis. Este campo de investigación es altamente pertinente pero inusualmente explotado, y merece atención dentro de la comunidad científica.

ii. OBJETIVOS DE LA TESIS

A la vista de todo lo anterior, el objetivo global de la tesis es contribuir en la recuperación de mezclas de gases residuales de origen industrial investigando principalmente dos tipos de tecnologías de separación de hidrógeno: membranas poliméricas y procesos de PSA, con objeto de obtener hidrógeno de elevada pureza. Para conseguir tal objetivo general, la investigación se ha centrado en proporcionar cuestiones metodológicas relacionadas con la recuperación de hidrógeno; evaluar el comportamiento de membranas comerciales poliméricas selectivas de hidrógeno usando mezclas de gases multi-componentes; y producir hidrógeno con la calidad apta para alimentar pilas de combustible a partir de una corriente gaseosa residual de origen industrial mediante un proceso de PSA.

Por consiguiente, se han definido los siguientes objetivos específicos:

- Efectuar una revisión del estado del arte de las corrientes gaseosas residuales que contienen hidrógeno de origen industrial con mayor potencial de ser recuperadas.
- Proporcionar una metodología para evaluar la viabilidad técnico-económica de varios subproductos gaseosos para integrarlos de forma sostenible en una cadena de suministro de hidrógeno.
- Identificar cuáles son las membranas selectivas de hidrógeno más apropiadas para las corrientes gaseosas residuales de estudio.
- Estudiar la permeación de gases puros y mezclas de gases multi-componentes de H_2, N_2, CH_4, CO, y CO_2 a diferentes condiciones de operación a través de membranas densas poliméricas.
- Evaluar en términos de rendimiento y rentabilidad la producción de hidrógeno con calidad apta para alimentar pilas de combustible a partir de una mezcla de gases que contiene H_2, N_2, CH_4, y Ar mediante un proceso de PSA con cuatro columnas.
- Perspectivas generales de futuras investigaciones e implementación industrial.

iii. ESTRUCTURA DE LA TESIS

El contenido de esta tesis se divide en cinco capítulos, impulsados por los principales objetivos previamente explicados.

Con el fin de introducir, comprender y estudiar las tendencias en investigación de la recuperación de corrientes gaseosas residuales, una introducción detallada es desarrollada en el **Capítulo 1**. Inicialmente, se ha explicado el hidrógeno como vector energético, enfocándose en su potencial como combustible libre de carbono para el transporte por carretera. Posteriormente, se identificaron cuáles son los gases residuales industriales con mayor potencial para recuperar hidrógeno. Luego, se introdujeron las principales técnicas de purificación de hidrógeno. Se ha puesto especial énfasis en los sistemas de membranas poliméricas, así como en las tecnologías de PSA, debido a que son las que exhiben mejores rendimientos, y por ello, las tecnologías estudias en profundidad en esta tesis. Al final de este capítulo, se presenta una descripción detallada de los requerimientos de calidad del hidrógeno para su aplicación en pilas de combustible.

En el **Capítulo 2**, se demuestra que los gases residuales ricas en hidrógeno pueden ser integradas dentro de una cadena de suministro para la generación de hidrógeno de forma distribuida. Este trabajo provee una metodología para evaluar la viabilidad tecno-económica de incorporar corrientes industriales residuales en una cadena de suministro de hidrógeno. Usando un modelo de optimización, el problema contribuye a satisfacer una demanda creciente de hidrógeno para aplicaciones estacionarias y para el transporte por carretera a lo largo de un horizonte temporal de 30 años. Se ha seleccionado la región del Norte de España como caso de estudio para ser analizado. Este trabajo ha sido llevado en colaboración con investigadores del Departamento de Ingeniería Química de la Universidad Carnegie Mellon, Pittsburgh, EE. UU.

En el **Capítulo 3**, se han evaluado los procesos basados en membranas como una tecnología alternativa para la separación de hidrógeno a través de su comportamiento real. Un análisis comparativo del rendimiento de membranas poliméricas selectivas de hidrógeno ha sido llevado a cabo, y aplicado a mezclas gaseosas residuales de origen industrial con el fin de obtener hidrógeno que cumpla con los requerimientos de calidad definidos en los estándares. Para ello, se ha diseñado y probado una instalación experimental de permeación de gases adecuada para mezclas de gases multi-componentes. Para evaluar el comportamiento de la permeación de mezclas de gases, la influencia de la composición de los gases de entrada, la temperatura y la presión se estudia a través de la permeabilidad, la selectividad y la pureza de hidrógeno.

En el **Capítulo 4**, los procesos de PSA como otra tecnología alternativa para la separación de hidrógeno se han evaluado en términos de rendimiento y coste usando gases de purga de la industria del amoniaco, como fuente prometedora de hidrógeno residual. Por tanto, se han estudiado cuales son las condiciones experimentales óptimas para producir hidrógeno con calidad apta para alimentar pilas de combustible usando una mezcla de gases mediante un proceso de PSA con cuatro columnas. Este trabajo ha sido desarrollado en el Departamento de Ingeniería Química de la Universidad de Oporto, Portugal, durante una estancia investigadora entre enero y abril de 2019.

Cada capítulo finaliza con una breve sección que trata principalmente con las abreviaturas y nomenclatura, así como con sus propias secciones de bibliografía y apéndices. Las conclusiones y futuras líneas de trabajo de la tesis son presentadas en el **Capítulo 5**, y este capítulo es traducido también al español. Finalmente, las contribuciones científicas del autor de la tesis son listadas en el **Apéndice I.**

REFERENCIAS

[1] International Renewable Energy Agency (IRENA), Global Energy Transformation: A Roadmap to 2050, (2018). www.irena.org.

[2] R.S. Cherry, A hydrogen utopia?, Int. J. Hydrogen Energy. 29 (2004) 125–129.

[3] J. Bellosta von Colbe, J.R. Ares, J. Barale, et al., Application of hydrides in hydrogen storage and compression: Achievements, outlook and perspectives, Int. J. Hydrogen Energy. 44 (2019) 7780–7808.

[4] J. Gao, M. Li, Y. Hu, et al., Challenges and developments of automotive fuel cell hybrid power system and control, Sci. China Inf. Sci. 62 (2019) 1–25.

[5] M.R. Rahimpour, A. Asgari, Production of hydrogen from purge gases of ammonia plants in a catalytic hydrogen-permselective membrane reactor, Int. J. Hydrogen Energy. 34 (2009) 5795–5802.

[6] S.C.T. J. Perrin, R. Steinberger-Wilkens, CertifHy project “Overview of the market segmentation for hydrogen across potential customer groups, based on key application areas,” 2015.

[7] M. Ball, M., Wietschel, The Hydrogen Economy: Opportunities and Challenges, Cambridge University Press, New York, 2009.

[8] G.T. F. Blank, M. Klages, S. Mock, DAIMLER: The Importance of Fuel Quality, (2017). www.hycora.eu/workshops.

CHAPTER 1

INTRODUCTION TO HYDROGEN SEPARATION TECHNIQUES

1.1 CURRENT ENERGY SITUATION

Uninterrupted availability of energy sources at an affordable price, also defined as energy security, is a high priority of every nation worldwide. Modern civilizations require a robust (sufficient of resources, reliable of infrastructure, and steady and affordable), sovereign (protected from potential threats from external agents); and resilient (the ability to withstand diverse disruptions) supply of energy.

Global energy demand history shows an increasing trend owing to the growth in world's population and industrialization, as it can be observed in Figure 1.1. The global recession was clearly noticeable for the primary energy consumptions which declined in 2008. The 2008 global financial crisis led to an important economic adjustment during the 2008-2013 period affecting developed economies, especially European Union (EU) countries. After that, the primary energy consumption progressively rose to the current values. In 2018, the global primary energy consumption was around 13900 Mtoe [1]. This means an increase of 2.9 % respect to the previous year, the fastest rate of growth since 2010, and almost double its 10-year average (1.5 %). Namely, all fuels grew faster than their 10-year averages. This acceleration, driven by natural gas and renewables, was particularly pronounced for natural gas, whose global consumption increasing by 5.3 % with respect to 2017, one of the strongest growth rates over 30 years. These figures are clearly connected to the "shale gas revolution" in the United States of America (USA), whose production of unconventional shale gas has soared dramatically, accounting for almost half of global growth in production. The recent shale gas supply boom has significant implications for energy security not only in the USA but also in the rest of the world [2].

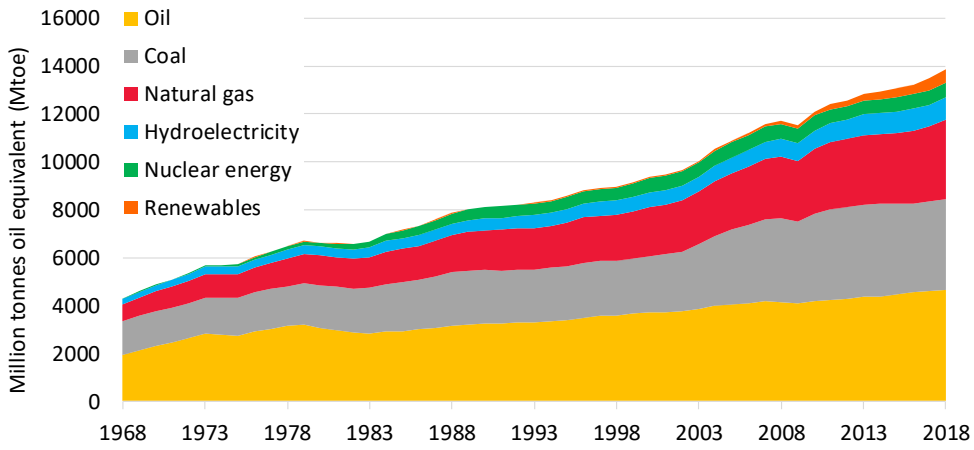

Figure 1.1 Primary energy world consumption by source

Overall, fossil fuels provide almost 84.7 % of the energy demands. Oil is the fuel mostly consumed, with 33.6 % of the global energy consumption and 1.5 % more than in the previous year. Although coal consumption grew by 1.4 %, being India and China the countries that contributed the most to this increase, coal's share in primary energy fell to 27.2%. Followed by the natural gas that accounted for 23.9 % in 2018, the contribution of hydroelectric and nuclear energy remained relatively flat at 6.8 % and 4.4 %, respectively. Renewable energy sources for power generation, led by wind and solar photovoltaic (PV), grew by 12.6 % in 2018, reaching 4.0 % of the global energy consumption, just behind nuclear.

Figure 1.2 shows the share of primary energy consumption by fuel and region in 2018. Natural gas is the major consumed fuel in the Middle East and Europe & Eurasia, whereas oil remains the dominant fuel in Africa and the Americas. Global coal consumption is heavily concentrated in the Asia Pacific region, while more than two thirds of nuclear consumption is concentrated in North America and Europe. In 2018, coal is still the dominant fuel in the Asia Pacific region, accounting for more than half of the regional energy mix. Regarding renewables, Asia Pacific, Europe and North America regions consumed more than 90 % of total renewable primary energy.

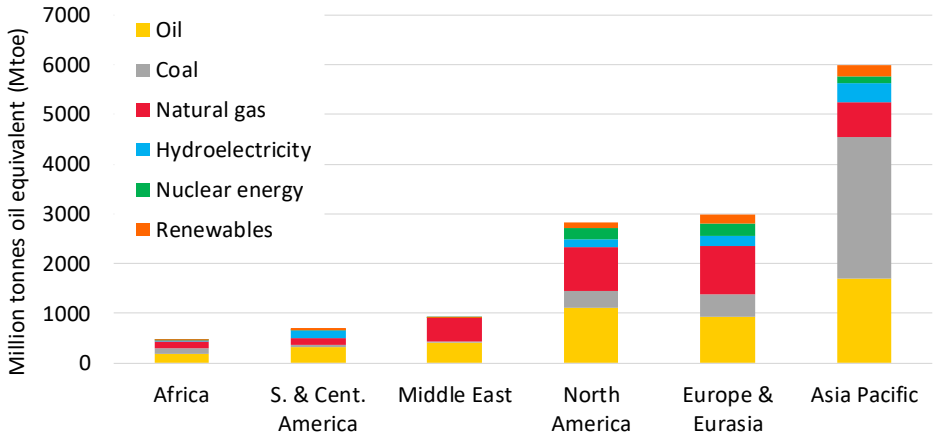

Figure 1.2. Primary energy regional consumption by fuel at 2018

The current fossil fuel-based energy system could lead to an unsustainable situation because of depletion of proved worldwide reserves of fossil fuels, climate change and conflicts over energy resources or infrastructure. Although reserves-to-production (R/P) ratios, as key factors to characterize the robustness of a certain fuel source, are notoriously fluid indicators, they still signal important vulnerabilities on energy security to policymakers, especially if they are near-term (< 10 - 20 years) [2].

As it can be seen in Figure 1.3, global R/P ratios shows that oil and natural gas reserves in 2018 accounted for around 50 years of current production, whereas world's coal stocks accounted for 132 years, and these are not as geographically concentrated as those of oil and natural gas. The biggest world oil reserves are heavily concentrated in Venezuela (17.5 %), closely followed by Saudi Arabia (17.2 %), then Canada (9.7 %), Iran (9.0 %) and Iraq (8.5 %), while the top countries in terms of proved gas reserves are Russia (19.8 %), Iran (16.2%) and Qatar (12.5 %). On the other hand, most of the world's coal reserves, especially anthracite and bituminous coal (70 %), are located in USA (24 %), Russia (15 %), Australia (14 %) and China (13%).

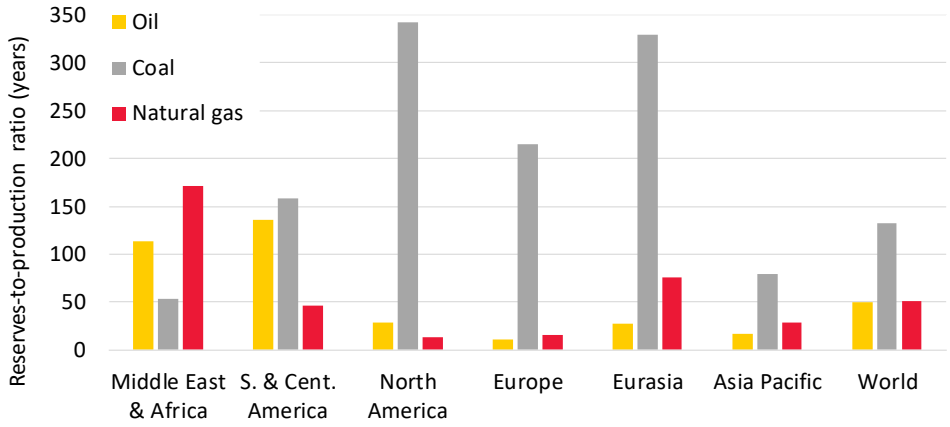

Figure 1.3. Fossil fuel reserves to production (R/P) ratio at 2018

Whereas energy security is primarily a national concern, climate change is mostly a global concern. Burning fossil fuels massively traded on the global scale, in addition to deforestation and farming, is one of the major causes of global warming on the planet, particularly through carbon emissions. Towards the achievement of a sustainable energy system, world's commitment to dealing with climate change has been defined under the Paris Agreement, agreed by 193 countries in 2015, to keep the global average temperature increase to "well below 2 °C". Nevertheless, according to the world's scientists, even a rise of 1.5 °C could be disastrous for ecosystems and societies over the coming decades [3]. To meet world's agreed climate target, worldwide stakeholders must pursue limit energy-related CO_2 emissions to their 1990 level by mid-century, 20 $GtCO_2$-eq annually, in order to preserve local air quality [4]. Energy production and use is currently the largest source of global greenhouse-gas (GHG) emissions (CO_2 and non-CO_2 combined), where transport accounted for one quarter of total GHG emissions, and specifically road transport accounted for 72 % of total GHG emissions of the sector [5].

The increase of CO_2 emissions over recent decades suggests a perceptible human influence on global ecosystems, as shown Figure 1.4. In the last twenty years, global energy-related CO_2 emissions grew by 48.5 %, from 21.3 $GtCO_2$ in 1990 to 33.9 $GtCO_2$ in 2018. With respect to 1968, the emissions have increased by 166.1 %. Even the climate-related goals, global CO_2 emissions from energy use rose in 2018 at the fastest rate seen for years as a directly consequence of the increase in energy growth. This is driven by both the increase of coal-burning in China and India, and the increase of oil used due to increasing the number of passenger cars on the planet [1]. Asia Pacific region accounted for 49.5 % of the global emissions in 2018, growing by 144.5 % over last twenty years. China is the major contributing country of the global carbon emissions (27.8 %, that grew by 4.7 % with respect to 2017), followed by USA (15.2 %, that grew by 2.5 % in 2018). In this regard, many countries rigorously pursue energy security policy initiatives without strong climate change agendas, aimed at reducing the GHG impacts from energy production and use.

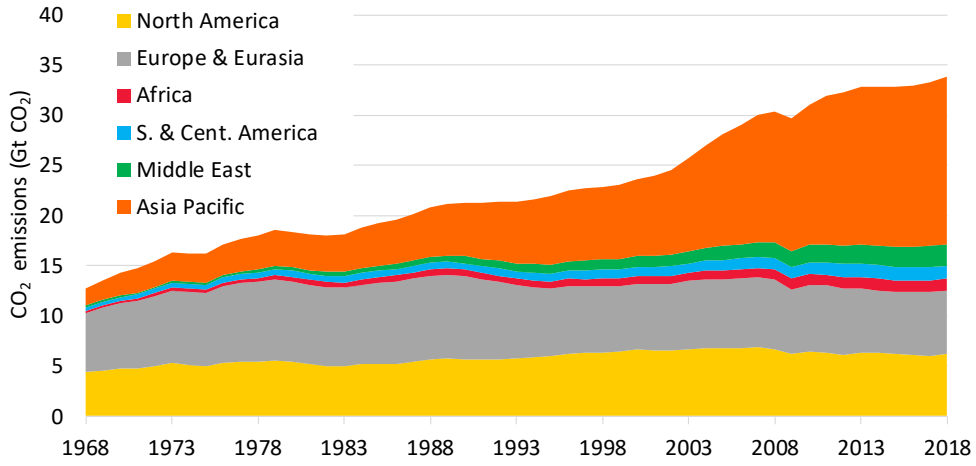

Figure 1.4. Historical evolution of energy-related CO_2 emissions by region

Alternative energy sources such as renewables are at the forefront of the drive to decarbonize our traditional system, together with electricity saving, fuel switching to low-carbon electricity generation and carbon capture and storage (CCS) [6]. Renewables-based power sources include modern biomass (in solid, liquid, and gaseous forms), wind, solar PV, solar thermal, geothermal, tide, waves, and ocean current energy. Renewable energy in power generation (excluding hydro) continued to increase by 14 % in 2018, wherein wind accounted for around 50 % of whole renewable power capacity and the share of solar PV power represents 24 %. Developing renewable infrastructure seeks not only to address commodity price volatilities in global fossil fuel markets, but also to reduce climate impacts of energy systems. However, intermittent-renewable energy sources, like wind and solar PV, are variable, largely

uncontrolled and sometimes hard to predict, causing a mismatch between supply and demand [7]. Electricity generated by renewable technologies cannot be effectively used to match the changing demand until the appropriate large-scale energy storage technologies are developed. In this context, pumped hydro storage currently dominates 96 % of the total global storage power capacity, with around 176 GW of capacity installed globally in mid-2017. Yet this is negligible compared with the total electric power production capacity, accounting for less than 2 % [8].

The versatility and unique properties of hydrogen, as a net zero-emission energy carrier (along with electricity and biofuels), open the way to accomplish this goal, being an important part of decarbonization strategies to reduce GHG emissions across the global energy system. Hence, hydrogen-based energy storage systems will lead the way for the transition to a decarbonized energy system, due to its significant potential for carbon neutrality along the entire hydrogen value chain.

1.2 HYDROGEN AS AN ENERGY CARRIER

Accounting for about 77 % of the mass of all normal matter, hydrogen is the most abundant element in the universe [9]. Like electricity, hydrogen is considered a secondary form of energy that does not exist freely on the Earth's surface, predominantly bound in water. Hydrogen is an odorless, tasteless and colorless gas that, even though the volumetric energy density of hydrogen at ambient temperature and pressure (0.0108 MJ L^{-1}) is lower than that of hydrocarbons, it has the largest energy content by weight (143 MJ kg^{-1}) [10–12]. Therefore, on a weight basis, the amount of fuel required to produce a given amount of energy is substantially reduced when hydrogen is utilized.

Likewise, hydrogen can be obtained from a number of primary or secondary energy sources, depending on regional availability, such us natural gas, coal, wind, solar, biomass, nuclear, and electricity using electrolysers. In this regard, hydrogen production processes can be grouped into three categories, as illustrated in Figure 1.5: photochemical, electrochemical and thermochemical processes. In the photochemical process, the energy input is direct absorption of photons of light, through photocatalytic, photoelectrochemical or photobiological technologies (i.e. metabolic processes using microorganisms such as microalgae, cyanobacteria, etc.). In the electrochemical route, the energy input is given as electricity followed by the production of hydrogen via water electrolysis, whereas the energy input in thermochemical processes, is given as high temperature heat [13],[14].

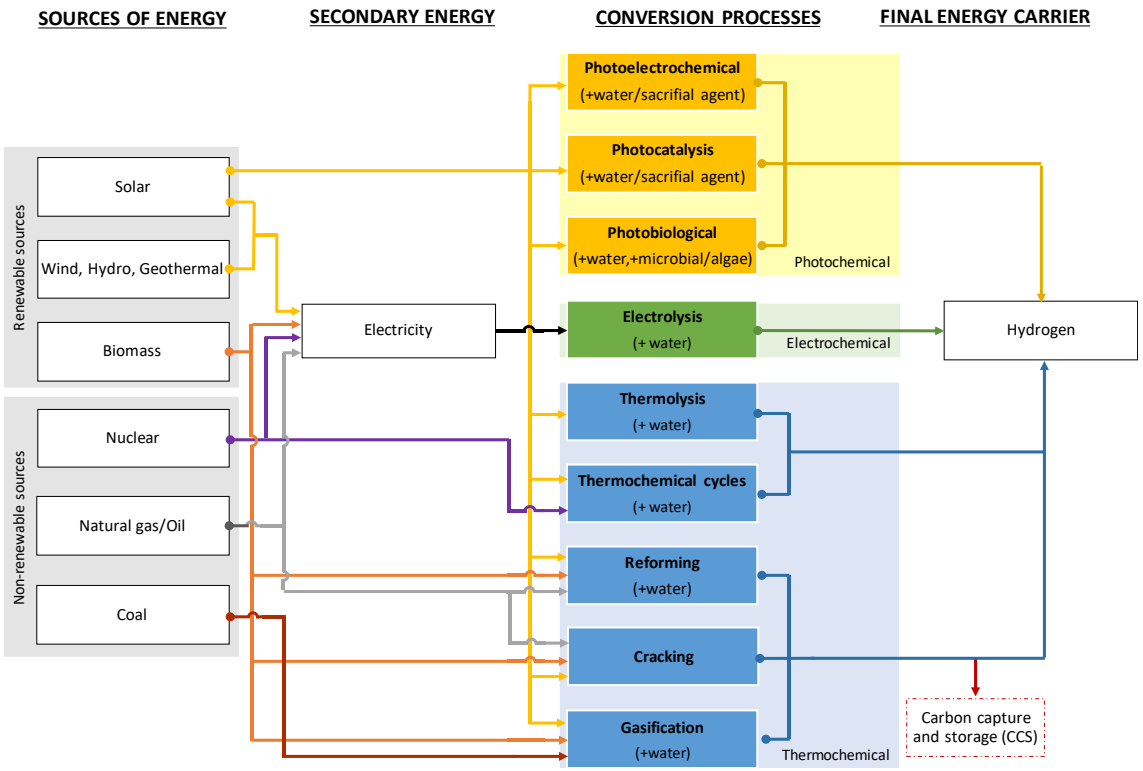

Figure 1.5. Hydrogen production routes. Modified from ref. [14–16]

Nowadays, about 96 % of the total hydrogen is produced from fossil fuel sources; divided into primary energy sources, about 48 % comes from natural gas (reforming), 30 % from heavy oils in refineries (cracking/decomposition) and 18 % from coal (gasification); the remaining 4 % is accounted for renewable sources, such as biomass-based technologies and water splitting techniques [11]. Therefore, worldwide production of hydrogen is responsible for CO_2 emissions of around 830 $MtCO_2$ per year [17].

While most of the hydrogen is currently being produced as “grey hydrogen” using mature technology, hydrogen production from carbon-lean and carbon-free energy sources has the potential to serve as a medium-to-long-term environmentally friendly alternative in a truly sustainable energy system. Likewise, the often called “blue hydrogen”, produced from non-renewable energy sources that meets the low-carbon threshold (i.e. steam-reforming with CCS) could therefore pave the way for the “green hydrogen” made from renewable electricity [18]. To achieve a hydrogen-based energy economy, all these hydrogen technologies must overcome their efficiency, cost, and safety challenges; thus, hydrogen production technologies are under research, development, and demonstration worldwide, and are on the way to mass market [7].

On the demand basis, hydrogen is an important industrial gas, being 90 % of the production consumed in the chemical and petrochemical sectors. The remaining 10 % of the produced hydrogen is used for mobility, electricity network (including storage of excess renewables) and heating, but it is still a very small fraction of the total consumption and under development. In energy terms, total annual hydrogen demand worldwide is currently around 330 Mtoe [17]. As shown in Figure 1.6, the chemical industry represents 63 % of the total industrial hydrogen demand, followed by crude-oil processing with a market share of 30 % and metal processing industry that accounts for 6 %. Hydrogen is also used in many other industrial processes, but together accounted for just 1 % of the industry market share. Ammonia, which is mostly used in the manufacture of fertilizers, is by far the largest consumer, representing 84 % of the total demand in the chemical sector [19].

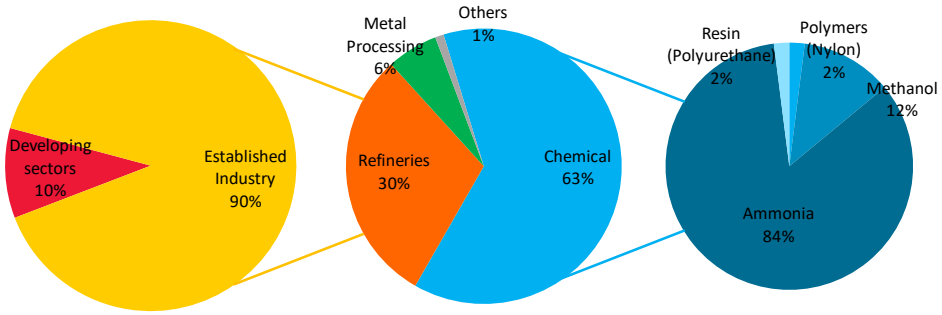

Figure 1.6. Hydrogen market share by segment and subsegment [19]

Demand for hydrogen has grown more than threefold since 1978 and continues to rise, as depicted in Figure 1.7 in 2018, world hydrogen demand reached 73.9 Mt H_2 in pure form; a further 45.0 Mt H_2 is used in chemical and petrochemical industries as part of a mixture of gases, such as synthesis gas, for fuel or feedstock. Asia and Pacific are the global leaders in hydrogen consumption representing one-third of the global consumption (33 %), followed by North America (28 %) and Western Europe (16 %) [20]. Besides its prominent role in its stand-alone markets, hydrogen-based energy storage systems play a key role as a bridge between intermittent electricity provided by alternative sources and the common fossil fuel-based energy system, evolving into a more integrated supply/demand system. Once it is produced, hydrogen acts essentially as a fuel gas opening the possibility of maintaining energy stored as long as needed, in units in the scale from kWh to GWh of energy [21]. To provide electricity back to the grid, hydrogen can be fed into a fuel cell or combustion engine where hydrogen gas is burnt. The main characteristic of the hydrogen combustion process is that it does not produce CO_2 but heat and water. But even when made from non-renewable energy sources, hydrogen still has certain advantages over fossil fuels, because of the high efficiency of such fuel cell systems [22].

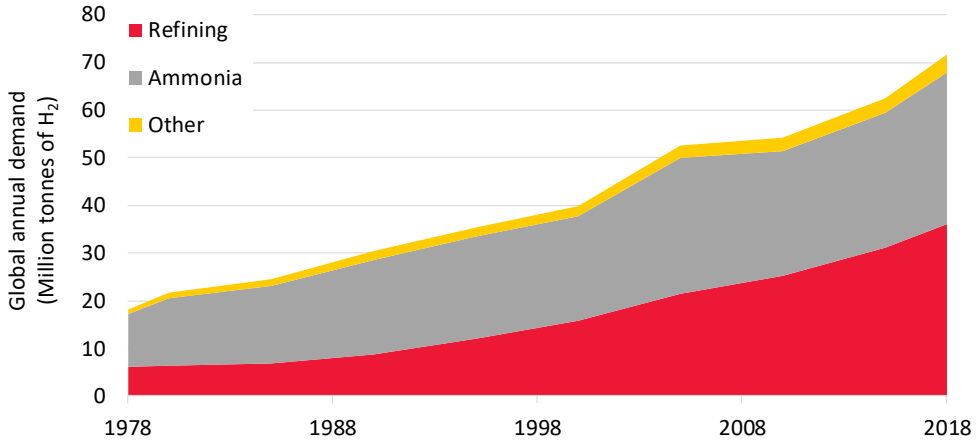

Figure 1.7. Global annual demand for hydrogen by sector [17]

At the same time, hydrogen-rich industrial waste streams are produced in relevant amounts considering both hydrogen generated due to excess of plant's capacity and by-product hydrogen [19]. With the aim of tackling this wasting of resources, this available surplus hydrogen that in some cases is simply vented or flared to the atmosphere, has also become attractive sources of feedstock for the manufacture of commodity chemicals such as ammonia or methanol, or even to be upgraded to fuel for both transportation and stationary applications.

1.3 SCREENING OF INDUSTRIAL SURPLUS HYDROGEN

Despite the fact that hydrogen is currently produced from a wide variety of primary or secondary energy sources, industrial surplus hydrogen is potentially one of the cheapest sources for producing hydrogen [23]. Currently, up to 0.5 Mt H_2 produced worldwide is currently vented to the atmosphere from several industrial users, while 22 Mt H_2 is simply used for on-site heat and power generation, even though cheaper energy sources could be used instead. In combination, this theoretically represents enough hydrogen to power 180 million fuel cell electric vehicles (FCEV) [17].

Generally, surplus hydrogen origin could be split into two different categories of industrial producers: captive and by-product industries. The former produced hydrogen as an intermediary input to on-site industrial processes (i.e. refineries, fertilizer plants and methanol industries) that accounts for 64 % of the hydrogen market in EU countries, while the latter generated hydrogen as by-product (i.e. petrochemical plants, steel mills or chlor-alkali plants) that constitutes 27 % of the market. The remaining 9 % consists in merchant hydrogen commercialization [24]. In the case of captive producers, hydrogen in excess may result when the installed capacities exceed internal consumption. On the other hand, depending on the

hydrogen-level of integration into the industrial plant, in some cases, wasted hydrogen from by-product industries is directly released to the atmosphere.

According to the above explained industrial categories, hydrogen loss in industrial waste gas streams could be estimated as up to 0.9 Mt H_2 per year in Europe, either in the form of excess of plant's capacity (up to 0.5 Mt H_2) or by-product hydrogen (0.2 to 0.4 Mt H_2). These figures have been estimated based on the EU hydrogen production in 2018, with two different excess margin scenarios (10 % for captive users and 10 to 20 % for by-product users), as it is projected the EU project "Roads2HyCom". In this regard, several studies have sought to quantify the amount of industrial surplus hydrogen available. The EU project "Roads2HyCom" produced a compilation of the surplus hydrogen production sites in Europe, in consonance with a previous hydrogen market report published in 1999 [25]. Nevertheless, the volume and flowrate of surplus hydrogen varies on a year basis because of changes in plant's capacity and the recycling of hydrogen in the integrated production sites. Despite these data are being largely based on qualitative approaches and not on a site-by-site assessment, this surplus hydrogen volume is quite significant and hydrogen recovery offers highly attractive opportunities.

The current use of industry's surplus hydrogen and hydrogen by-products could be split into internal or external uses. On the one hand, it may either be used for internal needs as a chemical feedstock or as an energy carrier for heat and power generation on-site. Alternatively, it could be sold as merchant hydrogen to specific industries, such as other captive users or even merchant companies. Hence, the hydrogen net balance of an industrial user strongly depends on the generated products and the processes involved, and therefore it could change largely between industrial plants. Nevertheless, the amount of hydrogen generally used by customers does not balance with the amount generated, and therefore, part of the hydrogen is wasted due to the inexistence of infrastructure for it to become merchantable [19].

The main hydrogen-rich waste gaseous stream by industrial producer are summarized in Table A.1.1 in the Appendix at the end of this chapter. Industrial waste streams with a hydrogen content higher than 50% are considered potential and promising sources for hydrogen recovery using separation techniques for its further use [26]. A detailed description of each industrial process step, which surplus hydrogen is generated, is outlined hereafter by industrial category.

1.3.1 CAPTIVE INDUSTRIES

As in the ammonia synthesis process depicted in Figure 1.8, a valuable hydrogen-rich gaseous stream is generated and, in some cases, wasted. Ammonia is commercially manufactured via Haber-Bosch process, which takes place at high pressure, *ca.* 250 atm, and a temperature of 450 °C, in the presence of an Fe-based catalyst after the reaction of N_2 and H_2 [27]. This production consumes about 1975 Nm^3 H_2 per ton of ammonia [19]. The SMR generally provides the H_2 required as a feedstock at the consumption site. The steam reforming is led by an endothermic reaction, which involves a catalytic conversion of a methane source, such as natural gas, and high-temperature steam into syngas, mainly consisting of a mix of CO and H_2. Then, water-gas shift reaction takes place at a lower temperature wherein CO from the syngas reacts with additional steam, forming CO_2 and more H_2. After CO_2 absorption, small amounts of CO and CO_2 are converted into CH_4 by reacting them in methanation reactor with H_2. The synthesis gas that contains a 3:1 ratio of H_2 and N_2, is then compressed and directed to the ammonia converter [28]. Ammonia is separated from the recycled gas by cooling/condensation, and even fresh synthesis gas is continuously added to the catalytic reaction, a portion of unconverted synthesis gas is returned to the loop. A stream of up to 180 – 240 Nm^3 H_2 per ton of ammonia is purged at high pressure to keep the inert gases concentration below a threshold value (up to 10 – 15 % of inert gases). Despite inert gases such as CH_4 or Ar do not hurt ammonia synthesis catalysts, they depress the H_2 and N_2 partial pressure [29]. These ammonia synthesis vent gases are often called as *ammonia purge gas (APG)*. In more recent designs, this hydrogen is mostly recovered and recycled to the synthesis loop via hydrogen recovery units (HRU), but some part of the cleaned purge gas is usually added to the reformer fuel, or even directly released to the atmosphere [19,30].

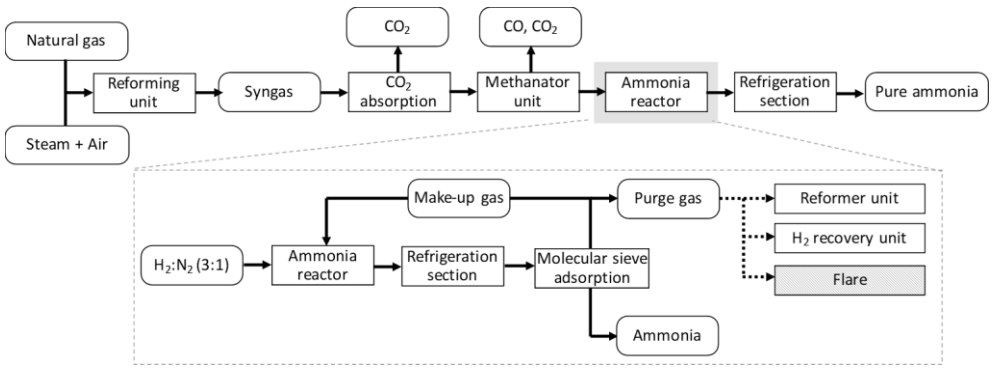

Figure 1.8. Origin of ammonia purge gas using Haber-Bosch process

Another hydrogen-containing gaseous stream is produced during methanol synthesis, which is schematized in Figure 1.9. This process involves the syngas catalytic conversion into methanol via hydrogenation of CO_2 and CO, both mildly exothermic reactions. The overall reaction is conducted at 300 - 400 °C and 50 - 300 bar, and contains a low $H_2/(2CO + 3CO_2)$ ratio, around 1.3 – 1.4 [28,31]. This production consumes about 1400 Nm^3 H_2 per ton of methanol [19]. As in the ammonia manufacturing, the syngas required as a feedstock is generally produced using natural gas reforming. At the methanol synthesis stage, the product of methanol reactors enters in a flash drum to separate gas phase from the liquid phase, called as crude methanol. The gas phase is mainly returned to the synthesis loop. To maintain the syngas rate within the methanol production unit, a portion of un-reacted syngas and some inert must be purged, like during ammonia synthesis. A stream of up to 125 Nm^3 H_2 is generated per ton of methanol, which is discharged at 10 – 45 °C and a pressure *ca.* 70 atm. Even though, this methanol synthesis vent gas, called as *methanol purge gas (MPG)*, is often valorized within several internal process steps; but also, some part is combusted in the flare.

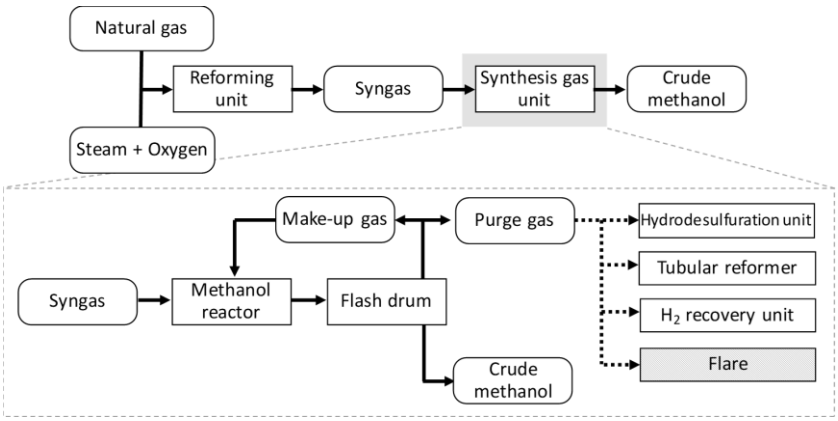

Figure 1.9. Origin of methanol purge gas using Lurgi Process

In oil refineries plants, another source of hydrogen concerns off-gas streams that are generated as a result of various separation and conversion processes [32]. Most of the make-up hydrogen supplied from the catalytic reforming unit is used to crack the heavier crudes as well as increase the hydrogen ratio in the molecules, and thus produce lighter crudes. All these processes allow hydrogen production only at a very limited purity of between 70 – 80 %. Generally, refinery off-gases contain mixtures of H_2 and light hydrocarbons [33]. Therefore, for further use of hydrogen, other than generation of process heat, a purification process is needed to increase the concentration over + 99 % [19]. Since petroleum industry increasingly adapt their production to their needs, this industrial surplus hydrogen is considered as the greatest near-term opportunity.

1.3.2 BY-PRODUCT INDUSTRIES

Among the various industrial sources of by-product hydrogen, chlor-alkali and sodium chlorate industries are considered one of the most promising low-cost hydrogen sources in the near term. Hydrogen off-gases from chlor-alkali plants may be produced through chlorine (Cl_2), hydrochloric acid (HCl) and sodium chlorate ($NaClO_3$) manufacturing. In this regard, high-purity hydrogen co-produced in manufacturing of chlorine and its derivatives, is often used as a feedstock for the production of other chemical products, such as ammonia (NH_3), hydrochloric acid (HCl) and hydrogen peroxide (H_2O_2), or even sold to merchant companies. Nevertheless, the current share of hydrogen streams emitted by chlor-alkali plants in EU countries acquire a 10 % of total hydrogen generated during their processes, but can vary from 2 to 53 % [34,35]. According to the statistics, this amount corresponds to *ca.* 33 kt H_2 emitted per year, considering these *chlor-alkali off-gases* as the most promising sources of hydrogen supply [29].

Figure 1.10 schematized the Cl_2 synthesis processes, wherein pure H_2 is co-produced. The basic principle of Cl_2 production process is the electrochemical splitting of an alkaline chloride solution (sodium chloride, NaCl or potassium chloride, KCl) into chlorine gas Cl_2, alkali hydroxide solution (caustic soda, NaOH or potassium hydroxide, KOH) and hydrogen, H_2. The brine is loaded in the anode compartment of such an electrolyser, which is powered by electricity. Whereas the chloride anion is oxidized on the anode to Cl_2, sodium or potassium ions are transported through the cation-selective membrane from the anode to the cathode compartment. Here, they recombine with hydroxyl ions to produce NaOH or KOH [36]. At the cathode, gaseous hydrogen, which partially is vented or flared, is manufactured independently of the type of electrolytic process used within the industry at a pre-set ratio of 300 Nm^3 H_2 per ton of Cl_2 [9]. The grade of these off-gases typically excesses 99.9 % of H_2 purity with minor traces of other components such as Cl_2, NO_x, H_2O, O_2 and HCl [32,37].

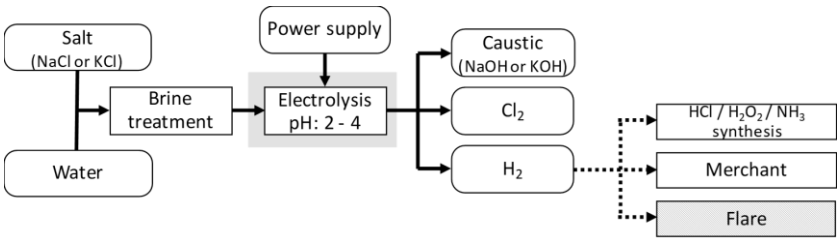

Figure 1.10. Origin of chlor-alkali off gas from chlorine making process

Another hydrogen stream is generated as by-product during HCl production, as illustrated in Figure 1.11. The production process consists on combusting Cl_2 and H_2 that feds into a burner at temperature above 2000 °C. The result is HCl, with subsequent absorption in demineralized water. To ensure a complete synthesis and prevent emissions of chlorine, excess of at least 5 % hydrogen compare to chlorine is charged to combustion chamber [38]. It has been estimated that 6 Nm^3 H_2 are produced in excess per ton of HCl, whereas a certain amount is partially emitted.

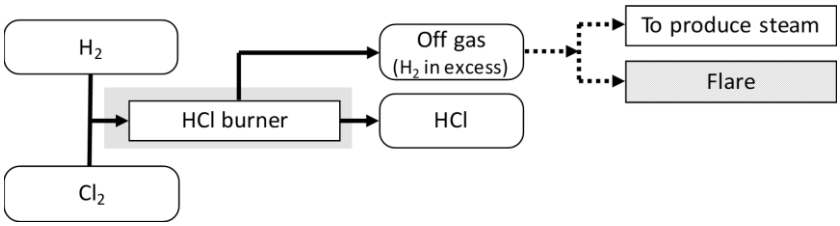

Figure 1.11. Origin of hydrogen-rich off gas from hydrochloric acid production

High-purity hydrogen off-gases from $NaClO_3$ production in chlor-alkali plants or pulp mills are another relevant source of by-product hydrogen. $NaClO_3$ is principally used to produce chlorine dioxide (ClO_2), which is commonly used as a bleaching agent in the pulp and paper industry to make a white fibre. The manufacture of $NaClO_3$ relies on the electrolysis of brine, also producing hydrogen as a co-product. Figure 1.12 schematized the $NaClO_3$ production process. Chlorine from the anode combines with the sodium hydroxide from the cathode and, due to the pH conditions, remains in solution forming hypochlorous acid and sodium hypochlorite, which is converted to sodium chlorate [39]. High-purity hydrogen, which is produced a rate of 668 Nm^3 H_2 per ton of $NaClO_3$, is often used as fuel for burners; but also, certain amount is simply flared. In all cases, output flow conditions are generally at temperature of 15 – 35 °C and atmospheric pressure [32],[40].

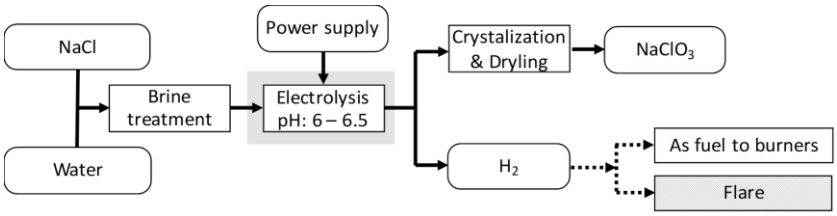

Figure 1.12. Origin of hydrogen-rich off gas from sodium chlorate synthesis

Another relevant hydrogen-containing off-gas is coke oven gas (COG), sometimes simply called “coke gas”, that comes coming from steel mills and coke plants. This is a by-product of coal carbonization to coke, which is co-generate in the coke-making. After leaving the coke oven,

raw COG is generally collected and treated to recover valuable products such as tar, light oil (mainly consisting of BTX (benzene, toluene and xylenes)), sulphur, and ammonia [41]. The cleaned COG is generally at atmospheric temperature and pressure, and *ca.* 425 Nm^3 COG is produced per ton of coke. Nowadays, most of this gas is simply used as fuel for the under-firing of coke oven batteries, in which only the thermal value of this stream is used, as well as in other processes of the steel plants. However, very often the excess of COG cannot be used in this way and so it is burnt directly in flare stacks, followed by discharged into the atmosphere, as depicted in Figure 1.13 [42]. In the case integrated steel mills with an on-site coke oven plant, around 3 % of the total COG produced is flared [41,43,44]. Likewise, only 20 – 40 % of the total COG produced in coking plants is recovered in alternative processes [45,46].

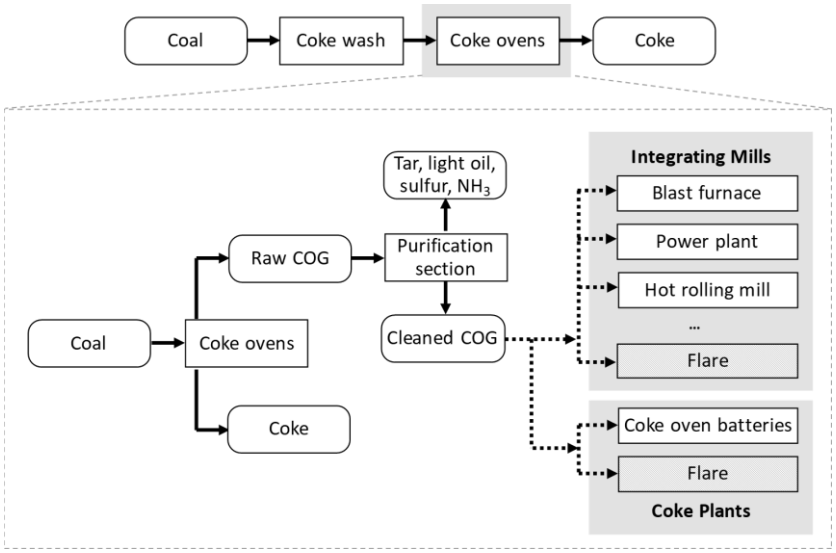

Figure 1.13. Origin of coke oven gas based primary steel production

In petrochemical plants, a large amount of hydrogen is produced as a by-product from dehydrogenation of the hydrocarbon molecules that involves the removal of hydrogen to generate more valuable products, such as ethylene or acetylene production [4]. Recovered hydrogen is either recycled to downstream process or sold for distribution on the merchant market [47].

1.4 VALORIZATION OPPORTUNITIES

These hydrogen-rich effluent gases would theoretically become attractive sources to be upgraded for hydrogen-based storage solutions. Especially, surplus hydrogen could be used to instantly supply early user centers at moderate prices during the transition phase towards a hydrogen-based energy system. Despite a large industrial market dominated by refineries and chemical plants, niche markets for hydrogen are likely to emerge in the short-to-medium term.

As depicted in Figure 1.14, these include valorizing hydrogen for use as a commodity in many industrial processes, hydrogen injection into the gas network, converting it to hydrogen-based fuels, providing a re-electrification pathway or using it as a fuel for mobility [7]. Within the hydrogen-to-chemical route, hydrogen can be used as a chemical feedstock in its stand-alone markets (i.e. oil refining, ammonia or methanol); but also, in a wide variety of applications characterized by very high prices and purity grade of hydrogen (i.e. healthcare, space industry, food and beverage industry, semiconductor fabrications or hospitals). Today, much of the refining and chemicals production sites are already concentrated in coastal industrial zones around the world (i.e. the North Sea in Europe, the Gulf Coast in North America and south-eastern China). Thus, coastal industrial hubs, which already have hydrogen pipeline network and storage infrastructure, are of special interest for hydrogen value chains [17].

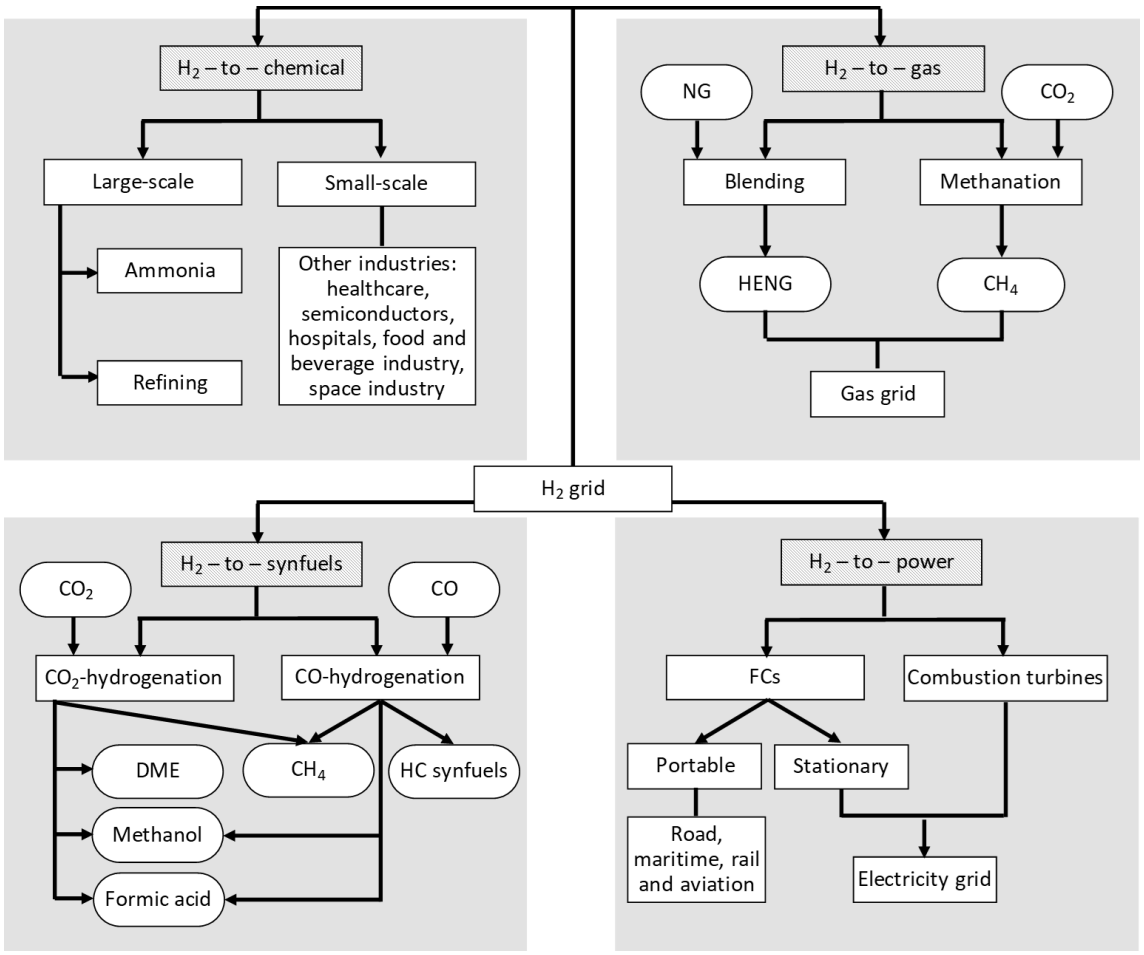

Note: Natural gas (NG), Hydrogen-enriched natural gas (HENG), Synthetic liquid fuels (Synfuels), Hydrocarbons (HC), dimethyl ether (DME), Fuel cells (FC).

Figure 1.14. Present and potential hydrogen niche markets

Otherwise, hydrogen can also be partially blended with natural gas in an existing gas grid or converted into synthetic methane, allowing its calorific value to be monetized. This is the so-called hydrogen-to-gas pathway. Furthermore, hydrogen-to-synfuels application relies on the use of hydrogen for producing synthetic liquid and gaseous fuels (i.e. methane, methanol and ammonia), which have a range of potential transport uses. To render fuels GHG-free, the carbon feedstock must be of biogenic origin or captured from the atmosphere using direct air capture (DAC) technologies [48]. Likewise, hydrogen-to-power solutions are found to have a major role, in which hydrogen can be re-electrified in a direct electrochemical process, via fuel-cell power plants, or using conventional thermal combustion turbines. But also, it is a fuel for hydrogen-powered vehicles, especially using fuel cells as efficient, reliable and clean prime mover technologies. Among the fuel cell technologies, polymer electrolyte membrane fuel cells (PEMFC) are one of the most promising electrochemical devices that could be fed with hydrogen to produce electricity in a very efficient and clean way. The advantages of PEMFC devices, such as rapid start-up, high electrical efficiency, silence, low pollutant emissions and ease of installation, motivate their application to portable, transportation and stationary end-uses [49].

Therefore, hydrogen demand for fuel cell applications is expected to grow rapidly in all end-sectors of the economy: industrial, transportation, residential and commercial. Especially, the transport growth makes this a key sector with increasing demand for “green hydrogen” as an attractive alternative to non-renewable energies [50]. The use of hydrogen as a future carbon-free road transport fuel represents a promising option towards the required profound transformation of the automotive industry. On such a tank-to-wheel basis, only hydrogen FCEVs and battery electric vehicles (BEVs) are fully CO_2 emission free. The advantages of FCEVs, which use PEMFCs, relative to current lithium-ion-powered BEVs include higher driving ranges (over 500 km) and rapid refueling (3 – 5 min). The most leading Asian automakers to introduce FCEVs onto the market in 2014 – 2020 timeframe are Toyota, Honda and Hyundai [9]. Accordingly, Toyota’s Mirai FCEV, Honda’s Clarity FCEV, and Hyundai’s Tucson-ix35 and NEXO FCEVs are commercially available, but also Mercedes-Benz has recently begun leasing and selling a plug-in hybrid electric vehicle with a fuel cell. Even thought, FCEV purchase prices are higher compared to conventional vehicles, and similarly to BEVs, due to their electrochemical power supply (on-board hydrogen storage and fuel-cell system); but they will decline considerably with increased manufacturing volumes in order to achieve better market uptake [51]. About 4,000 FCEVs were sold worldwide in 2018 accounting for a total stock of 12,000 fuel cell cars on the road, but this still represents a small fraction compared with the 2018 BEV stock of 5.1 million or the global car stock of more than 1 billion [17].

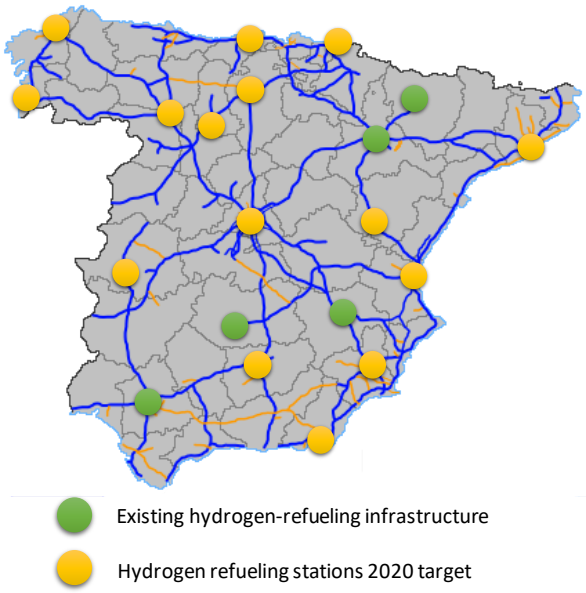

Figure 1.15. Estimated evolution of the hydrogen-refueling infrastructure in Spain. Modified from: [52]

Although in recent years, the prospects of a shift to a hydrogen economy have created great interest in the scientific community and social stakeholders, the success relies on the availability of the necessary infrastructures [53]. In the specific case of the mobility sector, the main obstacle hindering vehicles manufacturers and consumers from embracing FCEVs is mostly the lack of hydrogen infrastructure [54]. Several worldwide national strategies are focused on promoting alternative energy vehicles (AEV), such as the "AEV Strategy" in Spain for the period 2014 - 2020, which foreseen the extension of the current Spanish corridor with 6 hydrogen refueling stations (HRS) in different operating states to 20 plants in 2020. The present and future hydrogen refueling infrastructure is shown in Figure 1.15.

Hence, a number of works focused on the use of decision-support tools for the design and operation of hydrogen supply chains (HSC), have been reported addressing questions such as the design of the hydrogen fuel infrastructure applied at country, region and city levels with Almansoori and Shah leading the way [55]. Some studies include the selection of the production technology (primary and secondary energy sources) and hydrogen transmission forms (pipeline, truck and on-site schemes) through each node of the supply chain [56–64]. Also, most of these studies analyze hydrogen delivery modes in terms of capital and operation expenditure of the infrastructure focusing on the transportation sector [54,65,66]. Meanwhile, among the list of hydrogen-containing waste streams, some studies concentrated on the management, optimization, and utilization of steel-work off gases in integrated iron and steel plants [67–70]. However, little is focused on the optimization of various by-product gases to embed sustainability into a HSC.

Faced with this scenario, hydrogen produced at a cost around 1.5 - 3 € kg^{-1} could be competitive within the mobility sector, allowing hydrogen penetration into the mass markets. From the Table 1.1, steam-methane reforming process currently produce the lowest hydrogen cost below 2 € kg^{-1}, but it strongly correlates with the market price of natural gas and varies regionally. According to the European's 2030 vision, these prices would be viable by a diversity of clean production routes such as the conventional central steam-methane reforming (SMR) combined with CCS, and decentralized water electrolysis connected to wind or solar farms [71]. On the other hand, hydrogen sales price to mobility end-users is currently set at 9 - 10 € kg^{-1}, within the HRSs in Europe. Nevertheless, EU-targets of hydrogen sales price assessed at the pump by 2030 should be in the range of 4 - 6 € kg^{-1} to achieve cost parity with conventional fuels; but even these figures strongly depend on natural gas and electricity prices to achieve profitability [72,73].

Table 1.1. Current hydrogen production cost (€ kg^{-1}). Sources: [15,74,75]

Resources / Routes	Production cost
Natural Gas (SMR)	**0.8 – 2.0**
Coal (gasification)	**1.0 – 2.0**
Grid electricity EU-mix (electrolysis)	**3.75**
Wind (electrolysis)	**4 - 9**
Solar PV (electrolysis)	**5 - 20**
Geothermal	**9**
Hydropower	**5.4 - 7.9**
Biomass (gasification)	**3.8 - 9.8**
Nuclear	**1.4 - 5.4**

It has been estimated that the price of recovered hydrogen could be 1.5 to 2 times lower than the corresponding cost from centralized conventional SMR plants [26]. These figures highlight the potential and attractiveness of using these industrial waste streams as source of hydrogen. The need to compete against the fluctuations in fuel energy prices and promote the circular economy by upcycling the resources, leads to a great relevance of hydrogen-containing waste gas streams recovery using separation and purification techniques. Hydrogen-fuel quality requirements and available gas separation methods for hydrogen recovery are two important factors for estimating the real potential of industrial surplus hydrogen to feed fuel cell stacks. All this technologies are going to be introduced, and then focus in the most interesting among them, membrane technology and multicolumn PSA process, since the scope of this thesis is contributing to the assessment of these particular types of commercially proven hydrogen recovery techniques.

1.5 HYDROGEN PURIFICATION METHODS

Hydrogen separation is theoretically an entropy decrease process, and as a result, it cannot happen spontaneously without consumption of energy [76]. Currently, the most mature technologies to purify hydrogen can be distinguished into pressure swing adsorption (PSA), membrane systems and cryogenic distillation. Each of these separation methods has its unique capabilities and constraints. Table 1.2 summarizes important considerations when determining the choice of the best technology for upgrading hydrogen. The selection of the right purification system is basically influenced by several specific considerations, strictly related to the output to be obtained. The feed composition, the feed conditions (pressure and temperature), the plant's capacity, the capital and operating costs, and the final destination of the product strongly affect the choice of the hydrogen upgrading method [77]. But also, some useful project parameters, introduced by Miller in 1989, such as flexibility, reliability, turndown, scale economics and by-product value, are discussed below [78].

Table 1.2. Comparison between current technologies for hydrogen separation [79–81]

Features		**Units**	**Membrane**	**PSA**	**Cryogenic**
Means media		-	Polymers	Adsorbents	Cooling agents
Mechanism		-	Diffusivity and solubility	Surface sorption	Gas boiling temperatures
Hydrogen concentration	**Feed**	H_2 mol %	> 25	> 40	> 10
	Product	H_2 mol %	90 - 98	> 99.9	90 - 98
Operating conditions	**Temperature**	° C	0 - 100	RT	-183
	Feed pressure	bar	20 - 160	10 - 40	5 - 75
Hydrogen recovery		%	85 - 95	50 - 92	90 - 99
Hydrogen capacity		$Nm^3\ h^{-1}$	< 60,0000	30 – 400,000	10,000 – 90,000
Product pressure		bar	< 1/3 Feed pressure	Feed pressure	Feed/ Low pressure
Pre-treatment requirements		-	Minimum	None	CO_2, H_2O removal
Operating flexibility		-	Moderate	High	Low
Response to variations		-	Instantaneous	Rapid (5 - 15 min)	Slow
Start-up after the variations		-	10 min	1 h	8 - 24 h
Turndown		-	Down to 10 %	Down to 30 %	Down to 30 – 50 %
Reliability		-	100	95	Limited
Control requirement		-	Low	High	High
Capital cost		-	Low	Medium	High
Scale economics		-	Modular	Moderate	Good
By-product value		-	Moderate	No	Liquid HCs

The hydrogen product purity and the levels of specific product impurities are critical to process selection. Cryogenic and membrane processes normally produce hydrogen at 90 - 98 % vol., whereas the PSA process is the best choice when high-purity hydrogen above 99.9 % is required. The composition of the feed and its variability, either on a short- or long-term basis, has also a large impact on the selection of the upgrading process due to it influences the performance, reliability and pre-treatment required. While membrane and cryogenic systems are suitable for a wide range of feed compositions, PSA is more applicable for gas streams with hydrogen content above 60 %. Nevertheless, variability in feed quality conditions have little impact on PSA performance, showing a great ability to maintain hydrogen purity and recovery constant by a simple cycle time adjustment. In membrane processes, small feed composition changes can be managed by adjusting the feed-to-permeate pressure ratio, and it has essentially instantaneous response time and extremely short state-up time. On the contrary, the cryogenic process has very low flexibility, with response and star-up times not as rapid as for PSA and membrane systems.

The plant's capacity and feed/product pressures should be considered together because the three hydrogen purification processes have different scale economies. The membrane systems are the lowest capital cost choice for small product flow rates at high pressures ranging 20 - 160 bar, since the pressure drives the separation and the cost of the membrane system is proportional to the number of modules required. Nevertheless, the hydrogen product stream is produced at pressures much lower than the feed pressure using membranes and it may need recompression. PSA systems are applicable throughout a full range of capacities and produces hydrogen at essentially feed pressure, reducing compression steps afterwards and energy consumption. Differently from membrane systems, PSA units cannot take advantage of high available feed pressure, which normally operates at pressures ranging 10 - 40 bar. On the other hand, cryogenic systems have high capital cost at low product rates but have good economies of scale.

Furthermore, cryogenic process has the lowest turndown, meaning that it has the lowest capability to operate at reduced capacity of the initial design by maintaining product purity and recovery (i.e. low operating flexibility). On the contrary, even though the capacity is reduced to 10 % of the initial design, membrane systems are highly capable of keeping product purity. Regarding the reliability, the cryogenic process is considered to be less reliable than the PSA or membrane processes with respect to the on-stream factor that can cause unscheduled shutdowns.

While the three hydrogen purification systems are in the trade market, high capital costs and energy consumption are associated to the cryogenic distillation processes. Without liquid hydrocarbon recovery to offset the higher capital cost, especially ethylene and propylene from refinery off-gases, cryogenic methods cannot generally be justified over the other separation technologies. For all these reasons, this thesis is focused on the assessment of the two most valuable hydrogen clean-up technologies for the recovery of hydrogen from industrial waste gas streams: PSA and membrane systems.

1.5.1 HYDROGEN PSA PROCESS

1.5.1.1 Fundamentals of PSA technology

Adsorption processes are based on the selectivity that some porous solids have to attract adsorbate molecules to the particle's surface: outside and on the pore walls. Regarding the mechanism, most of the PSA processes are equilibrium driven, where the selectivity depends on differences in the equilibrium affinities [82]. The interactions between the solid surface (adsorbent/solid phase) and the gas molecules (adsorbate/fluid phase) used are the type of binding that correspond to physical adsorption (also known as physisorption). The physisorption is spontaneous and thus exothermal, releasing low heat of adsorption (10 – 60 kJ mol^{-1}). The adsorption forces are relatively weak, involving only Van der Waals attractions and electrostatic forces. Since physisorption is caused by intermolecular forces, the adsorbed species are also easier to desorb, so the physical adsorption is reversible to a certain extent [83].

The role of the adsorbents, typically alumina, silica gel, activated carbon or molecular sieves, is to provide the surface area for the selective sorption to take place: the selectivity and the adsorption capacity are important factors that must be taken into account when choosing the sorbent as well as the operating conditions for gas separation. The adsorption behavior of the porous material, is normally assessed by measuring the amount adsorbed at equilibrium state, which establishes the thermodynamic limit of the adsorbent loading for a given fluid phase, pressure and temperature. Adsorption equilibrium isotherms relate amount of adsorbate on adsorbent q_i^*, at different concentrations (partial pressures) of adsorbate in the bulk p_i, but at a fixed temperature. The separation ability is lost once the adsorbent has reached equilibrium with the fluid phase, so that is why the solid phase must be regenerated. The more linear or slightly nonlinear the isotherms, the better performance in PSA units. When isotherms are strongly nonlinear, the adsorbent regeneration is not possible unless vacuum or higher temperature is applied to desorb the loaded gases [9,84].

Industrial PSA units typically comprise multiple adsorbed vessels, which operate simultaneously in an adsorption- regeneration cycle, in such a way that each bed undergoes the same sequence of elementary steps, but at different times. Consequently, PSA systems may process a feed stream to produce a constant flow of product and tail gas. The adsorption step is carried out at high pressure to retain all impurities; whereas the regeneration step is performed by reducing the total pressure of the bed. Therefore, the purified hydrogen breaks through the column at near feed pressure, whereas the tail gas is at very low pressure to maximize hydrogen recovery. This operating mode eliminates compression steps afterwards, and therefore permits to reduce energy consumption. As illustrated in Figure 1.16, the inlet and exit streams are characterized by the molar fraction y_i , the volumetric flowrate Q_i, and the partial pressure p_i.

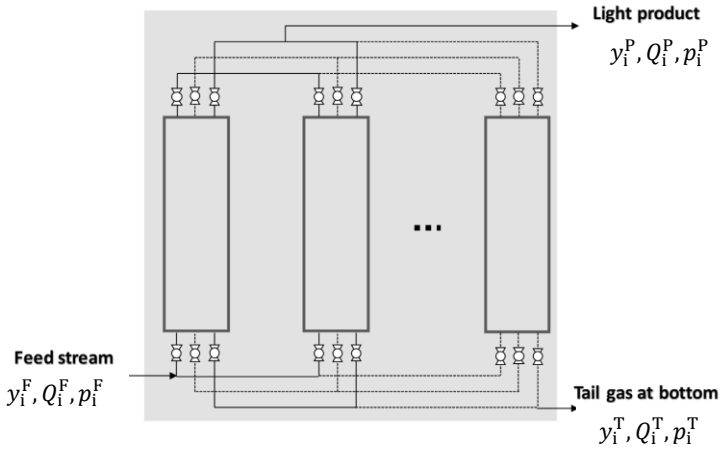

Figure 1.16. Basic black-box scheme of a PSA process for H_2 purification

The technology was commercially introduced in the 1960s by Skarstrom (Esso Research and Engineering Company), who established the standard and reference cycle of a PSA process as a sequence of four steps [85]:

- Adsorption (AD) – the feed gas is introduced in the packed column at the high cycle pressure, wherein the contaminants of the stream are retained while hydrogen is produced.
- Counter-current blowdown (BD) – immediately before the contaminants break through the column, the feed is interrupted and the column is depressurized down to the low cycle pressure through the bottom end, and waste gas is obtained.
- Counter-current purge (PP) – the column is washed with hydrogen through the top end with the feed end open at low cycle pressure.
- Pressurization (PPE) – the column is finally pressurized through the top end with recycled enriched gas (purified hydrogen).

1.5.1.2 State-of-the-art of PSA technology

High-purity hydrogen production from a gas mixture containing 60 - 90 % vol. H_2 by using PSA processes has become the state-of-the-art technology in the chemical and petrochemical industries. These systems accounts for over 85 % of the current hydrogen purification units installed around the world since the early 1970s [9],[86]. Many different PSA processes have been developed for purification of hydrogen during the last thirty years. The two most common gas streams to feed the PSA process are: i) SMR off gas after water - gas shift reaction (SMROG), and ii) refinery off gases from various sources (ROG), which compositions are detailed in Table A.1.1 in the Appendix section. Furthermore, Table 1.3 summarizes the performance of the most frequently PSA processes patented by different companies around the world. The high separation efficiency of these processes is self-evident. Nevertheless, hydrogen recoveries for the PSA systems are typically lower than those available for the other technologies, with recoveries above 80 % in large units with more than twelve columns and operation pressures above 20 bar [87].

Table 1.3. Process performance of four PSA process [88]

Process	Licensor	Adsorbent	nº columns	Feed gas	Primary product	Purity	Recovery	Secondary product
Poly-bed	UOP LCC	AC / 5A zeolite	10 beds	SMROG at 21 bar	H_2	99.999 %	86.0 %	-
LOFIN	Toyo Engineering	Silica gel / AC	4 beds + storage	ROG at 28 bar	H_2	99.96 %	86.3 %	-
Gemini	Air Products	AC / 5A zeolite	9 beds	SMROG at 18 bar	H_2	99.999 %	87.1 %	CO_2
Gemini-NH3	Air Products	AC / 5A zeolite	6 beds	SMROG at 18 bar	$N_2 + H_2$	$H_2 \approx 75\%$ $N_2 \approx 25\%$	$\approx 95\%$ $\approx 75\%$	CO_2

Note: Steam methane reforming off gas (SMROF), Refinery off gas (ROG)

Intensive research has been carried out to improve the performance of the PSA process, either in terms of hydrogen recovery or in unit size, focused on a variety of industrial effluents, such as SMR off gas [89], refinery off gases [90], coke oven gas [91,92] and coal gas [93]. The key development goals of PSA are to increase the yield of the units and to reduce the costs of smaller PSA systems [9]. With a growing demand of distributed hydrogen production, the challenge in hydrogen purification becomes more evident at small-scale PSA units, in which lower recovery values are found, *ca*. < 70 %, due to the lower operating pressure used that gives less flexibility for cycle optimization [94]. Also, it is reported that down-scaling PSA units to less 500 Nm^3 H_2 h^{-1} of production capacity is not economic [95]. In consequence, innovative materials can provide enhanced cyclic capacity that will reduce the size of the units [96,97]. A typical strategy to deal with the adsorption of so many gases is to employ columns filled with different layers of adsorbents. Two active research lines in materials science are the structural and chemical

modifications of activated carbons and the synthesis of mixed-cation exchanged zeolite frameworks [86]. Diverse types of cycle sequences are also being developed or even patented to efficiently use the adsorbent loading [98]. The recent developments in H_2 PSA units includes: rapid PSA (RPSA) processes, which operate with rotary valves and structured adsorbents and have very short total cycle time smaller than 30 seconds; sorption enhanced reaction process (SERP), that uses a sorber-reactor to produce hydrogen; and hybrid adsorbent membrane – PSA processes for improving hydrogen recovery [88]. However, only few studies have been focused on controlling hydrogen impurity for fuel-cell application and most of these efforts are focused on purifying reformate gas, from either methane, ethanol or methanol.

1.5.2 HYDROGEN-SELECTIVE POLYMERIC MEMBRANES

1.5.2.1 Fundamentals of gas permeation

A membrane is a physical barrier that selectively permits specific gases pass through to the permeate side driven by the chemical potential, while being able to retain the impermeable gases at the retentate side. For dense polymeric membranes, the driving force is the difference in fugacities for real gases and in partial pressure for gases where it can be assumed the ideal gas behavior [99]. Gas transport in dense, organic (polymeric) membranes (DPMs) is mostly described by the solution-diffusion mechanism. In this case, the permeating gas dissolves into the polymer at one face of the membrane, diffuses across the membrane and then is desorbed at the downstream face. Thus, permeability is a function of both gas diffusivity and solubility [100]. The solution-diffusion mechanism is driven by a difference in the thermodynamic activities existing at the upstream and downstream faces of the membrane as well as the interacting force working between the molecules that constitute the membrane material and the permeate molecules. The activity difference causes a concentration gradient that leads to diffusion in the direction of decreasing activity, as depicted in Figure 1.17.

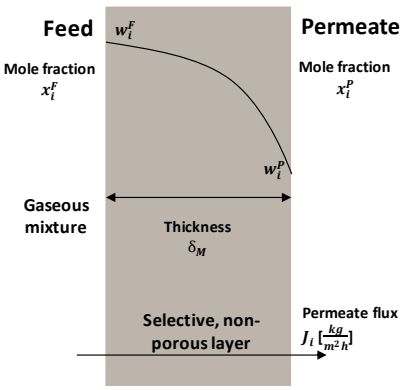

Figure 1.17. Schematic representation of gas permeation through the solution-diffusion mechanism

Fick's law is the simplest description of gas diffusion through a dense membrane with a constant diffusion coefficient assumption [101] :

$$J_{\mathrm{i}} = -D_{\mathrm{i}} \frac{\partial C_{\mathrm{i}}}{\partial x} \qquad \text{Eq. (1.1)}$$

with J_{i} the flux through the membrane of a component i, D_{i} is the diffusion coefficient and $\partial C_{\mathrm{i}}/\partial x$ is the driving force for gas transport. Assuming steady state conditions, this equation can be integrated to give:

$$J_{\mathrm{i}} = -D_{\mathrm{i}} \frac{C_{\mathrm{i},0} - C_{\mathrm{i},\delta}}{\delta} \qquad \text{Eq. (1.2)}$$

where $C_{\mathrm{i},0}$ and $C_{\mathrm{i},\delta}$ are the concentrations of component i in the membrane at the retentate side and the permeate side, respectively, and δ the thickness of the membrane. In ideal systems, Henry's law states a linear relationship between the concentration inside the membrane,C_{i} , and the gas partial pressure outside the membrane, p_{i}.

$$C_{\mathrm{i}} = S_{\mathrm{i}}\, p_{\mathrm{i}} \qquad \text{Eq. (1.3)}$$

where S_{i} (cm^3(STP) cm^{-3} bar^{-1}) is the solubility coefficient of component i in the membrane. Finally, combining the Eq. (1.2) with Eq. (1.3), and considering that the constant gas permeability P_{i} is equal to the product of the solubility S_{i} of the gas molecules into the membrane surface and the diffusivity D_{i} of the gas molecules penetrating in the membrane matrix, the local transmembrane flux of a given compound is calculated according to the given expression:

$$J_{\mathrm{i}} = P_{\mathrm{i}} \frac{\Delta p_{\mathrm{i}}}{\delta} = P_{\mathrm{i}} \frac{({p_{\mathrm{i}}}^{F} - {p_{\mathrm{i}}}^{P})}{\delta} \qquad \text{Eq. (1.4)}$$

Where Δp_{i} is equal to the difference between the ${p_{\mathrm{i}}}^{F}$and ${p_{\mathrm{i}}}^{P}$, which are the feed and permeate pressures, respectively. Thus, the pure-gas permeability coefficients are calculated using the following equation:

$$P_{\mathrm{i}} = \frac{{Q_{\mathrm{i}}}^{P} \cdot \delta}{A \cdot \Delta p_{\mathrm{i}}} = \frac{{Q_T}^{P} \cdot {x_{\mathrm{i}}}^{P} \cdot \delta}{A \cdot ({p_{\mathrm{i}}}^{F} - {p_{\mathrm{i}}}^{P})} \qquad \text{Eq. (1.5)}$$

where P_{i} is the pure-gas permeability coefficient, a normalized measure of flux of the membrane. It is usually expressed in Barrer (10^{-10} cm^3(STP) cm cm^{-2} s^{-1} $cmHg^{-1}$). The permeability is related to the permeate flow rate of a component i through the membrane ${Q_{\mathrm{i}}}^{P}$ (cm^3 s^{-1}), the area of the membrane A (cm^2), the selective layer thickness of the membrane δ (cm), and the

driving force for separation Δp_{i} (cmHg). The theoretical pure-gas selectivity $\propto_{i/j}$ of one gas, i, over another gas, j is defined in Eq. (1.6), where P_{i} and P_{j} are the permeabilities of gas i and gas j, respectively.

$$\propto_{\mathrm{i}/\mathrm{j}} = \frac{P_{\mathrm{i}}}{P_j} \qquad \text{Eq. (1.6)}$$

Whereas the order of gas permeability in rubbery polymers (polymers with glass transition temperatures, T_{g}, below the operating temperature) is governed principally by gas condensability, in glassy polymers (polymers with T_{g} above the operating temperature) the order is related to the size difference between the gas molecules and the size sieving ability of the polymer [102]. Concerning the theory, light gases (i.e. H_2, N_2) with very low solubility in polymeric materials, they only weakly affect the property and behavior of polymers, and do not influence the mutual diffusion and solubility parameters in the process of simultaneous transport of gases in mixture separation. For heavy gases (i.e. CO_2) with great solubility, the applicability of ideal permeation parameters is less predictable [103]. Hence, the following formula is used to calculate gas permeability coefficients for multicomponent gas mixtures [104,105]:

$$P_{\mathrm{i}} = \frac{{Q_{\mathrm{i}}}^P \cdot \delta}{A \cdot \Delta p_{\mathrm{i}}} = \frac{{Q_T}^P \cdot {x_{\mathrm{i}}}^P \cdot \delta}{A \cdot (p^F \cdot {x_{\mathrm{i}}}^F - p^P \cdot {x_{\mathrm{i}}}^P)} \qquad \text{Eq. (1.7)}$$

where P_{i} is the mixed-gas permeability coefficient of component i, and Δp_{i} (cmHg) is the gas component i partial pressure gradient across the membrane. Likewise, ${x_{\mathrm{i}}}^F$ and ${x_{\mathrm{i}}}^P$ are the mole fraction of component i in the feed and permeate stream, respectively. Moreover, the mixed-gas selectivity is calculated by this equation:

$$\propto_{\mathrm{i}/\mathrm{j}} = \frac{{x_{\mathrm{i}}}^P \cdot (p^F \cdot {x_j}^F - p^P \cdot {x_{\mathrm{j}}}^P)}{{x_j}^P \cdot (p^F \cdot {x_{\mathrm{i}}}^F - p^P \cdot {x_{\mathrm{i}}}^P)} \qquad \text{Eq. (1.8)}$$

where ${x_{\mathrm{j}}}^F$ and ${x_{\mathrm{j}}}^P$ are the mole fractions of component j in the feed and permeate stream, respectively.

1.5.2.2 State-of-the-art of membrane systems

A number of comprehensive reviews have been conducted on membrane sciences for hydrogen purification during the last few years [102,106–109]. These studies have identified three kind of membranes based on the materials, which are of polymeric, inorganic and metallic nature. As shown in Table 1.4, these membranes differ in terms of the hydrogen separation

performance and the applicable operation conditions [110]. The advantages of membrane technology over existing separation processes, such as high selectivity, low energy consumption, small footprint, moderate cost to performance ratio and compact and modular design, especially in small to medium capacity plants, have been widely reported, and thus, also motivate their application to hydrogen upgrading [87]. Compared with metal and inorganic membranes, DPMs are the dominating materials for gas separation membranes at present, because of the outstanding economy (lower material and manufacturing costs) and competitive performance (mild operation conditions) [99]. Although metal membranes, such as palladium-based membranes, could provide infinite permselectivity of hydrogen, apart from its inherent material cost, they are more suitable for use at high operating conditions (> 300 °C) to avoid embrittlement [111].

Table 1.4 Different membranes for hydrogen separation [110]

Membrane type	**Polymeric**	**Metallic**	**Ceramic**		**Carbon**
	Dense			**Microporous**	
Materials	Polymers	Groups III–V metals (Pd and alloys)	Ceramics	Silica, Alumina, Zeolites	Carbon proton conducting
Transport mechanism	Solution-diffusion	Solution-diffusion	Solution-diffusion	Molecular sieving	Surface diffusion; Molecular sieving
Temperature range	< 110 °C	150 - 700 °C	600 - 900 °C	200 - 600 °C	500 - 900 °C
Selectivity	Moderate	Very high (> 1000)	> 1000	5 - 139	4 - 20
H_2 flux (10^{-3} mol m^{-2} s^{-1}) at Δp=1 bar	Low-moderate	60 - 300	6 - 80	60 - 300	10 - 200
Cost	Low	Moderate-High	Low-moderate		

Also, hydrogen-selective membranes made of glassy polymers have preferences as membrane materials for separation of hydrogen in comparison with hydrogen-rejective membranes based on rubbery polymers; they are more permselective to hydrogen molecules and in many cases more permeable in comparison with rubbers [103]. Moreover, glassy polymeric membranes still exhibit better thermal stability and mechanical strength that rubbery hydrogen-rejective membranes [112,113]. After many years of development, membrane separation technology has been extensively applied in many industries with moderate hydrogen purity requirements, especially for natural gas upgrading/sweetening (90 % purity), and also as fuel gas (54 – 60 % purity). As a matter of fact, membrane manufacturing companies use a quite limited set of polymers as hydrogen-selective membrane materials such as polysulfones (PSF), polycarbonates (PC), cellulose acetates (CA), polyphenyloxides (PPO) and polyimides (PI), meanwhile new high performance tailor-made polymers are still under intensive research and development, but currently most of them are too expensive to be used at large scale [114]. Nowadays, the membrane gas separation industry is still growing and expanding very rapidly at

over 15 % yearly, and most of the large industrial gas companies have membrane affiliates [99,115]. Table 1.5 provides information on the first commercial hydrogen-selective membranes based on commercially polymers, even though some of the membranes have been modified through technologies under patent protection [99].

Table 1.5. Selectivity of commercially available polymeric membranes [116]

					Selecticity			
Membranes	Licensor	Country	Material	Modulo	H_2/CO_2	H_2/N_2	H_2/CH_4	H_2/CO
PRISM	Air Products	USA	Polysulfone	Hollow-fiber	2.5	56 - 80	80	40 - 56
MEDAL	Air Liquide	France	Polyimide, polyamide	Hollow-fiber	-	>200	>200	100
GENERON	MG	USA	Tetrabromo-polycarbonate	Hollow-fiber	3.5	90	120	100 -123
SEPAREX	UOP LCC	USA	Cellulose acetate	Spiral wound	2.4	72 - 80	60 - 80	30 - 66
UBE	UBE Industries	Japan	Polyimide	Hollow-fiber	3.8	88-200	100-200	50-125

However, membrane processes have several inherent limitations such as the moderate purity reported by state-of-art hydrogen-selective DPMs working with low pressure permeate at mild temperature conditions. This is because all membranes exhibit a trade-off between permeability—i.e., how fast molecules pass through a membrane material—and selectivity—i.e., to what extent the desired molecules are separated from the rest. While selectivity is the key to purity, the membrane area drives the capital cost [102]. Consequently, materials should be processed into thin, typically supported membranes, fashioned into high surface/volume ratio modules (up to 30.000 m^2 m^{-3} of packing density for hollow fiber (HF) modules), and used in optimized processes, as shown Figure 1.18.

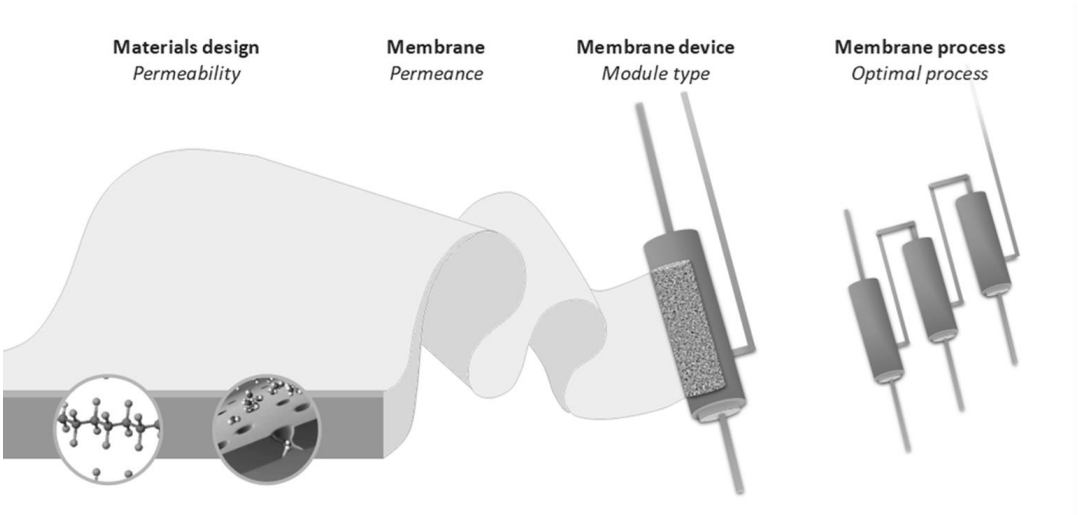

Figure 1.18. From intrinsic permeability-selectivity trade-off to practical performance. Modified from ref. [117]

Among the vast amounts of polymers that have been investigated, the general trend shown that highly permeable polymers possess low selectivities. At this point, gas permeation properties of various commercial polymers have been compiled by plotting the selectivity of different gas pairs versus the H_2 permeability in Robeson-type plots, as depicted in Figure 1.19. All gas permeability data were taken from Membrane Society of Australasia (MSA) database [118]. The Robeson upper - bound limits were included for each gas pairs showing the performance improvement compared to those publishing in 1991 and 2009; however, most of the polymeric membranes fabricated from commercial available polymers are still distant from the highlighted attractive area [119,120]. Although very limited research works have addressed the mixed permeation of CO through different polymers as the membrane material [121–124], it is known that CO transport behavior is similar to that of N_2 [125].

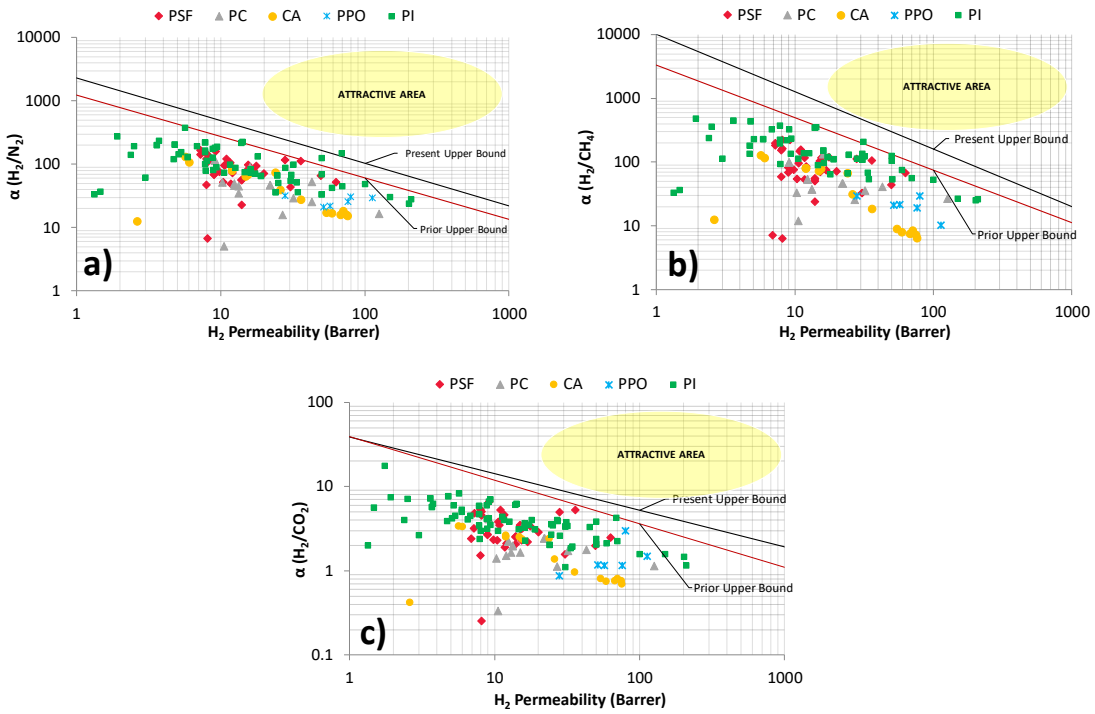

Figure 1.19. Comparison on desired selectivity and permeability for commercially available polymeric membranes for a) H_2/N_2 separation, b) H_2/CH_4 separation and c) H_2/CO_2 separation. ♦ PSF: Polysulfones; ▲ PC: Polycarbonates; ● CA: Cellulose acetate; ⁎ PPO: Polyphenyloxide; ■ PI: Polyimide

As it is illustrated, PIs are the largest group by far for hydrogen enrichment. As for hydrogen-selective DPMs, H_2 and CO_2 permeabilities fluctuated between 2.4 to 125 and 0.6 to 84.6 Barrer, respectively, resulting in H_2/CO_2 theoretical selectivities of 1.5 to 5.9. Looking to the Figure 1.19 c), these hydrogen-selective membranes fabricated from commercial polymers do not possess the desired H_2/CO_2 selectivity, and also the permeability of these membranes is not satisfactory, resulting in less than 10 Barrer due to the high diffusion resistance in the rigid glassy polymer

chains. Thus, H_2/CO_2 selectivity is still unfavorable to produce high-purity hydrogen. Nevertheless, almost all of the trade-off plots described in literature like Figure 1.19 are for pure gases (pure polymers; 35 °C). While Robeson-type plots are a useful new material screening tool, new features to assess the real performance of gas mixtures through conventional glassy polymers are required if the objective is to determine the feasibility of the membrane process for a specific industrial application [126].

Moreover, the permeability and selectivity of a membrane vary under different operating conditions (temperature, pressure, humidity and gas compositions, etc.) [99]. Thus, further research on the assessment of the performance of the available hydrogen separation membranes under different conditions is also a crucial factor for determining the feasibility of the membrane process for a specific industrial application. Furthermore, as for gas mixtures, the transport behavior of one component through the membrane is affected by the presence of other penetrants, which resulted in deviations from permeation data of pure gases. In addition, the non-ideal gas behavior of CO_2-containing mixture and the concentration polarization phenomenon, also cause the deviation from permeation data of pure gases [127]. Hence, using single gas permeation data to estimate the performance of gas mixtures may lead to confusing results and, for that reason, the membranes behavior during mixed gas measurements must be thoroughly analyzed [128,129].

1.6 FUEL QUALITY REQUIREMENTS FOR FUEL CELL SYSTEMS

Depending on the industrial origin, low-quality hydrogen streams detailed in above section, which could contain different types of contaminants, need to be purified using gas clean-up technologies [23]. Developments in hydrogen separation techniques are driven not only by cost and performance, but also by the purity requirements of the final application. Furthermore, contaminant levels involve a substantial direct impact on the hydrogen retail price [26]. That is, the lower the quality of hydrogen, the cheaper the price, but the more expensive the manufacturing technology of the cell that can process it. Thus, impurities can arise not only from hydrogen production process, but also from storage containers, station tubing and fuel lines up to the nozzle used. Additionally, except for halogen traces, no contaminants are present in the hydrogen product by using water electrolysis [130].

The International Standard ISO 14687 series titled “Hydrogen fuel – Product specification” must be the reference for the required quality grades of hydrogen fuel at global level. The ISO 14687 standard consists of three parts: Part 1 - for all types of applications, except those including PEMFCs; Part 2 - for road vehicle application; and Part 3 - for stationary application

[131–133]. According to these standards, quality levels depending on whether the hydrogen is in different states, as is described in Table 1.6. Hydrogen fuel should be complied with ISO 14687 standard, which states a hydrogen fuel index of 98 % to feed conventional internal combustion engines (Type I, Grade A), of 99.9 % for PEMFC stationary appliance systems (Type I, Grade E), and of 99.97 % for PEMFC road vehicle systems (Type I, Grade D).

Focusing on hydrogen supplied to fuel cell vehicles, the European Commission (EC) Directive 2014/94/EU on the deployment of an alternative fuels infrastructure sets out that "the hydrogen purity dispensed by hydrogen refueling points shall comply with the technical specifications included in the ISO 14687-2 standard" [134]. According to the latter regulation, the ultimate responsible to prove that their hydrogen is of suitable quality for fuel cell vehicles are the hydrogen providers at the fuel station. However, only online purity analyzers at the HRSs to monitor key impurities would be affordable in terms of cost and lead time associated with the hydrogen quality analysis to support the emerging hydrogen sector [135,136].

Table 1.6. Fuel hydrogen types and grades, and their applications

Fuel	Type	Grade	Applications	Purity (%)
GASEOUS	I	A	Internal combustion engines for transportation, residential or commercial appliances. (All applications, except fuel cells)	98
	I	B	Industrial fuel, for use e.g. in power generation or as a heat energy source	99.9
	I	C	Aircraft and space-vehicle ground support systems	99.995
	I	D	Fuel cells for vehicles	99.97
	I	E	Fuel cells for stationary applications Category 1 Category 2 Category 3	 50 50 99.9
LIQUID	II	A	Aircraft and space-vehicle on board propulsion systems and electrical energy requirements; land vehicles except fuel cells	99.995
	II	B	Fuel cells for transportation	99.97
SLUSH	III		Aircraft and space-vehicle on board propulsion systems	99.995

The maximum threshold limits for the fourteen gaseous contaminants specified in ISO 14687-2, which are identical to those listed in SAE J2719 standards from USA, are shown in Table A.1.2 in the Appendix. Total non-hydrogen gases must not exceed 300 ppm and these impurities can affect the fuel cell system in different ways, permanently or reversibly, as it is also described in Table A.1.2. Among these impurities, CO is one of the most critical ones poisoning the rare-metal-based electrocatalyst of the fuel cell by occupying the active sites and substantially reducing the number of sites for hydrogen adsorption and oxidation. Therefore, CO must be

reduced to an acceptable level, preferably below 0.2 ppm, for road vehicle applications. Other impurities have less negative impact on fuel-cell performance compared to CO. Inert gases, such as Ar, N_2 or CH_4 dilute the hydrogen affecting fuel-cell operation and the total gases do not exceed 300 ppm. Besides, concentrations of CO_2 must be lower than 2 ppm, which affect storages tank with metal hybrid alloys material and its reaction with water could results in CO formation. For this reason, high-purity hydrogen is beneficial not only to ensure that the impurities do not affect system operation and efficiency, but also to achieve lifetime targets of fuel cell systems to become a competitive alternative against burning off in flare systems [137].

ABBREVIATIONS

AD	adsorption
AEV	alternative energy vehicles
APG	ammonia purge gas
BD	blowdown
BEV	battery electric vehicles
CCS	carbon capture and storage
COG	coke oven gas
DAC	direct air capture
DPM	dense, organic (polymeric) membranes
EA	Environmental assessment
EU	European Union
FCEV	fuel cell electric vehicles
GHG	greenhouse-gas
HF	hollow fiber
HRS	hydrogen fuel station
HRU	hydrogen recovery unit
HSC	hydrogen supply chain
ISO	International Organization for Standardization
MPG	methanol purge gas
PEMFC	polymer electrolyte membrane fuel cells
PP	purge
PPE	pressurization
PSA	pressure swing adsorption
PV	photovoltaic

R/P reserves-to-production ratio

ROG refinery off-gas

RPSA rapid pressure swing adsorption

SAE Society of Automotive Engineers

SERP sorption enhanced reaction process

SMR steam-methane reforming

SMROG steam-methane reforming off-gas

STP standard temperature (0 °C or 273 K) and pressure (1 atm)

USA United States of America

NOMENCLATURE

Parameters

T_g glass transition temperatures (°C)

q^* molar concentration in the adsorbed phase (mol kg^{-1})

Δp pressure gradient across the membrane (cmHg)

A area of the membrane (cm^2)

D diffusion coefficient in the membrane ($cm^2\ s^{-1}$)

J flux through the membrane ($kg\ m^{-2}\ h^{-1}$)

P gas permeability coefficient (Barrer)

Q gas flow rate ($cm^3\ s^{-1}$)

S solubility coefficient in the membrane (cm^3 (STP) $cm^{-3}\ bar^{-1}$)

p gas partial pressure (bar)

y gas-phase mole fraction (-)

δ thickness of the membrane (cm)

Greek letters

$\propto_{i/j}$ selectivity of component i over component j (-)

Subscripts/superscripts

i, j gas components (-)

Units

toe tonne of oil equivalent

Mtoe million tonnes of oil equivalent: 1,000,000 toe

kWh kilowatt hour

MWh	megawatt hour: 1,000 kWh
GWh	gigawatt hour: 1,000,000 kWh
tCO_2	tonne CO_2
tCO_2-eq	tonne CO_2-equivalent
$GtCO_2$-eq	giga tonnes of CO_2-equivalent: 1,000,000,000 tCO_2-eq
ppm	particulates per million
µm	microgram: $1 \cdot 10^{-6}$ grams
€	euros
MM €	million €: 1,000,000 €
Barrer	10^{-10} cm^3 (STP) cm cm^{-2} s^{-1} $cmHg^{-1}$

REFERENCES

[1] BP Stats Review 2019, BP Statistical Review of World Energy 2019, (2019). www.bp.com.

[2] Global Energy Assessment (GEA), Toward a Sustainable Future, Cambridge University Press, Cambridge, UK and New York, NY, USA and the International Institute for Applied Systems Analysis, Laxenburg, Austria, 2012.

[3] S.I. Seneviratne, J. Rogelj, R. Séférian, R. Wartenburger, M.R. Allen, M. Cain, R.J. Millar, K.L. Ebi, N. Ellis, O. Hoegh-Guldberg, A.J. Payne, C.F. Schleussner, P. Tschakert, R.F. Warren, The many possible climates from the Paris Agreement's aim of 1.5 °C warming, Nature. 558 (2018) 41–49.

[4] A. Keramidas, K., Kitous, A. Després, J., Schmitz, POLES-JRC model documentation, JRC Technical Reports. Publications Office of the European Union, Luxembourg, 2017.

[5] International Energy Agency (IEA), Summary: Energy Technology Perspectives 2017, OECD/IEA. (2017). www.iea.org.

[6] A. Keramidas, K., Tchung-Ming, S., Diaz-Vazquez, A. R., Weitzel, M., Vandyck, T., Després, J., Schmitz, A., Rey Los Santos, L., Wojtowicz, K., Schade, B., Saveyn, B., Soria-Ramirez, Global Energy and Climate Outlook 2018: Sectoral mitigation options towards a low-emissions economy, European Union, Luxembourg, 2018.

[7] R. Debarre, B. Decourt, B. Lajoie, Hydrogen based energy-conversion FactBook, SBC Energy Inst. (2014). www.sbc.slb.com.

[8] International Renewable Energy Agency (IRENA), Electricity storage and renewables: Costs and markets to 2030, in: Int. Renew. Energy Agency, Abu Dhabi, 2017.

[9] D. Stolten, B. Emonts, Hydrogen Science and Engineering: Materials, Processes, Systems and Technology, Wiley-VCH, Weinheim, Germany, 2016.

[10] Y. Demirel, Energy: Production, conversion, storage, conservation, and coupling, in: Green Energy Technol., Springer-V, London, 2012.

[11] P. Nikolaidis, A. Poullikkas, A comparative overview of hydrogen production processes, Renew. Sustain. Energy Rev. 67 (2017) 597–611.

[12] T.N.V. Magdalena Momirlana, The properties of hydrogen as fuel tomorrow in sustainable energy system for a cleaner planet, Int. J. Hydrogen Energy. 30 (2005) 795–802.

[13] S. Rahmouni, N. Settou, B. Negrou, A. Gouareh, GIS-based method for future prospect of hydrogen demand in the Algerian road transport sector, Int. J. Hydrogen Energy. 41 (2016) 2128–2143.

[14] E.K. and S. Sherif, S.A., Goswami, D. Yogi, Stefanakos, Handbook of hydrogen energy, CRC Press, Boca Raton, Florida, 2014.

[15] T. Abbasi, S.A. Abbasi, 'Renewable' hydrogen: Prospects and challenges, Renew. Sustain. Energy Rev. 15 (2011) 3034–3040.

[16] Shell Deutschland Oil GmbH, Shell Hydrogen Study: Hydrogen as energy carrier and fuel - Facts, trends and perspectives, 2017.

[17] International Energy Agency (IEA), The future of hydrogen: Seizing today's opportunities, (2019). www.iea.org.

[18] Energy Efficiency & Renewable Energy, Hydrogen Production Pathways, (2017).

[19] D. Fraile, J.C. Lanoix, P. Maio, A. Rangel, A. Torres, CertifHy project. Overview of the market segmentation for hydrogen across potential customer groups, based on key application areas., 2015.

[20] The Freedonia Group, World Hydrogen: Industry study with forcasts for 2013 & 2018, Cleveland,Ohio, 2010.

[21] J. Bellosta von Colbe, J.R. Ares, J. Barale, M. Baricco, E. Al., Application of hydrides in hydrogen storage and compression: Achievements, outlook and perspectives, Int. J. Hydrogen Energy. 44 (2019) 7780–7808.

[22] J. Gao, M. Li, Y. Hu, H. Chen, Y. Ma, Challenges and developments of automotive fuel cell hybrid power system and control, Sci. China Inf. Sci. 62 (2019) 1–25.

[23] M. Ball, M., Wietschel, The hydrogen economy: Opportunities and challenges, Cambridge University Press, New York, 2009.

[24] A. Wokaun, E. Wilhelm, Transition to hydrogen: Pathways toward clean transportation, Cambridge University Press, New York, 2011.

[25] Ludwig-Bölkow-Systemtechnik GmbH (LBST), Identification of hydrogen by-product sources in the European Union, 1998.

[26] M.G. Shalygin, S.M. Abramov, A.I. Netrusov, V. V. Teplyakov, Membrane recovery of hydrogen from gaseous mixtures of biogenic and technogenic origin, Int. J. Hydrogen Energy. 40 (2015) 3438–3451.

[27] European Commission, Reference Document on Best Available Techniques for the Manufacture of Large Volume Inorganic Chemicals – Ammonia, Acids and Fertilisers, I (2007) 418.

[28] P. Basu, Production of Synthetic Fuels and Chemicals from Biomass, in: Biomass Gasification, Pyrolysis and Torrefaction, Academic Press, Cambridge, Massachusetts, 2018.

[29] R.L. Schendel, C.L. Mariz, J.Y. Mak, Is permeation competitive?, Hydrocarb. Process. 62 (1983).

[30] D. Favreau, S. Vinot, Roads2HyCom Project: Fuel cells and hydrogen in a sustainable energy economy, (2009).

[31] X. Deng, H. Wang, H. Huang, M. Ouyang, Hydrogen flow chart in China, Int. J. Hydrogen Energy. 35 (2010) 6475–6481.

[32] N. Kanellopoulos, Small-Scale Gas to Liquid Fuel Synthesis, CRC Press Book, Boca Raton, Florida, 2015.

[33] W.L. W. Malaty, R.H. Mccue, D.J. Brown, Producing olefins by pyrolytic cracking of refinery off-gas, EP2616416A1, 2013.

[34] European Commission, Reference Document on Best Available Techniques for the Production of Chlor-alkali, 2014.

[35] Chlor-alkali company personal communication, (2017).

[36] M. Paidar, V. Fateev, K. Bouzek, Membrane electrolysis—History, current status and perspective, Electrochim. Acta. 209 (2016) 737–756.

[37] C. Hunter and G. Deligiannis, Canadian hydrogen survey 2004-2005 : capacity, production and surplus update, Toronto, Canada, 2005.

[38] SGL Group - The Carbon Company, Brochure Systems HCl Syntheses, Germany, 2008.

[39] L. Nylen, Doctoral Thesis: Influence of the electrolyte on the electrode reactions in the chlorate process, KTH – Chemical Science and Engineering, 2008.

[40] W.C. Chang, A.Y.J. Huang, D.R. Huang, T.Y. Chen, An economic evaluation on the purification and storage of waste hydrogen for the use of fuel cell scooters, Int. J. Green Energy. 13 (2016) 1608–1614.

[41] European Commission, Reference Document on Best Available Techniques for Iron and Steel Production, 2013.

[42] W.H. Chen, M.R. Lin, T.S. Leu, S.W. Du, An evaluation of hydrogen production from the perspective of using blast furnace gas and coke oven gas as feedstocks, Int. J. Hydrogen Energy. 36 (2011) 11727–11737.

[43] International Energy Agency (IEA), Tracking Industrial Energy Efficiency and CO2 Emissions, 2007.

[44] B. de Lamberterie et al., ESTEP-EUROFER Steel production - energy efficiency working group, Final report, 2014. https://cordis.europa.eu/pub/estep/docs/wg7-final-report.pdf.

[45] J.M. Bermúdez, A. Arenillas, R. Luque, J.A. Menéndez, An overview of novel technologies to valorise coke oven gas surplus, Fuel Process. Technol. 110 (2013) 150–159.

[46] R. Razzaq, C. Li, S. Zhang, Coke oven gas: Availability, properties, purification, and utilization in China, Fuel. 113 (2013) 287–299.

[47] A. Mivechian, M. Pakizeh, Performance comparison of different separation systems for H2 recovery from catalytic reforming unit off-gas streams, Chem. Eng. Technol. 36 (2013) 519–527.

[48] M. Götz, J. Lefebvre, F. Mörs, A. McDaniel Koch, F. Graf, S. Bajohr, R. Reimert, T. Kolb, Renewable Power-to-Gas: A technological and economic review, Renew. Energy. 85 (2016) 1371–1390.

[49] M. Díaz, A. Ortiz, I. Ortiz, Progress in the use of ionic liquids as electrolyte membranes in fuel cells, J. Memb. Sci. 469 (2014) 379–396.

[50] M.R. Rahimpour, A. Asgari, Production of hydrogen from purge gases of ammonia plants in a catalytic hydrogen-permselective membrane reactor, Int. J. Hydrogen Energy. 34 (2009) 5795–5802.

[51] Z.P. Cano, D. Banham, S. Ye, A. Hintennach, J. Lu, M. Fowler, Z. Chen, Batteries and fuel cells for emerging electric vehicle markets, Nat. Energy. 3 (2018) 279–289.

[52] Ministerio de Industria Energía y Turismo (MINETUR), Estrategia de Impulso del vehículo con energías alternativas (VEA) en España (2014-2020), 2015.

[53] J. Kim, I. Moon, Strategic design of hydrogen infrastructure considering cost and safety using multiobjective optimization, Int. J. Hydrogen Energy. 33 (2008) 5887–5896.

[54] C. Yang, J. Ogden, Determining the lowest-cost hydrogen delivery mode, Int. J. Hydrogen Energy. 32 (2007) 268–286.

[55] A. Almansoori, N. Shah, Design and operation of a future hydrogen supply chain: Multi-period model, Int. J. Hydrogen Energy. 34 (2009) 7883–7897.

[56] S. De-León Almaraz, C. Azzaro-Pantel, L. Montastruc, M. Boix, Deployment of a hydrogen supply chain by multi-objective/multi-period optimisation at regional and national scales, Chem. Eng. Res. Des. 104 (2015) 11–31.

[57] S. De-León Almaraz, C. Azzaro-Pantel, L. Montastruc, S. Domenech, Hydrogen supply chain optimization for deployment scenarios in the Midi-Pyrénées region, France, Int. J. Hydrogen Energy. 39 (2014) 11831–11845.

[58] G. Guillén-Gosálbez, F.D. Mele, I.E. Grossmann, A bi-criterion optimization approach for the design and planning of hydrogen supply chains for vehicle use, AIChE J. 56 (2010) 650–667.

[59] M. Dayhim, M.A. Jafari, M. Mazurek, Planning sustainable hydrogen supply chain infrastructure with uncertain demand, Int. J. Hydrogen Energy. 39 (2014) 6789–6801.

[60] A. Almansoori, N. Shah, Design and operation of a stochastic hydrogen supply chain network under demand uncertainty, Int. J. Hydrogen Energy. 37 (2012) 3965–3977.

[61] N. Johnson, J. Ogden, A spatially-explicit optimization model for long-term hydrogen pipeline planning, Int. J. Hydrogen Energy. 37 (2012) 5421–5433.

[62] S. Cho, J. Kim, An optimization-based planning of investment strategies for a renewable energy supply system from biomass utilization, Korean J. Chem. Eng. 33 (2016) 2808–2819.

[63] N.V.S.N. Murthy Konda, N. Shah, N.P. Brandon, Dutch hydrogen economy: Evolution of optimal supply infrastructure and evaluation of key influencing elements, Asia-Pacific J. Chem. Eng. 7 (2012) 534–546.

[64] S. Hwangbo, I.-B. Lee, J. Han, Mathematical model to optimize design of integrated utility supply network and future global hydrogen supply network under demand uncertainty, Appl. Energy. 195 (2017) 257–267.

[65] M. Sahdai, Review of modelling approaches used in the HSC context for the UK, Int. J. Hydrogen Energy. 42 (2017) 24927–24938.

[66] S. Samsatli, I. Staffell, N.J. Samsatli, Optimal design and operation of integrated wind-hydrogen-electricity networks for decarbonising the domestic transport sector in Great Britain, Int. J. Hydrogen Energy. 41 (2016) 447–475.

[67] J. Lundgren, T. Ekbom, C. Hulteberg, M. Larsson, C.-E. Grip, L. Nilsson, P. Tunå, Methanol production from steel-work off-gases and biomass based synthesis gas, Appl. Energy. 112 (2013) 431–439.

[68] Q. Chen, Y. Gu, Z. Tang, W. Wei, Y. Sun, Assessment of low-carbon iron and steel production with CO2 recycling and utilization technologies: A case study in China, Appl. Energy. 220 (2018) 192–207.

[69] H. Kong, E. Qi, H. Li, G. Li, X. Zhang, An MILP model for optimization of byproduct gases in the integrated iron and steel plant, Appl. Energy. 87 (2010) 2156–2163.

[70] W.C. Cho, D. Lee, C.H. Kim, H.S. Cho, S.D. Kim, Feasibility study of the use of by-product iron oxide and industrial off-gas for application to chemical looping hydrogen production, Appl. Energy. 216 (2018) 466–481.

[71] Hydrogen Europe's Strategic Plan 2020-2030, Hydrogen: enabling a zero emission Europe, 2018.

[72] R. Berger, Fuel Cell Electric Buses - Potential for Sustainable Public. Transport in Europe, 2015.

[73] FCH JU, Study on early business cases for H2 in energy storage and more broadly power to H2 applications, 2017.

[74] H. Dagdougui, R. Sacile, C. Bersani, A. Ouammi, Hydrogen infrastructure for energy applications: Production, storage, distribution and safety, Academic Press, Cambridge, Massachusetts, 2018.

[75] U.S.D. of Energy, Request for Information (RFI) - H2@Scale (Hydrogen at Scale): Enabling affordable, reliable and secure energy options across multiple sectors [DE-FOA-0001965], 2018.

[76] F.G. Kerry, Industrial gas handbook: Gas separation and purification, CRC Press Book, Boca Raton, Florida, 2007.

[77] Y. Alqaheem, A. Alomair, M. Vinoba, A. Pérez, Polymeric Gas-Separation Membranes for Petroleum Refining, Int. J. Polym. Sci. 2017 (2017) 19.

[78] J. Miller, G.Q.; Stoecker, Selection of a hydrogen separation process, in: Natl. Pet. Refiners Assoc. Annu. Meet., San Francisco, CA (USA), 1989.

[79] Nitin Patel, Bill Baade, Leong Wah Fong, Vinay Khurana, Creating value through refinery hydrogen management, 2006. www.h2alliance.com.

[80] M. Elsherif, Z.A. Manan, M.Z. Kamsah, State-of-the-art of hydrogen management in refinery and industrial process plants, J. Nat. Gas Sci. Eng. 24 (2015) 346–356.

[81] A.K. Pabby, S.S.H. Rizvi, A.M. Sastre, Handbook of membrane separations: Chemical, pharmaceutical, food, and biotechnological applications, second edition, CRC Press Book, Boca Raton, Florida, 2015.

[82] M.D. LeVan, Pressure Swing Adsorption: Equilibrium Theory for Purification and Enrichment, Ind. Eng. Chem. Res. 34 (1995) 2655–2660.

[83] K. Seshan, Pressure swing adsorption, in: Appl. Catal., Elservier, 1989: p. 180.

[84] C.A. Grande, Advances in Pressure Swing Adsorption for Gas Separation, ISRN Chem. Eng. 2012 (2012) 1–13.

[85] C.W. Skarstrom, Method and apparatus for fractionating gas mixtures by adsorption, U.S. Patent 2,944,627, 1969.

[86] S. Shivaji, T.C. Golden, Pressure Swing Adsorption Technology for Hydrogen Production, in: Hydrogen and Syngas Production and Purification Technologies, John Wiley & Sons, Inc., Hoboken, New Jersey, 2009: pp. 414–450.

[87] I. Uehara, Separation and purification of hydrogen, in: O. Tokyo (Ed.), Energy Carriers Convers. Syst. Vol. 1., EOLSS, Paris, 2008: pp. 268–282.

[88] L. Zhou, Adsorption - Progress in fundamental and application research, World Scientific Publishing Company, Singapore, 2007.

[89] F.V.S. Lopes, C.A. Grande, A.E. Rodrigues, Activated carbon for hydrogen purification by pressure swing adsorption: Multicomponent breakthrough curves and PSA performance, Chem. Eng. Sci. 66 (2011) 303–317.

[90] A. Malek, S. Farooq, Hydrogen purification from refinery fuel gas by pressure swing adsorption, AIChE J. 44 (1998) 1985–1992.

[91] J. Yang, C.H. Lee, Adsorption dynamics of a layered bed PSA for H2 recovery from coke oven gas, AIChE J. 44 (1998) 1325–1334.

[92] H. Ahn, J. Yang, C.H. Lee, Effects of feed composition of coke oven gas on a layered bed H2 PSA process, Adsorption. 7 (2001) 339–356.

[93] S. Ahn, Y.W. You, D.G. Lee, K.H. Kim, M. Oh, C.H. Lee, Layered two- and four-bed PSA processes for H2 recovery from coal gas, Chem. Eng. Sci. 68 (2012) 413–423.

[94] Foundation for Research and Technology Hellas, Final Report Summary - HY2SEPS-2 project (Hybrid Membrane- Pressure Swing Adsorption (PSA) Hydrogen Purification Systems), 2015. https://cordis.europa.eu/project/rcn/101420.

[95] M. Haydn, K. Ortner, T. Franco, W. Schafbauer, A. Behrens, B. Dittmar, S. Hummel, M. Sulik, M. Rüttinger, A. Venskutonis, L.S. Sigl, Metal-supported palladium membranes for hydrogen separation, Powder Metall. 58 (2015) 250–253.

[96] P. Brea, J.A. Delgado, V.I. Águeda, M.A. Uguina, Comparison between MOF UTSA-16 and BPL activated carbon in hydrogen purification by PSA, Chem. Eng. J. 355 (2019) 279–289.

[97] F. Relvas, R.D. Whitley, C. Silva, A. Mendes, Single-Stage Pressure Swing Adsorption for Producing Fuel Cell Grade Hydrogen, Ind. Eng. Chem. Res. 57 (2018) 5106–5118.

[98] L.T. Biegler, L. Jiang, V.G. Fox, Recent advances in simulation and optimal design of pressure swing adsorption systems, Sep. Purif. Rev. 33 (2004) 1–39.

[99] H. Yin, A.C.K. Yip, A review on the production and purification of biomass-derived hydrogen using emerging membrane technologies, Catalysts. 7 (2017) 297.

[100] S. Matteucci, Y. Yampolskii, B.D. Freeman, I. Pinnau, Transport of gases and vapors in glassy and rubbery polymers, in: Mater. Sci. Membr. Gas Vap. Sep., John Wiley & Sons, Ltd, England, 2006: pp. 1–47.

[101] A. Fick, Ueber Diffusion, Ann. Phys. 94 (1855) 59–86.

[102] J.A. Ritter, A.D. Ebner, State-of-the-art adsorption and membrane separation processes for hydrogen production in the chemical and petrochemical industries, Sep. Sci. Technol. 42 (2007) 1123–1193.

[103] Y. Yampolskii, E. Finkelshtein, Permeability of polymers, in: Membrane Materials for Gas and Vapor Separation: Synthesis and Application of Silicon-Containing Polymers, John Wiley & Sons Ltd, England, 2016: pp. 1–15.

[104] S. Basu, A.L. Khan, A. Cano-Odena, C. Liu, I.F.J. Vankelecom, Membrane-based technologies for biogas separations, Chem. Soc. Rev. 39 (2010) 750–768.

[105] R. Bounaceur, E. Berger, M. Pfister, A.A. Ramirez Santos, E. Favre, Rigorous variable permeability modelling and process simulation for the design of polymeric membrane gas separation units: MEMSIC simulation tool, J. Memb. Sci. 523 (2017) 77–91.

[106] P. Li, Z. Wang, Z. Qiao, Y. Liu, X. Cao, W. Li, J. Wang, S. Wang, Recent developments in membranes for efficient hydrogen purification, J. Memb. Sci. 495 (2015) 130–168.

[107] J.J. Conde, M. Maroño, J.M. Sánchez-Hervás, Pd-based membranes for hydrogen separation: Review of alloying elements and their influence on membrane properties, Sep. Purif. Rev. 46 (2017) 152–177.

[108] D.F. Sanders, Z.P. Smith, R. Guo, L.M. Robeson, J.E. McGrath, D.R. Paul, B.D. Freeman, Energy-efficient polymeric gas separation membranes for a sustainable future: A review, Polymer (Guildf). 54 (2013) 4729–4761.

[109] R.W. Baker, B.T. Low, Gas separation membrane materials: A perspective, Macromolecules. 47 (2014) 6999–7013.

[110] K. Liu, C. Song, V. Subramani, Hydrogen and syngas production and purification technologies, Wiley-AIChE, Hoboken, New Jersey, 2009.

[111] D. Alique, D. Martinez-Diaz, R. Sanz, J.A. Calles, Review of supported Pd-based membranes preparation by electroless plating for ultra-pure hydrogen production, Membranes (Basel). 8 (2018) 1–39.

[112] J.D. Perry, K. Nagai, W.J. Koros, Polymer membranes for hydrogen separations, MRS Bull. 31 (2006) 745–749.

[113] L. Shao, B.T. Low, T.S. Chung, A.R. Greenberg, Polymeric membranes for the hydrogen economy: Contemporary approaches and prospects for the future, J. Memb. Sci. 327 (2009) 18–31.

[114] P. Bakonyi, N. Nemestóthy, K. Bélafi-Bakó, Biohydrogen purification by membranes: An overview on the operational conditions affecting the performance of non-porous, polymeric and ionic liquid based gas separation membranes, Int. J. Hydrogen Energy. 38 (2013) 9673–9687.

[115] L.M.P. E. Drioli, G. Barbieri, Gas-separation Issues with Membranes, in: Membr. Eng. Treat. Gases, RSC Publising, Cambridge, 2011: pp. 1–318.

[116] A. Basile, S. Mozia, R. Molinari, Current Trends and Future Developments on (Bio-) Membranes: Photocatalytic Membranes and Photocatalytic Membrane Reactors, Elsevier Inc., United States, 2018.

[117] H.B. Park, J. Kamcev, L.M. Robeson, M. Elimelech, B.D. Freeman, Maximizing the right stuff: The trade-off between membrane permeability and selectivity, Science. 356 (2017) 1138–1148.

[118] Aaron Thornton, Membrane Society of Australasia database, (2019). www.membrane-australasia.org.

[119] L.M. Robeson, Correlation of separation factor versus permeability for polymeric membranes, J. Memb. Sci. 62 (1991) 165–185.

[120] L.M. Robeson, The upper bound revisited, J. Memb. Sci. 320 (2008) 390–400.

[121] F.P. McCandless, Separation of binary mixtures of CO and H2 by permeation through polymeric films, Ind. Eng. Chem. Process Des. Dev. 11 (1972) 470–478.

[122] A.B. Hinchliffe, PhD Thesis: Separation of hydrogen carbon monoxide using polymer membranes, Aston University, 1991.

[123] M. Peer, S.M. Kamali, M. Mahdeyarfar, T. Mohammadi, Separation of hydrogen from carbon monoxide using a hollow fiber polyimide membrane: Experimental and simulation, Chem. Eng. Technol. 30 (2007) 1418–1425.

[124] O.C. David, D. Gorri, A. Urtiaga, I. Ortiz, Mixed gas separation study for the hydrogen recovery from H2/CO/N2/CO2 post combustion mixtures using a Matrimid membrane, J. Memb. Sci. 378 (2011) 359–368.

[125] G. Zarca, I. Ortiz, A. Urtiaga, Copper(I)-containing supported ionic liquid membranes for carbon monoxide/nitrogen separation, J. Memb. Sci. 438 (2013) 38–45.

[126] M. Galizia, W.S. Chi, Z.P. Smith, T.C. Merkel, R.W. Baker, B.D. Freeman, 50th Anniversary Perspective: Polymers and mixed matrix membranes for gas and vapor separation: A review and prospective opportunities, Macromolecules. 50 (2017) 7809–7843.

[127] W.J. Koros, G.K. Fleming, Membrane-based gas separation, J. Memb. Sci. 83 (1993) 1–80.

[128] F. Wu, L. Li, Z. Xu, S. Tan, Z. Zhang, Transport study of pure and mixed gases through PDMS membrane, Chem. Eng. J. 117 (2006) 51–59.

[129] S.S. Dhingra, E. Marand, Mixed gas transport study through polymeric membranes, J. Memb. Sci. 141 (1998) 45–63.

[130] J.L. Aprea, Quality specification and safety in hydrogen production, commercialization and utilization, Int. J. Hydrogen Energy. 39 (2014) 8604–8608.

[131] ISO 14687: Hydrogen Fuel: Product Specification, Part 1: All applications except proton exchange membrane (PEM) fuel cell for road vehicles, 2009.

[132] ISO 14687: Hydrogen Fuel: Product Specification, Part 2: Proton exchange membrane (PEM) fuel cell applications for road vehicles, (2009).

[133] ISO 14687: Hydrogen Fuel: Product Specification, Part 3: Proton exchange membrane (PEM) fuel cells applications for stationary appliances, (2009).

[134] European Parliament and Council of the European Union, Directive 2014/94/EU of the European Parliament and of the Council of 22 October 2014 on the deployment of alternative fuels infrastructure, 2014.

[135] A. Murugan, A.S. Brown, Review of purity analysis methods for performing quality assurance of fuel cell hydrogen, Int. J. Hydrogen Energy. 40 (2015) 4219–4233.

[136] T. Bacquart, A. Murugan, M. Carré, B. Gozlan, F. Auprêtre, F. Haloua, T.A. Aarhaug, Probability of occurrence of ISO 14687-2 contaminants in hydrogen: Principles and examples from steam methane reforming and electrolysis (water and chlor-alkali) production processes model, Int. J. Hydrogen Energy. 43 (2018) 11872–11883.

[137] G.T. F. Blank, M. Klages, S. Mock, DAIMLER: The Importance of Fuel Quality, (2017). www.hycora.eu/workshops.

[138] S.H. Cho, K.T. Chue, J.N. Kim, A two stage PSA for argon and hydrogen recovery from ammonia purge gas, Chem. Eng. Commun. 163 (1998) 97–109.

[139] Q. Sun, J. Liu, A. Liu, X. Guo, L. Yang, J. Zhang, Experiment on the separation of tail gases of ammonia plant via continuous hydrates formation with TBAB, Int. J. Hydrogen Energy. 40 (2015) 6358–6364.

[140] T. Dong, L. Wang, A. Liu, X. Guo, Q. Ma, G. Li, Q. Sun, Experimental study of separation of ammonia synthesis vent gas by hydrate formation, Pet. Sci. 6 (2009) 188–193.

[141] Environmental assessment (EA/ HU / 029) - Fertiberia, S.A. in Palos de la Frontera (Huelva), 2007.

[142] Z. Wu, W. Wenchuan, The recovery of ammonia from purge gas, (2017). www.cryobridge.com/Ammonia.pdf.

[143] Trondheim Arthur, Master thesis: Control structure design for methanol process, Norwegian University of Science and Technology, 2010.

[144] S. Agahzamin, A. Mirvakili, M.R. Rahimpour, Investigation and recovery of purge gas streams to enhance synthesis gas production in a mega methanol complex, J. CO2 Util. 16 (2016) 157–168.

[145] V.K. Arora, Monetise off-gases for low cost ammonia, Pet. Technol. Q. 20 (2015) 91–96.

Table A.1.1. Major hydrogen-rich off gas streams by origin

Origin	Industry	Exhaust gas mixture	H_2	N_2	CO_2	CO	CH_4	+ C_nH_{2n}	Other	T (°C)	P (bar)	Ref.
CAPTIVE INDUSTRIES	Ammonia	Ammonia purge gas	54 - 67	19 - 26	-	-	8 - 15	-	2 - 4 Ar, < 2,500 ppm NH_3	15 - 30	100 - 150	[138–141]
		Periodic off gases	18 - 20	6 - 7	-	-	15 - 16	-	1 - 3 Ar, 54 - 58 NH_3	15 - 30	22	[31,142]
	Methanol	Methanol purge gas	60 - 72	2 - 11	7 - 11	3 - 5	6 - 23	-	< 0.1% Ar	15 - 45	70	[31,143,144]
		Expanded gas	27 - 36	1 - 8	34 - 44	2 - 14	13 - 18	-	-	-	-	[26,144]
	Oil refining	SMR off gas	70 - 80	traces	15 - 25	1 - 3	3 - 6	-	-	21 - 38	4 - 30	[86]
		Refinery off gas	65 - 90	-	-	-	3 - 20	4 – 8 C_2H_6, 1 – 3 C_3H_8, <0.5% C_4+		21 - 38	4 - 30	[86]
		Catalytic reformer off gas	70 - 90	-	-	-	10 - 30		ppm HCl, aromatics	15 - 30	15 - 30	[81]
		Pt-based reformer off gas	87 - 93	-	-	-	3 - 4	3 - 10	-	-	-	[26]
		Hydrocracker off gas	75 - 90	-	-	-	yes	yes	-	15 - 30	50 - 200	[81]
		Hydrotreater purge gas	50 - 75	-	-	-	yes	yes	-	15 - 30	5 - 20	[81]
		FCC off gas	15 - 50	-	-	-	yes	yes	olefins	15 - 30	5 - 20	[81]
BY-PRODUCT INDUSTRIES	Petro-chemical	Ethylene off gas	80 - 90	-	yes	yes	yes	-	-	15 - 30	15 - 30	[81]
		MTBE off gas	80 - 85	yes	yes	yes	yes	-	-	-	-	[32]
		Acetylene flue gas	50 - 63	1 - 2	3 -	27 - 30	5 - 8	-	-	-	-	[26]
		Styrene monomer off gas	90 - 95	-	yes	-	yes		-	-	-	[32]
		Propane DH purge	80	yes	yes	yes	yes	yes	-	-	-	[32]
		Butane DH purge	72	-	0.1 - 0.5	0.1 - 0.5	13	1 - 3	-	-	-	[26]
		Toluene HDA purge	50 - 60	-	-	-	yes	yes	-	-	-	[145]
	Steelmaking	Coke oven gas	55 - 66	3 - 6	2 - 3	5 - 8	21 - 27	-	-	15 - 30	5 - 20	[45,67]
	Chlor-alkali	Chlorine off gas	> 99.9	-	-	-	-	-	< 10 ppm O_2	15 - 20	Positive	[32,35]
		Hydrochloric acid off gas	> 99	-	-	-	-	-	traces HCl and Cl_2	15 - 20	Positive	[35]
		Sodium chlorate off gas	> 99	-	-	-	-	-	50 – 100 ppm O_2	15 - 20	Positive	[35,37]

Note: Fluid catalytic cracking (FCC), Methyl tertiary butyl ether (MTBE), Dehydrogenation (DH), Butane dehydrogenation (BDH), Hydrodealkylation (HDA)

Table A.1.2. Hydrogen fuel index and impurities specified in ISO 14687-2

Specification	Threshold
Hydrogen Fuel Index (A)	99.97 % vol.
Total Gases (B)	300.0 ppm

Contaminants		Effect of FCs			Type of effect		
Individual components	**Threshold**	**Onboard storage**	**FC performance**	**Catalyst poison**	**Reversible**	**Irreversible**	**Comments**
Water	5.0 ppm	X	X				Ice formation in storage tank and potential for unwanted ion transport (K^+ and Na^+).
Total Hydrocarbons (C)	2.0 ppm		X				Adsorb to catalyst surface or preventing access to hydrogen. Methane is an inert that dilutes hydrogen.
Oxygen	5.0 ppm	X					Reacts with metal hybrid storage material.
Helium	300.0 ppm		X				Inert gases dilute the hydrogen resulting in affecting system operation and efficiency.
Nitrogen and Argon	100.0 ppm		X				
Carbon dioxide	2.0 ppm	X					Affect storages tank with metal hybrid alloys material. Reaction with water could results in CO formation.
Carbon monoxide	0.2 ppm		X	X	X		Severe catalyst contaminant
Total sulfur compounds	0.004 ppm		X	X		X	Severe contaminant degrading fuel cell performance
Formaldehyde	0.01 ppm		X		X		More severe effect than that of CO due to slower recovery kinetics
Formic Acid	0.2 ppm		X		X		More severe effect than that of CO due to slower recovery kinetics
Ammonia	0.1 ppm		X			X	Reacts with protons in the membrane/ionomer to form NH_4^+ ions, which affect the ion exchange capacity.
Total halogenated compounds	0.1 ppm		X			X	Degradation fuel cell performance
Particulate size	10.0 µm		X			X	Erosion of gaskets, fuel cell stack, clogging of filters and valves
Particulate Concentration (D)	1.0 µg/L					X	

NOTES: A. The Hydrogen Fuel Index is the value obtained with the value of Total Gases measured in % subtracted from 100%. B. Total Gases = Sum of all impurities listed on the table except particulates. C. Total Hydrocarbons may exceed 2 ppm only due to the presence of methane, provided that the total gases do not exceed 300 ppm. D. µg/L @ NTP = micrograms per liter of hydrogen fuel at 0°C and 1 atmosphere pressure.º

CHAPTER 2

UPCYCLING OF SURPLUS HYDROGEN INTO A HYDROGEN SUPPLY CHAIN

2.1 INTRODUCTION

The prospects of a shift to a hydrogen economy have created great interest in the scientific community and social stakeholders in the recent years, although its success relies on the availability of the necessary infrastructures [1]. In the specific case of the mobility sector, the main obstacle hindering vehicles manufacturers and consumers from embracing hydrogen fuel cell electric vehicles (FCEVs) is mostly the lack of hydrogen infrastructure [2].

A number of works focused on the use of decision-support tools for the design and operation of hydrogen supply chain (HSC), have been reported addressing questions such as the design of the hydrogen fuel infrastructure applied at country, region and city levels with Almansoori and Shah leading the way [3]. Some studies include the selection of the production technology (primary and secondary energy sources) and hydrogen transportation forms (pipeline, truck and on-site schemes) through each node of the supply chain [4–13]. Also, most of these studies analyze hydrogen delivery modes in terms of capital and operation expenditure of the infrastructure focusing on the transportation sector [2,4,14]. Moreover, Europe roadmaps expect an increased hydrogen demand in both road vehicle transportation and residential/commercial sectors [15]. Recent evidence suggests that steam methane reforming (SMR) with carbon capture and storage (CCS) is expected the most economically and environmental attractive technology to produce hydrogen while renewable source infrastructures like wind and solar farms continue developing [4,16,17]. The assessment of environmental, economic and risk aspects by using multi-objective optimization-based approaches has been also reported [7,18–22]. Interesting studies were conducted establishing efficient investment strategies over a specific timeframe by using multi-period optimization models [8,9,23]. The final decision will define the time when stakeholders shall make their investments in developing the hydrogen infrastructure regarding payback and profit. Finally, economies of scale are necessary in order to compare the advantages of centralized versus distributed production, as well as the impact in the transportation costs [16].

As it has been mentioned in the previous Chapter 1, hydrogen-rich industrial waste streams could become attractive sources of distributed feedstock to be upgraded to hydrogen fuel for both transportation and stationary applications. Meanwhile, among the list of hydrogen-containing waste streams, some studies concentrated on the management, optimization, and utilization of steel-work off gases in integrated iron and steel plants [24–27]. Nonetheless, little is focused on the optimization of various by-product gases to embed sustainability into HSC. To the best of our knowledge, reported optimization models for HSCs had not yet been considered

the competitiveness of upcycling hydrogen-rich waste gas sources for its reuse in both transportation and residential sectors. Hence, this chapter reports the techno-economic feasibility of a HSC with contribution of upcycled hydrogen-rich waste gas sources to fuel both stationary and road transport applications [28]. The methodology is based on optimizing a mixed-integer programming model (MILP) to determine the optimal investment plan for developing hydrogen recovery and distribution infrastructure, while maximizing the net present value (NPV). Using scenario analyses, the techno-economic modelling is applied over the 2020 - 2050 period at regional scale in northern Spain, 4,135.4 km^2 and 11,723,776 inhabitants.

2.2 METHODOLOGY

The methodology framework of this work is proposed in Figure 2.1. The HSC incorporating industrial waste gas sources has been designed by adapting the procedure reported by A. Almansoori et al. (2009) [3]. The optimization problem embeds the infrastructure elements required throughout the future HSC (levels: production, purification, conditioning, delivery and market niches), in order to maximize the economic performance across the entire value chain, subject to several constraints. For that purpose, a mathematical formulation with the objective of maximizing net present value (NPV) is proposed. The NPV considers detailed cash flow with taxation, capital depreciation, transportation, and operation costs. The input block consists of all the databases, scenarios, hypothesis and assumptions. Then, decision-making tools were used to optimize the design problem for a specific case study. Lastly, snapshots and results concerning the objective function and the decision variables are the main outputs.

The corresponding problem is stated as follows. Given:

- the potential sources for hydrogen recovery composition and their quality;
- a set of suppliers with their corresponding time-dependent supply of surplus hydrogen;
- locations of the key stakeholders in the target region: suppliers, merchants, and customers;
- a set of allowed routes between the three stakeholders, the transportation mode between them, the delivery distance between both routes; supplier-to-merchant and merchant-to-customer;
- hydrogen demand forecast by customer for both transport and residential sectors;
- raw material and product prices;
- a set of production, purification and conditioning technologies, and their yields to upgrade raw materials to hydrogen product, as well as their capacity at different scales;

- investment and operating costs of each intermediate technology, transportation mode, depreciation, and the residual values at the end of the time horizon;
- financial data (such as discount and tax rates).

The goal of the proposed model is to provide the optimum answer to the following questions: how much, where and when stakeholders shall make their investments for a particular demand scenario over a 30-year period. The outputs provided by the model are:

- optimal investment plan for all the merchants considered and related logistics;
- location (single- or multi-plant), type, scale, and number of intermediate technologies, as well as production rates;
- sourcing and supply routes for the raw materials and product considered;
- connections between the stakeholders, and hydrogen flows through the network.

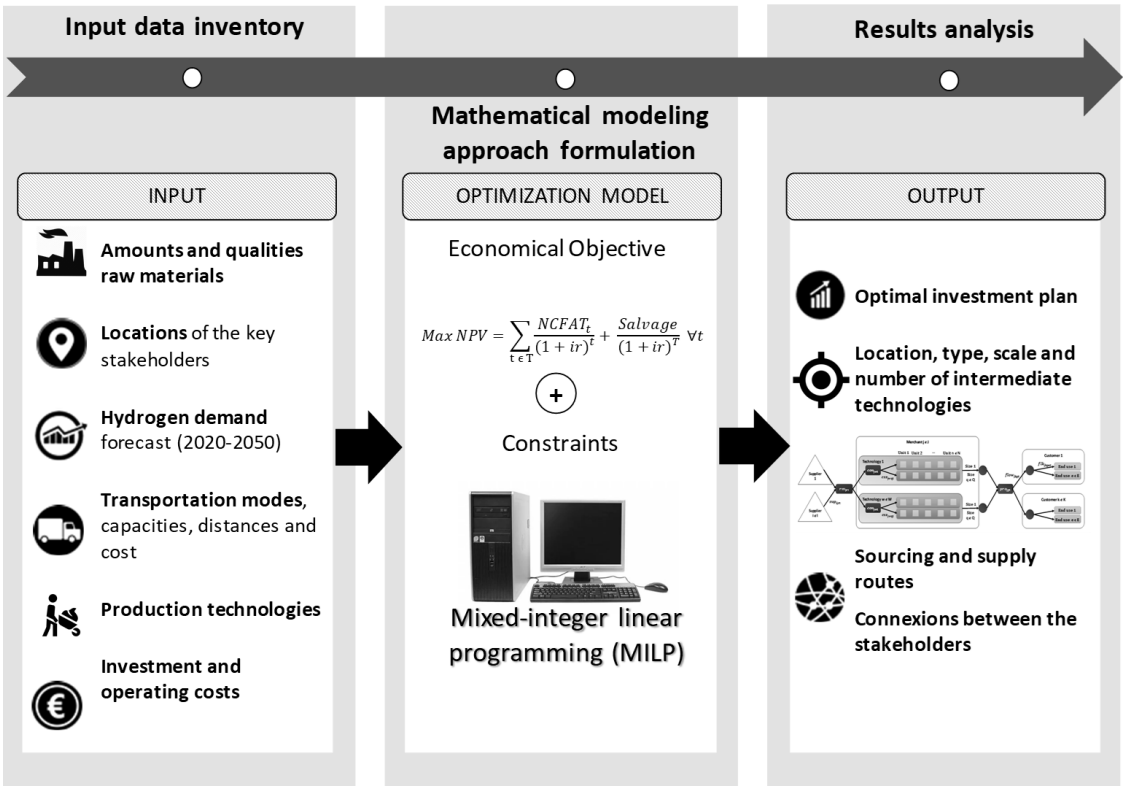

Figure 2.1. Methodology framework for the proposed model

2.3 CASE STUDY

This work is focused on the techno-economic feasibility of the upcycling of hydrogen-containing multicomponent gas mixtures to feed stationary and portable fuel cells using decision-making tools, geographically located in the north of Spain and over the 2020 - 2050

period. At the early stages of design, one of the main goals of this study is to identify and critically analyze the potential of the upcycling of industrial waste gaseous streams to be integrated in a HSC [29].

The optimization model has been developed by integrating technology selection and operation, hydrogen demand forecast, geographical information, capital investment models, and economic models. Some parameters have been collected from recent publications, INE [30] and Eurostat [31], industrial reports, and data provided by companies. Detailed input data used to solve the mathematical model is described in the following sections.

2.3.1 STUDY AREA DESCRIPTION

The proposed model is focused on two main industrial waste streams that have been selected because of the following reasons: (i) both hydrogen sources are gaseous waste streams with hydrogen content higher than 50 %, and they are currently flared or released; (ii) both industries develop their activities in stable markets and; (iii) both hydrogen sources are by-product gaseous streams with low market price.

The first hydrogen source corresponds to high purity hydrogen off gases of the chlor-alkali industry denoted as raw material "R99" because its composition is almost pure hydrogen gas. The second most valuable by-product considered in the optimization model is coke oven gas (COG), which is produced at integrated steel mills and coke making industries. Hereafter, this raw material has been denoted as "R50" because the average hydrogen composition is between 36 – 62 % vol. The composition of these hydrogen-containing effluent gases is detailed in Table A.1.1 in the previous Chapter 1. Furthermore, Table 2.1 summarizes the estimated volume of surplus hydrogen with a pre-set ratio (hydrogen produced per ton of chemical product) that depends on its origin [32–35].

Table 2.1. Waste hydrogen streams by origin and final use

Raw material	Industry	Waste streams	H_2 flowrate	Flared/ Vented (%)	Recovered (%)
R50	Steel mills	Coke Oven Gas	209 $Nm^3 H_2$ t $coke^{-1}$	3	97
	Coke plants			60 - 80	20 - 40
R99	Chlor-alkali industry	Cl_2 production	300 $Nm^3 H_2$ t Cl_2^{-1}	10	90
		HCl production	6 $Nm^3 H_2$ t HCl^{-1}	10	90
		$NaClO_3$ production	668 $Nm^3 H_2$ t $NaClO_3^{-1}$	10	90

Taking into account the above-mentioned raw materials for surplus hydrogen, the availability of both hydrogen sources over the whole period was estimated as follows:

$$Supply_{\mathrm{irt}} = Sup_{\mathrm{ir}} \cdot \left(1 + \frac{SF_{\mathrm{irt}}}{100}\right) \quad \text{Eq. (2.1)}$$

with $Supply_{\mathrm{irt}}$ (t raw material year^{-1}) as the estimated supply for raw material r at supplier i in period t, calculated based on the current estimated supply for raw material by supplier Sup_{ir} (t raw material year^{-1}) and the growth rate of each industry market over the 2020 - 2050 period SF_{irt} (%). This factor was estimated based on projections for chlor-alkali and basic iron and steel markets until 2022 and 2025 [36–38], respectively, and then using a conservative linear growth of 5 % per year, as shown in Figure 2.2.

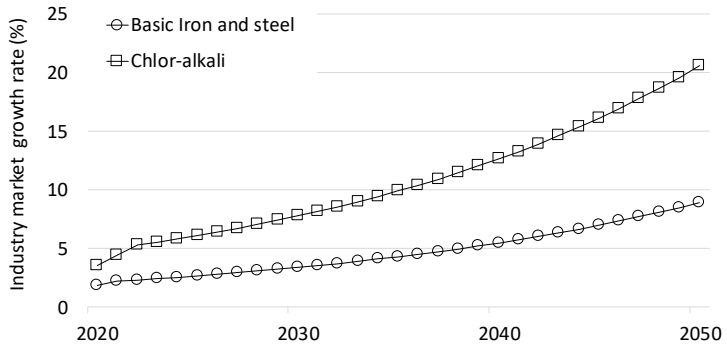

Figure 2.2. Growth rate of each industrial market. Circles denote chlor-alkali market growth rate; squares denote steel market growth rate.

The current estimated supply Sup_{ir} (t raw material year^{-1}) is determined from the plant's capacity $\dot{m}_{\mathrm{ir}}$ (t product day^{-1}), the pre-set ratio of raw material produced per ton of chemical product R_{r} (t raw material t product^{-1}), the emission factor EF_{ir} (%), and the hydrogen feed fraction $y^{F}_{\mathrm{H_2}r}$ (% vol.); and is given by Eq. (2.2):

$$Sup_{ir} = \dot{m}_{\mathrm{ir}} \cdot R_{\mathrm{r}} \cdot EF_{\mathrm{ir}} \cdot y^{F}_{\mathrm{H_2}r} \quad \text{Eq. (2.2)}$$

Table 2.2 summarizes the plant's capacity of each supplier, which have been obtained from the Environmental Assessment (EA) of each industrial company at the present time. Furthermore, Table 2.3 shows the projections of the surplus hydrogen by supplier until 2050.

Table 2.2. Plant's capacity by supplier at the present time

		Region	Latitude	Longitude	Type of product	$\dot{m}_{ir}$ (t product day^{-1})
supplier i ∈ I	**25**	Asturias	43.295530	-5.681080	Coke	352
	26	Asturias	43.370010	-5.840700	Coke	229
	27	Asturias	43.541169	-5.725317	Coke	3014
	28	Guipúzcoa	43.254883	-1.946582	HCl	52
					Cl_2	11
					$NaClO_3$	33
	29	Huesca	41.926459	0.174920	Cl_2	85
	30	Huesca	41.927672	0.163954	HCl	82
					Cl_2	11
					$NaClO_3$	126
	31	Tarragona	41.114081	1.185894	Cl_2	233
					HCl	38
	32	Cantabria	41.927672	0.163954	Cl_2	173
	33	Pontevedra	43.374621	-4.043224	HCl	93

Table 2.3. Availability of surplus hydrogen by supplier and timeframe

			$Supply_{irt}$ (t raw material year^{-1})			
		Raw material r ∈ R	2020	2030	2040	2050
supplier i ∈ I	**25**	R50	24054.7	24421.2	24919.1	25730.2
	26		15623.9	15861.9	16185.4	16712.2
	27		8821.5	8955.8	9138.5	9435.9
	28	R99	86.4	90.4	94.3	100.7
	29		85.9	89.9	93.7	100.1
	30		296.2	309.9	323.4	345.2
	31		236.2	247.1	257.8	275.2
	32		174.8	182.9	190.8	203.7
	33		1.9	2.0	2.1	2.2
Total R50 (t R50 year^{-1})			$4.8 \cdot 10^4$	$4.9 \cdot 10^4$	$5.0 \cdot 10^4$	$5.2 \cdot 10^4$
Total R99 (t R99 year^{-1})			881.0	922.0	962.0	1027.0

Moreover, the geographic distribution of the future hydrogen market comprises a number of stakeholders that correspond to the three nodes of the hydrogen network, as illustrated in Figure 2.3 [33]. We select the northern Spain region with a population of 11,723,776 inhabitants and 4,135.4 km^2 of land for the case study to be analyzed.

- **Suppliers (ID numbers: 25 - 33):** Industrial factory sites that produce hydrogen-rich waste streams as by-product. In the studied region, nine supply industries have been identified; three of them generate the R50 raw material (ID: 25 - 27), and the other six suppliers produce R99 (ID: 28 - 33).

- **Merchants (ID numbers: 1 - 17):** The major industrial gas manufacturers and responsible of raw materials transformation into the final hydrogen products. In our case, eleven plant sites and/or filling stations owned by industrial gas companies (ID: 1 - 11), such as Air Liquide S.A., Praxair Inc., Abelló Linde S.A., Messer Ibérica de Gases S.A. and Sociedad Española de Carburos Metalicos S.A. (Air Products Group) [3]. In addition, we have also considered that surplus hydrogen could also be recovered on-site at the supplier's plants and could directly be marketed to customers. Therefore, six out of the nine suppliers (ID: 12 - 17) will be considered as transforming nodes, depending on the throughput managed.

- **Customers (ID numbers: 46 - 82):** Final markets are aggregated into thirty-six urban areas with more than 100,000 inhabitants [39]. The hydrogen is distributed to the final end-users to be used as fuel for both road vehicle transportation and residential/commercial sectors. The hydrogen demand forecast per client and end-use is stated in detail at the end of this chapter.

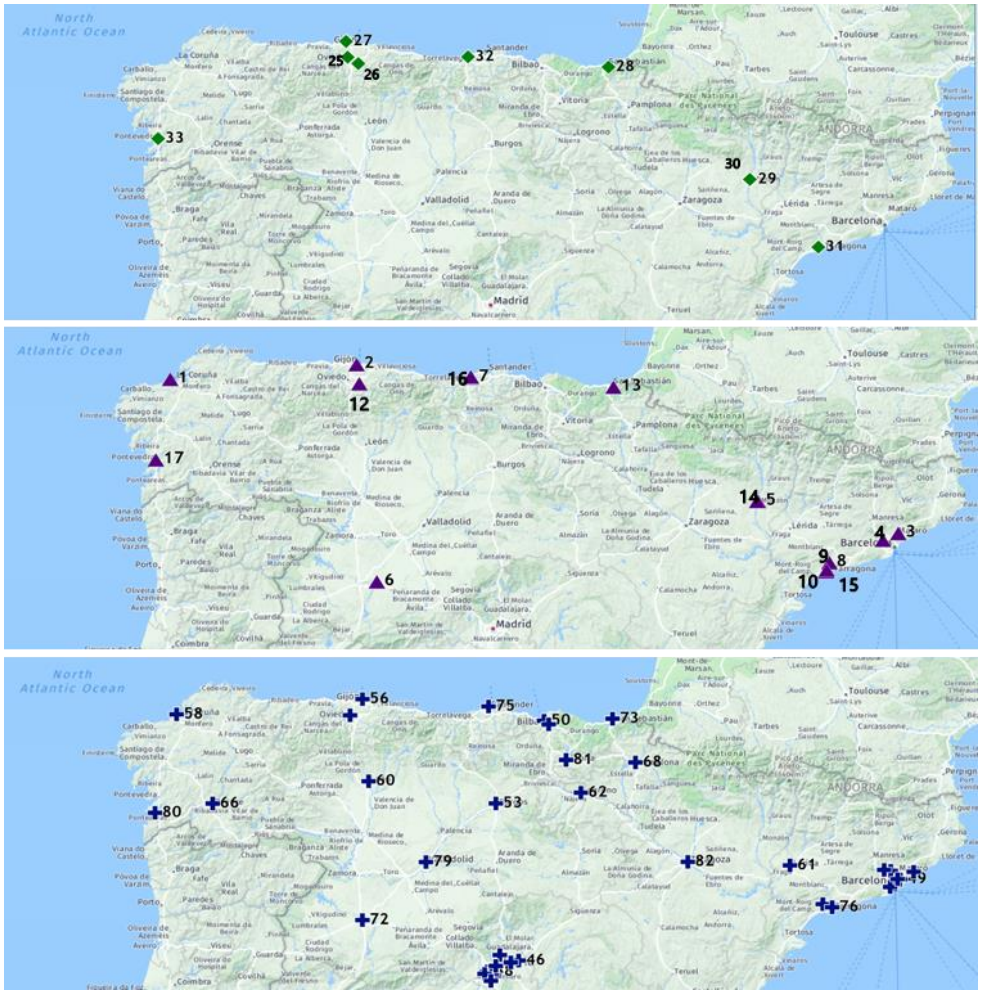

Figure 2.3. Geographic breakdown studied ◆ Supplier Company i ϵ I; ▲ Merchant company j ϵ J; ✚ Customer area k ϵ K.

2.3.2 DATA COLLECTION

2.3.2.1 Hydrogen demand forecast

In this study, two scenarios concerning two levels of hydrogen demand for road vehicle transportation and residential/commercial sectors have been considered. The first scenario, named pessimistic (s1) has been estimated considering a low hydrogen penetration ratio, whereas the other scenario, named optimistic (s2) has been estimated with a higher penetration ratio. The hydrogen market penetration ratio for the above mentioned end-users has been collected from The European Hydrogen Energy Roadmap [15], and summarized in Table 2.4.

Table 2.4. Demand scenarios of hydrogen penetration ratio by end-user and timeframe

			period t ϵ T			
	scenario s ϵ S	**end use e ϵ E**	**2020**	**2030**	**2040**	**2050**
H_2 market penetration (%)	s1	e1: Road transport	0.7	8.4	16.6	25.3
		e2: Commercial/residential	0.0	0.7	3.0	6.7
	s2	e1: Road transport	1.4	16.8	33.2	50.6
		e2: Commercial/residential	1.0	6.0	10.0	13.5
H_2 demand (kt H_2 $year^{-1}$)	Total s1		8.9	120.8	271.5	458.8
	Total s2		40.1	335.6	629.4	921.8

Furthermore, hydrogen demand curves for the north of Spain by end-user concerning both scenarios s1 and s2 are represented in Figure 2.4 and Figure 2.5, respectively. The potential demand of hydrogen in two demand scenarios is computed according to Eq. (2.3) [6].

$$Demand_{\mathrm{kset}} = \frac{Pop_{\mathrm{k}} \cdot FE \cdot sf_{\mathrm{ke}}}{LHV} \cdot dsat_{\mathrm{set}} \qquad \text{Eq. (2.3)}$$

where the total demand for each customer $Demand_{\mathrm{kset}}$ (kt H_2 $year^{-1}$) results from the population in location Pop_{k} (inhabitants), the final energy consumption per capita in Spain FE (toe hab^{-1} $year^{-1}$), the share of final energy consumption in location per end-use sf_{ke} (%), the hydrogen lower heating value LHV (MJ kg^{-1}) and the market penetration ratio $dsat_{\mathrm{set}}$ (%) per scenario, end use and timeframe [15,30,39,40]. The demand has also been estimated according to the methods described in Refs. [3,16,41,42] focused on transportation sector to support the reliability of these calculations. In appendix at the end of this chapter, the hydrogen demand forecast per client in northern Spain is given in further detailed by final end-use for each scenario.

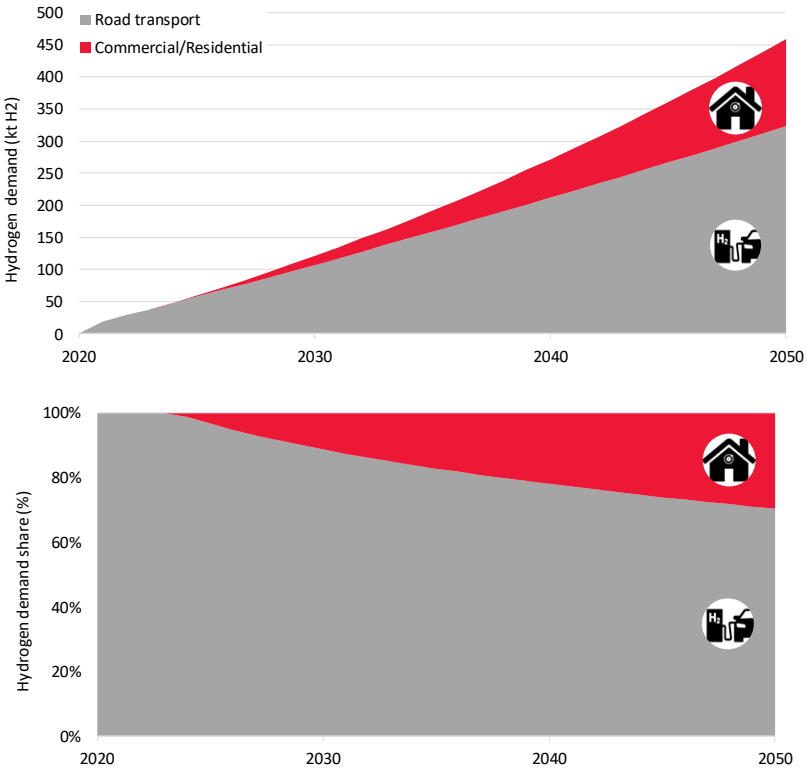

Figure 2.4. Hydrogen demand curves for scenario s1 in northern Spain by end-user

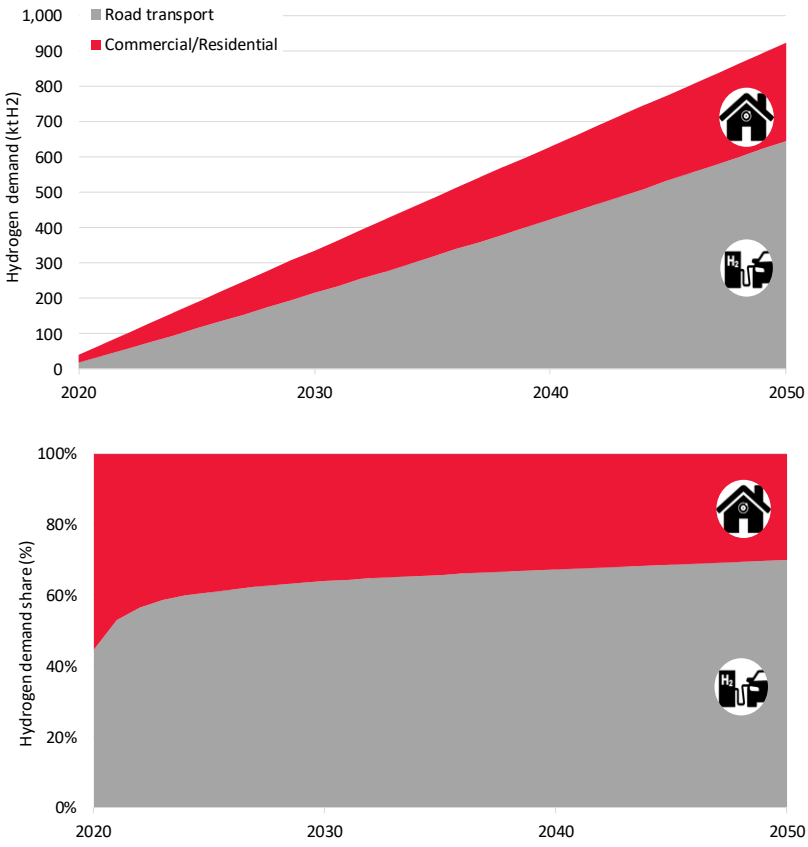

Figure 2.5. Hydrogen demand curves for scenario s2 in northern Spain by end-user

2.3.2.2 Techno-economic data

The final value-added product, named P99, is manufactured applying different sequences of intermediate technologies, which have been considered in this work as illustrated Figure 2.6. The characteristics of the product P99 have been defined in compliance with the standards ISO 14687, which defines quality specifications for hydrogen. According to this regulation, pure hydrogen could be used to meet hydrogen demand for both transportation and residential sectors using polymer electrolyte membrane fuel cells (PEMFC) [43,44]

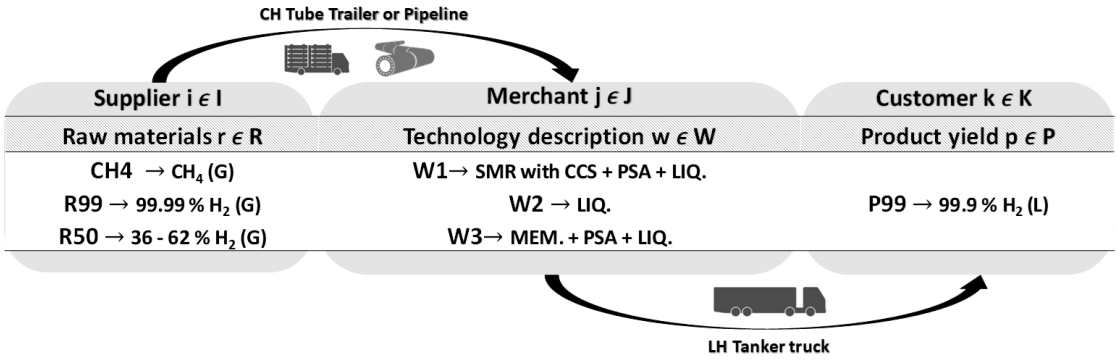

Figure 2.6. Waste gas streams-based HSC studied for the north of Spain

As already mentioned in preceding Chapter I, centralized SMR with CCS has been considered as benchmark technology in order to satisfy the expected demand for hydrogen [4]. The reaction between natural gas, mainly CH_4, and steam in a catalytic converter strips away the hydrogen atoms, while CO_2 is generated as byproduct and then, handled by the CCS [45]. With regard to the upcycling of surplus hydrogen, we have selected a combination of two of the most mature technologies for hydrogen purification: membrane technology (MEM) followed by pressure swing adsorption (PSA) [46,47]. In a recent work, Alqaheem, Y. et al (2017) compare current purification technologies for hydrogen recovery, and state that purification technologies are limited by, among other reasons, the hydrogen feed composition. Consequently, industrial gaseous waste streams are pre-enriched via hydrogen-selective membrane separation and further upgrade to the required quality by PSA [48,49]. The final product requires a liquefaction stage.

In this study, methane is considered an inexhaustible source, where methane transportation costs are included in the raw material price for merchants. The prices forecast of hydrogen and methane have been estimated based on projections for each material until 2030, and then both have been considered as constant, as shown in Figure 2.7.

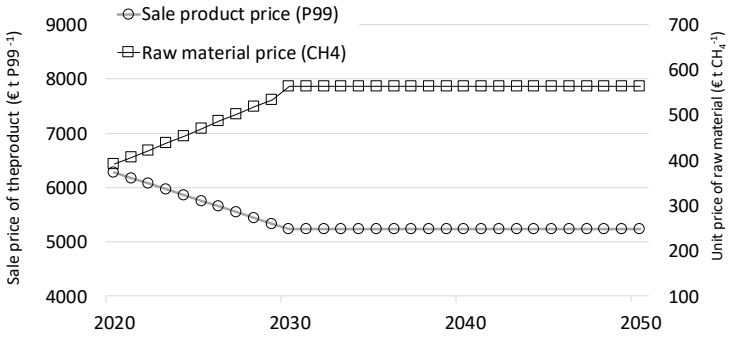

Figure 2.7. Price forecast of the finished product based on left-Y axis and the unit price of raw material based on right-Y axis.

Each transformation technology type incurs in fixed capital CI_{wq} (MM €), and unit production costs CO_{wq} (€ t H_2^{-1}) as function of its capacity. In order to account for the economies of scale of the technologies, the six-tenths-factor rule has been used to estimate the fixed capital costs based upon the investment cost of a reference case as follows [50]:

$$\mathrm{CI}_{wq1} = \mathrm{CI}_{wq2} \cdot \frac{Q_{\mathrm{w1}}}{Q_{\mathrm{w2}}}^{0.6} \cdot UF_{\mathrm{w}} \qquad \text{Eq. (2.4)}$$

where CI_{wq2} (MM €) and Q_{w2} (€ t H_2^{-1}) are the base capital costs as well as the reference hydrogen product flow rate. Thus, the investment cost has been associated to a design production capacity of 175,200 t H_2 $year^{-1}$ for SMR with CCS, of 1,178 t H_2 $year^{-1}$ for PSA, of 1,423 t H_2 $year^{-1}$ for MEM, and of 10,950 t H_2 $year^{-1}$ for LIQ, as summarized in Table 2.5. Moreover, UF_{w} as the update factor for each technological process accounts for changes that result from inflation. For simplification, it was assumed that the production costs CO_{wq}, are directly proportional to the base reference.

Table 2.5. Reference case of investment and operating costs by technology

Intermediate technology	capacity q ϵ Q (t H_2 $year^{-1}$)	Capital cost (MM €)	Unit operating cost (€ t H_2^{-1})	References
SMR + CCS	175,200	345	1,170	[5,6,51]
MEM	1,423	1.85	280	[52,53]
PSA	1,178	1.82	196	[52,53]
LIQ	10,950	133	356	[51,54,55]

Each of these technologies can be designed at five different production scales [5]. For larger plant capacities, fixed capital investments increase while unit operational costs decrease. Furthermore, the efficacy of each technological process was calculated as the amount of hydrogen produced per ton of raw material consumed. Table 2.6 summarizes the fixed cost and operating cost by technology.

Table 2.6. Investment cost and unit operating cost by technology at different sizes

technology w ϵ W	Efficacy (t H_2 t raw material^{-1})	capacity q ϵ Q (t H_2 year^{-1})	Capital cost (MM €)	Unit operating cost (€ t H_2^{-1})
w1 → SMR with CCS + PSA + LIQ.	0.321 [56]	200	10	3457
		1000	26	3019
		10000	104	2458
		50000	273	2026
		200000	627	1602
w2 → LIQ.	0.998 [55]	200	3	361
		1000	9	361
		10000	35	356
		50000	93	338
		200000	213	271
w3 → MEM+ PSA + LIQ.	0.430 [53,57]	200	5	941
		1000	12	841
		10000	48	832
		50000	126	814
		200000	289	746

2.3.2.3 Delivery costs

The delivery costs depend on the selected mode of transportation, which relies on the transported flow and distance [58]. The selection of the transportation mode depends on the transported flow. Specifically, for small and intermittent demands, liquid delivery is cheaper than using pipelines. For lower demands, and short distance delivering compressed gas cylinders is a good alternative [42], [2]. We considered that raw materials are transported as compressed gaseous hydrogen (CH2) by tube trailer, and the final hydrogen products are shipped as liquid hydrogen (LH2) by truck. We have considered the corresponding unit transportation cost for each type of hydrogen delivery mode that are collected in Table 2.7.

Table 2.7. Road transportation parameters

Parameter	Description	Value	Units	Reference
$p_{\mathbf{CH2,delivery}}$	Trailer GH2 unit operation cost	10.04	€ km^{-1}· t H_2^{-1}	[5]
$p_{\mathbf{LH2,delivery}}$	Tanker LH2 unit operation cost	0.50	€ km^{-1}· t H_2^{-1}	[59]

This work considers straight-line distances between two geographical coordinates for each stakeholder: supplier-to-merchant and merchant-to-customer. Detailed information about the distances between stakeholders is presented in Tables A.2.3 and Tables A.2.4 included in the appendix section of this Chapter 2.

2.3.3 ASSUMPTIONS

The study is based on the following assumptions:

- the amount of raw materials emitted or flared, is based on statistical assumptions and not on a site-by-site assessment.
- the growth rate of chlor-alkali and steel markets are assumed constant.
- the model is prepared to design a network capable of satisfying a given hydrogen demand forecast over time.
- all intermediate technologies will be located at merchant companies where the investors own 100 % equity.
- no existing plants are considered at the beginning of the planning horizon.
- in order to account for the economies of scale of technologies, the six-tenths-factor rule has been used.
- no reduction in costs due to learning or technology improvements is considered,
- the facility costs accrue from the moment it is put on service.
- the selling price for P99 is the same as the retail price for hydrogen in the transportation sector (99.9 % LH2).
- the unit transportation cost of raw materials R99 and R50 is equal and considered on a mass basis.
- due to the complexity involved, our study case has not included the following cost and facilities: storage units, compression units for hydrogen-compressed transportation, refueling stations, etc.

Table 2.8 establishes the key operational assumptions considered for the resolution of the problem.

Table 2.8. Key operational assumptions

Parameter	Description	Value	Unit	Reference
ρ_{H_2}	hydrogen density	0.09	kg Nm^{-3}	[60]
ρ_{CH_4}	methane density	0.65	kg Nm^{-3}	[61]
ρ_{COG}	coke oven gas density	0.62	kg Nm^{-3}	[62]
LHV_{H_2}	hydrogen lower heating value	120.0	MJ kg^{-1}	[60]
LHV_{CH_4}	methane lower heating value	47.1	MJ kg^{-1}	[63]
FE	Final energy consumption in Spain (2016)	1.5	toe hab^{-1} $year^{-1}$	[63]
-	electricity price	0.04 – 0.06	€ kWh^{-1}	[63]
-	EUR/USD	1.12	$ $€^{-1}$	[64]
-	EUR/GBP	0.87	£ $€^{-1}$	[64]
-	toe/electricity conversion factor	0.086	toe MWh^{-1}	[63]
-	energy conversion factor	3,600	MWh MJ^{-1}	[63]

Additionally, Table 2.9 indicates the main economical parameters, while Table 2.10 summarizes the final energy consumption factor by region and sector.

Table 2.9. Main economical parameters

Parameter	Description	Value	Unit	Reference
t_{ope}	annual network operating period	365	day year^{-1}	[16]
DEP	useful life of intermediate technologies	30	year	[16]
ir	discount rate	8	%	[65]
φ	industrial tax rate	33	%	[66]
sv	salvage value	20	%	-

Table 2.10. Final energy consumption by region and sector

	Final energy consumption by sector (%)				
Autonomous Community	**Industry**	**Transport**	**Residential/ Services**	**Primary**	**Reference**
Aragón	37.1	34.5	18.7	9.7	[67]
Asturias	67.6	17.8	13.6	1.0	[68]
Cataluña	27.3	42.3	27.3	3.1	[69]
Galicia	42.2	33.6	24.2	-	[70]
Madrid	8.6	52.8	37.0	1.3	[71]
Navarra	34.8	39.1	20.1	6.1	[72]
País Vasco	40.0	38.2	20.3	1.4	[73]
ESPAÑA 2015	**25.1**	**40.4**	**29.9**	**3.5**	[63]

2.4 OPTIMIZATION MODEL

An optimization modeling approach based on multi-scenario mixed-integer linear programming (MILP) has been developed. The mathematical model was implemented in JuMP (Julia for Mathematical Optimization) and the experiments were conducted in the Intel (R) Core (TM) i7-7700 (3.60GHz) computer, and 32 GB of RAM. The optimization solver used was Gurobi 7.0.2. This work has been carried out in collaboration with the PhD candidate Braulio Brunaud and Prof. Ignacio E. Grossmann of the Department of Chemical Engineering at the Carnegie Mellon University, Pittsburg, US.

In the proposed formulation, the next sequence was followed: the raw material, r ϵ R, that comes from supplier, i ϵ I, is delivered to merchant company, j ϵ J. Inside these factory sites, hydrogen product form, p ϵ P, is produced from technologies w ϵ W including different technological processes. Then, it is distributed to customers, k ϵ K, according to the final end-use, e ϵ E. Table 2.11 shows the sets of parameters considered in the multi-period problem.

Table 2.11. Sets of parameters considered in the mathematical model

Set	Description	Values
I	Set of suppliers, indexed by i	[25:33, 100]
J	Set of potential merchants, indexed by j	[1:17]
K	Set of customers, indexed by k	[46:82]
R	Set of raw materials, indexed by r	[CH4, R99, R50]
P	Set of products, indexed by p	[P99]
T	Set of time periods, indexed by t	[2020:2050]
W	Set of technologies, indexed by w	[w1, w2, w3]
Q	Set of sizes for technologies, indexed by q	[200 1,000 10,000 50,000 200,000]
N	Set of units for technologies, indexed by n	[1:5]
E	Set of end-uses, indexed by e	[e1, e2]
S	Set of scenarios, indexed by s	[s1, s2]

Furthermore, Figure 2.8 shows a graphical representation of the connection between the decision variables. According to that, raw material and product's flows within the network are measured per unit of time and hence referred to as flow variables.

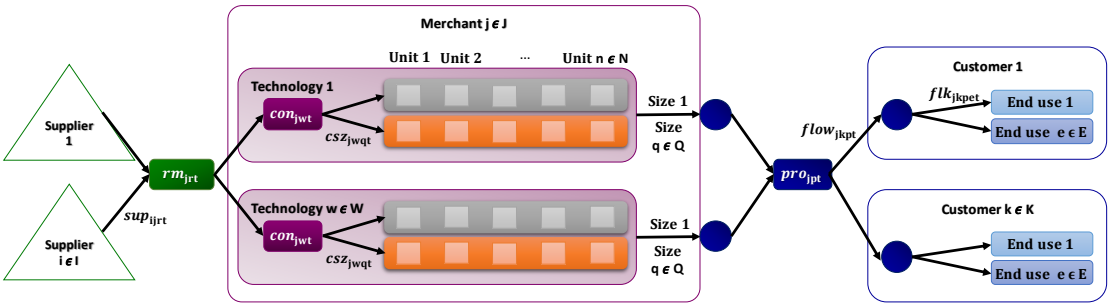

Figure 2.8. Superstructure of connections for the waste gaseous streams-based HSC

A total of seven flow variables have been considered in this work, as can be seen in Table 2.12. Furthermore, to indicate the initial state of the technologies, two binary variables have been established: ys_{jwqnt} to indicate if the transformation technology starts to operate or no at any given time, while y_{jwqnt} indicates if the transformation technology is operating or no. The operational planning model regarding plant's capacity, production, transportation, and mass balance relationships is considered together with the constraints of these activities. The corresponding constraints and relationships are grouped into four classes: mass balances, demand satisfaction, technology capacity, and decision constraints.

Table 2.12. Decision variables

Binary variables: y ϵ {0,1}	
$ys_{\mathrm{jwqnt}} = 1$	If unit n at the size q of technology w starts operating, 0 otherwise.
$y_{\mathrm{jwqnt}} = 1$	If unit n at the size q of technology w is operating, 0 otherwise.

Flow variables: x ≥ 0	
sup_{ijrt}	Supply of raw material r
rm_{jrt}	Amount of raw material r received
con_{jwt}	Amount of raw material r consumed
csz_{jwqt}	Amount of raw material r consumed at size q
pro_{jpt}	Amount of the finished product p produced
$flow_{\mathrm{jkpt}}$	Flow of the finished product p consumed
flk_{jkpet}	Flow of the finished product p consumed for end use e

Regarding mass balances, the mathematical formulation has been adapted from Ref. [7] according to our case study. Eq. (2.5) enforces the supply of raw material to be equal or lower than the available maximum sourcing. The set of constraints Eqs. (2.6) – (2.11), determines the raw material and product balances within the merchant companies.

Supply $$\sum_{\mathrm{j}\,\epsilon\,\mathrm{J}} sup_{\mathrm{ijrt}} \leq Supply_{\mathrm{irt}} \quad \forall\, \mathrm{i, r, t}$$ Eq. (2.5)

Raw material arrival $$rm_{\mathrm{jrt}} = \sum_{\mathrm{j}\,\epsilon\,\mathrm{J}} sup_{\mathrm{ijrt}} \quad \forall\, \mathrm{j, r, t}$$ Eq. (2.6)

Raw material partition $$rm_{\mathrm{jrt}} = \sum_{\mathrm{w}\,\epsilon\,\mathrm{W}} con_{\mathrm{jwt}} \quad \forall\, \mathrm{j, r, t}$$ Eq. (2.7)

Size Distribution $$con_{\mathrm{jwt}} = \sum_{\mathrm{q}\,\epsilon\,\mathrm{Q}} csz_{\mathrm{jwqt}} \quad \forall\, \mathrm{j, r, t}$$ Eq. (2.8)

Produced Amount $$pro_{\mathrm{jpt}} = \sum_{\mathrm{w}\,\epsilon\,\mathrm{W}_p} \alpha_w \cdot con_{\mathrm{jwt}} \quad \forall\, \mathrm{j, p, t}$$ Eq. (2.9)

Flow Distribution $$pro_{\mathrm{jpt}} = \sum_{\mathrm{k}\,\epsilon\,\mathrm{K}} flow_{\mathrm{jkpt}} \quad \forall\, \mathrm{j, p, t}$$ Eq. (2.10)

Flow use $$flow_{\mathrm{jkpt}} = \sum_{\mathrm{k}\,\epsilon\,\mathrm{K}} flk_{\mathrm{jkpet}} \text{ if } \mathrm{PE_{pe}} > 0 \quad \forall\, \mathrm{j, p, e, t}$$ Eq. (2.11)

Regarding the demand constraint, Eq. (2.12) ensures the product's demand compliance, at every customer, for every end use and at every period.

Demand $$\sum_{\mathrm{k}\,\epsilon\,\mathrm{K}} \sum_{\mathrm{p}\,\epsilon\,\mathrm{P}} PE_{\mathrm{pe}} \cdot flk_{\mathrm{jkpet}} = Demand_{\mathrm{ket}} \quad \text{if } PE_{\mathrm{pe}} > 0 \;\; \forall\, \mathrm{j, p, e, t}$$ Eq. (2.12)

Concerning the technology capacity constraint, Eq. (2.13) is applied to limit the amount of finished product the capacities of the production plant assuming discrete capacities.

Capacity $$csz_{\mathrm{jwqt}} \leq \sum_{\mathrm{n}\,\epsilon\,\mathrm{N}} q \cdot y_{\mathrm{jwqnt}} \quad \forall\, \mathrm{j,w,q,t}$$ Eq. (2.13)

Finally, a set of constraints have been established for the decision variables. In Eq. (2.14), zero-manufacturing technologies are installed at the beginning of the period time. The set of Eqs. (2.15) – (2.16) considers the no-negativity, and symmetry breaking to avoid redundancies.

Initial state $$y_{\mathrm{jwqnt}} = 0 \quad \forall\, \mathrm{j,w,q,\ n,\ t}$$ Eq. (2.14)

Start-up $$y_{\mathrm{jwqnt}} - y_{\mathrm{jwqnt-1}} \leq ys_{\mathrm{jwqnt}} \quad \forall\, \mathrm{j,w,q,n,t} \geq 2$$ Eq. (2.15)

Symmetry Breaking $$y_{\mathrm{jwqnt}} \leq y_{\mathrm{jwq(n-1)t}} \quad \forall\, \mathrm{j,w,q,n,t} \geq 2$$ Eq. (2.16)

The objective of the optimization mathematical model based on scenarios is maximizing the NPV (MM €) over a 30-year time horizon, where the investors owned 100 % equity. This economic target is based as the sum of a time series of cash flows discounted to the present year over a specified interest rate (minimum rate of return), as presented in the following Eq. (2.17) based on Refs. [74,75].

$$Max\ NPV = \sum_{\mathrm{t}\,\epsilon\,\mathrm{T}} \frac{NCFAT_{\mathrm{t}}}{(1+ir)^{\mathrm{t}}} + \frac{Salvage}{(1+ir)^{\mathrm{T}}} \quad \forall\, \mathrm{t}$$ Eq. (2.17)

In this equation, ir (%) represents the interest rate. The net cash flow after taxes $NCFAT_{\mathrm{t}}$ (MM € year $^{-1}$), in each time period is obtained from the net cash flow before taxes $NCFBT_{\mathrm{t}}$ and the corporate income tax CTI_{t} that corresponds to the period. Besides, the net cash flow before taxes $NCFBT_{\mathrm{t}}$ are given by the difference between the revenues S_{t}, and the total operating costs TOC_{t}, plus the corresponding fixed capital investment cost FCI_{t}.

$$NCFAT_{\mathrm{t}} = NCFBT_{\mathrm{t}} - CTI_{\mathrm{t}} = S_{\mathrm{t}} - TOC_{\mathrm{t}} - FCI_{\mathrm{t}} - CTI_{\mathrm{t}} \quad \forall\ \mathrm{t} = 1, \ldots, \mathrm{T}-1$$ Eq. (2.18)

Furthermore, in the calculation of the cash flow of the last time period (t = T), it is necessary to take into account the fact that part of the total fixed capital investment FCI_{t}, may be recovered at the end of the time horizon by yearly deductions for depreciation, which represents the salvage value of the network.

$$NCFAT_{\mathrm{t}} = NCFBT_{\mathrm{t}} - CTI_{\mathrm{t}} = S_{\mathrm{t}} - TOC_{\mathrm{t}} - FCI_{\mathrm{t}} - CTI_{\mathrm{t}} + Salvage \quad \forall\, \mathrm{t} = \mathrm{T}$$ Eq. (2.19)

Here, the revenues or incomes S_t, are determined from sales of final products, whereas the total operating cost TOC_t, includes: the raw material purchase RM_t, the operating costs associated with production plant site OC_t, and the total transportation costs between supply chain entities TC_t, as shown in Eq. (2.20).

$$TOC_t = RM_t + TC_t + OC_t \quad \forall\, t \qquad \text{Eq. (2.20)}$$

Likewise, the corporate income tax CTI_t, is calculated from the taxable income TI_t, applying an industrial interest rate φ, at a 33 %, and they are given by the following equations:

$$CTI_t = \begin{cases} TI_t \cdot \varphi & if\ TI_t > 0 \\ 0 & if\ TI_t < 0 \end{cases} \quad \forall\, t \qquad \text{Eq. (2.21)}$$

$$TI_t = S_t - TOC_t - DEP_t \quad \forall\, t \qquad \text{Eq. (2.22)}$$

In Eq. (2.22), depreciation expenses of the capital invested is based on the straight-line method where the capital investment CI_{wq}, is determined from the capacity expansions made in merchant companies during the entire time horizon. Thus, substituting Eq. (2.18) to Eq. (2.22) into the Eq. (2.17), and rearranging all these equations into a common formula, the net present value is given by Eq. (2.23).

$$Max\ NPV = \sum_{t \in T} \frac{(1-\varphi)\cdot(S_t - RM_t - TC_t - OC_t) - FCI_t}{(1+ir)^t} + \sum_{t \in T} \frac{\varphi \cdot DEP_t}{(1+ir)^t} + \frac{Salvage}{(1+ir)^T} \qquad \text{Eq. (2.23)}$$

By substituting all the economic terms by the decision variables, the objective function is fully given as follows:

$$\begin{aligned} \mathrm{Max}\ NPV = \sum_{t \in T} \frac{(1-\varphi)}{(1+ir)^t} \Bigg[& \sum_{j \in J} \sum_{k \in K} \sum_{p \in P} SP_{pt} \cdot flow_{jkpt} - \sum_{i \in I} \sum_{r \in R} \sum_{p \in P} RP_{rt} \cdot rm_{irt} \\ & - \sum_{j \in J} \left(\sum_{i \in I} \sum_{r \in R} CTS_{ij} \cdot sup_{ijrt} + \sum_{k \in K} \sum_{p \in P} CTS_{jk} \cdot flow_{jkpt} \right) \\ & - \sum_{j \in J} \sum_{w \in W} \sum_{q \in Q} CO_{wq} \cdot csz_{jwqt} \Bigg] \\ & - \sum_{j \in J} \sum_{w \in W} \sum_{q \in Q} \sum_{n \in N} \mathrm{CI}_{wq} \cdot \mathrm{ys}_{jwqnt} + \sum_{t \in T} \frac{\varphi}{(1+ir)^t} \\ & \cdot \left[\frac{1}{DEP} \sum_{j \in J} \sum_{w \in W} \sum_{q \in Q} \sum_{n \in N} \sum_{\tau=0}^{DEP-1} CI_{wq} \cdot y_{jwqn(t-\tau)} \right] + \frac{(1-sv)}{(1+ir)^T} \\ & \cdot \left[\sum_{j \in J} \sum_{w \in W} \sum_{q \in Q} \sum_{n \in N} \sum_{\tau=1}^{DEP} CI_{wq} \cdot \left(1 - \frac{\tau}{\mathrm{DEP}}\right) y_{jwqn(t-\tau+1)} \right] \end{aligned} \qquad \text{Eq. (2.24)}$$

Furthermore, the process economics is additionally assessed by the levelized cost of H_2 $Cost_{H_2}$, entails the total investment costs FCI_t, as well as the annual operating costs TOC_t. Thus, the levelized cost of H_2 $Cost_{H_2}$, is calculated as the equivalent annual costs EAC, divided by the estimated product mass flow rate pro_{jpt}, and the annual operation time t_{ope}, and is described by the following formula [76]:

$$Cost_{H_2} = \frac{EAC}{pro_{jpt} \cdot t_{ope}} \quad \text{Eq. (2.25)}$$

where the equivalent annual costs EAC, were annualized taking into account the interest rate ir of 8 % , and the plant's lifetime of 30 years each technology, DEP. The equivalent annual costs are given by Eq. (2.26):

$$EAC = FCI_t \cdot \frac{ir}{1-(1+ir)^{-DEP}} + TOC_t \quad \text{Eq. (2.26)}$$

Because of the complexity of the proposed model, a truncation-relaxation approach has been used in order to solve the MILP model in reasonable computational time, achieving near-optimal solutions (5 % optimality gap) in less than 2 h [6,16,77,78]. The first step consists of the solution of a truncated MILP to determine the location of production plants at the end of the horizon only for year 2050. From this initial assessment, merchant companies that have not been selected in the first step are eliminated. Next, in the second step, is divided into two sub-steps: 1) Linear programming (LP) relaxation of resulting multi-period MILP is solved by removing those units, suppliers, merchants, and raw materials that are not selected; and 2) reduced multi-period MILP is solved. The optimality gaps have been set to 2 % and 5 % for the first and second step, respectively. The size of the MILP problem is summarized in Table 2.13, where s1 corresponds to a low demand scenario and s2 is the optimistic one.

Table 2.13. Computational outputs solved with the two-step hierarchical procedure

scenario s ϵ S	Step	Number of variables		No. of constraints	Gap (%)	CPU time (s)
		Integer	Continuous			
s1	Step 1	10,200	5,542	10,020	2.0	200.9
	Step 2	45,360	30,318	74,958	5.0	616.6
s2	Step 1	31,875	5,542	27,340	2.0	423.2
	Step 2	165,375	35,371	176,390	5.0	5,306.0

2.5 RESULTS AND DISCUSSION

This section shows the main results obtained by application of the proposed model. The solution provides information about the most economical pathway to integrate the upcycling of industrial waste gaseous streams to be integrated in a HSC for northern Spain. To understand the sensitivity of the techno-economic impact of integrating upcycled surplus hydrogen into a HSC, as well as the strategic and operational decisions, two case studies was set up for analysis. The case studies were built to understand the influence of the hydrogen demand scenarios: pessimistic (s1) and optimistic (s2). They are described as follows:

- Case 1: leads to the optimization of the network infrastructure for the fulfillment of low hydrogen demand s1, allowing the model to determine: i) the amount of hydrogen-rich waste streams (R50 and R99) converted into liquefied hydrogen at the merchant's plants, and ii) the optimum plant site locations of SMR with CCS, so that the NPV is maximized.
- Case 2: the optimization problem set in Case 1 is modified for the fulfillment of high hydrogen demand s2.

2.5.1 INVESTMENT NETWORK

Case 1 leads to a solution with NPV of 941 MM €, where the revenue derived from hydrogen sales of 33,700 MM € can absorb the costs, with a total investment of almost 4,400 MM €. The overall hydrogen network needs 14 years to recover its original investment, when net cash flow equals zero, as illustrated Figure 2.9. Although investment costs are significantly high because of building more plants over the time period, the revenue of opening plants closer to the potential customers compensates the investment, operational and logistics costs.

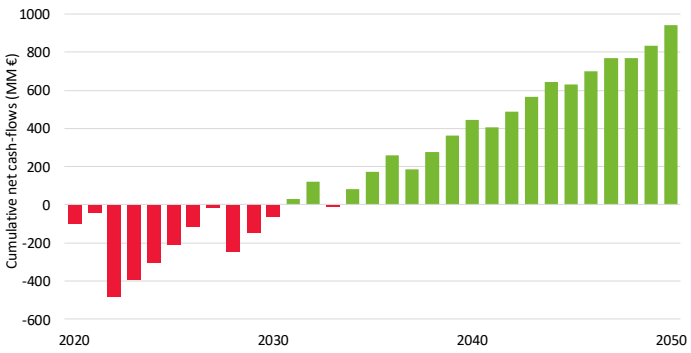

2020 - 2050	
Objective Value = 940.0 MM €	
Item	**Value (MM €)**
Income	33682
Investment	4367
Purchase	9984
Operation	9710
TranspIJ	178
TranspJK	469
Depreciation	2211
Salvage	432

Figure 2.9. Investment plan and cumulative yearly net cash-flows for the entire network for Case 1

Regarding the production costs over the entire period, methane costs correspond to the most significant share with 49.4 % of the total cost. The impact of the surplus hydrogen transformation costs on the overall operating and maintenance (O&M) costs are not substantial. On the other extreme, transportation costs account for 3.1 % of the total production costs. Furthermore, no single hydrogen production method is optimally used to produce enough hydrogen to fulfill the expected demand on its own, thus various types of raw materials are transformed into hydrogen. The optimal solution of the integrated surplus HSC leads to the installation of ten units of different technologies until 2050 in northern Spain: w1 (7 units), w2 (2 units) and w3 (1 unit), as depicted in Figure 2.10.

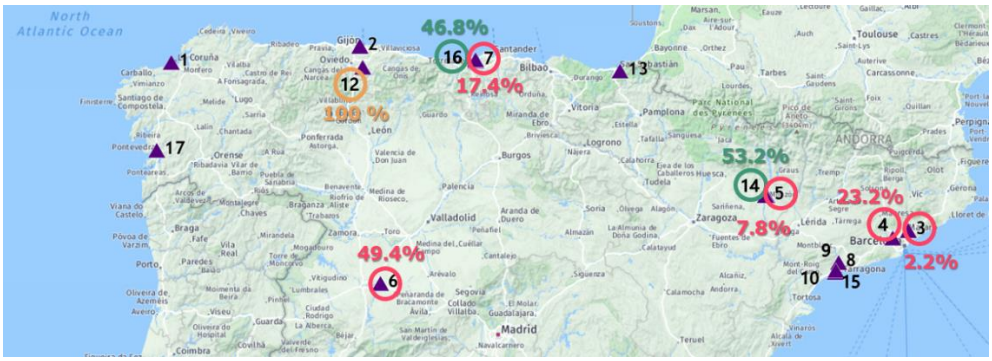

Figure 2.10. Network structure in 2050 by ▲ Merchant company j ϵ J and technology w ϵ W for Case S1; ■ w1→ SMR with CCS + PSA + LIQ.; ■ w2→ LIQ.; ■ w3→ MEM + PSA + LIQ.

Investment in w1 technology is profitable for high capacity plants and in the proximity of customers to minimize logistics costs. Table 2.14 outlines the investment plan for Case 1 by merchant and transformation technology. Most of the methane is transformed close to the biggest urban areas where economic activities and population concentrations are stronger. For instance, the integrated approach identifies that 49.4 % of the total consumed methane is transformed in Salamanca by merchant (j=6) covering nearly the entire demand of urban areas at the Autonomous Community of Madrid, where only the municipality of Madrid accounts for about 32 % of the total hydrogen demand. As described in Table 2.15, merchant (j=6) is followed by merchant (j=4) with a methane consumed share of 23.2 %, then closely merchant (j=7) with a 17.4 %, merchant (j=5) with 7.8 % and finally merchant (j=3) with 2.2 %. Thus, centralized hydrogen productions are ideal routes to the future global hydrogen-incorporated economy in highly populous areas at low market penetration.

Table 2.14. Investment plan by merchant for Case 1

Merchant j ∈ J	Latitude	Longitude	Period t ∈ T	Technology w ∈ W	capacity q ∈ Q (t H_2 $year^{-1}$)	Capital cost (MM €)
12	43.295530	-5.681080	2020	W3	50,000	116.3
14	41.926459	0.174920	2020	W2	1,000	8
16	43.374621	-4.043224	2020	W2	1,000	8
6	40.975060	-5.423241	2022	W1	200,000	605.2
4	41.469317	2.011355	2028	W1	200,000	605.2
7	43.363694	-4.037977	2033	W1	200,000	605.2
6	40.975060	-5.423241	2037	W1	200,000	605.2
5	41.926824	0.181189	2041	W1	200,000	605.2
6	40.975060	-5.423241	2045	W1	200,000	605.2
3	41.550429	2.237328	2048	W1	200,000	605.2

As mentioned above, a combination of three merchant's plant sites have been identified as the key hotspots to obtain on-site liquefied hydrogen from industrial waste streams based upon w2 and w3 technologies. Initially, industrialized hydrogen is transformed on-site and decentralized production technologies such as PSA and membrane systems will play a pivotal role in introducing hydrogen for early market penetration. Since suppliers of R50 are concentrated in the northern part of the region, almost the totality of this raw material is purified in a single facility of 50,000 t H_2 $year^{-1}$ of capacity located in Asturias at merchant (j=12). The overall investment is 116.3 MM € in 2020 with a payback period of less than three years. The main sources of supply are coking plants instead of integrated steel mills where the amount of R50 available is slightly lower due to the applied emission factor.

Table 2.15. Share of raw material consumed by merchant for Case 1

Supplier i ∈ I	Merchant j ∈ J	Raw material r ∈ R	Supply (kt raw material)	Total flow (kt raw material)	Share (%)
25	12	R50	745.9	1497.5	49.8
26	12	R50	498.1	1497.5	33.3
27	12	R50	253.5	1497.5	16.9
28	14	R99	2.9	29.3	9.8
29	14	R99	2.9	29.3	9.8
30	14	R99	9.9	29.3	33.7
31	16	R99	7.9	29.3	26.8
32	16	R99	5.8	29.3	19.9
33	16	R99	0.1	29.3	0.2
100	3	CH4	398.4	17837.7	2.2
100	4	CH4	4134.0	17837.7	23.2
100	5	CH4	1394.7	17837.7	7.8
100	6	CH4	8807.5	17837.7	49.4
100	7	CH4	3103.1	17837.7	17.4

Because suppliers of R99 are spread over the entire target region, a combination of two optimal merchants close to the markets was identified. While the former is located in Huesca at merchant (j=14) that consumes 53.2 % of the total R99, the latter is located in Santander at merchant (j=16) accounting for 46.8 % of the total R99 transformation. The optimal capacity installed of technology w2 at both factory sites reaches 1,000 t H_2 $year^{-1}$ with an investment per plant site of 8 MM € in 2020 and a payback period of six years. The main sources of R99 come from chlor-alkali industries with larger capacity, the largest quantity of surplus streams is reused in the hydrogen network. Thus, decentralized on-site hydrogen production by the upcycling of industrial surplus hydrogen is the best choice for market uptake and for avoiding costly distribution infrastructure until the demand increases.

In contrast, the number of installations built up in Case 2 is higher than in Case 1, as shown in Table 2.16. Furthermore, the case study based upon optimistic scenario s2 leads to an optimal solution where the revenue of 78,900 MM € absorbs the costs, with a total investment of 8,600 MM € and a payback period of 14 years.

Table 2.16. Results of the proposed mathematical model by hydrogen demand scenario

		scenario s1	**scenario s2**
NPV maximization (MM €)		941.0	2366.0
Number of facilities by technology w ϵ W	w1	7	16
	w2	2	3
	w3	1	2
Location of merchant company j ϵ J		3,4,5,6,7,12,14,16	4,6,8,12,14,16

2.5.2 SURPLUS HYDROGEN FLOWRATES

As summarized in Table 2.17, in Case 1, the full amount of R99 is utilized with an inflow of 29.3 kt R99 over the next 30 years due to the model constraints. On the other hand, the model determines that the optimal amount of R50 converted into liquefied hydrogen is 96.9 % of the total amount available in northern Spain over the entire period, which is 1497.0 kt R50. This conversion is achieved primarily due to the fact that the maximum capacity of the technology w3 used to transform R50 is reached in the year 2038, and building more facilities is not economically feasible due to the fixed capital investment costs.

Table 2.17. Total surplus hydrogen flowrates for Case 1

Raw material r ϵ R	**Maximum supply (kt raw material)**	**Surplus used (kt raw material)**	**H_2 produced (kt H_2)**	**H_2 demand (kt H_2)**
R99	29.3	29.3	29.2	6399.0
R50	1546.0	1497.0	643.9	

Based on figures shown in Table 2.17, R99 is able to meet 0.5 % of the total hydrogen demand in the north of Spain for the whole time period, whereas the amount of liquefied hydrogen produced from R50 is able to cover a much larger hydrogen demand accounting for 10.1 % of the total hydrogen demand. As expected, the purification of R50 stands out as the most profitable solution on account of the large available volume of this industrial waste stream. Consequently, the rest of the hydrogen produced to fulfill demand is obtained from CH4 using SMR with CCS as benchmark technology while producing the least CO_2 emissions compared to the rest of the commercially available technologies.

Thus, the use of inexpensive surplus hydrogen sources may have a central role in the early phase of hydrogen infrastructure build up in the north of Spain. As it was predicted in the demand curves based on scenario s1, cleaned hydrogen is beginning to be incorporated into the road vehicle sector from the year 2020, while hydrogen that feeds stationary fuel cells for residential and commercial sectors starts to be used from the year 2024. Figure 2.11 and Figure 2.12 show the fulfilled hydrogen demand by year with raw materials R50 and R99, respectively.

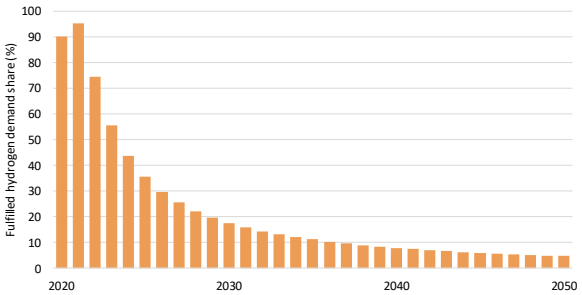

period t ϵ T	H_2 produced (kt H_2 $year^{-1}$)	H_2 demand (kt H_2 $year^{-1}$)	Share (%)
2020	8.1	8.9	90.2
2030	21.1	120.8	17.5
2040	21.5	271.5	7.9
2050	21.5	458.8	4.7

Figure 2.11. Fulfilled hydrogen demand with raw material R50 by year for Case 1

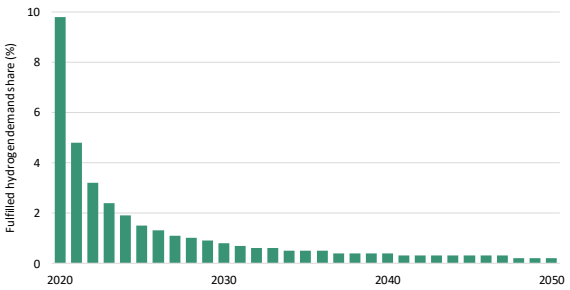

period t ϵ T	H_2 produced (kt H_2 $year^{-1}$)	H_2 demand (kt H_2 $year^{-1}$)	Share (%)
2020	0.9	8.9	9.8
2030	9.2	120.8	0.8
2040	9.6	271.5	0.4
2050	10.2	458.8	0.2

Figure 2.12. Fulfilled hydrogen demand with raw material R99 by year for Case 1

As illustrated in Figure 2.13, in Case 1, surplus hydrogen (R50 and R99) would be sufficient to cover the hydrogen demand for transport applications between the years 2020 and 2022 in the target study region. In Case 2, although the share of surplus hydrogen contribution to cover hydrogen demand is slightly lower than in the other case study, hydrogen demand would also be partially fulfilled by upcycling industrial hydrogen-rich waste gas streams. Therefore, surplus hydrogen will also play an important role in initiating the transition into a hydrogen economy with localized plants of SMR with CCS; this will support the demand before expanding to less populous areas forming a more decentralized green hydrogen production.

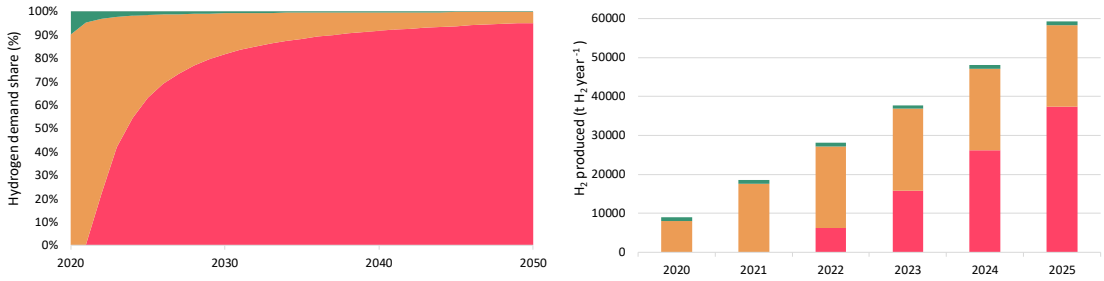

Figure 2.13. Fulfilled hydrogen demand with raw materials CH4; R99; R50 by year for Case 1

Analyzing the surplus hydrogen flowrates by customer, it can be observed that though raw material R50 is partially marketed to all final end-users, it has an essential contribution when the production of the final product is closer to the customers. The key hotspot demand markets, whereby surplus hydrogen has a central role, are displayed in Figure 2.14. As shown in Table 2.18, merchant (j=12) located in Asturias, which produce a total of 643.9 kt H_2 in the overall period, may fulfill hydrogen demand based on scenario s1 by more than 40 % in several municipalities, such as Gijón (k=56), A Coruña (k=58), Orense (k=66), Oviedo (k=67) and Vigo (k=80).

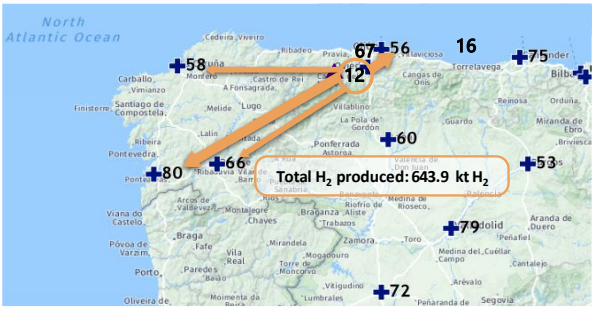

Figure 2.14. Total hydrogen produced for the overall 30-year period at ▲ Merchant company with raw material R50, by ✚ the key hotspots demand markets

Table 2.18. Total R50 flowrates for the key customers by end use

		end use e1			end use e2		
Merchant j ϵ J	**Customer k ϵ K**	**H_2 produced (kt H_2 $year^{-1}$)**	**H_2 demand (kt H_2 $year^{-1}$)**	**Share (%)**	**H_2 produced (kt H_2 $year^{-1}$)**	**H_2 demand (kt H_2 $year^{-1}$)**	**Share (%)**
12	56	61.3	105.5	58.1	6.0	15.0	40.0
	58	76.5	78.3	97.8	18.5	23.9	77.3
	66	31.8	34.0	93.5	9.4	10.4	90.3
	67	85.1	85.1	100.0	12.1	12.1	100.0
	80	93.9	93.9	100.0	27.3	28.7	95.1

With regard to raw material R99, it can be observed in Table 2.19 that merchant (j=14) located in Huesca, which produce a total of 15.5 kt H_2 in the overall 30-years period, may fulfill hydrogen demand by more than 3 % in Logroño (k=62) and Zaragoza (k=82). On the other hand, merchant (j=16) located in Santander, which produce a total of 13.7 kt H_2 within the time horizon, may partially fulfill hydrogen demand by more than 4 % in Baracaldo (k=50) and Santander (k=75). Figure 2.15 displays the key hotspots demand markets of hydrogen produced from raw material R99 for the overall 30-year period.

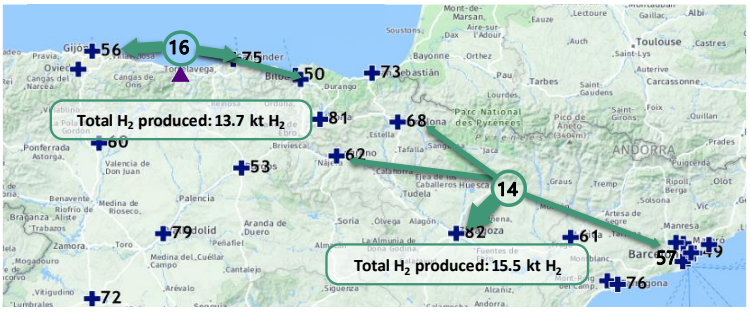

Figure 2.15. Total hydrogen produced for the overall 30-year period at ▲ Merchant company with raw material ■ R99, by ✚ the key hotspots demand markets

Table 2.19. Total R99 flowrates for the key customers by end use

		end use e1			end use e2		
Merchant j ϵ J	**Customer k ϵ K**	**H_2 produced (kt H_2 $year^{-1}$)**	**H_2 demand (kt H_2 $year^{-1}$)**	**Share (%)**	**H_2 produced (kt H_2 $year^{-1}$)**	**H_2 demand (kt H_2 $year^{-1}$)**	**Share (%)**
14	62	0.8	29.0	2.6	0.8	18.6	4.4
	82	5.6	217.6	2.6	2.6	50.2	5.1
16	75	2.0	66.6	3.1	1.8	20.9	8.4
	50	2.2	36.6	5.9	-	-	-

Based on Eqs. (2.25) – (2.26), the average levelized cost of hydrogen produced from R99 using w2 technology on merchant (j=14) basis, and taking into account the annual capital costs is around 1.36 € kg H_2^{-1}. The hydrogen levelized cost drops from 1.52 to 1.30 € kg H_2^{-1}, from the beginning until the last years of the time horizon varying due to the yearly amount of hydrogen produced. Regarding the average of producing hydrogen from R50 using w3 technology, it is

around 1.69 € kg H_2^{-1}, and ranges between 2.40 to 1.64 € kg H_2^{-1} during the 30-years of period, whereby also varies the hydrogen demand fulfilled by this raw material. Therefore, our study confirms that the price of upcycled hydrogen is in the range of 1.5 to 2 times lower than the price of hydrogen obtained by SMR with CCS, as summarized in Table 2.20. These findings support the notion that industrial waste gaseous streams can be integrated in a hydrogen-based scenario of the energy system as potential sources of hydrogen fuel.

Table 2.20. Average hydrogen levelized cost by technology

raw material $r \in R$	merchant $j \in J$	Total operating costs (MM € year^{-1})	Equivalent annual costs (MM € year^{-1})	H_2 produced (kt H_2 year^{-1})	Levelized cost (€ kg H_2^{-1})
CH4	6	322.23	376.98	94.24	4.00
R99	14	0.22	0.71	0.52	1.36
R50	12	25.8	36.10	21.46	1.68

2.6 CONCLUSIONS

In this chapter, we have addressed the identification of the optimal hydrogen supply chain (HSC) for the north of Spain, 4,135.4 km^2 and 11,723,776 inhabitants, which integrates hydrogen-rich waste gas sources and converts them into liquefied hydrogen, by maximizing the net present value (NPV) as the objective function. This research has a twofold objective: i) on the one hand, it provides the methodology to assess the techno-economic feasibility of reusing surplus hydrogen gases promoting the shift to the Circular Economy and, ii) on the other hand, it contributes to the penetration of renewable energies expressed as low cost fuel cell devices to power stationary and mobile applications.

Optimal decisions are provided by using a mathematical modeling approach regarding the technology selection, facility location and sizing, and yearly production planning. The optimization modeling approach based on multi-scenario multi-period mixed-integer linear programming (MILP) has been applied to the northern Spain region, having identified a pull of 3 possible raw materials, 8 possible suppliers, 17 merchants, 3 conversion technologies, 36 customers and 1 unique product, leading to the optimum HSC over a 30-year period.

Within a more sustainable framework, new features to accommodate industrial hydrogen-rich waste streams into a hydrogen supply chain have been developed to determine how and when stakeholders shall invest in developing the hydrogen infrastructure. The obtained results, which for the first time analyze the economic advantages of integrating upcycled industrial hydrogen in HSCs, could support future decision-making policies and the methodology could be extended to different spatial regions and timeframes.

The analysis has been performed over two scenarios of hydrogen demand s1 and s2, and the results show that as long as both scenarios of hydrogen demand apply, all generated case studies lead to a solution with positive NPVs. The results confirm that the use of inexpensive surplus hydrogen sources such as R50 and R99 offers an economic solution to cover hydrogen demand in the very early stage of transition to the future global hydrogen-incorporated economy, especially when surplus hydrogen generation is closer to the demand markets. Moreover, hydrogen production via purification systems stands out as the most profitable solution with payback periods lower than 6 years, which strongly depends on the available volume of the industrial waste streams.

In conclusion, a waste-to-energy route based on industrial hydrogen-rich gas sources has been evaluated from both economic and ecological perspectives. In future work, investigating the economic feasibility of the integrated surplus hydrogen supply chain taking into account the presence of inherent uncertainties on significant input parameters might prove important. Particularly, raw material and product prices uncertainty, technology's efficacies and the variability of the hydrogen composition in the raw material R50.

ABBREVIATIONS

CCS	carbon capture and storage
CH2	compressed gaseous hydrogen
COG	coke oven gas
FCEV	fuel cell electric vehicles
GHG	greenhouse-gas
HSC	hydrogen supply chain
INE	Spanish Statistical Office
ISO	International Organization for Standardization
JuMP	Julia for Mathematical Optimization
LH2	liquid hydrogen
LIQ	liquefaction facility
MEM	membrane system
MILP	mixed-integer linear programming
NPV	net present value
O&M	operating and maintenance
PDE	partial differential equation
PEMFC	polymer electrolyte membrane fuel cells

PSA pressure swing adsorption

SMR steam-methane reforming

NOMENCLATURE

Cost-related parameters

CI_{wq} investment cost of manufacturing technology w ϵ W at the size q ϵ Q (MM €)

CO_{wq} unit operating cost of manufacturing technology w ϵ W at the size q ϵ Q (€·tH_2^{-1})

α_{w} efficacy of manufacturing technology (t H_2·t raw material^{-1})

PE_{pe} inverse of the proportion of the product p ϵ P required to satisfy end use e ϵ E (%)

RP_{rt} unit price of raw material r ϵ R in the period t ϵ T (€· t raw material^{-1})

SP_{pt} sale price of the product p ϵ P in the period t ϵ T (€· t product^{-1})

$Supply_{\mathrm{irt}}$ supply of raw material r ϵ R at the supplier i ϵ I in the period t ϵ T (t raw material · year^{-1})

CTS_{ij} transportation cost of the raw material r ϵ R from the supplier i ϵ I to the merchant j ϵ J (t raw material · year^{-1})

$Demand_{\mathrm{ket}}$ client's demand k ϵ K for end use e ϵ E in the period t ϵ T and scenario s ϵ S (t product· year^{-1})

CTS_{jk} transportation cost of the finished product p ϵ P from merchant j ϵ J to the customer k ϵ K (t product· year^{-1})

Units

toe	tonne of oil equivalent
MJ	megajoule: 1,000,000 joules
kWh	kilowatt hour
MWh	megawatt hour: 1,000 kWh
€	euros
MM €	million €: 1,000,000 €

REFERENCES

[1] J. Kim, I. Moon, Strategic design of hydrogen infrastructure considering cost and safety using multiobjective optimization, Int. J. Hydrogen Energy. 33 (2008) 5887–5896.

[2] C. Yang, J. Ogden, Determining the lowest-cost hydrogen delivery mode, Int. J. Hydrogen Energy. 32 (2007) 268–286.

[3] A. Almansoori, N. Shah, Design and operation of a future hydrogen supply chain: Multi-period model, Int. J. Hydrogen Energy. 34 (2009) 7883–7897.

[4] M. Sahdai, Review of modelling approaches used in the HSC context for the UK, Int. J. Hydrogen Energy. 42 (2017) 24927–24938.

[5] P. Nunes, F. Oliveira, S. Hamacher, A. Almansoori, Design of a hydrogen supply chain with uncertainty, Int. J. Hydrogen Energy. 40 (2015) 16408–16418.

[6] N. Sabio, M. Gadalla, G. Guillén-Gosálbez, L. Jiménez, Strategic planning with risk control of hydrogen supply chains for vehicle use under uncertainty in operating costs: A case study of Spain, Int. J. Hydrogen Energy. 35 (2010) 6836–6852.

[7] G. Guillén-Gosálbez, F.D. Mele, I.E. Grossmann, A bi-criterion optimization approach for the design and planning of hydrogen supply chains for vehicle use, AIChE J. 56 (2010) 650–667.

[8] M. Dayhim, M.A. Jafari, M. Mazurek, Planning sustainable hydrogen supply chain infrastructure with uncertain demand, Int. J. Hydrogen Energy. 39 (2014) 6789–6801.

[9] A. Almansoori, N. Shah, Design and operation of a stochastic hydrogen supply chain network under demand uncertainty, Int. J. Hydrogen Energy. 37 (2012) 3965–3977.

[10] N. Johnson, J. Ogden, A spatially-explicit optimization model for long-term hydrogen pipeline planning, Int. J. Hydrogen Energy. 37 (2012) 5421–5433.

[11] S. Cho, J. Kim, An optimization-based planning of investment strategies for a renewable energy supply system from biomass utilization, Korean J. Chem. Eng. 33 (2016) 2808–2819.

[12] N.V.S.N. Murthy Konda, N. Shah, N.P. Brandon, Dutch hydrogen economy: Evolution of optimal supply infrastructure and evaluation of key influencing elements, Asia-Pacific J. Chem. Eng. 7 (2012) 534–546.

[13] S. Hwangbo, I.-B. Lee, J. Han, Mathematical model to optimize design of integrated utility supply network and future global hydrogen supply network under demand uncertainty, Appl. Energy. 195 (2017) 257–267.

[14] S. Samsatli, I. Staffell, N.J. Samsatli, Optimal design and operation of integrated wind-hydrogen-electricity networks for decarbonising the domestic transport sector in Great Britain, Int. J. Hydrogen Energy. 41 (2016) 447–475.

[15] HyWays project, The European Hydrogen Energy Roadmap: A sustainable pathway for the European Energy Transition, (2007). www.hyways.de.

[16] M. Moreno-Benito, P. Agnolucci, L.G. Papageorgiou, Towards a sustainable hydrogen economy: Optimisation-based framework for hydrogen infrastructure development, Comput. Chem. Eng. 102 (2017) 110–127.

[17] M. Voldsund, K. Jordal, R. Anantharaman, Hydrogen production with CO2 capture, Int. J. Hydrogen Energy. 41 (2016) 4969–4992.

[18] N.V.S.N. Murthy Konda, N. Shah, N.P. Brandon, Optimal transition towards a large-scale hydrogen infrastructure for the transport sector: The case for the Netherlands, Int. J. Hydrogen Energy. 36 (2011) 4619–4635.

[19] J. Kim, Y. Lee, I. Moon, Optimization of a hydrogen supply chain under demand uncertainty, Int. J. Hydrogen Energy. 33 (2008) 4715–4729.

[20] R.S. Kumar, A. Choudhary, S.A.K.I. Babu, S.K. Kumar, A. Goswami, M.K. Tiwari, Designing multi-period supply chain network considering risk and emission: a multi-objective approach, Ann. Oper. Res. 250 (2017) 427–461.

[21] S. De-León Almaraz, C. Azzaro-Pantel, L. Montastruc, L. Pibouleau, O.B. Senties, Assessment of mono and multi-objective optimization to design a hydrogen supply chain, Int. J. Hydrogen Energy. 38 (2013) 14121–14145.

[22] N. Sabio, A. Kostin, G. Guillén-Gosálbez, L. Jiménez, Holistic minimization of the life cycle environmental impact of hydrogen infrastructures using multi-objective optimization and principal component analysis, Int. J. Hydrogen Energy. 37 (2012) 5385–5405.

[23] A. Hugo, P. Rutter, S. Pistikopoulos, A. Amorelli, G. Zoia, Hydrogen infrastructure strategic planning using multi-objective optimization, Int. J. Hydrogen Energy. 30 (2005) 1523–1534.

[24] J. Lundgren, T. Ekbom, C. Hulteberg, M. Larsson, C.-E. Grip, L. Nilsson, P. Tunå, Methanol production from steel-work off-gases and biomass based synthesis gas, Appl. Energy. 112 (2013) 431–439.

[25] Q. Chen, Y. Gu, Z. Tang, W. Wei, Y. Sun, Assessment of low-carbon iron and steel production with CO2 recycling and utilization technologies: A case study in China, Appl. Energy. 220 (2018) 192–207.

[26] H. Kong, E. Qi, H. Li, G. Li, X. Zhang, An MILP model for optimization of byproduct gases in the integrated iron and steel plant, Appl. Energy. 87 (2010) 2156–2163.

[27] W.C. Cho, D. Lee, C.H. Kim, H.S. Cho, S.D. Kim, Feasibility study of the use of by-product iron oxide and industrial off-gas for application to chemical looping hydrogen production, Appl. Energy. 216 (2018) 466–481.

[28] M. Yáñez, A. Ortiz, B. Brunaud, I.E. Grossmann, I. Ortiz, Contribution of upcycling surplus hydrogen to design a sustainable supply chain: The case study of Northern Spain, Appl. Energy. 231 (2018) 777–787.

[29] M. Yánez, A. Ortiz, I. Ortiz, B. Brunaud, E. Grossmann, Surplus hydrogen reuse using decision-making techniques in northern Spain, in: Proc. EHEC'18, 2018.

[30] Spanish National Statistics Institute (INE), Renovable 2050: Un informe sobre el potencial de las energías renovables en la España peninsular - Situación actual y escenarios para el 2050, (2004) 40–88. pg. 21.

[31] Ec.europa.eu., Natural gas price statistics, (2018). www.ec.europa.eu/eurostat.

[32] X. Zhang, S. Wang, H. Chen, L. Zhou, System design and economic evaluation of coke oven gas utilization projects, in: Asia-Pacific Power Energy Eng. Conf. APPEEC, 2010.

[33] D. Fraile, J.C. Lanoix, P. Maio, A. Rangel, A. Torres, CertifHy project. Overview of the market segmentation for hydrogen across potential customer groups, based on key application areas., 2015.

[34] European Commission, Reference Document on Best Available Techniques for the Production of Chlor-alkali, 2014.

[35] Daniel Braxenholm, Doctoral Thesis: By-Product Hydrogen to Fuel Cell Vehicles, Chalmers University of Technology, Gothenburg, Sweden, 2016.

[36] Infinium Global Research, Global Chlor-Alkali Market: Trends Analysis & Forecasts to 2021, 2017.

[37] PWC, Steel in 2025: quo vadis?, 2015. www.pwc.com.

[38] Euromonitor International, Basic Iron and Steel in Spain: ISIC 271, 2018. www.euromonitor.com.

[39] Spanish National Statistics Institute (INE), Cifras oficiales de población de los municipios españoles: Revisión del Padrón Municipal, (2016). www.ine.es.

[40] Office of Energy Efficiency and Renewable Energy's Fuel Cell Technologies, H2tool, (2019). www.h2tools.org.

[41] S. Rahmouni, N. Settou, B. Negrou, A. Gouareh, GIS-based method for future prospect of hydrogen demand in the Algerian road transport sector, Int. J. Hydrogen Energy. 41 (2016) 2128–2143.

[42] S. De-León Almaraz, C. Azzaro-Pantel, L. Montastruc, S. Domenech, Hydrogen supply chain optimization for deployment scenarios in the Midi-Pyrénées region, France, Int. J. Hydrogen Energy. 39 (2014) 11831–11845.

[43] ISO 14687: Hydrogen Fuel: Product Specification, Part 2: Proton exchange membrane (PEM) fuel cell applications for road vehicles, (2009).

[44] ISO 14687: Hydrogen Fuel: Product Specification, Part 3: Proton exchange membrane (PEM) fuel cells applications for stationary appliances, (2009).

[45] S.E. Hosseini, M.A. Wahid, Hydrogen production from renewable and sustainable energy resources: Promising green energy carrier for clean development, Renew. Sustain. Energy Rev. 57 (2016) 850–866.

[46] Y. Yampolskii, B. Freeman, Membrane Gas Separation, John Wiley & Sons Inc, England, 2010.

[47] Y. Alqaheem, A. Alomair, M. Vinoba, A. Pérez, Polymeric Gas-Separation Membranes for Petroleum Refining, Int. J. Polym. Sci. 2017 (2017) 19.

[48] W. Liemberger, M. Groß, M. Miltner, M. Harasek, Experimental analysis of membrane and pressure swing adsorption (PSA) for the hydrogen separation from natural gas, J. Clean. Prod. 167 (2018) 896–907.

[49] W. Liemberger, M. Groß, M. Miltner, H. Prazak-Reisinger, M. Harasek, Extraction of green hydrogen at fuel cell quality from mixtures with natural gas, Chem. Eng. Trans. 52 (2016) 427–432.

[50] H.R. Perry, W.G. Green, Perry's Chemical Engineers' Handbook. 8th Edition., McGraw-Hill, New York, 2013.

[51] D. Favreau, S. Vinot, Roads2HyCom Project: Fuel cells and hydrogen in a sustainable energy economy, (2009).

[52] A. Mivechian, M. Pakizeh, Hydrogen recovery from Tehran refinery off-gas using pressure swing adsorption, gas absorption and membrane separation technologies: Simulation and economic evaluation, Korean J. Chem. Eng. 30 (2013) 937–948.

[53] R.L. Schendel, C.L. Mariz, J.Y. Mak, Is permeation competitive?, Hydrocarb. Process. 62 (1983).

[54] U.S. DRIVE Patnership., Hydrogen Production Technical Team Roadmap, U. S. Drive. (2013) 98.

[55] A. Alekseev, Hydrogen Liquefaction, in: Hydrog. Sci. Eng. Mater. Process. Syst. Technol., 2016: pp. 733–761.

[56] T. Jordan, HySafe - Chapter 2. Hydrogen Technologies, 3 (2006) 2223–2231. www.hysafe.net.

[57] L.M.P. E. Drioli, G. Barbieri, Gas-separation Issues with Membranes, in: Membr. Eng. Treat. Gases, RSC Publising, Cambridge, 2011: pp. 1–318.

[58] M. Reuß, T. Grube, M. Robinius, P. Preuster, P. Wasserscheid, D. Stolten, Seasonal storage and alternative carriers: A flexible hydrogen supply chain model, Appl. Energy. 200 (2017) 290–302.

[59] J.H. Han, J.H. Ryu, I.B. Lee, Modeling the operation of hydrogen supply networks considering facility location, Int. J. Hydrogen Energy. 37 (2012) 5328–5346.

[60] Spanish Hydrogen Association (AeH2), Los números del hidrógeno, (2017). www.aeh2.org.

[61] D. Kreith, Frank & Goswami, Handbook of energy efficiency and renewable energy, CRC Press, Boca Raton, Florida, 2007.

[62] European Commission, Reference Document on Best Available Techniques for Iron and Steel Production, 2013.

[63] Ministerio de Industria Energía y Turismo (MINETUR), La Energía en España 2015, 2015. www.minetur.es.

[64] Currency Converter, Eur. Cent. Bank. (2017). sdw.ecb.europa.eu/curConverter.do.

[65] Informe de Estabilidad Financiera, Banco de España, Eurosistema, 2017.

[66] Trading Economics, Spain Corporate Tax Rate, (2017). www.tradingeconomics.com.

[67] Gobierno de Aragón, Boletín Nº 29 de Coyuntura Energética en Aragón, 2015. www.aragon.es.

[68] Fundación Asturiana de la Energía, Energía en Asturias: Datos Energéticos del Principado de Asturias, 2015.

[69] Instituto de Estadística de Cataluña, Consumo final de energía. Por sectores, (2014). www.idescat.cat.

[70] Instituto Enerxético de Galicia, Balance Enerxético de Galicia, 2015. www.inega.gal.

[71] Fundación de la Energía de la Comunidad de Madrid, Balance Energético de la Comunidad de Madrid, 2015. www.fenercom.com.

[72] Gobierno de Navarra., Balance Energético de Navarra, (2015). www.navarra.es.

[73] Ente Vasco de la Energía, Euskadi Energia, 2015. www.eve.eus.

[74] C.L. Gargalo, A. Carvalho, K. V. Gernaey, G. Sin, Supply Chain Optimization of Integrated Glycerol Biorefinery: *GlyThink* Model Development and Application, Ind. Eng. Chem. Res. 56 (2017) 6711–6727.

[75] G. Guillén-Gosálbez, I.E. Grossmann, Optimal design and planning of sustainable chemical supply chains under uncertainty, AIChE J. 55 (2009) 99–121.

[76] B. Ohs, M. Falkenberg, M. Wessling, Optimizing hybrid membrane-pressure swing adsorption processes for biogenic hydrogen recovery, Chem. Eng. J. (2019) 452–461.

[77] F. Andersen, F. Iturmendi, S. Espinosa, M.S. Diaz, Optimal design and planning of biodiesel supply chain with land competition, Comput. Chem. Eng. 47 (2012) 170–182.

[78] M. Martín, I.E. Grossmann, Optimal integration of renewable based processes for fuels and power production: Spain case study, Appl. Energy. 213 (2018) 595–610.

Table A.2.1 Hydrogen demand forecast per client for scenario s1 in northern Spain

		period $t \in T$							
		2020		2030		2040		2050	
customer $k \in K$		e1	e2	e1	e2	e1	e2	e1	e2
46	Alcalá de Henares	177	0	2119	286	4188	1251	6383	2851
47	Alcobendas	102	0	1226	165	2423	724	3693	1649
48	Alcorcón	151	0	1810	244	3578	1069	5453	2435
49	Badalona	156	0	1867	232	3689	1018	5622	2320
50	Baracaldo	65	0	785	80	1551	352	2363	802
51	Barcelona	1161	0	13926	1734	27521	7594	41945	17305
52	Bilbao	225	0	2702	277	5340	1212	8138	2761
53	Burgos	122	0	1461	208	2887	912	4400	2079
54	Fuenlabrada	175	0	2100	283	4151	1240	6326	2825
55	Getafe	159	0	1911	258	3777	1128	5756	2571
56	Gijón	188	0	2262	146	4469	641	6812	1461
57	Hospitalet Llobregat	184	0	2206	275	4359	1203	6644	2741
58	La Coruña	140	0	1678	233	3317	1020	5055	2325
59	Leganés	169	0	2025	273	4001	1195	6098	2724
60	León	82	0	988	101	1952	443	2976	1010
61	Lérida	100	0	1196	149	2363	652	3602	1486
62	Logroño	52	0	621	181	1227	793	1870	1806
63	Madrid	2854	0	34243	4616	67671	20214	103137	46063
64	Mataró	91	0	1087	148	2147	648	3273	1478
65	Móstoles	185	0	2224	300	4395	1313	6699	2992
66	Orense	61	0	728	101	1440	443	2194	1009
67	Oviedo	152	0	1824	118	3605	517	5495	1178
68	Pamplona	134	0	1610	160	3182	699	4850	1593
69	Parla	112	0	1349	182	2665	796	4062	1814
70	Reus	75	0	897	112	1773	489	2702	1115
71	Sabadell	150	0	1803	224	3563	983	5430	2240
72	Salamanca	100	0	1199	171	2369	749	3611	1706
73	San Sebastián	121	0	1457	149	2879	653	4387	1489
74	S. Coloma de Gramanet	85	0	1014	126	2004	553	3055	1260
75	Santander	119	0	1428	204	2822	892	4301	2033
76	Tarragona	95	0	1135	141	2243	619	3418	1410
77	Tarrasa	155	0	1862	232	3680	1015	5609	2314
78	Torrejón de Ardoz	114	0	1374	185	2715	811	4137	1848
79	Valladolid	208	0	2497	356	4934	1560	7520	3554
80	Vigo	168	0	2014	280	3981	1224	6067	2790
81	Vitoria	160	0	1915	196	3785	859	5769	1957
82	Zaragoza	389	0	4665	489	9218	2141	14050	4878
H_2 demand (t H_2 year^{-1})		**8934**	**0**	**107207**	**13615**	**211862**	**59624**	**322899**	**135870**
		8934		120822		271486		458769	

Table A.2.2 Hydrogen demand forecast per client for scenario s2 in northern Spain

		period t ϵ T							
		2020		2030		2040		2050	
customer k ϵ K		e1	e2	e1	e2	e1	e2	e1	e2
46	Alcalá de Henares	353	467	4238	2542	8376	4317	12766	5791
47	Alcobendas	204	270	2452	1471	4846	2497	7386	3350
48	Alcorcón	302	399	3621	2171	7155	3687	10905	4947
49	Badalona	311	380	3733	2068	7378	3512	11244	4712
50	Baracaldo	131	131	1569	715	3101	1214	4727	1629
51	Barcelona	2321	2836	27853	15431	55042	26203	83890	35155
52	Bilbao	450	453	5404	2462	10679	4181	16276	5610
53	Burgos	243	341	2922	1854	5773	3148	8799	4224
54	Fuenlabrada	350	463	4201	2519	8302	4278	12653	5740
55	Getafe	319	421	3822	2292	7553	3892	11512	5222
56	Gijón	377	239	4523	1303	8938	2212	13623	2968
57	Hospitalet Llobregat	368	449	4412	2444	8718	4150	13287	5568
58	La Coruña	280	381	3357	2073	6633	3520	10110	4722
59	Leganés	337	446	4049	2429	8003	4124	12197	5533
60	León	165	165	1976	900	3905	1529	5951	2051
61	Lérida	199	244	2392	1325	4727	2250	7204	3019
62	Logroño	103	296	1242	1610	2454	2735	3740	3669
63	Madrid	5707	7550	68486	41073	135342	69748	206275	93574
64	Mataró	181	242	2173	1318	4294	2237	6545	3002
65	Móstoles	371	490	4448	2668	8791	4530	13398	6078
66	Orense	121	165	1457	900	2879	1528	4388	2050
67	Oviedo	304	193	3649	1051	7211	1784	10990	2394
68	Pamplona	268	261	3220	1420	6364	2412	9699	3236
69	Parla	225	297	2697	1617	5330	2747	8123	3685
70	Reus	149	183	1794	994	3545	1688	5403	2264
71	Sabadell	300	367	3605	1997	7125	3392	10859	4551
72	Salamanca	200	280	2398	1522	4739	2584	7222	3466
73	San Sebastián	243	244	2913	1327	5757	2254	8775	3024
74	S. Coloma de Gramanet	169	207	2028	1124	4008	1908	6109	2560
75	Santander	238	333	2856	1812	5644	3078	8602	4129
76	Tarragona	189	231	2270	1257	4485	2135	6836	2865
77	Tarrasa	310	379	3724	2063	7360	3504	11218	4701
78	Torrejón de Ardoz	229	303	2747	1648	5429	2798	8274	3754
79	Valladolid	416	582	4994	3169	9869	5381	15041	7219
80	Vigo	336	457	4029	2488	7961	4225	12134	5668
81	Vitoria	319	321	3830	1745	7570	2964	11537	3976
82	Zaragoza	777	800	9330	4350	18437	7386	28100	9910
H_2 demand (t H_2 $year^{-1}$)		17865	22266	214414	121152	423723	205732	645798	276016
		40131		335566		629455		921814	

Table A.2.3. Distance between supplier and merchant companies, in km

		merchant j ϵ J																
		1	**2**	**3**	**4**	**5**	**6**	**7**	**8**	**9**	**10**	**11**	**12**	**13**	**14**	**15**	**16**	**17**
supplier i ϵ I	**25**	225	25	678	664	503	259	133	614	615	614	533	15	302	502	615	133	263
	26	212	19	693	678	518	269	146	629	631	629	544	0	315	517	630	145	254
	27	222	3	689	675	515	286	138	627	629	627	560	20	318	524	640	148	261
	28	527	307	392	381	228	383	170	347	352	347	540	315	0	227	351	170	556
	29	724	513	177	161	1	478	380	119	124	119	510	518	228	1	123	381	731
	30	723	512	177	162	1	478	379	119	125	120	510	517	227	0	124	380	730
	31	832	627	100	80	123	555	498	10	2	10	524	630	351	124	0	498	830
	32	357	137	554	540	381	290	1	496	499	496	524	145	170	380	498	0	392
	33	105	269	906	889	731	313	392	831	830	831	570	254	556	730	830	392	0

Table A.2.4. Distance between merchant company and customer, in km

customer k ∈ K	ID	merchant j ∈ J																
		1	2	3	4	5	6	7	8	9	10	11	12	13	14	15	16	17
	46	528	389	485	464	337	182	325	394	388	394	210	381	330	336	389	327	492
	47	505	372	506	485	355	158	314	415	410	416	212	363	332	353	411	316	467
	48	508	385	527	506	379	152	335	436	430	436	188	375	359	378	431	337	465
	49	904	692	11	20	180	644	558	90	98	90	619	697	399	181	96	559	909
	50	442	222	471	458	301	327	85	418	422	418	522	231	85	300	421	86	473
	51	899	689	19	16	176	637	555	82	89	82	610	694	397	177	88	556	904
	52	448	228	464	452	294	327	91	411	415	411	518	236	79	293	414	92	478
	53	404	210	499	483	323	209	117	427	428	428	409	209	176	322	428	118	408
	54	515	393	527	506	380	157	343	435	429	436	181	383	364	379	430	344	470
	55	517	393	520	500	374	161	341	429	423	430	184	383	360	373	424	342	474
	56	227	6	684	670	510	286	133	623	625	623	558	24	302	509	624	132	275
	57	895	685	24	14	172	631	551	76	83	75	604	689	394	173	81	552	899
	58	6	217	895	880	719	362	352	827	827	827	637	207	522	718	827	352	109
	59	514	390	522	501	375	158	338	431	425	431	186	380	359	374	426	340	471
	60	249	102	655	639	479	181	151	583	583	584	456	88	304	478	584	151	255
	61	769	561	135	117	51	510	429	68	74	68	516	565	279	52	73	430	773
	62	499	291	400	385	225	298	164	335	337	336	443	294	97	224	337	164	510
	63	511	383	514	494	366	158	328	423	418	424	197	373	348	365	419	330	470
	64	917	704	17	37	193	531	569	109	117	109	638	710	408	194	115	570	924
	65	508	386	531	510	383	547	338	440	434	440	184	376	363	382	435	340	463
	66	122	218	840	823	665	857	332	764	763	764	520	201	493	664	763	332	67
	67	211	20	693	678	518	710	146	629	630	629	542	1	316	517	630	146	253
	68	556	340	350	337	180	366	204	297	302	298	504	346	54	179	301	204	576
	69	520	398	526	505	381	542	348	434	428	435	176	388	368	380	429	350	475
	70	824	620	104	83	116	119	490	11	9	11	520	623	343	117	8	491	823
	71	889	678	11	12	166	28	543	83	93	83	614	683	383	167	91	544	896
	72	351	283	664	644	499	681	298	578	574	578	290	268	399	497	575	299	297
	73	524	303	399	387	235	414	167	354	359	354	545	312	8	234	358	167	554
	74	900	689	11	17	177	22	555	87	95	87	617	694	396	178	93	556	906
	75	376	155	539	526	368	555	22	484	487	484	533	165	152	367	487	21	413
	76	836	632	96	75	126	111	501	9	6	9	528	635	354	127	5	502	835
	77	881	670	19	10	157	36	535	77	87	77	608	675	376	159	85	536	887
	78	522	387	495	475	347	512	326	404	398	405	205	378	336	346	400	328	484
	79	359	222	579	561	408	597	198	499	497	499	336	212	290	407	497	200	336
	80	126	284	909	892	735	926	402	832	831	833	559	266	564	733	831	402	21
	81	473	259	429	415	255	446	125	370	373	370	478	264	74	254	372	126	493
	82	649	448	259	241	93	277	322	182	182	183	428	449	198	91	182	322	649

CHAPTER 3

MEMBRANE-BASED TECHNOLOGIES AS AN ALTERNATIVE FOR HYDROGEN SEPARATION

3.1 INTRODUCTION

A broad range of technologies, i.e. pressure swing adsorption (PSA), membrane systems and cryogenic distillation, are available in the market and compete each other for hydrogen upgrading purposes. The advantages of membrane technology over existing separation processes, such as high selectivity, low energy consumption, small footprint, moderate cost to performance ratio and compact and modular design, especially in small to medium capacity plants, have been widely reported [1].

A number of comprehensive reviews have been conducted on membrane sciences for hydrogen purification during the last few years [2–6]. These studies have identified three kind of membranes based on the materials, which are of polymeric, inorganic and metallic nature. These membranes differ in terms of the hydrogen separation performance and the applicable operation conditions [7]. Compared with metal and inorganic membranes, dense, organic (polymeric) membranes (DPMs) are the dominating materials for gas separation membranes at present, because of the outstanding economy (lower material and manufacturing costs) and competitive performance (mild operation conditions) [8]. Although metal membranes, such as palladium-based membranes, could provide infinite permselectivity of hydrogen, apart from its inherent material cost, they are more suitable for use at high operating conditions (> 300 °C) to avoid embrittlement [9]. After many years of development, membrane separation technology has been extensively applied in many industries However, membrane processes have several inherent limitations such as the moderate purity reported by state-of-art hydrogen-selective DPMs working with low pressure permeate at mild temperature conditions. This is because among the vast number of polymers that have been investigated, the general trend shown is that highly permeable polymers possess low selectivities. Moreover, the permeability and selectivity of a membrane vary under different operating conditions (temperature, pressure, humidity and gas compositions, etc.) [8]. Thus, further research on the assessment of the performance of the available hydrogen separation membranes under different conditions is also a crucial factor for determining the feasibility of the membrane process for a specific industrial application. Furthermore, as for gas mixtures, the transport behavior of one component through the membrane is affected by the presence of other penetrants, which resulted in deviations from permeation data of pure gases. In addition, the non-ideal gas behavior of CO_2-containing mixture and the concentration polarization phenomenon, also cause the deviation from permeation data of pure gases [10]. Hence, using single gas permeation data to estimate the

performance of gas mixtures may lead to confusing results and, for that reason, the membranes behavior during mixed gas measurements must be thoroughly analysed [11,12].

Hence, in the present work, we aimed to test conventional DPMs using synthetic multi-component gaseous mixtures based on three of most suitable industrial hydrogen-rich waste gases, which compositions and outlet conditions are detailed in Table 3.1. In this way, a comparative performance analysis of commercially available polymeric membranes for hydrogen separation is developed and applied to industrial waste gas mixtures to obtain high-purity hydrogen. Therefore, the aim here is to investigate the permeation of pure gases and multicomponent mixtures of H_2, N_2, CH_4, CO, and CO_2 at different operation conditions through dense polymeric films. Furthermore, the impacts of other important process parameters such as temperature and pressure on the performance of the membranes were investigated. Hence, new knowledge on membrane behavior related to real process conditions are revealed for commercially available DPMs. The results render to the status of a membrane-based hydrogen recovery process applicable to industrial-scale waste gas streams.

Table 3.1. Case study industrial waste gas streams parameters [13–15]

		Gas composition (% vol.)						
Industrial sources	**ID**	**H_2**	**N_2**	**CO_2**	**CO**	**CH_4**	**T (°C)**	**P (bar)**
Ammonia industry	APG	58.6	25.7	-	-	15.7	15 - 30	> 100
Steelmaking process	COG	60.2	4.7	2.1	6.8	26.2	15 - 30	5 - 20
Methanol production	MPG	63.1	11.3	11.1	3.4	11.2	15 - 45	70

3.2 EXPERIMENTAL PROCEDURE

3.2.1 DENSE POLYMERIC MEMBRANE MATERIALS

The first step consists of making a comparative analysis of available polymeric membranes to select the material that offers the best performance for hydrogen recovery from aforementioned waste gas streams. Due to the relative high hydrogen content within the gas mixtures exhausted under mild temperature conditions, and also the required high-purity hydrogen to comply with ISO 14687 series, a polymer with high selectivity towards hydrogen and reasonable permeability over a long period of usage is needed. Also, materials should be processed into thin, typically supported membranes, fashioned into high surface/volume ratio modules (up to 30.000 m^2 m^{-3} of packing density for hollow fiber (HF) modules), and used in optimized processes [16].

Due to their high hydrogen selectivity with respect to CO_2, N_2, CH_4 and CO, in order to obtain the maximum hydrogen purity to meet the quality standards of fuel cells, we decided to study the permeation behavior of the three commercial DPMs summarized in Table 3.2. Membrane thicknesses were measured using a digital micrometer Mitutoyo Digmatic Series 369 (accuracy ± 0.001 mm). For each membrane, five repetitions were made at different points along the organic material, where average values and standard deviations were obtained. The membrane thicknesses for polyetherimide (PEI), polyethersulfone (PES) and polybenzimidazole (PBI) were determined to be 27.4 ± 1.1, 29.2 ± 1.1 and 58.4 ± 0.5 µm, respectively. All gases in this study had purities higher than 99.9 % and were supplied by Air Liquide.

Table 3.2. Properties of the commercial studied H_2-selective membranes

Brand Names	Short name	Supplier	T_g (°C)	ρ (g cm^{-3})
ULTEM® 1000B	PEI	GoodFellow from SABIC	217	1.27
Ultrason® E	PES	GoodFellow from BASF	222	1.37
Celazole®	PBI	PBI Performance Products	427	1.30

3.2.2 PERMEATION SET-UP

In lab-scale experiments, commercial flat hydrogen selective membranes based on polymers were tested in order to separate multicomponent gas mixtures. A schematic illustration of the set-up indicating the coupled equipment is presented in Figure 3.1. The permeation set-up confers the possibility of performing pure and mixed gas permeation experiments, at predetermined gas concentrations and flow rate levels.

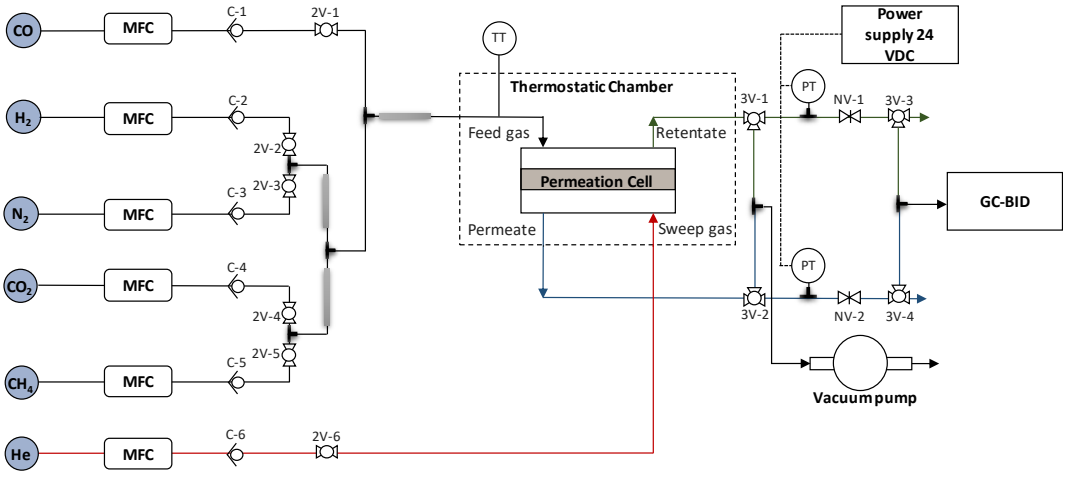

Figure 3.1. Mixed-gas permeation set-up. MFC, flow controller; C, check valve; 2V, 2-way valve; 3V, 3-way valve; TT, thermocouple; PT, pressure transducer; NV, Needle valve; GC-BID, gas analyzer. Feed gas (black); Sweep gas (red); Permeate (blue); Retentate (green).

Henceforth, gas separation experiments were carried out by means of multicomponent mixed gas separation tests using a continuous flow permeation cell. The membrane modules consist of two stainless steel 316 cylindrical chambers pressed onto each other, where the membranes have been placed on a porous metallic plate (Mott Corp., US. 3.5" OD, 0.2" W, media grade 20, 316L stainless steel) and sealed by Kalrez® O-rings. The studied membranes are cut off from the dried polymeric film in circular shape and after the insertion in the permeation cell, it results an effective membrane area of 55.4 cm^2. The feed and sweep gas flowrates were controlled using Bronkhorst digital mass flow controllers' series F-201CV (0–0.1 $L_N\,min^{-1}$) for all gases, except for H_2 that was F-201CV (0–0.2 $L_N\,min^{-1}$). The gas permeates through the membrane material and after it is removed by a sweep gas (Helium). Two pressure transducers, from Ashcroft series GC-35 (0 – 8 bar) followed by a needle valve and placed at each side of the membrane, are used to set the transmembrane pressure for the separation according to the experimental design.

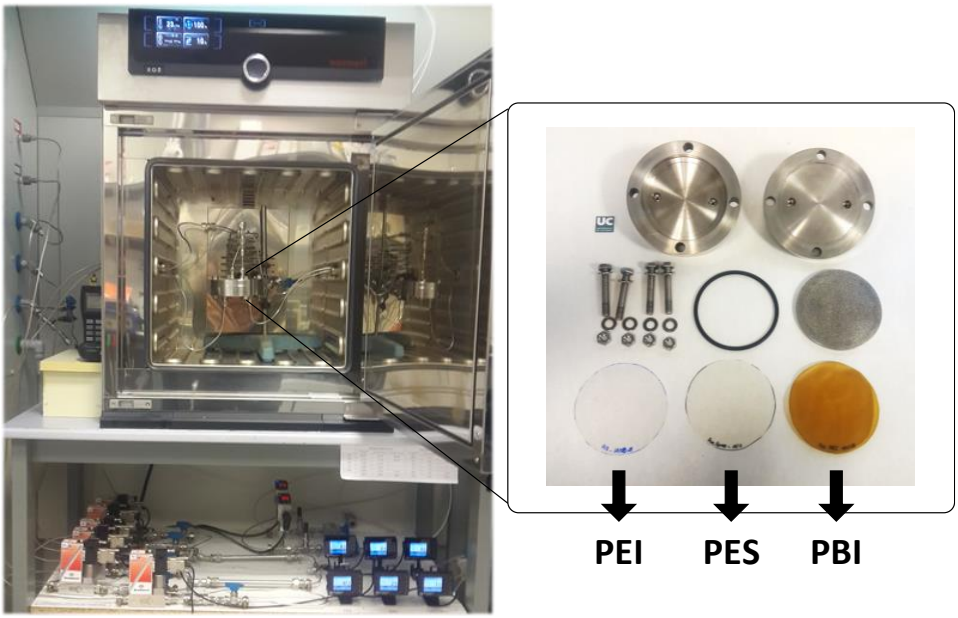

Figure 3.2. Photography of the experimental permeation set – up

The membrane testing apparatus is placed in a thermostatic chamber (Memmert Excel) to ensure isothermal operation and an additional thermocouple was placed in order to control the input temperature of the gases. Figure 3.2 shows a photographic image taken from the experimental setup. The composition of permeate and retentate streams was real-time analyzed by gas chromatography (Tracera GC-2010) equipped with a Barrier Ionization Discharge (BID) detector of ppb quantity level. The GC is suited with two columns, 1) molecular sieve capillary column (SH/Rt®/Msieve 5A) for H_2, N_2 , CO, and CH_4 separation and 2) fused silica capillary column (Carboxen® 1010 Plot) for CO_2 separation.

Due to the differences in concentration at permeate and retentate sides of the membrane, two gas chromatographic methods were developed: one for analyzing gas concentrations at low levels and the other for higher volume concentrations. An example of both gas chromatograms is shown in Figure 3.3. The first method is applied to detect gas mixture concentrations at the permeate side, while the second method is used for analyzing the retentate stream. The only difference between these two methods is the split ratio, which is set at 1:5 for the first method, and 1:50 for the second one. To generate the calibration curves for each gas component, a minimum of three calibration points (with the fit forced through zero) were obtained by analyzing gas mixture standards in triplicate. For all gas components (H_2, N_2, CH_4, CO and CO_2), the relative standard deviation (% RSD) for peak area of three consecutive injections was not more than 1.5 % at different concentration levels, showing high repeatability for the proposed method to monitor even ppm levels of each gas specie. Additionally, the values of the determination coefficient (R^2) for all gas component were found to be higher than 0.90, showing a good linearity property of the proposed method. The total acquisition time of the proposed gas chromatographic methods for analyzing permeate and retentate streams was 9 minutes. Helium is employed as the carrier gas in both columns with a constant pressure of 4.5 bar.

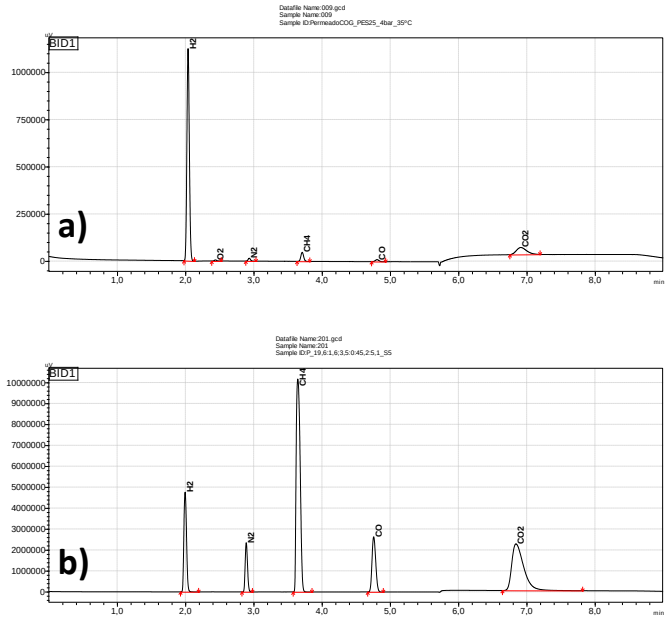

Figure 3.3. Example of the resulting chromatograms of a) hydrogen-rich permeate stream and b) retentate stream

Before starting a series of experiments, a vacuum pump was used to evacuate the whole permeation setup from undesired species and purge on the low pressure side of the equipment. The permeate side was kept under slightly higher ambient conditions ($p^P \approx 0.1$ barg) to detect leaks by pressure decay. Constant steady-state values of retentate and permeate flux and

composition were reached in less than 2 h. During this period the composition of the permeate stream was continuously analyzed, while the retentate was analyzed at least three times. Thus, once the constant steady-state is reached, the permeability of gases for each test is assessed using at least the last three injections, whose RSD for peak area was not more than 1.5 %. In this regard, gas permeability coefficients and selectivities were calculated by using Eqs. (1.7) – (1.8) as detailed in the previous Chapter 1.

A series of experiments was carried out to assess permeation and separation properties of the membranes. The process variables examined were the operation temperature, feed pressure, and the inlet gas composition described above in Table 3.1. When the same membrane was used for several tests, the experimental runs were conducted in the order of increasing CO_2 content in the inlet gas composition as follows: APG (H_2/ N_2/ CH_4 (% vol.): 58.6/ 25.7/ 15.7) , then COG (H_2/ N_2/ CO_2/ CO/ CH_4 (% vol.): 60.2/ 4.7/ 2.1/ 6.8/ 26.2) and MPG (H_2/ N_2/ CO_2/ CO/ CH_4 (% vol.): 63.1/ 11.3/ 11.1/ 3.4/ 11.2). The design boundaries for temperature were selected in the range of 25 to 45 °C, since the industrial gaseous waste streams under study are usually released to the air at room temperature. Beyond temperature and gas composition, the upstream pressure effect was also studied in the range of 4 to 7 barg. To sum up, the impact of the process variables on the real membrane performance was investigated, at the conditions given in Table 3.3.

Table 3.3. Operation experimental conditions for mixed gas experiments

Constant parameters	**Value**
Feed gas flowrate, Q^F (ml min^{-1})	75
Sweep gas flowrate, Q^S (ml min^{-1})	7 - 15
Effective area, A (cm^2)	55.4
Variable parameters	**Value**
Temperature, T (°C)	25/35/45
Upstream pressure, p^F(barg)	4/5.5/7
Feed gas composition, ${x_i}^F$ (%vol.)	APG/COG/MPG

3.3 RESULTS AND DISCUSSION

This section shows the main results obtained by investigating the permeation of pure gases and multicomponent gas mixtures of H_2, N_2, CH_4, CO, and CO_2 through dense polymeric films. Also, using experimental results of mixed gas separations, permeability has been evaluated as a function of temperature, pressure and feed concentration.

3.3.1 PURE GAS EXPERIMENTS

First, single gas permeation experiments were performed to obtain and compare permeability coefficients with literature data and also to have a benchmark for the multicomponent gas experiments. Table 3.4 shows the permeability data of pure gases for three DPMs: PEI, PES and PBI, in addition to values reported in literature. The pure-gas measurements were conducted at a constant temperature of 35 °C and a transmembrane pressure of 3.5 to 5.5 bar, until constant steady-state values of permeate flux and composition. The permeability error is determined by the membrane thickness standard deviation and each membrane sample was measured in two replicates. Based on the permeability values determined, it was revealed that the membranes allowed the gases to permeate in the following order: H_2 >> CO_2 > N_2 ≈ CO ≈ CH_4, where this phenomenon represents the hydrogen-selective characteristic of the membranes. It was noticeable that H_2 permeability was always higher than CO_2 permeability for all the membranes, and correlates with the kinetic diameter of the gases with H_2 as the smallest one (2.89 Å) compared to CO_2 with bigger size (3.3 Å), and then follow by N_2 (3.64 Å), CO (3.76 Å) and CH_4 (3.8 Å). The kinetic diameters are not only related to the gas molecular size, but also to their molecular structure [17]. H_2 is a small and non-condensable gas so that it can easily permeate through the membranes unlike the other pure gases. According to the obtained values, the performance results for the given membranes showed two different ranges of permeability coefficients. Thus, H_2 permeability values obtained with PEI and PES membranes are 10 times higher than those obtained with PBI membrane. This is possibly related to the polymers' chemical and physical properties. It was known that PBI-based materials exhibits higher density (1.3 g cm^{-3}) than other glassy polymers (PEI: 1.27 g cm^{-3}, PSF: 1.24 g cm^{-3}, etc.), which renders low flexibility and rigid chain-packing structure [18]. Thus, the immobilization of the polymer matrix would result in lesser free volume for gas diffusion, which finally presented lower permeability. It can be observed that the selected membranes provide H_2 permeability and ideal selectivity values well-agreed with the previously reported data in the literature for other PEI, PES and PBI membranes. However, it must be pointed out that, for a transmembrane pressure of 5.5 bar and regardless of the membrane used, the achievable H_2/CO_2 selectivity is slightly lower than the ideal values obtained from the literature. Nevertheless, H_2/N_2 and H_2/CH_4 selectivities are higher to a certain extent that those previously reported. The differences observed can be partially attributed to the fact that some results reported in literature have been obtained by the traditional time-lag technique. No previous data of the given membranes have been reported regarding CO, thus the obtained values constitute original data for these polymeric materials.

Table 3.4. Pure gas permeation properties of different polymeric membranes

		Permeability (Barrer)						Ideal selectivity				Polymer properties			Operating conditions		
Membrane	Membrane type	H_2	He	CO_2	N_2	CH_4	CO	H_2/CO_2	H_2/N_2	H_2/CH_4	H_2/CO	T_g (°C)	ρ (g cm^{-3})	δ_N (µm)	T (°C)	Δp (bar)	Ref.
PEI	**ULTEM® 1000B**	**7.9 ± 0.3**	**-**	**2.1 ± 0.1**	**0.03± 0.001**	**0.05 ± 0.002**	**0.04 ± 0.002**	**3.7**	**281**	**155**	**196**	**217**	**1.27**	**25**	**35**	**5.5**	**This work**
		8.9 ± 0.5	**-**	**2.2 ± 0.1**	**0.03± 0.002**	**0.05 ± 0.003**	**0.04 ± 0.002**	**4.1**	**330**	**168**	**223**	**217**	**1.27**	**25**	**35**	**3.5**	
	ULTEM® 1010	-	8.80	1.5	0.05	0.04	-	5.9	163.0	220.0	-	215	-	-	35	3.5	[30]
	ULTEM® XH6050	-	9.40	1.3	0.05	0.04	-	7.1	184.3	261.1	-	-	1.27	-	35	10 (3.5 H_2)	[34]
	-	7.8	-	1.3	0.05	0.04	-	5.9	166.0	222.9	-	215	-	-	30	-	[35]
	ULTEM® 1000	-	-	-	0.05	-	-	-	-	-	-	218	1.27	25	35	10	[36]
	-	-	-	1.3	-	0.04	-	-	-	-	-	215	1.28	-	35	10	[37]
	ULTEM® 1000	-	-	2.4	-	0.09	-	-	-	-	-	214	1.26	-	25	10	[38]
	ULTEM® 1000	6.9	-	1.6	0.05	0.03		4.4	133	238	-	215	-	-	35	5	[39]
PES	**Ultrason® E**	**10.5 ± 0.4**	**-**	**5.6 ± 0.2**	**0.08± 0.003**	**0.2 ± 0.01**	**0.11 ± 0.004**	**1.9**	**131**	**52**	**95**	**222**	**1.37**	**25**	**35**	**5.5**	**This work**
		12.0 ± 0.5	**-**	**3.1 ± 0.1**	**0.09± 0.01**	**0.2 ± 0.01**	**0.11 ± 0.01**	**3.8**	**130**	**58**	**106**	**222**	**1.37**	**25**	**35**	**3.5**	
	Radel® A	-	-	3.2	0.07	0.10	-	-	-	-	-	-	-	HF	RT	1.36 – 13.6	[40]
	Radel® A - 300	5.8	7.6	-	0.10	-	-	-	73.7	-	-	-	-	film	25	10	[41]
	Radel® A	9.0	9.1	3.4	0.13	0.11	-	2.7	70.0	82.7	-	-	-	60-70	35	2-35	[42]
	Radel® A	9.0	9.1	3.4	0.13	0.11	-	2.7	70.6	81.3	-	-	-	-	35	10 (2 H_2/He)	[43]
PBI	**Celazole®**	**0.52 ± 0.004**	**-**	**0.3 ± 0.2**	**0.002± 0**	**0.001± 0**	**0.004± 0**	**2.0**	**260**	**> 400**	**130**	**427**	**1.30**	**55**	**35**	**5.5**	**This work**
		0.77 ± 0.02	**-**	**0.3 ± 0.2**	**0.002± 0**	**0.001± 0**	**0.004± 0**	**3.0**	**198**	**> 400**	**198**	**427**	**1.30**	**55**	**35**	**3.5**	
	Celazole®	0.53	-	0.22	0.016	-	-	2.4	33.7	-	-	427	1.30	-	23	20	[44]
	Celazole®	1.74	-	0.88	0.063	-	-	2.0	27.9	-	-	427	1.30	-	80	20	[44]
	Tailor-made	0.6	1.05	0.16	0.005	0.002	-	3.8	125	333.3	-	416	1.33	40	35	20	[18]
	Tailor-made	76.8	-	3.33	0.78	-	-	23.0	98.3	-	-		1.37		250	1.5 – 3.5	[32]

3.3.2 MIXED GAS EXPERIMENTS

In this analysis, the impact of operating conditions (temperature, pressure and inlet mixed-gas composition) over permeability, selectivity and outlet gas purity was studied for each membrane. For synthetic gas mixtures based on real industrial hydrogen-rich waste gases, the performance of three DPMs: PEI, PES and PBI, were characterized to assess the appropriateness of the each membrane for a given separation task.

3.3.2.1 Temperature effect on mixed-gas permeation

The temperature effect on gas permeability through the DPMs was studied over a temperature range of 25 to 45 °C for the different synthetic waste gas streams, at $\Delta p \approx 5.5$ bar. As it is illustrated in Figure 3.4, all gas permeabilities were increased at higher temperatures. Generally, for DPMs, the temperature affects the energies of the gas molecules as well as the mobility of the polymeric chains of the membrane. Thus, a temperature increment in the membrane changes the flexibility of the polymeric chains, which improves the gas motion through the membrane [19,20].

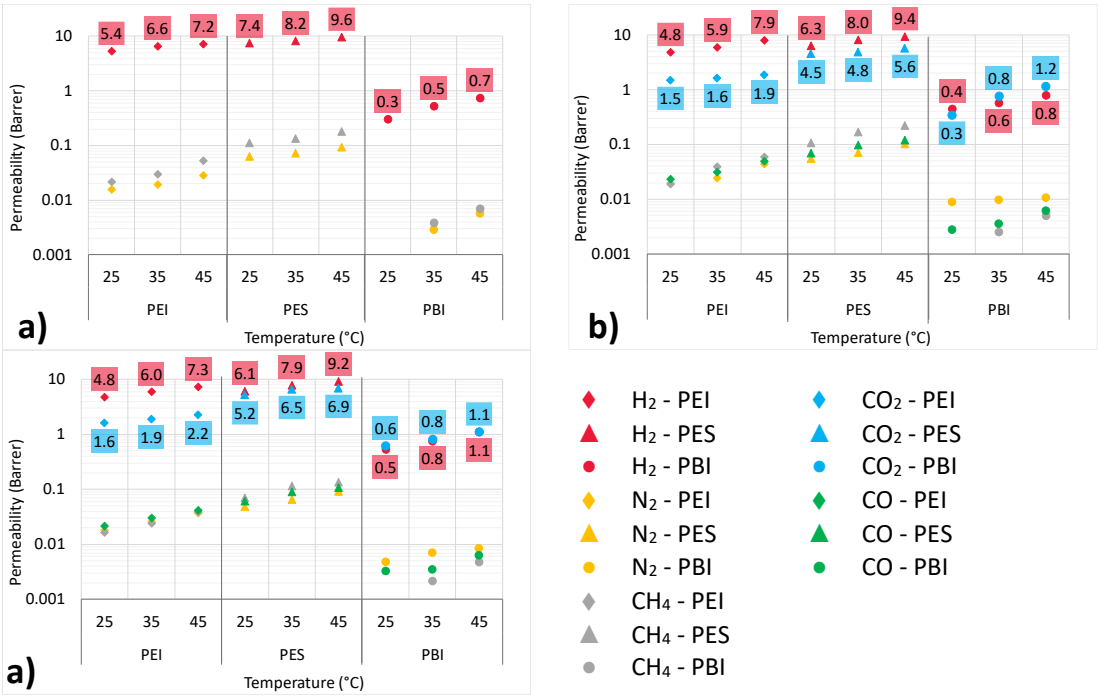

Figure 3.4. Temperature effect of mixed-gas permeabilities, measured at $\Delta p \approx 5.5$ bar: a) APG, b) COG and c) MPG

As it is represented in Figure 3.5 and regardless of the DPM used, all studied cases H_2/N_2, H_2/CH_4 and H_2/CO selectivity values decrease with temperature, while H_2/CO_2 increases. These results are in agreement with previous studies [21,22]. This behavior can be attributed to the changes of the transport properties (i.e. diffusion and solubility) of specific gases included in the mixed gas mixtures, with raising the temperature. Theoretically, elevating the temperature enhances gas diffusion, while on the other hand, reduces solubility in a significant manner. In the case of CO_2, as the temperature increased the regime was shifted from diffusion-limited to sorption-limited because of the higher dependence of diffusivity on temperature. Thus, increasing rate of CO_2 permeability with temperature was lower than the increasing rate of H_2 and therefore the H_2/CO_2 selectivity increased [21,22].

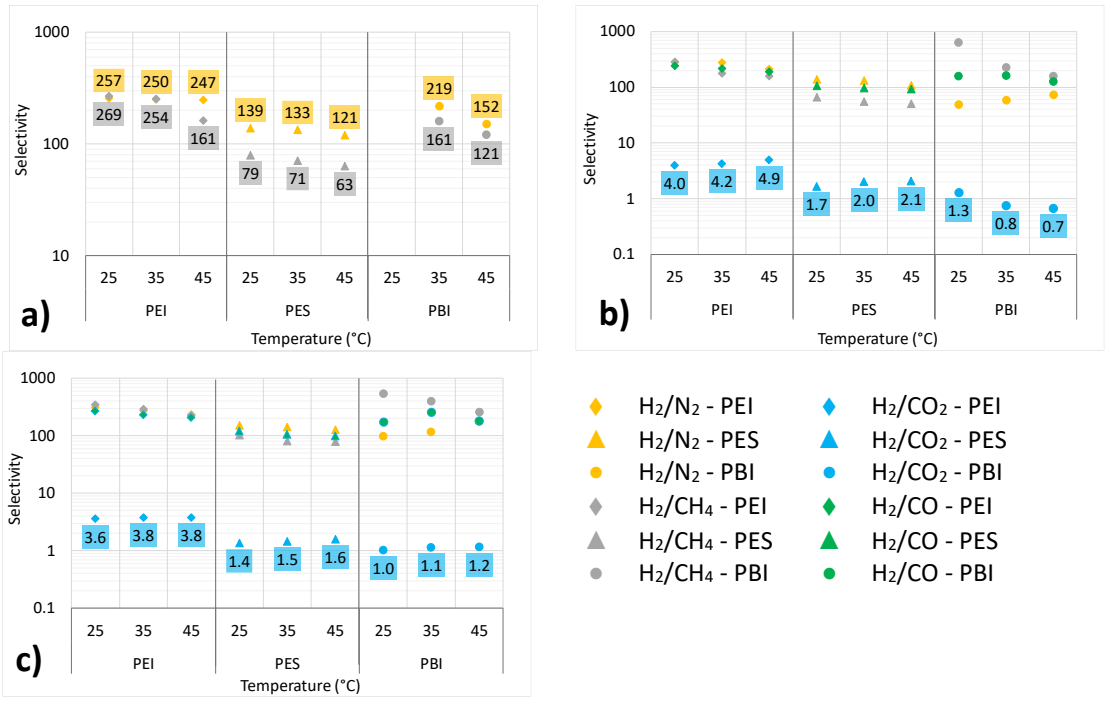

Figure 3.5. Temperature effect of mixed-gas selectivities, measured at $\Delta p \approx 5.5$ bar: a) APG, b) COG and c) MPG

As it is seen in Figure 3.5, the achievable H_2/CO_2 selectivity of PEI membrane increased from 3.96 at 25 °C to 4.86 at 45 °C using COG, while this increase is less pronounced using MPG from 3.60 at 25 °C to 3.80 at 45 °C. These behavior is also showed by PES membrane, raising the temperature the H_2/CO_2 selectivity values enhanced from 1.65 at 25 °C to 2.07 at 45 °C using COG, whereas the performance improvement is less evident using MPG from 1.37 at 25 °C to 1.57 at 45 °C. However, mixed gas permeability results from PBI membrane lead to higher CO_2 permeability values, showing a non-hydrogen-selective behavior at the temperature range under study.

Furthermore, to explore the dependence of the gas permeability on temperature, the data were correlated with the Arrhenius equation:

$$P_{\mathrm{i}} = P_0 \cdot e^{\left(-\frac{E_p}{RT}\right)} \qquad \text{Eq. (3.1)}$$

with P_0 as the pre-exponential factor, E_p as the permeation activation energy, T as the temperature and R as the ideal gas constant (8.314 J mol^{-1} K^{-1}). E_p values for the transport of each gas through each membrane were obtained from the slope of permeability (in logarithmic form) versus the reciprocal temperature. The specific E_p parameters at $\Delta p \approx$ 5.5 bar for permeation of H_2, N_2, CH_4, CO and CO_2 are summarized in Table 3.5. The permeation activation energy increased in the order CO_2 <H_2 <CO <N_2 <CH_4, the same as reported in other glassy polymeric membranes [23,24]. These glassy polymers present high values for the activation energy of permeation for CH_4, N_2 and CO, and therefore, the permeability coefficients strongly depend on temperature. The dependency on temperature for hydrogen as the smallest of the gases is much weaker. The very low E_p value of CO_2 compared with the other gases, could be attributed primarily to the lower energy consumption for CO_2 diffusion, which means that sorption rather than diffusion dominates the response of permeation to temperature for this gas molecule [25].

Table 3.5. Activation energy of H_2, N_2, CH_4, CO and CO_2 permeation through DPMs

		E_p (kJ mol^{-1})				
Membrane	**Mixed gas**	**H_2**	**N_2**	**CH_4**	**CO**	**CO_2**
PEI	APG	11.5	22.5	34.3	-	-
	COG	19.5	31.4	44.1	28.2	8.9
	MPG	16.4	28.0	33.1	25.2	13.4
PES	APG	9.9	15.3	18.5	-	-
	COG	15.1	23.4	28.3	21.3	8.6
	MPG	15.5	23.9	25.8	21.9	11.1
PBI	APG	34.9	55.5	47.1	-	-
	COG	31.1	6.9	99.1	30.8	43.7
	MPG	27.4	6.8	98.2	24.4	17.8

3.3.2.2 Pressure effect on mixed-gas permeation

The permeability coefficients of each gas were also measured as a function of the upstream feed pressure ranging from 4 to 7 barg for each synthetic waste gas stream and membrane material, and at 35 °C. Furthermore, the permeate side was kept under slightly higher atmospheric pressure. The permeability of mixed gases through the DPMs, as a function of the pressure difference, is presented in Figure 3.6, while selectivity in Figure 3.7.

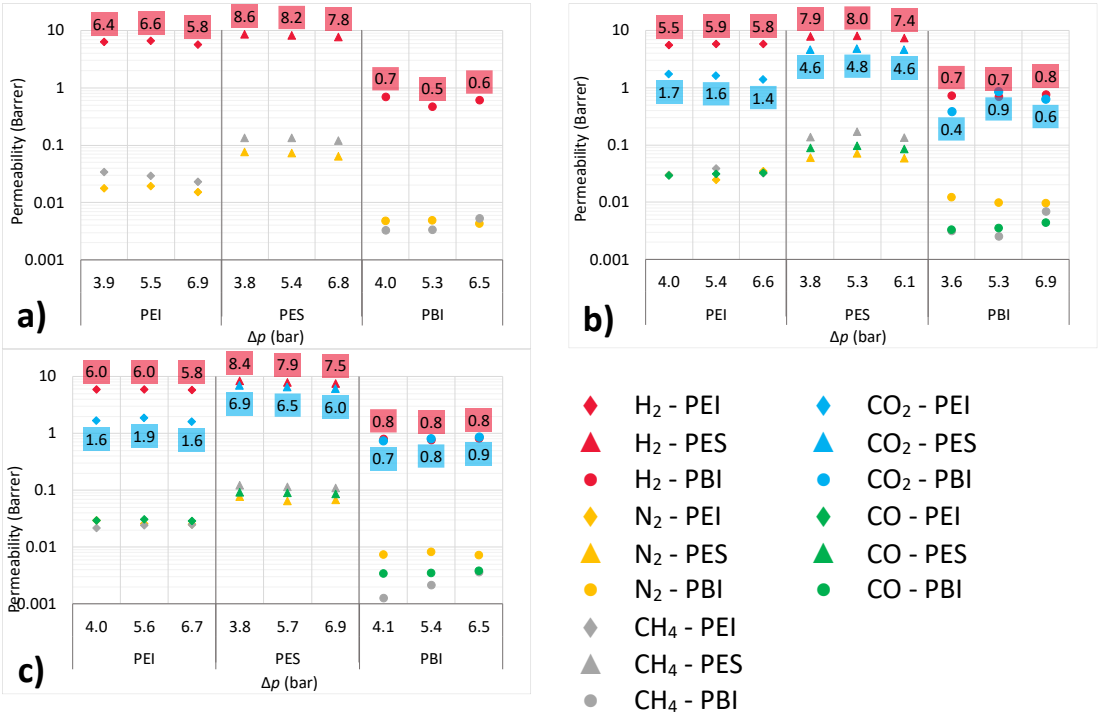

Figure 3.6. Pressure effect of mixed-gas permeabilities, measured at 35 °C: a) APG, b) COG and c) MPG

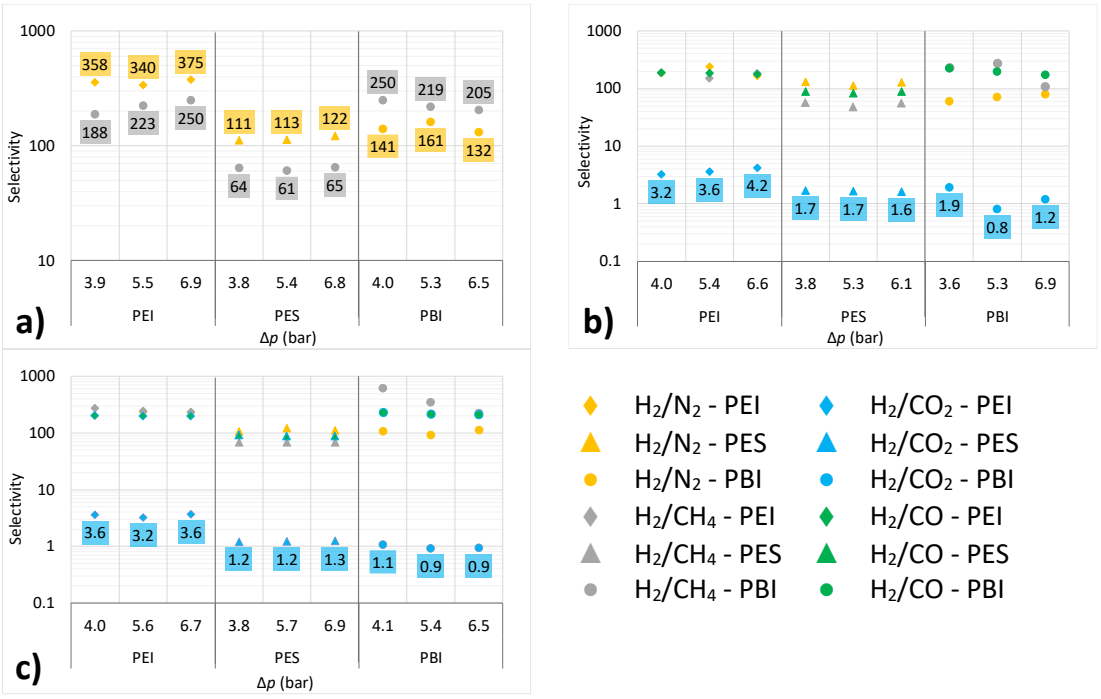

Figure 3.7. Pressure effect of mixed-gas selectivities, measured at 35 °C: a) APG, b) COG and c) MPG

Upon increasing the applied pressure, the permeability of low-sorbing penetrants (i.e. H_2, N_2, CH_4, CO) as feed gas exhibit non-significant change with pressure (< 15 % deviations), although a slight decrease can be intuited. This is a classical behavior in glassy polymeric membranes, where the transport is more diffusion dependent for less soluble penetrants. Initially, diffusion increases with applied pressure.

On the other hand, the compaction effect leads to less diffusion rate of low-sorbing gases, which causes the permeability to decrease with pressure [26,27]. Meanwhile the permeability tendency observed for CO_2 showed a decreasing trend when the transmembrane pressure increased. The decrease is related to the interaction of CO_2 molecules with the polymer matrix, and according to the dual-sorption model, the Langmuir sorption sites become saturated with gas molecules [20,28].

3.3.2.3 Comparing membrane performance

Experiments with multicomponent gas mixtures of H_2, N_2, CH_4, CO and CO_2 were performed. Other than membrane-penetrant interactions, there is also the interaction between the gas penetrants, which results in different results depending on the gas mixture and hydrogen-selective membrane used. Figure 3.8 shows the Robeson's trade-off lines between the selectivity and permeability for H_2/N_2, H_2/CH_4 and H_2/CO_2.

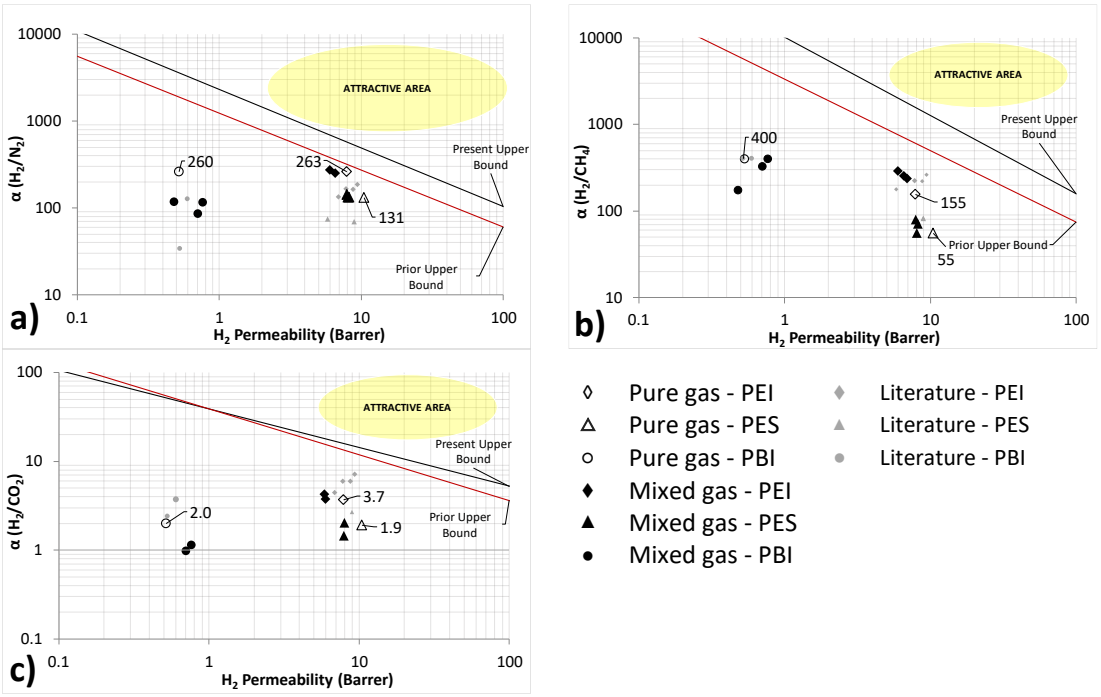

Figure 3.8. Separation performance with single and mixed gases, measured at 35 °C and $\Delta p \approx 5.5$ bar: a) H_2/N_2, b) H_2/CH_4 and c) H_2/CO_2

Although single gas permeabilities are similar to those reported in previous research, competitive sorption effect results in a slight drop in the permeability of H_2 with respect to pure gases using PEI and PES membranes. This effect was ascribed to the fact that the permeability of gases in mixed gas experiments is overall affected by the presence of CO_2 in the mixture of gases [29,30]. As a matter of fact, these interactions depend on several factors, such as the number of components in the mixture, type of components and operating parameters [31].

However, mixed-gas experimental results using PBI membrane showed higher H_2 permeabilities than pure gas tests, as it has been observed by other authors in literature [32]. For all the studied membranes, there is no coupling or competitive sorption between H_2 and N_2, CO and CH_4, with slight deviations between ideal and mixed-gas selectivity values of less than 4.7 % in PES, 11.2 % in PEI and 15.0% in PBI. Light gases (i.e. H_2, N_2) with very low solubility in polymer materials, they only weakly affect the property and behavior for polymers, and do not influence the mutual diffusion and solubility parameters in the process of simultaneous transport of gases in the separation of the mixture.

Nevertheless, the experimental results implied that the growing presence of CO_2 in the feed gas mixture caused difficulties in the whole separation process, due to the fact that this high-sorbing gas can fairly be dissolved in the membrane. For heavy gases (i.e. CO_2) with high solubility, the applicability of ideal permeation parameters implies higher uncertainty in predicting permeation results [33]. According to these results, although the DPMs do not cross the upper bound established in 2008, most of the membranes under study lay close to the upper bound found previously, in 1991.

3.3.2.4 Gas composition effect on hydrogen purity

Besides the above-mentioned variables, the inlet gas composition of the mixture to be separated is another factor that affects the overall performance of the membrane. Thus, tertiary and quinary mixed-gas experiments ($H_2/N_2/CH_4/CO/CO_2$) were performed by applying three different inlet gas compositions based on industrial waste gas streams (APG, COG and MPG), where hydrogen content is *ca.* 60 %. As might be expected because of permeability and selectivity values obtained, PEI membrane attained the highest hydrogen gas purities, followed by PES and PBI membranes.

Based on Figure 3.9, after permeation using PEI membrane at the given conditions (cell dimensions, flowrates, operating parameters), hydrogen in permeate reached up to 99.7 % vol. H_2 from APG, 98.8 % from COG and 95.4 % from MPG. Then, the product purity drops using PES membrane down to 99.2 % vol. H_2 from APG, 97.0 % from COG and 89.3 % from MPG. Regarding PBI membrane, hydrogen purities are quite similar to those obtained using PES, as 99.4 % vol. H_2 from APG and 96.1 % from COG, whereas the purity value decays down to 86.6 % when MPG is used as feed gas stream.

Regardless the DPMs studied, the purification yield was slightly lower using MPG as feed gas, possibly due to the existence of higher CO_2 content in the inlet stream. Thus, hydrogen purity is strongly affected by the CO_2 feed concentration, while the results showed that hydrogen purity remains almost constant to temperature and pressure changes in these ranges. This implies that the enrichment degree of hydrogen as the fastest gas penetrant was considerably dependent on the amount of carbon dioxide in the feed gas. The experimental results implied that the growing amount of carbon dioxide present in the feed gas caused a decrease in the enriched hydrogen permeate stream.

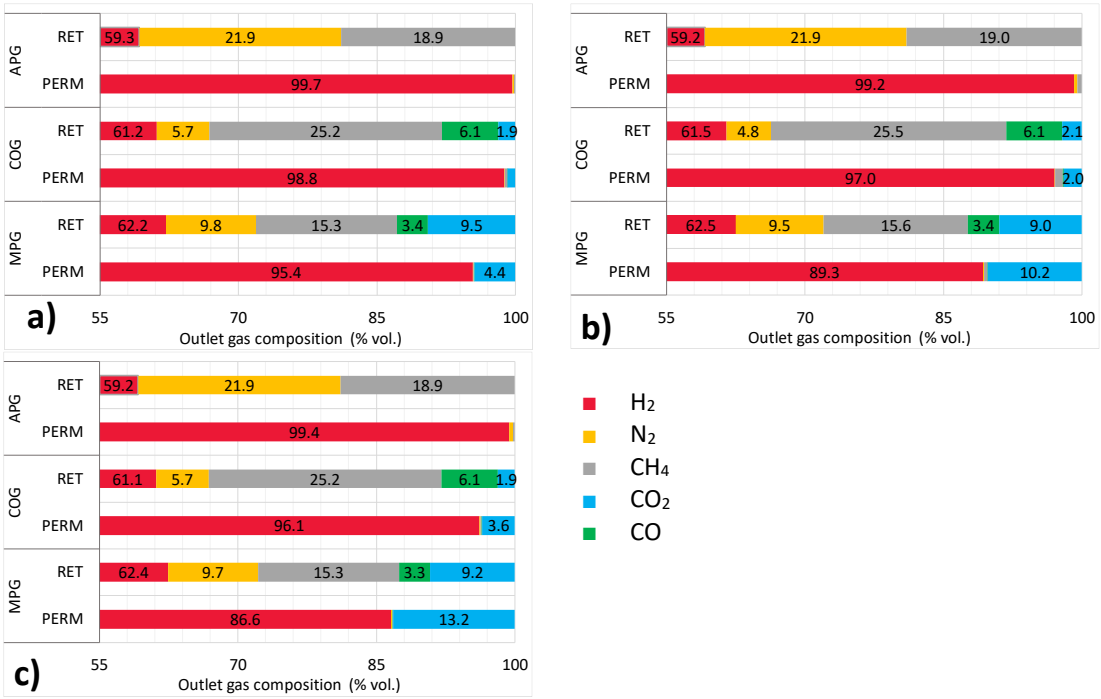

Figure 3.9. Composition of permeate (PERM) and retentate (RET) streams as function of feed gas, measured at 35 °C and $\Delta p \approx 5.5$ bar. a) PEI, b) PES and c) PBI membranes

Even though these results are still far from the quality requirements to feed fuel cells (> 99.9 %), they give relevant knowledge on membrane hydrogen purification yield to the scientific community, as the first upgrading step before further purification. In consequence with the results of state-of-the-art membranes studied in flat sheet form, PEI membrane achieve the highest purity of hydrogen, while simultaneously showed higher permeability and H_2/CO_2 selectivity. Although the maximum hydrogen purity obtained using PEI membrane was 99.7 % vol. H_2 from APG, 98.8 % from COG and 95.4 % from MPG, it would be necessary further upgrading to meet fuel cell quality standards. This could be done through the use of cascade membrane module systems or coupling it with conventional processes, such as hybrid membrane-PSA systems.

3.4 CONCLUSIONS

This chapter reports new data on the performance of commercial polymer-based membranes for hydrogen selective separations, which serves as the basis for the evaluation of the membrane technologies for hydrogen recovery from industrial waste gases. The permeation of pure gases and multicomponent mixtures of H_2, N_2, CH_4, CO, and CO_2 at different operation conditions through dense polymeric films has been investigated. Moreover, operating conditions that govern the practical feasibility of different membranes are discussed. In this way, new knowledge on membrane behavior related to real process conditions is revealed for commercially available polymeric membranes. This work renders valuable insights into the status of a membrane-based processes for hydrogen recovery applicable to industrial waste gas streams. Furthermore, the effect of process parameters on the performance of hydrogen-selective polymeric membranes was investigated. In this paper, mixed-gas permeation through three different non-porous polymeric membranes (PEI, PES, PBI) has been studied over three different synthetic waste gas streams (COG, APG and MPG). Also, the influence of temperature, transmembrane pressure and feed gas composition on gas permeation was examined. The major findings of this study are as follows;

- In the mixed gas system, all gas permeabilities were increased when increasing temperature. Even so, H_2/N_2, H_2/CH_4 and H_2/CO selectivity values decrease with temperature, while H_2/CO_2 selectivity increases.
- Permeability of low-sorbing penetrants (i.e. H_2, N_2, CH_4, CO) as feed gas exhibit insignificant change with pressure, whereas the permeability tendency observed for CO_2 showed a decreasing trend upon increasing the transmembrane pressure.
- Strong dependency of H_2 permeability on CO_2 concentration inducing this gas a decay of H_2/CO_2 selectivity in mixed-gas experiments for the studied membranes.
- Competitive sorption effect results in a drop in the permeability of H_2 with respect the pure gases using PEI and PES membranes, meanwhile the opposite effect was observe using PBI membrane.

In addition, with the experimentally obtained permeances, the required membrane area for a specific separation can be calculated and the optimum operational conditions can be found. Although the maximum hydrogen purity obtained using PEI membrane was 99.7 % vol. H_2 from APG, 98.8 % from COG and 95.4 % from MPG, it would be necessary further upgrading of the permeate stream to the required quality to comply with ISO 14687 series.

ABBREVIATIONS

APG	ammonia purge gas
CA	cellulose acetate
COG	coke oven gas
HF	hollow fibers
MPG	methanol purge gas
PBI	polybenzimidazole
PC	polycarbonate
PEI	polyetherimide
PEMFC	proton exchange membrane fuel cell
PES	polyethersulfone
PI	polyimide
PPO	polyphenyloxide
PSA	pressure swing adsorption
PSF	polysulfones
RT	room temperature
ISO	International Organization for Standarization
ICE	internal combustion engines
DPM	dense, organic (polymeric) membranes
RSD	relative standard deviation
RSD	relative standard deviation
OD	outside diameter
W	width
RET	retentate stream
PERM	permeate stream
MSA	Membrane Society of Australasia database
GC	gas chromatography
BID	barrier ionization discharge
MFC	flow controller
TT	thermocouple
PT	pressure transducer
NV	needle valve

NOMENCLATURE

Parameters

E_p	permeation activation energy (kJ mol^{-1})
P_0	pre-exponential factor (Barrer)

T_g glass transition temperature (°C)

Δp pressure gradient across the membrane (bar)

A area of the membrane (cm^2)

P gas permeability coefficient (Barrer)

Q gas flow rate ($cm^3\ s^{-1}$)

R ideal gas constant ($J\ mol^{-1}\ K^{-1}$)

T operating temperature (°C)

p pressure (barg)

x mole fractions of component (% mol.)

δ thickness of the membrane (cm)

Greek letters

$\propto_{i/j}$ selectivity of component i over component j

ρ membrane density ($g\ cm^3$)

Subscripts/superscripts

i, j gas components

F feed

P permeate

S sweep gas

REFERENCES

[1] I. Uehara, Separation and purification of hydrogen, in: O. Tokyo (Ed.), Energy Carriers Convers. Syst. Vol. 1., EOLSS, Paris, 2008: pp. 268–282.

[2] P. Li, Z. Wang, Z. Qiao, et al., Recent developments in membranes for efficient hydrogen purification, J. Memb. Sci. 495 (2015) 130–168.

[3] J.A. Ritter, A.D. Ebner, State-of-the-art adsorption and membrane separation processes for hydrogen production in the chemical and petrochemical industries, Sep. Sci. Technol. 42 (2007) 1123–1193.

[4] J.J. Conde, M. Maroño, J.M. Sánchez-Hervás, Pd-based membranes for hydrogen separation: Review of alloying elements and their influence on membrane properties, Sep. Purif. Rev. 46 (2017) 152–177.

[5] D.F. Sanders, Z.P. Smith, R. Guo, et al., Energy-efficient polymeric gas separation membranes for a sustainable future: A review, Polymer (Guildf). 54 (2013) 4729–4761.

[6] R.W. Baker, B.T. Low, Gas separation membrane materials: A perspective, Macromolecules. 47 (2014) 6999–7013.

[7] K. Liu, C. Song, V. Subramani, Hydrogen and syngas production and purification technologies, Wiley-AIChE, Hoboken, New Jersey, 2009.

[8] H. Yin, A.C.K. Yip, A review on the production and purification of biomass-derived hydrogen using emerging membrane technologies, 7 (2017) 297.

[9] D. Alique, D. Martinez-Diaz, R. Sanz, et al., Review of supported Pd-based membranes preparation by electroless plating for ultra-pure hydrogen production, Membranes (Basel). 8 (2018) 1–39.

[10] W.J. Koros, G.K. Fleming, Membrane-based gas separation, J. Memb. Sci. 83 (1993) 1–80.

[11] F. Wu, L. Li, Z. Xu, et al., Transport study of pure and mixed gases through PDMS membrane, Chem. Eng. J. 117 (2006) 51–59.

[12] S.S. Dhingra, E. Marand, Mixed gas transport study through polymeric membranes, J. Memb. Sci. 141 (1998) 45–63.

[13] J.M. Bermúdez, A. Arenillas, R. Luque, et al., An overview of novel technologies to valorise coke oven gas surplus, Fuel Process. Technol. 110 (2013) 150–159.

[14] S.H. Cho, K.T. Chue, J.N. Kim, A two stage PSA for argon and hydrogen recovery from ammonia purge gas, Chem. Eng. Commun. 163 (1998) 97–109.

[15] S. Agahzamin, A. Mirvakili, M.R. Rahimpour, Investigation and recovery of purge gas streams to enhance synthesis gas production in a mega methanol complex, J. CO2 Util. 16 (2016) 157–168.

[16] W.F. Yong, T.S. Chung, M. Weber, et al., New polyethersulfone (PESU) hollow fiber membranes for CO2 capture, J. Memb. Sci. (2018).

[17] S. Matteucci, Y. Yampolskii, B.D. Freeman, et al., Transport of gases and vapors in glassy and rubbery polymers, in: Mater. Sci. Membr. Gas Vap. Sep., John Wiley & Sons, Ltd, England, 2006: pp. 1–47.

[18] S.C. Kumbharkar, P.B. Karadkar, U.K. Kharul, Enhancement of gas permeation properties of polybenzimidazoles by systematic structure architecture, J. Memb. Sci. 286 (2006) 161–169.

[19] S.M. Nadakatti, J.H. Kim, S.A. Stern, Solubility of light gases in poly(n-butyl methacrylate) at elevated pressures, J. Memb. Sci. 108 (1995) 279–291.

[20] D.H. Malagón-Romero, A. Ladino, N. Ortiz, et al., Characterization of a polymeric membrane for the separation of hydrogen in a mixture with CO2, Open Fuels Energy Sci. J. 9 (2016) 126–136.

[21] S. Shishatskiy, C. Nistor, M. Popa, et al., Polyimide asymmetric membranes for hydrogen separation: Influence of formation conditions on gas transport properties, Adv. Eng. Mater. 8 (2006) 390–397.

[22] O.C. David, D. Gorri, A. Urtiaga, et al., Mixed gas separation study for the hydrogen recovery from H2/CO/N2/CO2 post combustion mixtures using a Matrimid membrane, J. Memb. Sci. 378 (2011) 359–368.

[23] L.A. El-Azzami, E.A. Grulke, Dual mode model for mixed gas permeation of CO2, H2, and N2 through a dry chitosan membrane, J. Polym. Sci. Part B Polym. Phys. 45 (2007) 2620–2631.

[24] K. Tanaka, H. Kita, K. Okamoto, et al., Gas permeability and permselectivity in polyimides based on 3,3',4,4'-biphenyltetracarboxylic dianhydride, J. Memb. Sci. 47 (1989) 203–215.

[25] J. Marchese, E. Garis, M. Anson, et al., Gas sorption, permeation and separation of ABS copolymer membrane, J. Memb. Sci. 221 (2003) 185–197.

[26] I.N. Mohamad, R. Rohani, M.S. Mastarmasdar, et al., Permeation properties of polymeric membranes for biohydrogen purification, Int. J. Hydrogen Energy. 41 (2016) 4474–4488.

[27] M.A. Abd. Hamid, Y.T. Chung, R. Rohani, et al., Miscible-blend polysulfone/polyimide membrane for hydrogen purification from palm oil mill effluent fermentation, Sep. Purif. Technol. 209 (2019) 598–607.

[28] O.C. David, D. Gorri, K. Nijmeijer, et al., Hydrogen separation from multicomponent gas mixtures containing CO, N2 and CO2 using Matrimid® asymmetric hollow fiber membranes, J. Memb. Sci. 419–420 (2012) 49–56.

[29] W.F. Yong, T.S. Chung, M. Weber, et al., New polyethersulfone (PESU) hollow fiber membranes for CO2 capture, J. Memb. Sci. 552 (2018) 305–314.

[30] L. Hao, P. Li, T.S. Chung, PIM-1 as an organic filler to enhance the gas separation performance of Ultem polyetherimide, J. Memb. Sci. 453 (2014) 614–623.

[31] M. Sadrzadeh, M. Amirilargani, K. Shahidi, et al., Pure and mixed gas permeation through a composite polydimethylsiloxane membrane, Polym. Adv. Technol. 22 (2011) 586–597.

[32] X. Li, R.P. Singh, K.W. Dudeck, et al., Influence of polybenzimidazole main chain structure on H2/CO2 separation at elevated temperatures, J. Memb. Sci. 461 (2014) 59–68.

[33] Y. Yampolskii, E. Finkelshtein, Permeability of polymers, in: Membr. Mater. Gas Vap. Sep. Synth. Appl. Silicon-Containing Polym., John Wiley & Sons Ltd, England, 2016: pp. 1–15.

[34] J. Xia, S. Liu, P.K. Pallathadka, et al., Structural determination of extem XH 1015 and its gas permeability comparison with polysulfone and ultem via molecular simulation, Ind. Eng. Chem. Res. 49 (2010) 12014–12021.

[35] V. Abetz, T. Brinkmann, M. Dijkstra, et al., Developments in membrane research: From material via process design to industrial application, Adv. Eng. Mater. 8 (2006) 328–358.

[36] Y. Wang, L. Jiang, T. Matsuura, et al., Investigation of the fundamental differences between polyamide-imide (PAI) and polyetherimide (PEI) membranes for isopropanol dehydration via pervaporation, J. Memb. Sci. 318 (2008) 217–226.

[37] T.A. Barbari, W.J. Koros, D.R. Paul, Polymeric membranes based on bisphenol-A for gas separations, J. Memb. Sci. 42 (1989) 69–86.

[38] H. Koolivand, A. Sharif, M.R. Kashani, et al., Functionalized graphene oxide/polyimide nanocomposites as highly CO2-selective membranes, J. Polym. Res. 21 (2014) 1–12.

[39] M.G. García, J. Marchese, N.A. Ochoa, Improved gas selectivity of polyetherimide membrane by the incorporation of PIM polyimide phase, J. Appl. Polym. Sci. 134 (2017) 1–11.

[40] Y. Li, T.-S. Chung, Silver ionic modification in dual-layer hollow fiber membranes with significant enhancement in CO2/CH4 and O2/N2 separation, J. Memb. Sci. 350 (2010) 226–231.

[41] D. Wang, Doctoral Thesis: Polyethersulfone hollow fibre gas separation membranes prepared from solvent systems containing onsolvent additives, National University of Singapore, 1996.

[42] Y. Li, T.S. Chung, Highly selective sulfonated polyethersulfone (SPES)-based membranes with transition metal counterions for hydrogen recovery and natural gas separation, J. Memb. Sci. 308 (2008) 128–135.

[43] Z. Huang, Y. Li, R. Wen, et al., Enhanced gas separation properties by using nanostructured PES-zeolite 4A mixed matrix membranes, J. Appl. Polym. Sci. 101 (2006) 3800–3805.

[44] P.P. Products, Datasheet Polybenzimidazole, 2017.

APPENDIX

Table A.3.1. Configuration of the gas chromatograph

GC-TRACERA 2010	**Column A**	**Column B**
Column type	Molecular sieve	Fused silica
Column ID	SH/Rt®/Msieve 5A	Carboxen® 1010 Plot
Dimensions	30m x 0.5 mm, ID=0.53 mm	30m x 0.5 mm, ID=0.32 mm
Separating species	H_2, N_2, CH_4, CO	CO_2
Injector mode	SPL	WBI
Carrier gas	He	
Detector type	BID (Barrier Dischage Ionization)-2010 Plus A	

Table A.3.2. Gas chromatographic method for analyzing the permeate stream

GC-TRACERA 2010	**Column A**	**Column B**
Column type	Molecular sieve	Fused silica
Separating species	H_2, N_2, CH_4, CO	CO_2
Column temperature program (°C)	100°C (9 min)	100°C (9 min)
Column flow (ml min^{-1})	6.45	1.12
Linear velocity (cm sec^{-1})	46.1	23.0
Carrier gas	He	
Flow control mode	Initial pressure at 50 kPa	
Pressure program	Pressure at 50 kPa (2 min)	Pressure at 50 kPa (1 min) + 20 kPa min^{-1} to 120 kPa (4 min)
Injection mode	Split (5:1)	Direct
Injection port temperature (°C)	150	150
Detector temperature (°C)	250	250
Discharge gas flow (ml min^{-1})	50	50
Injection size (µL)	500	500

The configuration and conditions of the gas chromatographic methods for analyzing permeate and retentate streams are detailed in Tables A.3.1 - A.3.3, respectively. The total acquisition time of both proposed methods was 9 min. For the proposed method to analyze the permeate stream, the retention times were 2.028 min for H_2, 2.910 min for N_2, 3.698 min for CH_4, 4.584 min for CO, and 6.894 min for CO_2, with a window width of 5 %. For the second method to detect gas concentrations at retentate side, the retention times were 1.984 min for H_2, 2.883 min for N_2, 3.666 min for CH_4, 4.487 min for CO, and 6.579 min for CO_2, with also a window width of 5%.

Table A.3.3. Gas chromatographic method for analyzing the retentate stream

GC-TRACERA 2010	**Column A**	**Column B**
Column type	Molecular sieve	Fused silica
Separating species	H_2, N_2, CH_4, CO	CO_2
Column temperature program (°C)	100°C (9 min)	100°C (9 min)
Column flow (ml min^{-1})	6.45	1.12
Linear velocity (cm sec^{-1})	46.1	23.0
Carrier gas	He	
Flow control mode	Initial pressure at 50 kPa	
Pressure program	Pressure at 50 kPa (2 min)	Pressure at 50 kPa (1 min) + 20 kPa min^{-1} to 120 kPa (4 min)
Injection mode	Split (50:1)	Direct
Injection port temperature (°C)	150	150
Detector temperature (°C)	250	250
Discharge gas flow (ml min^{-1})	50	50
Injection size (µL)	500	500

CHAPTER 4

PRESSURE SWING ADSORPTION AS AN ALTERNATIVE FOR UPCYCLING OF SURPLUS HYDROGEN

4.1 INTRODUCTION

In the ammonia synthesis process, a stream of up to 180 – 240 Nm^3 per ton of ammonia is purged to keep the inert gases concentration below a threshold value; this stream contains large hydrogen quantities, which could be recovered. The general output conditions and its composition are detailed in Table 4.1. In more recent designs, this hydrogen is mostly recovered and recycled to the synthesis loop via membrane contactors or cryogenic systems, but some part of the cleaned purge gas is usually added to the reformer fuel, or even directly released to the atmosphere [1,2].

Table 4.1. Case study of ammonia purge gas (APG) parameters [3–5]

Specifications	Value
Purge gas flow rate ($Nm^3\ t^{-1}\ NH_3$)	180 - 240
Purge gas pressure (bar)	150 - 200
Temperature (°C)	*ca.* 20
Gas composition (% vol.)	-
H_2	58.0
N_2	25.0
CH_4	15.0
Ar	2.0

A significant research effort has been already undertaken to upgrade ammonia synthesis vent gas (hereinafter called ammonia purge gas (APG)), which contains impurities, and improve hydrogen end-use. In 1998, Soon-Haeng Cho et al. reported a two-stage pressure swing adsorption (PSA) process packed with 13X zeolite for argon and hydrogen recovery, simultaneously [6]. Although that study obtained high-hydrogen purity (> 99 %) in a pilot-plant PSA, there is a lack of information regarding hydrogen recovery and the impurity content of the light product stream. Among other purification technologies under study, a catalytic Pd–Ag membrane reactor to produce pure hydrogen from ammonia purge gases has been reported by Rahimpour et al. [7,8]. Recently, a different research work evaluated the integrated configuration of the catalytic H_2-permselective membrane reactor and a solid oxide fuel cell for the flare and purge gas recovery from ammonia plants [9]. In 2013, Karami et al. modeled the ammonia separation from purge gases in microporous hollow fiber membrane contactors [10]. Qiang Sun et al. stated the separation of tail gases of ammonia plant via continuous hydrates formation with tetra-n-butylammonium bromide (TBAB) [11]. Recently, Okedi et al. examines the effect of ammonia decomposition product gas mix (containing $75H_2$:$25N_2$) to supply a polymer electrolyte membrane fuel cells (PEMFC) operating in dead-ended anode mode. To our knowledge, no study has yielded significant results in terms of performance as well as cost for upgrading H_2 via four-column PSA unit using purge gases from ammonia industry.

In this chapter, the overall goal was to evaluate experimentally a four-column PSA process for purifying hydrogen-containing gas that meets the fuel cell requirements, by using a multicomponent gas mixture as a simulated APG. Within the major aim, a number of specific objectives were identified. Firstly, the adsorption equilibrium isotherms of H_2, N_2, CH_4, and Ar on several commercially adsorbents were obtained and, the most suitable adsorbent was selected and further characterized. Then, adsorptive properties of the selected adsorbent were confirmed by single and multicomponent breakthrough runs and simulations. Once the breakthrough times were obtained for a single column, a design-of-experiments (DoE) was conducted to optimize the lab four-column PSA unit to produce target hydrogen purities at maximum recoveries. In addition to the technical performance, a brief economic analysis is provided for the hydrogen purification.

This work was developed in the Faculty of Engineering in the University of Porto (FEUP), in Porto, Portugal, during a three-month research stay, under the supervision of Prof. Dr. Adélio Miguel Magalhães Mendes, and in collaboration with the PhD candidate Frederico Relvas.

4.2 EXPERIMENTAL PROCEDURE

4.2.1 MATERIALS

For accomplishing the hydrogen purification, a set of four commercial adsorbents was selected based on the removal of weak adsorbates (N_2 and Ar), and the corresponding properties are presented in Table 4.2. These adsorbents are an activated carbon (2GA-H2, Kuraray CO., Ltd., Japan) and zeolites LiX (ZEOX Z12-07, Zeochem AG, Switzerland), 13X (13XBFK, CWK-Chemiewerk Bad Köstritz, Germany) and 5A (5ABFK, CWK). Figure 4.1 shows photographs of these four adsorbents.

Table 4.2. Physical properties of the studied adsorbents

Adsorbent	Type	Cation	Structure	d_p (mm)	ρ_p (g cm^{-3})
AC	Pellet	-	Amorphous	1.2	2.1 ± 0.1
13X	Spherical	Na^+	X	1.6 - 2.5	2.3 ± 0.1
5A			A	1.6 - 2.5	2.3 ± 0.1
LiX		Li^+	X	0.4 - 0.8	2.4 ± 0.1

Prior to the isotherm measurements, zeolites were regenerated at 375 °C overnight under synthetic flow of air. After regeneration, the temperature was allowed to decrease slowly at 1 °C min^{-1}. Helium pycnometry was performed to determine the structural volume of the samples and then the density of the adsorbents ρ_p. For the multicomponent breakthrough experiments, a tank was used to prepare the synthetic gas mixture under study. All gases in this study had purities higher than 99.99 % and were supplied by Linde.

Figure 4.1. Photos of the adsorbent materials under study

4.2.2 METHODS

4.2.2.1 Equilibrium isotherms

4.2.2.1.1 Experimental set-up

Single-component adsorption isotherms were obtained using the volumetric method, described elsewhere [12] and pictured in Figure 4.2, for H_2, N_2, CH_4 and Ar at different temperatures (20 °C, 40 °C and 60 °C) and pressure up to 7 bar. By a mass balance, assuming ideal gas behavior and knowing the pressure decay inside the sample vessel or Tank B, which initially has been evacuated to P < 0.01 mbar using a vacuum pump, it is possible to determine the amount of adsorbed gas.

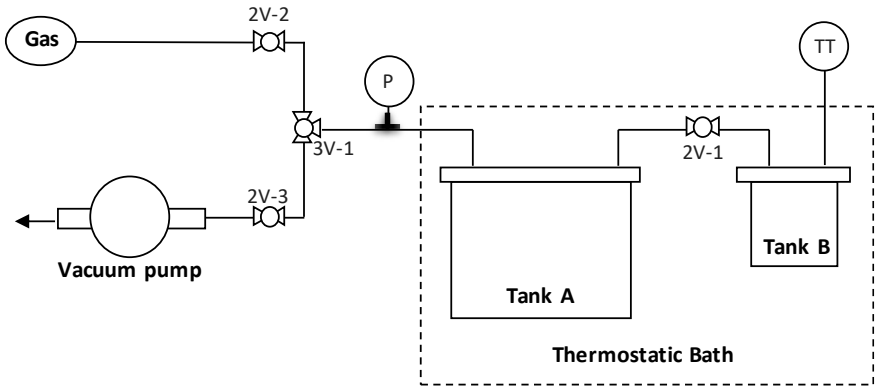

Figure 4.2. Sketch of volumetric method apparatus. 2V, 2-way valve; 3V, 3-way valve; TT, thermocouple; P, pressure transducer.

4.2.2.1.2 Adsorption isotherm models

In this work, adsorption equilibrium isotherms were fitted to the dual site Langmuir (DSL) equation, according to Eq. (4.1). This model was selected because it has good accuracy for fitting the experimental isotherm data, which is more accurate than Langmuir model [13].

$$q_{\mathrm{i}}^{*} = \frac{q_{\mathrm{max},1} \cdot b_1 \cdot P_{\mathrm{i}}}{1 + b_1 \cdot P_{\mathrm{i}}} + \frac{q_{\mathrm{max},2} \cdot b_2 \cdot P_{\mathrm{i}}}{1 + b_2 \cdot P_{\mathrm{i}}} \qquad \text{Eq. (4.1)}$$

where q_{i}^{*} is the molar concentration in the adsorbed phase (mol kg^{-1}), $q_{\mathrm{max},1}$ and $q_{\mathrm{max},2}$ are the maximum adsorbed concentration on sites 1 and 2, respectively (mol kg^{-1}); P_{i} is the partial pressure in the gas phase (bar); and b_1 and b_2 are the affinity constants for site 1 and 2, respectively (bar^{-1}). Obtaining the adsorption isotherms at three different temperatures, T_1 to T_3, allows determining the heats of adsorption using Eqs. (4.2) – (4.3), where b_∞ is the pre-exponential factor of the affinity constant and R is the gas constant. For the breakthrough simulations, which are further described below, it was assumed that the heats of adsorption on the first and second sites are equal ($\Delta H_1 = \Delta H_2$).

$$b_1 = b_{\infty,1} \cdot \mathrm{e}^{\Delta H_1 / \mathrm{R}T} \qquad \text{Eq. (4.2)}$$

$$b_2 = b_{\infty,2} \cdot \mathrm{e}^{\Delta H_2 / \mathrm{R}T} \qquad \text{Eq. (4.3)}$$

Thus, parameters $q_{\mathrm{max},1}$, $q_{\mathrm{max},2}$, $b_{\infty,1}$, $b_{\infty,2}$, ΔH were calculated by a non-linear data fitting of the experimental adsorption isotherms, minimizing the residual sum of squares RSS, as follows:

$$RSS\ (\%) = \sum_{T=T_1}^{T_3} \sum_{k=1}^{N} \left(q_{\mathrm{i,exp}}^{*} - q_{\mathrm{i,mod}}^{*}\right)^2 \qquad \text{Eq. (4.4)}$$

with $q_{\mathrm{i,exp}}^{*}$ and $q_{\mathrm{i,mod}}^{*}$ as the experimental and estimated adsorbed concentration, respectively; k is the number of data points per experimental isotherm and gas component; and N is total number of experimental points. The equilibrium separation factor $\alpha_{\mathrm{i/j}}$ was used to assess the adsorbent ability to separate the gases under study, which is usually expressed using Eq. (4.5) [14,15]:

$$\alpha_{\mathrm{i/j}} = \frac{q_{\mathrm{i}}^{*} / q_{\mathrm{j}}^{*}}{P_{\mathrm{i}} / P_{\mathrm{j}}} \qquad \text{Eq. (4.5)}$$

where q_{i}^{*} and q_{i}^{*} are the molar loading of species i and j at partial pressure of P_{i} and P_{j}, respectively, under the process conditions. Therefore, separation factor in equilibrium-based separation processes indicates the effectiveness of the separation performance between gases i and j by the considered adsorbent, and therefore they are discussed in the following section.

4.2.2.2 Adsorption breakthroughs

4.2.2.2.1 Experimental set-up

A set of breakthrough experiments was carried out in a fixed-bed column for the selected 5A zeolite adsorbent, recording the history of the outlet stream composition. From the breakthrough curves, the amount of gas adsorbed can be evaluated allowing to validate the adsorption equilibrium isotherms. Moreover, one can evaluate the duration of the adsorption step in the PSA cycle [16].

Single and multicomponent breakthrough experiments were conducted in an experimental set-up as described elsewhere [17] and schematically pictured in Figure 4.3. The lab set-up is placed in a thermostatic chamber to ensure isothermal operation, where the packed column with the selected adsorbent is equipped with two thermocouples and two pressure transducers at the entrance and the exit of the column; the process pressure is handled using a high precision backpressure regulator (Equilibar EB1LF2). The feed flow rate is controlled using Bronkhorst mass flow controllers' series F-201C (0–0.1 L_N min^{-1}), F-112CV (0–1 L_N min^{-1}) and F-201CV (0–10 L_N min^{-1}), and a mass flow meter series F-111C (0–3 L_N min^{-1}) for measuring the exit flowrate. The composition of the outlet gas is determined using a mass spectrometer (Pfeiffer GSD 301 O2). The characteristics of the column and the experimental conditions are detailed in Table 4.3.

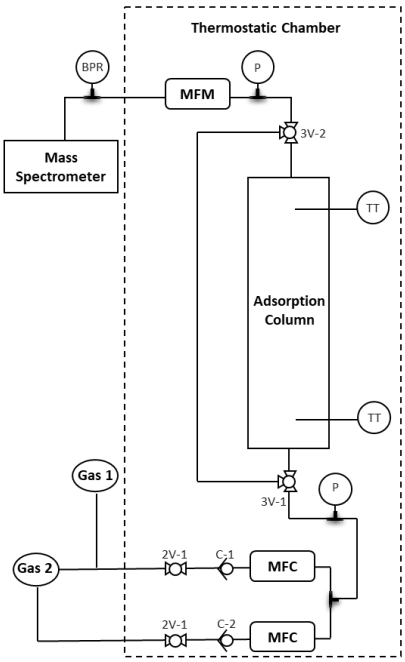

Figure 4.3. Single adsorption column flow diagram. MFC, flow controller; MFM, flow meter; 2V, 2-way valve; 3V, 3-way valve; C, check valve; TT, thermocouple; P, pressure transducer; BPR, back pressure regulator.

Adsorption and desorption breakthrough measurements were carried out at 40 °C, varying the pressure and feed flow rate. After each adsorption assay, desorption breakthroughs were performed passing pure He through the column. Owing to the available mass spectrometer could not operate with streams with a molar hydrogen concentration > 20 %, the measurements were carried out using gas mixtures balanced with He.

Table 4.3. Characteristics of the column and experimental conditions

Column characteristics	**Value**
L_{bed} (cm)	33.8
d_{in} (cm)	3.16
d_0 (cm)	3.49
TT distance (cm)	2.5
Adsorbent type	5A zeolite
m_{ads} (g)	193.12
Feed conditions	**Value**
He:N_2	75:25
He:Ar	98:2
He:CH_4	85:15
He:H_2	80:20
He:H_2:N_2:Ar:CH4	38:20:25:2:15
Q_{F} (L_N min^{-1})	0.5 / 2.75
P (bar)	1 / 4.5
T(°C)	*ca.* 40

4.2.2.2.2 Modeling and simulation of breakthrough curves

The breakthrough curves were simulated using Aspen Adsorption® V.10; the partial differential equations (PDEs) corresponding to mass, energy and momentum balances are discretized over an uniform grid using algebraic approximations with suitable boundary and initial conditions. The first order space derivative was approximated using an upwind differencing scheme (UDS) applied in 60 nodes. The resulting ordinary differential equations (ODEs) are further integrated in time. Accordingly, a non-isothermal and non-adiabatic model was applied using measured parameters (isotherm parameters, bed geometry, etc.) and other properties, for instance, heat capacity and conductivity, as input values found in the literature. The main assumptions of the mathematical model used for simulating breakthrough curves are [16,18]:

- ideal gas behavior throughout the column.
- negligible radial gradients (P, T, y).
- non-isothermal and non-adiabatic conditions with gas and solid heat conduction.
- the adsorption rate is approximated by the linear driving force (LDF) model.

- convection with constant dispersion for all components through the bed based on the axial dispersed plug flow-model.
- adsorption equilibrium described by DSL isotherms, forcing the heat of adsorption of each site to be equal.
- pressure drop described by Ergun's equation.
- constant heat transfer coefficients.
- constant and homogeneous bed porosity along the bed length.

According to these assumptions, the governing equations and input values are fully explained in Appendix at the end of this chapter. After that, this model was validated by comparing simulations with breakthrough experiments.

4.2.2.3 Experimental PSA unit

4.2.2.3.1 Process description

A four-column PSA was optimized to produce hydrogen for fuel cells applications from a synthetic mixture based on purge gases from ammonia industry. A photograph of the PSA unit is shown in Figure 4.4, and a sketch of the PSA unit, described elsewhere [19], is shown in Figure 4.5. The PSA unit was packed with 5A zeolite and a fifth column was used as a tank to store part of the product needed for the selected adsorption cycle. Additionally, two tanks were installed, one for minimizing pressure fluctuations and the other for collecting the light product. The packed columns were made of stainless steel with a length of 34.5 cm, an inner diameter of 2.7 cm, and a wall thickness of 0.15 cm. Three Bronkhorst mass flow meters' series F-112AC (0 - 20 $L_N\ min^{-1}$), F-111C (0 - 2 $L_N\ min^{-1}$), and F-111B (0 - 3 $L_N\ min^{-1}$) were used to measure the flow rate of the feed, purge and product streams, respectively. A needle valve was placed at the top of the columns to regulate the purge and backfill flowrates. A Bronkhorst pressure controller series P-702CV (0 - 10 bar) was placed after the product tank to maintain constant light product pressure. Four pressure transducers at the bottom of each bed were used to obtain the pressure history during operation. Check valves and solenoid valves were installed to direct the flow according to the PSA cycle and prevent reverse flow. The analysis of the cyclic steady state outlet gas composition was performed using an online gas chromatograph (Dani GC 1000 equipped with a TCD detector). N_2 and Ar concentration was measured as a whole concentration. The detection limit in all cases, N_2 + Ar and CH_4 concentrations, were assumed to be < 100 ppm. All instruments were connected to a computer using a data acquisition card (LabView interface); a routine written in the LabView platform was used for acquiring all data while a Visual Basic routine was used for controlling the solenoid valves according to the PSA cycle.

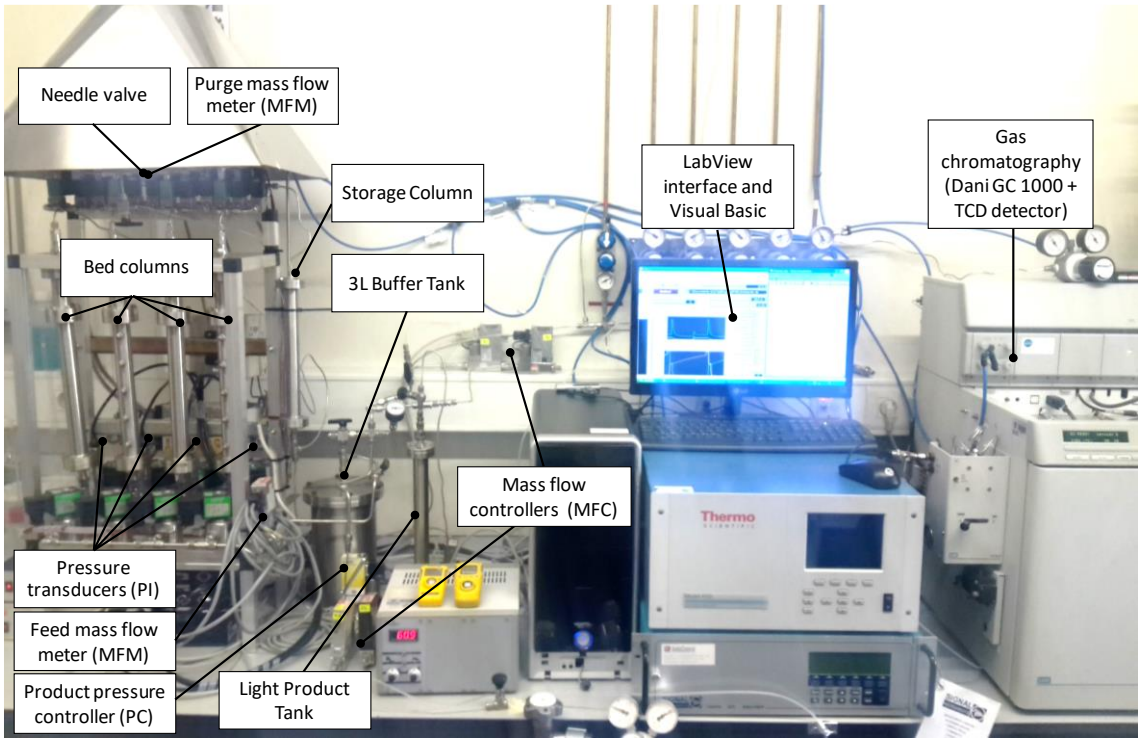

Figure 4.4. Pilot plant PSA system

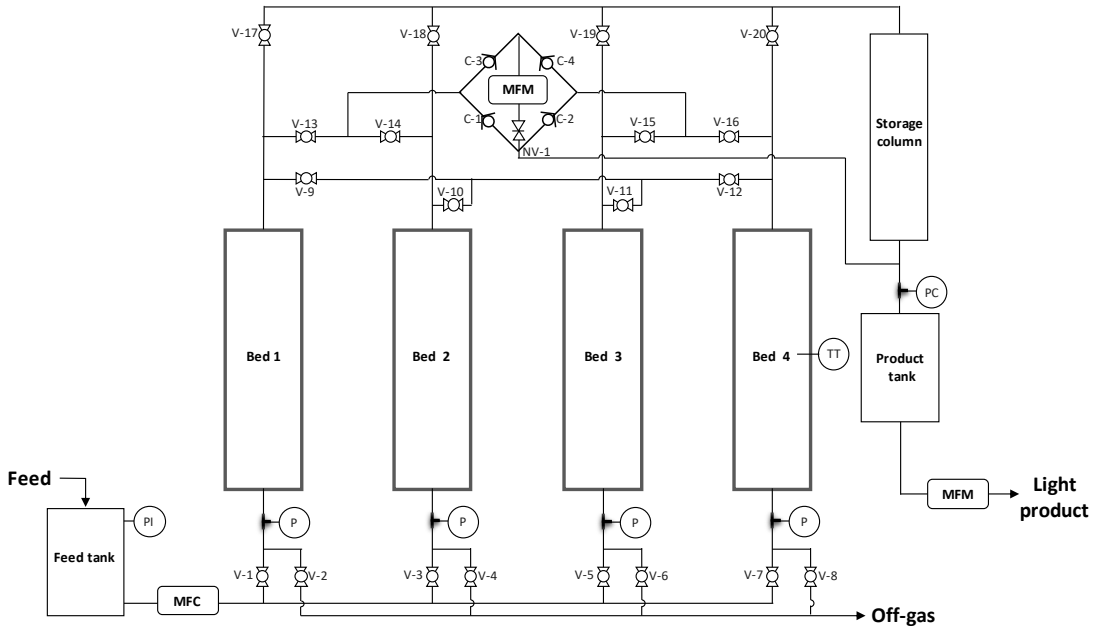

Figure 4.5. Schematic of the four-column PSA system. MFC, flow controller; MFM, flow meter; V, Solenoid vales; C, check valve; NV, Needle valve; TT, thermocouple; P, pressure transducer; PC, pressure controller.

During the PSA cycle, each column runs 9 elementary steps with different durations resulting in a 12-events cycle as described (following the step sequences of Bed 1): I) adsorption (AD) at the high pressure, II) H_2 product is split in two parts (AD/BF); one part of the stream flows to the storage column and the other is conducted to pressurize (backfill) Bed 2, which is the next adsorption bed, III) depressurization pressure equalization (DPE) down to an average pressure between Bed 1 and Bed 3, IV) blowdown (BD) to the low cycle pressure, V) purge with H_2 product (PG), VI) Idle (IDLE), VII) first pressurization pressure equalization (FPPE) up to an average pressure between Bed 1 and Bed 3, VIII) backfill with H_2 product (BF) and IX) second pressurization pressure equalization (SPPE) with the effluent from the producing Bed 4.

Before operation, the PSA was pressurized with H_2 at the adsorption high pressure. The cyclic sequence for the process and a typical pressure history along the cycle are given in Table 4.4 and Figure 4.6, respectively. The longer cycle steps (AD, PG, IDLE, BF) have a duration of t_{ad}= 60 - 90 s, whereas the shorter cycle steps (AD/BF, DPE, BD, FPPE, SPPE) were fixed at t_{eq}= 4 s.

Table 4.4. Sequence of 12-events PSA cycle

Events	**1**	**2**	**3**	**4**	**5**	**6**	**7**	**8**	**9**	**10**	**11**	**12**
Bed 1	AD		AD/BF	DPE	BD	PG		IDLE		FPPE	BF	SPPE
Bed 2	FPPE	BF	SPPE	AD		AD/BF	DPE	BD	PG		IDLE	
Bed 3	PG	IDLE		FPPE	BF	SPPE	AD		AD/BF	DPE	BD	PG
Bed 4	DPE	BD	PG	IDLE		FPPE	BF	SPPE	AD			AD/BF

Note: Adsorption (AD), providing backfill (AD/BF), depressurization pressure equalization (DPE), blowdown (BD), purge (PP), idle (IDLE), first pressurization pressure equalization (FPPE), backfill (BF), second pressurization pressure equalization (SPPE).

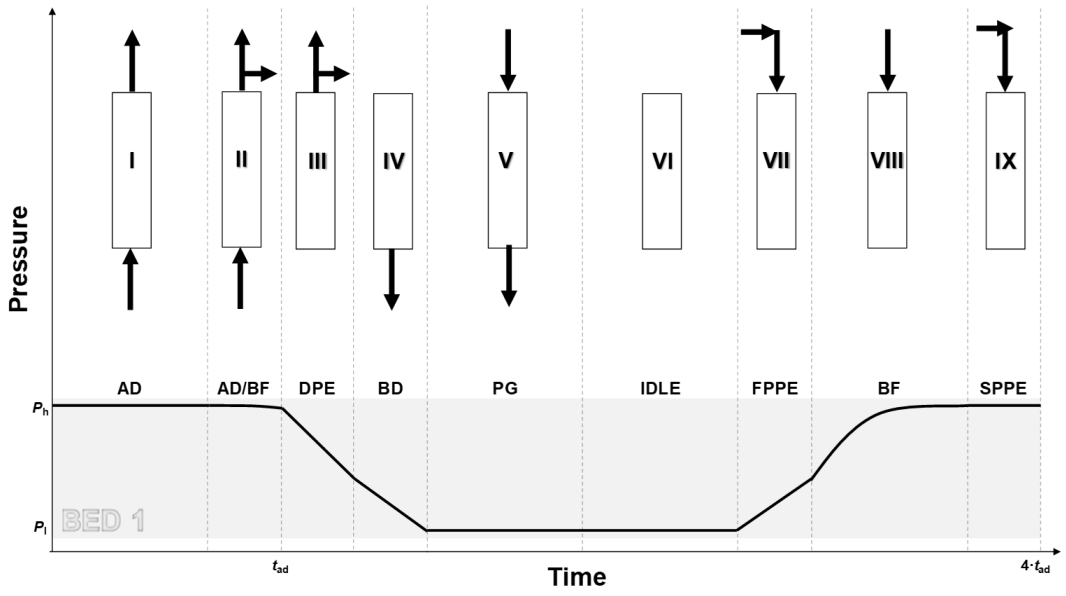

Figure 4.6. Schematic diagram of the cycle sequences used in the PSA experiments

4.2.2.3.2 Experimental design

In this study, 9-step 4-bed PSA experiments were carried out under various operating conditions. The system performance depends on several process variables such as temperature of operation, cycle sequence, high and low operating pressures, purge-to-feed P/F ratio, etc.

Herein, P/F ratio; adsorption pressure, P_{h}; and adsorption time, t_{ad}, which includes time of elementary steps I and II, $t_{\mathrm{ad}} = t_{\mathrm{I}} + t_{\mathrm{II}}$, were selected as three dimensionless factors. Other variables were preset at defined values, such as low operating pressure P_{l} = 1 bar; feed flow rate, Q_{F} = 2 L_N min^{-1} and equalization time, t_{eq} = 4 s. To compare performances among the PSA operations, the performance indicator parameters were assessed in terms of hydrogen purity, HP, as well as productivity and recovery, HR, defined as shown in the following Eqs. (4.6) – (4.8) [13,20]:

$$HP = \frac{\int_0^{t_{\mathrm{ad}}} y_{\mathrm{H_2}}^P \cdot Q^P dt}{\sum_{i=1}^{n} \int_0^{t_{\mathrm{ad}}} y_i^P \cdot Q^P dt} \cdot 100 \qquad \text{Eq. (4.6)}$$

$$HR = \frac{\int_0^{t_{\mathrm{ad}}} y_{\mathrm{H_2}}^P \cdot Q^P dt}{\int_0^{t_{\mathrm{ad}}} y_{\mathrm{H_2}}^F \cdot Q^F dt} \cdot 100 \qquad \text{Eq. (4.7)}$$

$$Productivity = \frac{\sum_{i=1}^{n} \int_0^{t_{\mathrm{ad}}} y_i^P \cdot Q^P dt}{m_{\mathrm{ads}} \cdot t_{\mathrm{cycle}}} \qquad \text{Eq. (4.8)}$$

The influence of the aforementioned factors on the system performance has been assessed and optimized following a DoE methodology [21]. This creates a factorial experimental plan by both reducing the number of experimental runs required and also maximizing the accuracy of the results obtained [22]. Response surface methodology (RSM) uses multiple regression analysis to relate predicted response with the independent factors [23]. RSM analysis was conducted using the statistical software JMP 7.0 (SAS Institute Inc.). In this work, it was used a central composite design (CCD) method for the factorial study that combines two-level three-factorial points, 2^3, plus 2x3 axial points, with two replicas at the center point, leading to a total number of sixteen experiments [24] (See Figure 4.7).

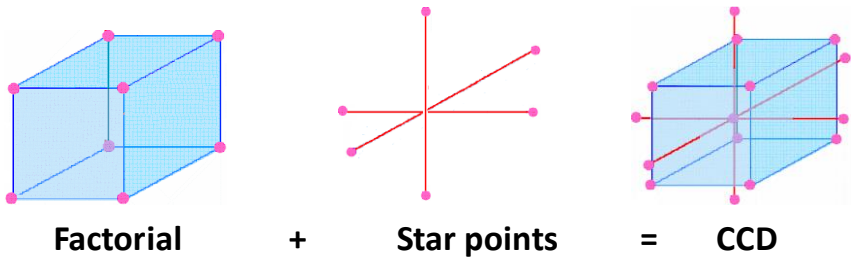

Figure 4.7. Central composite design (CCD) method

For generating design matrices, three dimensionless factors X_i, for each independent factor, ranging from -1 to +1 as the lower and upper limits, have been coded according to:

$$X_1 = \frac{t_{ad} - \bar{t}_{ad}}{\frac{t_{ad,+1} - t_{ad,-1}}{2}}; \quad X_2 = \frac{P_h - \bar{P}_h}{\frac{P_{h,+1} - P_{h,-1}}{2}}; \quad X_3 = \frac{P/F - \overline{P/F}}{\frac{P/F_{+1} - P/F_{-1}}{2}} \qquad \text{Eq. (4.9)}$$

The experimental values were fitted to an empirical second-order polynomial equation, which describes the effect of the selected factors upon the process responses as represented in Eq. (4.10):

$$\hat{y}\,(HP; HR) = \beta_0 + \beta_1 X_1 + \beta_2 X_2 + \beta_3 X_3 + \beta_4 X_2 X_1 + \beta_5 X_1 X_3 + \beta_6 X_2 X_3 + \beta_7 {X_1}^2 + \beta_8 {X_2}^2 + \beta_9 {X_3}^2 \qquad \text{Eq. (4.10)}$$

where (β_0), (β_1, β_2, β_3), (β_4, β_5, β_6), and (β_7, β_8, β_9) represent the intercept, linear, interaction, and quadratic coefficients, respectively. The analysis of variance (ANOVA) of the data was performed to assess the fitness of the polynomial model. The parameters significance was characterized by the p-value, while the coefficient of determination R^2, and the root-mean-square error RMSE, were used to assess the model fitness and accuracy. According to Eq. (4.10), optimization of the response $\hat{y}$ can be applied based on purity requirements for industrial use, road vehicle or stationary applications; meanwhile hydrogen recovery is maximized. Conforming to screening experiments and literature data, the ranges of the factors as well as the operating conditions of the PSA tests were selected and shown in Table 4.5.

Table 4.5. Operating conditions of the PSA runs

Column characteristics		**Value**
L_{bed} (cm)		35
d_{in} (cm)		2.7
d_0 (cm)		3.0
TT distance (cm)		15
Adsorbent type		5A zeolite
m_{ads} (g)		136.1 ± 0.7
Fixed conditions		**Value**
H_2:N_2:Ar:CH_4 (% vol.)		58:25:15:2
Q_F (L_N min^{-1})		2
P_l (bar)		1
T(°C)		*ca.* 25
t_{eq} (s)		4
t_{cycle} (s)		$4 \cdot t_{ad}$
Minimum number of PSA cycles		40
Variable conditions		
Symbol	**Lower bound**	**Upper bound**
P/F (-)	0.1	0.2
t_{ads} (s)	60	90
P_h (bar)	7	9

4.3 RESULTS AND DISCUSSION

4.3.1 ADSORPTION EQUILIBRIA

Adsorption isotherms of the pure gases H_2, N_2, CH_4, and Ar were obtained on the material adsorbents given in Table 4.2, for three temperatures (20 °C, 40 °C and 60 °C) and pressures up to 7 bar. According to the adsorption isotherms plotted in Figures 4.8 - 4.11, a general trend can be seen for all the candidate adsorbents. The order of adsorption capacity on the studied adsorbents up to 7 bar is H_2 < Ar < N_2 < CH_4. It is also observed that the adsorbed concentration increases with pressure with a linear trend for H_2 and Ar, and slightly favorable isotherms for N_2 and CH_4. On the contrary, the adsorption capacity decreases when the temperature increases due to the exothermic behavior, according to Eq. (4.1). As illustrated in Figures 4.8 - 4.11, dotted lines represent the DSL model, which is shown to suitably represent the experimental data due to it has good flexibility for fitting it. The parameters of the DSL model are summarized in Tables 4.6 - 4.9 for each adsorbent under study.

In the 5A zeolite, the adsorbed concentration of H_2 at 20 °C and 2 bar is 0.049 mol kg^{-1}, which is in agreement with similar studies in literature; i.e., ≈ 0.036 mol kg^{-1} at 20 °C [25] and ≈ 0.028 mol kg^{-1} at 25 °C [26]. Regarding the equilibrium adsorbed concentrations of other adsorbates at the same conditions, Ar is 0.331 mol kg^{-1}, N_2 is 0.967 mol kg^{-1} and CH_4 is 1.503 mol kg^{-1}. For this material, relatively lower adsorbed concentrations have been reported in literature; i.e., for N_2, ≈ 0.5 - 0.8 mol kg^{-1} at 20 - 30 °C and CH_4, ≈ 1.2 - 1.4 mol kg^{-1} at 30 °C [25,27,28]. In contrast, there is a lack of data for the adsorbed concentration of Ar on this material. The adsorption isotherms confirm that 5A zeolite is a suitable adsorbent for hydrogen purification due to its low H_2 adsorption capacity compared with the values obtained for the other gases (N_2, CH_4, and Ar). The adsorption heat of the studied gases follows the same trend as the adsorption capacities described above, and these parameters are in accordance with those reported for N_2 and CH_4 on zeolite 5A elsewhere [25,27].

For 13X zeolite, the adsorption capacities of pure gases at 20 °C and 2 bar are 0.045 mol kg^{-1} of H_2, 0.283 mol kg^{-1} of Ar, 0.646 mol kg^{-1} of N_2 and 1.033 mol kg^{-1} of CH_4. These values are relatively slower in comparison with the above-mentioned results using 5A zeolite, thus the equilibrium separation factors of H_2 over the other gases are expected to be lower.

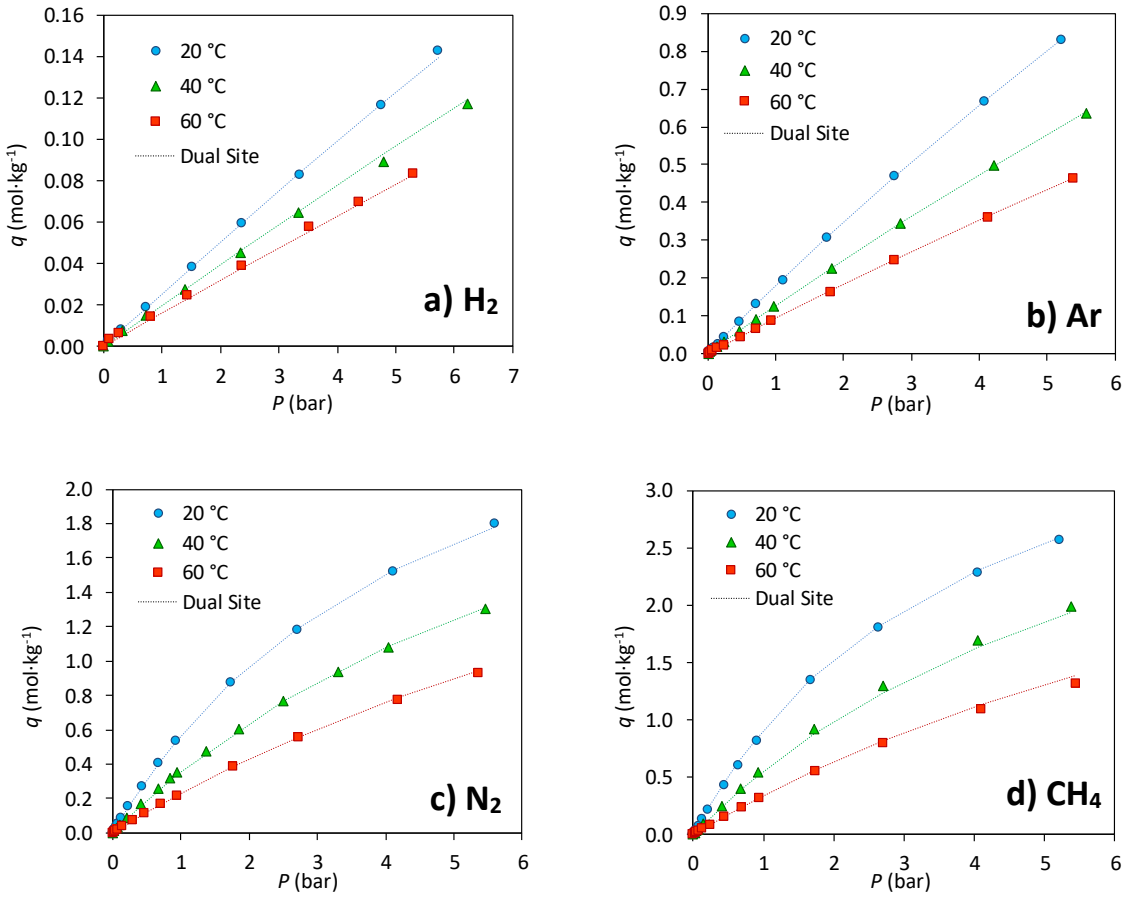

Figure 4.8. Adsorption isotherms on 5A zeolite for a) H_2, b) Ar, c) N_2 and d) CH_4 at 20 °C (blue); 40 °C (green); and 60 °C (red).

Table 4.6. Dual-site Langmuir parameters on 5A zeolite

Parameter	Units	H_2	N_2	CH_4	Ar
$q_{max,1}$	mol kg^{1}	2.58	2.37	2.79	1.69
$b_{\infty,1}$	bar^{-1}	$2.01 \cdot 10^{-4}$	$3.60 \cdot 10^{-5}$	$1.91 \cdot 10^{-5}$	$1.63 \cdot 10^{-4}$
$\Delta H_1 = \Delta H_2$	kJ mol^{-1}	9.45	20.88	23.13	13.88
$q_{max,2}$	mol kg^{-1}	0.39	0.95	1.76	5.0
$b_{\infty,2}$	bar^{-1}	$3.12 \cdot 10^{-5}$	$4.85 \cdot 10^{-5}$	$1.90 \cdot 10^{-5}$	$6.99 \cdot 10^{-5}$
RSS	%	$5.64 \cdot 10^{-5}$	$1.98 \cdot 10^{-3}$	$2.48 \cdot 10^{-2}$	$6.10 \cdot 10^{-5}$

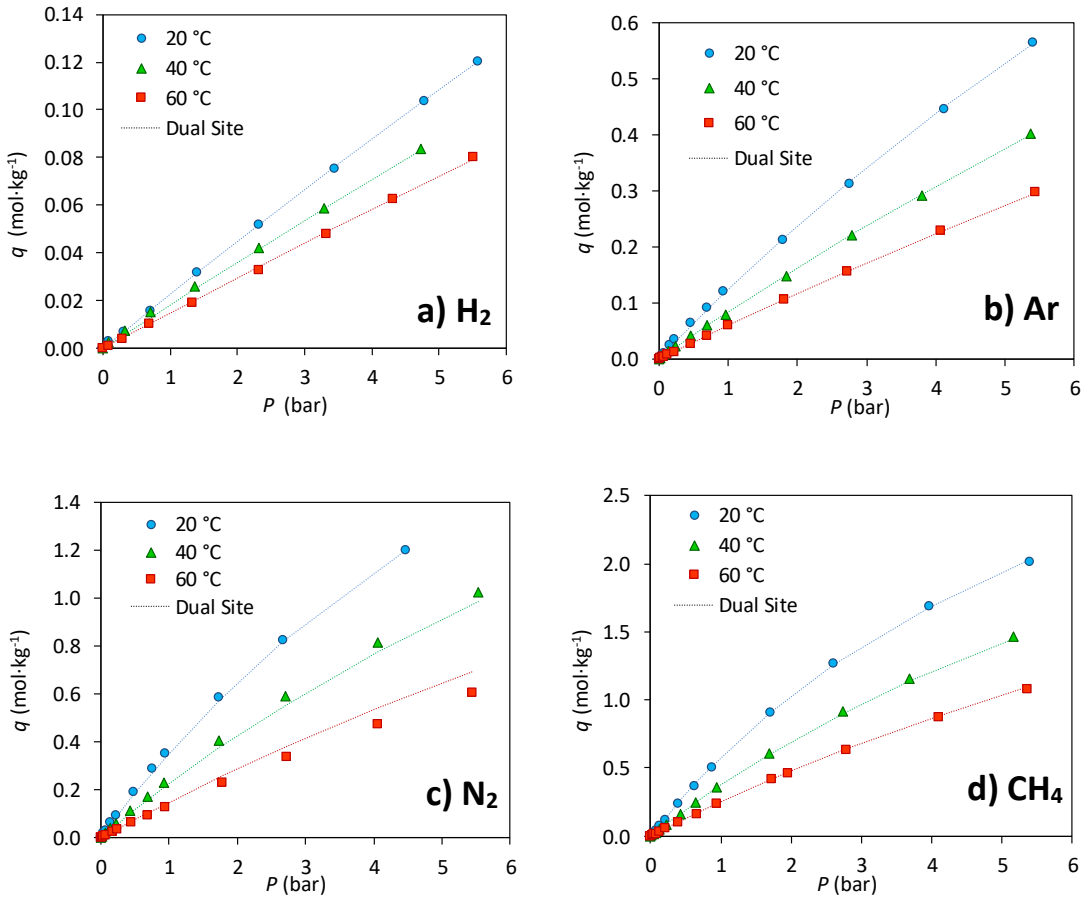

Figure 4.9. Adsorption isotherms on 13X zeolite for a) H_2, b) Ar, c) N_2 and d) CH_4 at 20 °C (blue); 40 °C (green); and 60 °C (red).

Table 4.7. Dual-site Langmuir parameters on 13X zeolite

Parameter	Units	H_2	N_2	CH_4	Ar
$q_{max,1}$	mol kg^{-1}	0.78	2.90	2.56	2.93
$b_{\infty,1}$	bar^{-1}	$1.28 \cdot 10^{-4}$	$3.94 \cdot 10^{-5}$	$7.07 \cdot 10^{-5}$	$8.18 \cdot 10^{-5}$
$\Delta H_1 = \Delta H_2$	kJ mol^{-1}	8.63	18.65	18.51	15.32
$q_{max,2}$	mol kg^{-1}	1.43	1.12	2.14	4.24
$b_{\infty,2}$	bar^{-1}	$3.97 \cdot 10^{-4}$	$6.31 \cdot 10^{-5}$	$7.08 \cdot 10^{-5}$	$1.02 \cdot 10^{-5}$
RSS	%	$1.81 \cdot 10^{-5}$	$2.33 \cdot 10^{-2}$	$2.25 \cdot 10^{-3}$	$2.29 \cdot 10^{-4}$

Other samples of this material in literature show similar capacities; i.e., for N_2, ≈ 0.5 mol kg^{-1} and CH_4, ≈ 1.1 mol kg^{-1} [29] at 25 °C and 2 bar, and for H_2, ≈ 0.04 mol kg^{-1} and CH_4, ≈ 0.45 mol kg^{-1} [30] at 35 °C and 2.5 bar. No data has been found concerning the adsorbed concentration of Ar on the given material. Besides, the heat adsorption of the gases are in the range of those reported for N_2 and CH_4 by other authors [27,31].

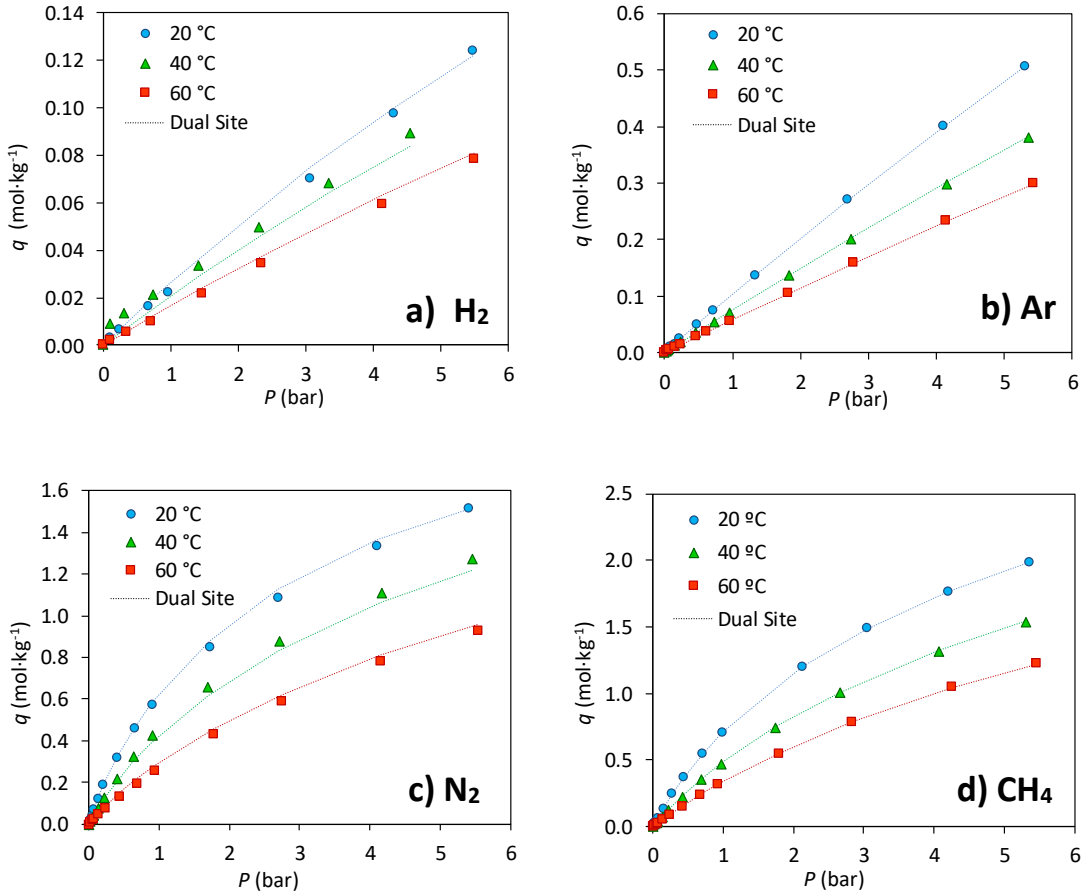

Figure 4.10. Adsorption isotherms on LiX zeolite for a) H_2, b) Ar, c) N_2 and d) CH_4 at 20 °C (blue); 40 °C (green); and 60 °C (red).

Table 4.8. Dual-site Langmuir parameters on LiX zeolite

Parameter	Units	H_2	N_2	CH_4	Ar
$q_{max,1}$	mol kg^{-1}	0.31	2.22	3.04	5.47
$b_{\infty,1}$	bar^{-1}	$7.77 \cdot 10^{-4}$	$6.10 \cdot 10^{-5}$	$4.31 \cdot 10^{-5}$	$1.42 \cdot 10^{-5}$
$\Delta H_1 = \Delta H_2$	kJ mol^{-1}	10.11	20.70	18.57	11.97
$q_{max,2}$	mol kg^{-1}	0.28	0.15	1.39	0.15
$b_{\infty,2}$	bar^{-1}	$7.39 \cdot 10^{-4}$	$6.22 \cdot 10^{-5}$	$2.48 \cdot 10^{-5}$	$1.46 \cdot 10^{-5}$
RSS	%	$3.00 \cdot 10^{-4}$	$1.91 \cdot 10^{-2}$	$7.12 \cdot 10^{-4}$	$9.65 \cdot 10^{-5}$

In the LiX zeolite adsorbent, the amount adsorbed of pure gases at 20 °C and 2 bar is ≈ 0.051 mol kg^{-1} of H_2, ≈ 0.203 mol kg^{-1} of Ar, ≈ 0.960 mol kg^{-1} of N_2 and ≈ 1.153 mol kg^{-1} of CH_4. These values obtained in this work are in accordance with findings reported by Y. Park et al (2014), at 20 °C and *ca.* 2 bar; i.e., for H_2 ≈ 0.09 mol kg^{-1}, for Ar ≈ 0.27 mol kg^{-1}, for N_2 ≈ 1.16 mol kg^{-1}, and for CH_4 ≈ 1.36 mol kg^{-1} [32]. Looking at these values, LiX zeolite exhibits the best adsorption capacity of N_2 as compared to 5A or 13X zeolites, although Ar capacity is slightly slower than for 5A zeolite.

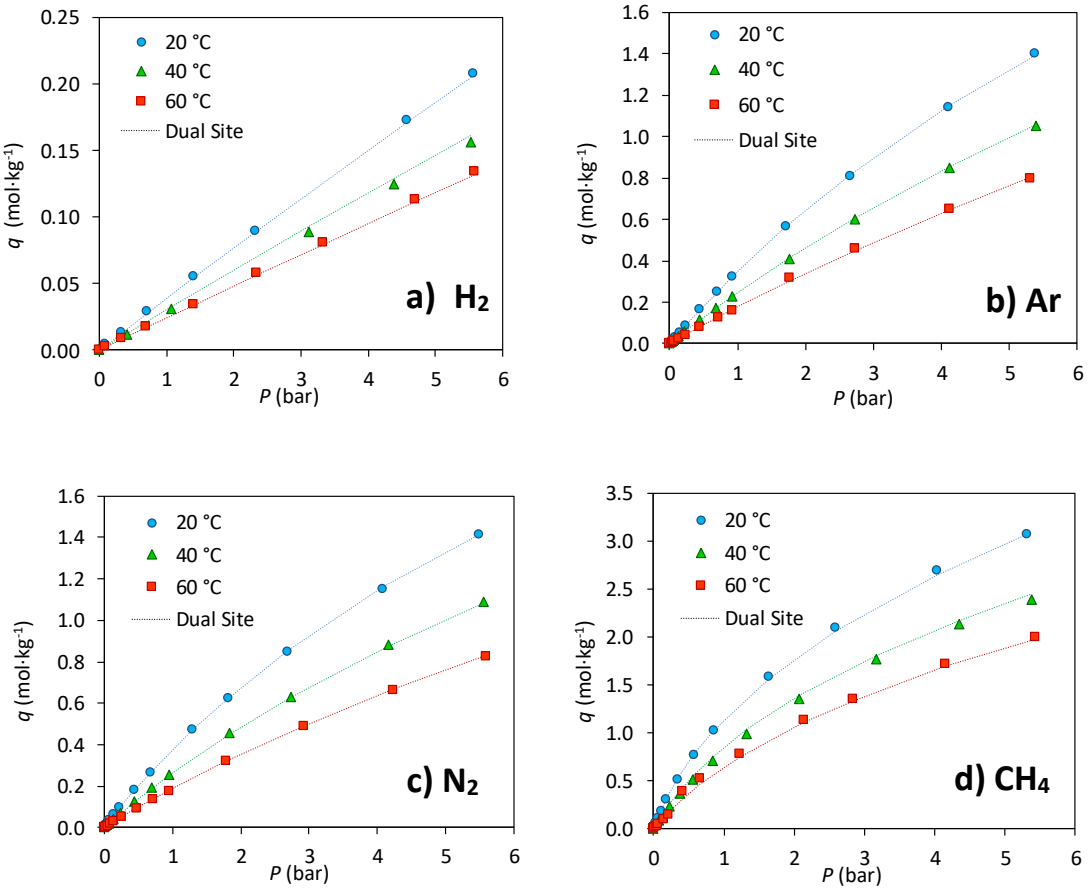

Figure 4.11. Adsorption isotherms on AC activated carbon for a) H_2, b) Ar, c) N_2 and d) CH_4 at 20 °C (blue); 40 °C (green); and 60 °C (red).

Table 4.9. Dual-site Langmuir parameters on AC activated carbon

Parameter	Units	H_2	N_2	CH_4	Ar
$q_{max,1}$	mol kg^{-1}	0.90	3.92	1.22	4.39
$b_{\infty,1}$	bar^{-1}	3.64·10^{-4}	1.64·10^{-5}	1.45·10^{-5}	2.21·10^{-5}
$\Delta H_1 = \Delta H_2$	kJ mol^{-1}	9.65	15.57	16.33	14.54
$q_{max,2}$	mol kg^{-1}	4.38	0.04	7.63	4.24
$b_{\infty,2}$	bar^{-1}	9.66·10^{-5}	3.28·10^{-3}	8.32·10^{-5}	1.02·10^{-5}
RSS	%	8.89·10^{-5}	3.01·10^{-4}	3.11·10^{-2}	6.83·10^{-4}

In the activated carbon AC adsorbent, the amount adsorbed of H_2 at 20 °C and 2 bar is 0.077 mol kg^{-1} of H_2, which values compare very well with previously reported values; ≈ 0.06 - 0.11 mol kg^{-1} at 20 - 25 °C and 2 – 2.5 bar [29,32]. The adsorption capacities of the other adsorbates at the same conditions are 0.678 mol kg^{-1} of Ar, 0.676 mol kg^{-1} of N_2, and 1.765 mol kg^{-1} of CH_4. These obtained results are consistent with those of older studies at 20 °C and *ca.* 2 bar; i.e., for Ar ≈ 0.78 mol kg^{-1}, N_2 ≈ 0.75 mol kg^{-1} and CH_4 ≈ 1.94 mol kg^{-1} [32].

To compare the performance of the adsorbents, equilibrium separation factors of H_2 over the other gases (H_2:N_2:CH_4:Ar, 58:25:15:2 %v/v) are summarized in According to Eq. (4.5), the separation factor depends on the relative equilibrium quantities of each adsorbed species under the process conditions. Therefore, the partial pressure of each gas was stated considering a pressure swing between high pressure, P_h ≈ 9 bar, and the pressure, P_l ≈ 1 bar, which were used during the PSA operation.

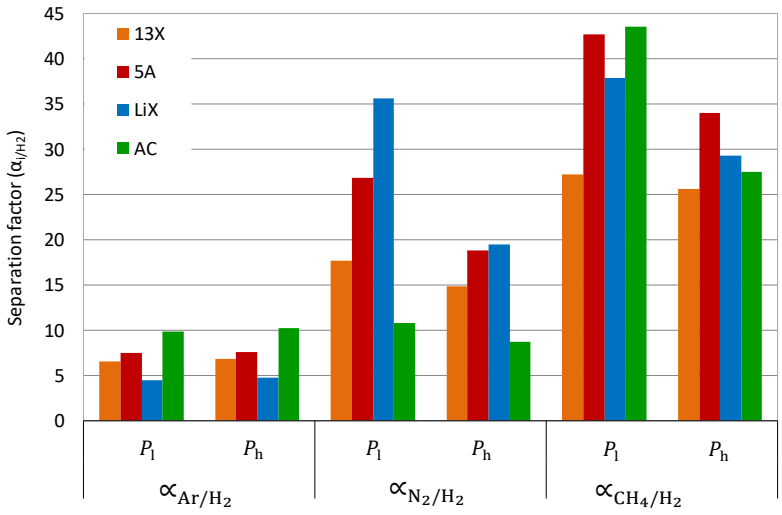

Figure 4.12. Separation factor between H_2 and the other gases i, at P_h and P_l pressures for different adsorbents; LiX (blue), 13X (orange), 5A (red) and AC (green).

Figure 4.12 shows that the Ar/H_2 separation factor is the lowest for all adsorbents followed by N_2 and then CH_4. This means that Ar is a tricky gas to separate from H_2 without decreasing hydrogen recovery. Furthermore, zeolite LiX has the lowest Ar/H_2 separation factor, 4.6, followed by zeolites 13X, 6.7; 5A, 7.6, and the highest value is obtained by activated carbon AC, 10.2. On the contrary, LiX zeolite has the highest N_2/H_2 separation factor, 19 - 37, with a considerable difference between pressure swing values as it is expected looking at the isotherm curvature. This zeolite is followed by 5A zeolite, 19 - 27; 13X, 14 - 18 and AC, 8 - 11. Regarding CH_4/H_2 separation factor, the zeolite 5A accounts for the highest values, 34 - 43, followed by AC, 27 - 45, LiX, 29 - 39, and then 13X, 25 - 28. According to these results, activated carbon AC is the best adsorbent for Ar removal, whereas LiX and 5A zeolites perform better to remove N_2 and CH_4, respectively, from the feed.

In this regard, others have shown that the use of activated carbon in an argon controlling hydrogen PSA increases hydrogen recovery from a feed gas with Ar, N_2 and CO as minor adsorbable impurities [33]. Nonetheless, given that, the bulk density of zeolite is higher than for AC, 728 kg m^{-3} and 600 kg m^{-3}, respectively, and that the separation factor is only 1.3 times higher, the benefit of using an additional AC layer is almost negligible. However, due to its well-balanced N_2/H_2 and CH_4/H_2 separation factors and acceptable Ar removal performance, 5A zeolite appears as the best choice for purifying H_2 from ammonia purge gas stream; besides zeolite 5A is a robust cost-effective adsorbent. For that reason, this material was further characterized.

4.3.2 BREAKTHROUGH EXPERIMENTS

Breakthrough experiments are required to study the adsorption bed dynamics and to validate the mathematical model. Accordingly, breakthrough curves were measured at different operational conditions of feed flowrate and pressure according to Table 4.3. The results of the single component adsorption and desorption breakthroughs of H_2, Ar, N_2 and CH_4 on 5A zeolite are illustrated in Figure 4.13. The reversibility of single breakthroughs was confirmed as the adsorption and desorption values fall on the same trend line.

The breakthrough times of single component for H_2, Ar, N_2 and CH_4 are approximately 31 s, 80 s, 190 s and 270 s, respectively, at 1 bar and 0.5 L_N min^{-1}, whereas the values change to 29 s, 70 s, 130 s and 200 s, respectively, at 4.5 bar and 2.75 L_N min^{-1}. This indicates that the first impurity to break through the column is Ar, followed by N_2 and CH_4. The results show that Ar adsorbs only slightly and H_2 adsorbs significantly less than Ar. However, the fast breakthrough of Ar on zeolite 5A may negatively affect H_2 purity and recovery. Therefore, H_2 product of the PSA unit packed with zeolite 5A is expected to be controlled by the concentration of Ar.

Moreover, Figure 4.14 reports the inner-temperature profiles at the bottom and the top of the column for the breakthrough curves depicted in Figure 4.13. Due to the low amount of H_2 and Ar adsorbed, the temperature peaks corresponding to these components were negligible. Likewise, the temperature remains nearly constant for Ar and H_2 desorption breakthroughs, while a temperature decrease is observed for N_2 and CH_4.

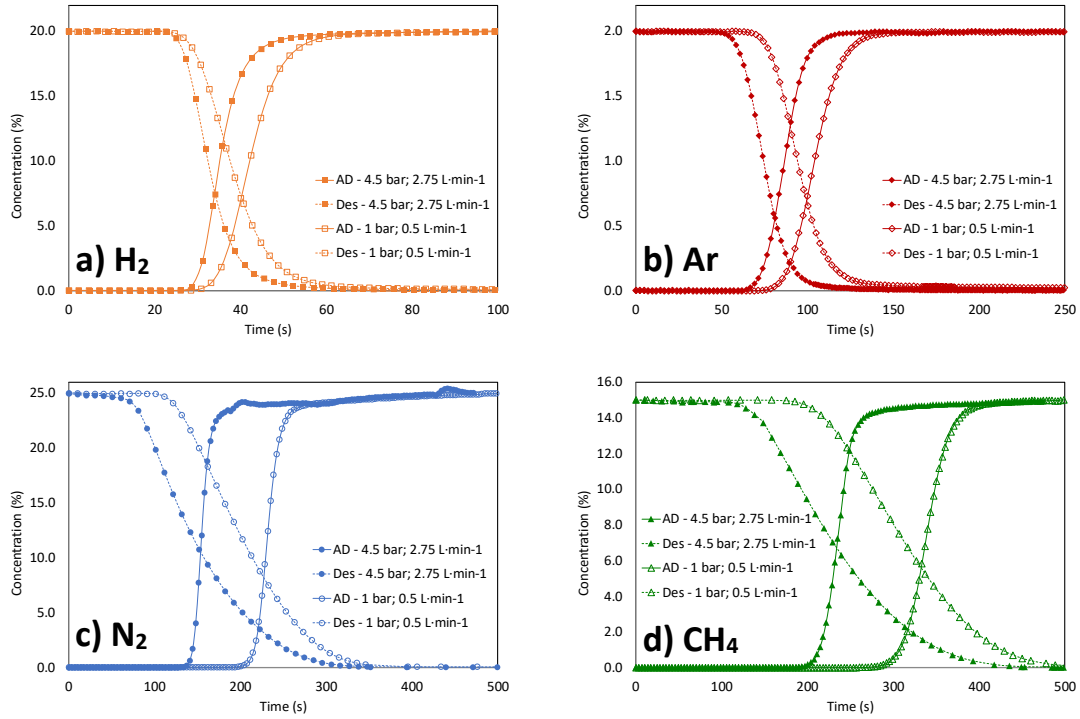

Figure 4.13. Single component adsorption and desorption breakthroughs of a) H_2, b) Ar, c) N_2 and d) CH_4 on 5A zeolite. Solid lines, adsorption; dashed line, desorption.

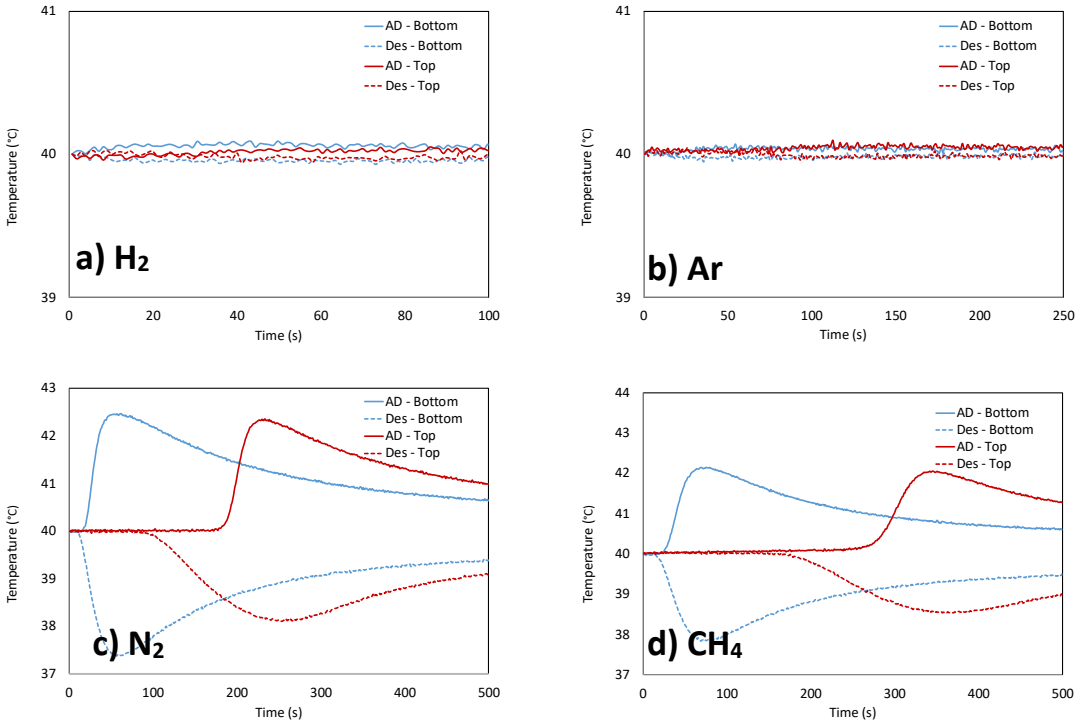

Figure 4.14. Temperature history of the single component breakthroughs of a) H_2, b) Ar, c) N_2 and d) CH_4, at 0.5 L_N min^{-1}, 1 bar and 40 °C. Solid lines, adsorption; dashed line, desorption.

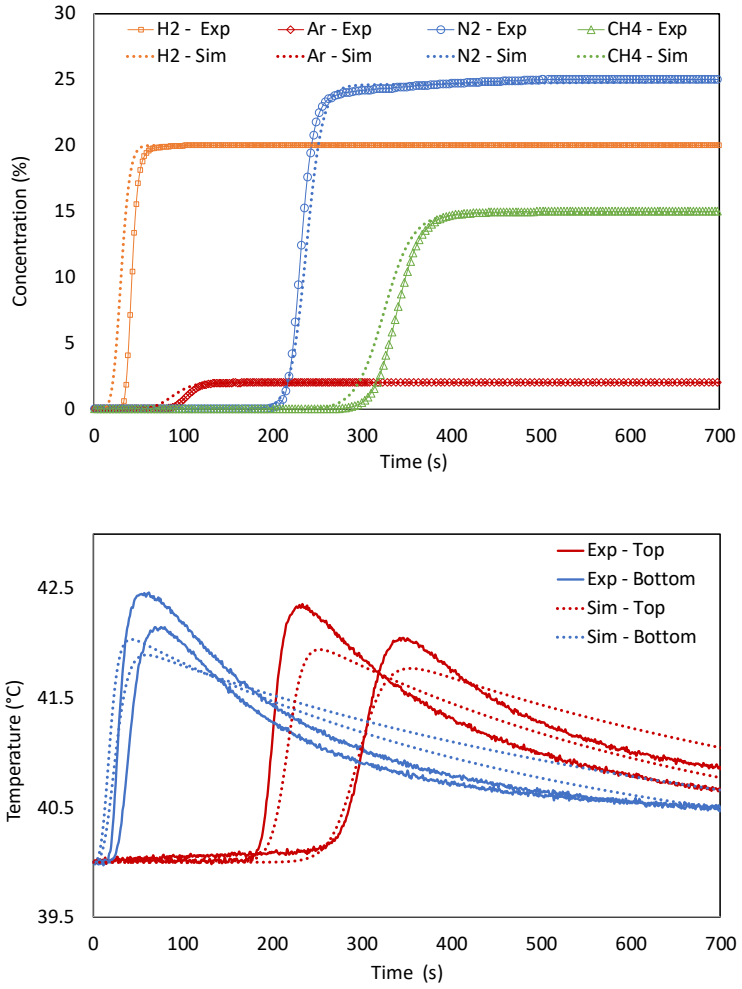

Figure 4.15. Comparison between the simulation and the experimental single component breakthrough data, at 0.5 L_N min^{-1}, 1 bar and 40 °C. Solid lines, experimental data; dotted lines, simulated data.

The comparison of the simulation results with the experimental single component and multicomponent data for 5A zeolite packed bed at 0.5 L_N min^{-1}, 1 bar and 40 °C, is included in Figure 4.15 and Figure 4.16, respectively. Looking at the single breakthrough curves shown in Figure 4.15, it is observed the time required for each single component in He as carrier gas to reach the inlet concentration at the outlet. Despite the simplifications, the dynamic mathematical model is in reasonable agreement with the experimental breakthrough curves for the concentration and temperature. The breakthrough curves are predicted with a slight advanced breakthrough time and temperature not exceeding 20 s and 1 °C, respectively. Regarding the temperature effect, the temperate history at the bed inlet (T – Bottom) displays only one peak corresponding to all components of the mixture, since the different components have not been separated yet. In turn, at the top of the column (T – Top), the two peaks of temperature, at ca. 43.0 °C, at instants 190 s and 270 s correspond to the adsorption heat generated by the concentration fronts of adsorbates N_2 and CH_4, respectively.

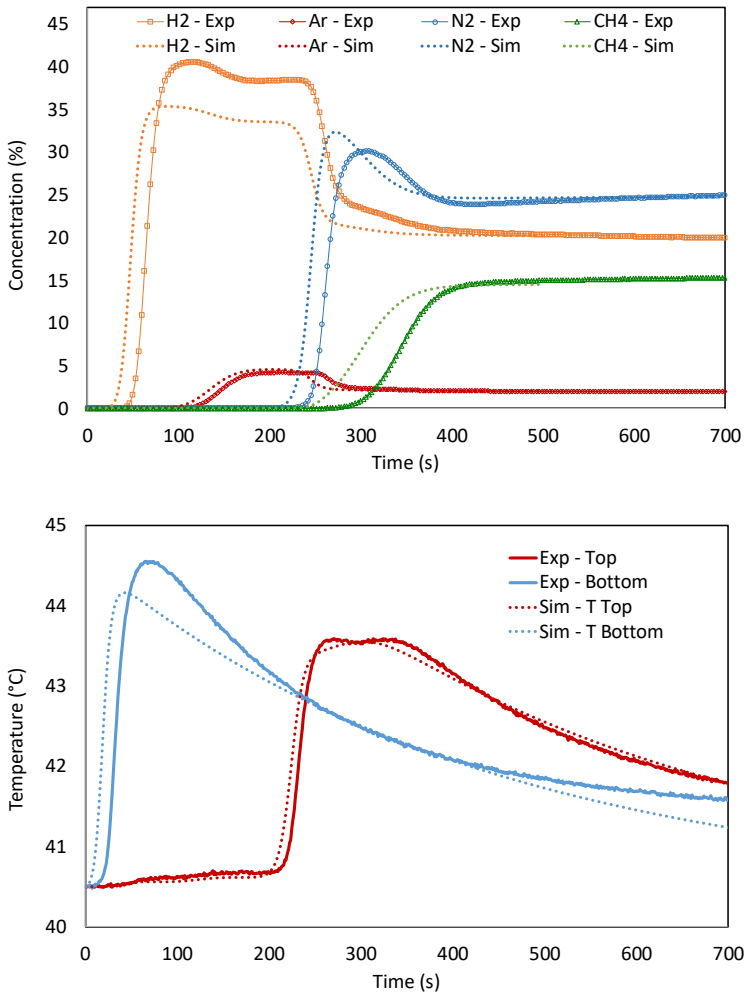

Figure 4.16. Comparison between the simulation and the experimental multicomponent breakthrough data, at 0.5 L_N min^{-1}, 1 bar and 40 °C. Solid lines, experimental data; dotted lines, simulated data.

Furthermore, as depicted in Figure 4.16, the breakthrough times for H_2, Ar, N_2 and CH_4 from a four-component mixture in a carrier gas are very similar to the values given above for single component breakthroughs. In this case, the model values also express the trend of the experimental data: the concentration reached by H_2 at the outlet of the packed bed, 40 % vol. H_2, is greater than its input concentration, 20 % vol. Then, H_2 concentration decreases gradually due to other components of the mixture, for which the adsorbent gas a higher adsorption capacity, start to break through the column. Finally, the concentration of all the gas species approaches to the concentration at the inlet.

4.3.3 PSA RESULTS

A set of PSA experiments were performed as indicated in Table 4.5, to optimize the lab four-column PSA unit to produce target hydrogen purities at maximum recoveries. To reach the cyclic steady-state, the four-bed PSA unit was operated experimentally for at least 40 cycles, until the product concentration history remained constant. Table 4.10 summarizes a total of 24 PSA tests performed, including the experimental results obtained for each run as well as the modeled results. Runs #1 to #16 were designed based on CCD methodology, while runs #17 to #24 were undertaken as screening experiments and replicates for assessing the experimental reproducibility. The results show that CH_4 concentrations were below the detection limit of the gas analyzer, except for run #21 at P/F = 0.04.

Table 4.10. Performance of the cyclic PSA unit

	DoE factors			Experimental process responses					RSM predictions	
run nº	P_h (bar)	t_{AD} (s)	*P/F* (-)	HP (%vol.)	y_{N2+Ar} (ppm)	y_{CH_4} (ppm)	HR (%)	*Productivity* (mol_{H2}/kg·day)	HP (%vol.)	HR (%)
1	7	90	0.11	99.51	4940	<100	71.4	391.6	99.52	71.9
2	8	75	0.20	99.99	<100	<100	43.3	237.7	100.0	43.6
3	8	75	0.21	+99.98	<100	<100	43.2	237.1	100.0	43.1
4	9	75	0.20	+99.98	<100	<100	37.2	203.8	99.99	36.7
5	8	60	0.23	+99.98	<100	<100	28.1	154.2	99.99	28.5
6	7	60	0.15	99.98	183	<100	49.4	271.0	99.99	49.4
7	8	75	0.14	+99.98	<100	<100	50.9	279.2	99.99	51.4
8	8	75	0.14	+99.98	<100	<100	50.3	275.8	99.99	50.8
9	8	75	0.09	99.84	1551	<100	62.1	340.7	99.85	60.8
10	9	90	0.09	99.89	1111	<100	61.6	337.1	99.87	61.7
11	9	90	0.10	99.88	1170	<100	60.7	333.4	99.90	59.7
12	7	60	0.09	99.82	1764	<100	60.6	334.0	99.81	61.0
13	8	90	0.18	99.92	752	<100	56.2	308.1	99.90	56.3
14	7	75	0.19	99.96	447	<100	54.9	301.4	99.94	54.2
15	9	60	0.13	+99.98	<100	<100	37.4	205.3	100.0	36.7
16	9	60	0.16	+99.98	<100	<100	29.7	162.7	100.0	30.7
17	9	90	0.16	99.97	325	<100	40.0	219.6	99.99	51.5
18	7	90	0.09	99.12	8820	<100	75.4	413.6	99.41	75.1
19	9	75	0.10	99.99	<100	<100	52.5	283.1	99.97	53.4
20	9	75	0.08	99.93	740	<100	55.9	306.6	99.94	56.6
21	8	90	0.04	98.27	16043	1272	79.5	436.0	99.41	77.4
22	8	75	0.06	99.49	5090	<100	68.1	373.5	99.71	68.0
23	9	60	0.17	+99.98	<100	<100	30.9	170.0	100.0	30.0
24	9	90	0.16	99.98	245	<100	51.4	282.0	99.99	51.9

Two empirical models, previously described by Eq. (4.10), were fitted for hydrogen purity and recovery, from the CCD results, using the statistical software JMP. Model parameters of model 1 for describing hydrogen purity, HP, and model 2 for describing hydrogen recovery, HR, as well as the statistical and regression parameters are presented in Table 4.11. Both models were considered statistically highly significant, p-values smaller than 0.001 % (p-value < 0.0001); moreover, the empirical models describe accurately the experimental results with determination coefficients of R^2 = 0.985 and R^2 = 0.997, for HP and HR, respectively.

Table 4.11. ANOVA for response surface models

	Model 1, HP		**Model 2, HR**	
Parameter	**Estimate**	**p-value**	**Estimate**	**p-value**
β_0	99.99	<.0001	51.5	<.0001
β_1	-0.10	<.0001	9.2	<.0001
β_2	0.10	<.0001	-7.5	<.0001
β_3	0.19	<.0001	-17.5	<.0001
β_4	0.08	<.0001	0.3	0.464
β_5	0.07	0.014	4.1	0.003
β_6	-0.13	<.0001	-1.3	0.189
β_7	-0.04	0.004	-0.7	0.198
β_8	-0.05	0.001	1.4	0.024
β_9	-0.24	<.0001	6.4	0.005
R^2	0.985		0.997	
RMSE	0.02		0.92	
p-value	<0.0001		<0.0001	

4.3.3.1 The effect of independent factors on responses

The response surfaces of these models are displayed in Figure 4.17, for adsorption pressures at 7 bar (green), 8 bar (blue) and 9 bar (red). This figure shows similar surface shapes for the three pressures. As it can be seen, an increase in adsorption pressure leads to a purity increase (Fig. 4.17 (a)) whereas the recovery (Fig. 4.17 (b)) and productivity drop. The same trend is observed increasing the P/F ratio while the opposite trend is observed increasing t_{ad}. The maximum product purity occurs at the P/F ratio upper bound because P/F enhances the adsorbent regeneration. However, the recovery and productivity decreases, as P/F ratio increased, due to higher amount of H_2 used in the purge step. An optimal value of t_{ad} should allow enough time for H_2 concentration front to leave the adsorption bed, and it should be short enough to avoid the impurities front to breakthrough.

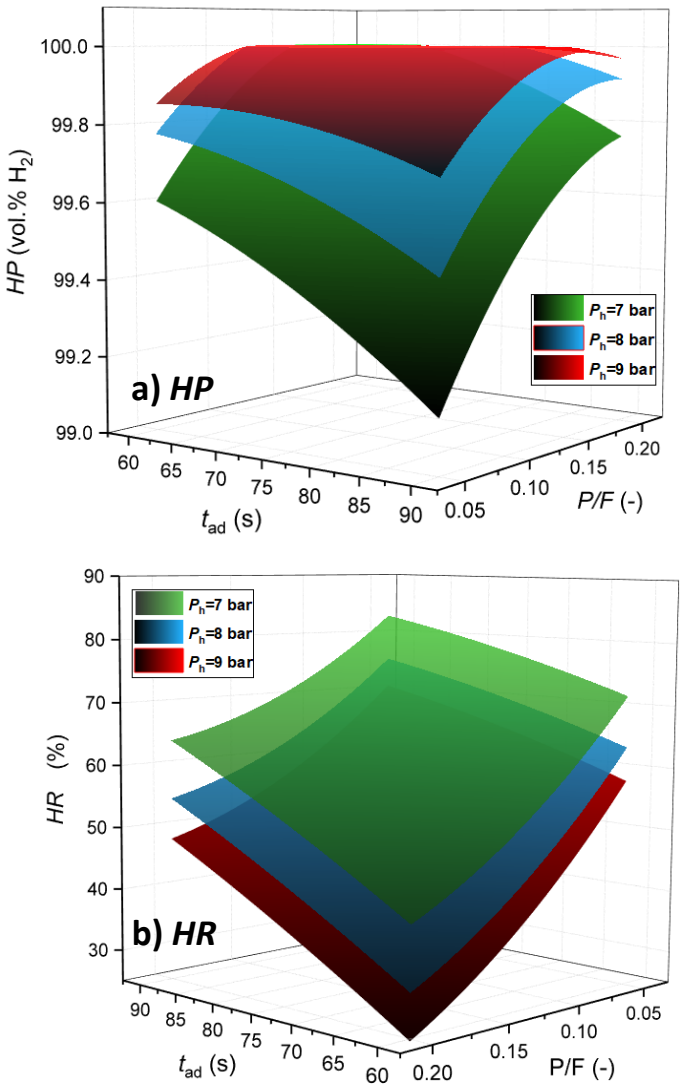

Figure 4.17. Response surface for hydrogen purity HP and recovery HR, as a function of the independent variables t_{ad} and P/F ratio at 7 bar (green); 8 bar (blue); and 9 bar (red).

4.3.3.2 Process optimization

The four-column PSA system was optimized for delivering three different hydrogen qualities: high purity for PEMFC road vehicle systems (Type I, Grade D), medium purity for PEMFC stationary appliance systems (Type I, Grade E) and lower purity for industrial use to feed conventional internal combustion engine (ICE) (Type I, Grade A), in compliance with ISO 14687 standards [34–36]. The optimization was performed maximizing the recovery for each hydrogen quality using the desirability function of JMP software application, as follows:

- Opt #1, maximizes the recovery and sets the H_2 purity to 99.97 %vol.
- Opt #2, maximizes the recovery and sets the H_2 purity to 99.9 % vol.
- Opt #3, maximizes the recovery and sets the H_2 purity to 98.0 % vol.

Then, additional experiments were performed under the optimal conditions predicted by the model. The obtained experimental and model results can be found in Table 4.12.

Table 4.12. Optimal DoE parameters and experimental and RSM predicted PSA results

	DoE factors			Experimental process responses					RSM pred.	
run nº	P_h (bar)	t_{AD} (s)	P/F (-)	HP (%vol.)	y_{N_2+Ar} (ppm)	y_{CH_4} (ppm)	HR (%)	*Productivity* ($mol_{H2}/kg \cdot day$)	HP (%vol.)	HR (%)
Opt #1	9	84	0.11	99.97	281	<100	55.5	304.4	99.97	54.8
Opt #2	9	83	0.08	99.92	831	<100	61.0	334.8	99.90	60.3
Opt #2.1	9	83	0.08	+99.98	<100	<100	61.0	334.8	-	-
Opt #3	7	90	0.09	99.25	7514	<100	75.3	413.1	99.11	75.6

Note: The optimization Opt #2.1 indicates that the inert content (N_2+Ar) observed for Opt #2 is mostly Ar.

As it can be seen, the RSM predicted optimum performance parameters very close to the experimental values. For obtaining PEMFC mobility grade of H_2 at 99.97 % vol. (Opt #1), a recovery of 55.5 % was experimentally obtained, while the model predicted recovery was 54.8 % for P_h = 9 bar; P/F = 0.1; t_{ad} = 84 s. That corresponds to a productivity of 304 mol_{H2} $kg_{ads}^{-1}day^{-1}$ and 282 ppm of Ar. Setting the H_2 concentration to 99.9 % vol. (Opt #2), the forecasted optimum operating conditions were P_h= 9 bar; P/F = 0.08; t_{ad} = 83 s. For these operating conditions, the experimental recovery was 61.0 %, while the forecasted recovery was 60.3. The productivity was 335 mol_{H2} $kg_{ads}^{-1}day^{-1}$ and 831 ppm of Ar. Setting H_2 content to 98 % vol. (Opt #3), for P_h= 7 bar; P/F = 0.09; t_{ad} = 90 s, an experimental and model recoveries of 75.3 % and 75.6 %, respectively, were obtained, corresponding to a productivity of 413 mol_{H2} $kg_{ads}^{-1}day^{-1}$ and 7514 ppm of inerts. Additionally, the experimental run Opt #2.1 was performed but with a feed stream free of Ar (H_2:N_2:CH_4; 60:25:15 vol. %). This allowed evaluating the contribution of Ar to the inert content at the product stream, since Ar and N_2 were quantified as one. An experimental purity of 99.98 % was obtained, which indicates that the inert gases concentration at the product stream was mostly Ar.

Even though the achieved recoveries are assumed to be very conservative due to the PSA system has only 4 absorbers fed at a relatively low pressure ≤ 9 bar, these recoveries should be higher at real conditions by taking advantage of the significant pressure swing growth, due to the pressure of APG wasted is already high (150 – 200 bar). It is well know that the increased pressure equalization steps directly relates to improved recovery in a multi-bed PSA at a cost of reducing purity [37]. Furthermore, a greater number of adsorption beds primary helped to improve recovery, but also leads to an increase in the PSA capital costs, which are often critical for small-scale applications.

4.3.4 ECONOMIC BENEFITS

The use of surplus hydrogen from industrial processes provides a cheaper hydrogen source that can be used as a transportation fuel for road vehicle applications. The cost of hydrogen produced from waste streams of ammonia plants, using a small-PSA unit, was estimated and compared to the conventional steam methane reforming (SMR) pathway as the most cost-effective option. The comparison also considers the compression of the purified hydrogen to 350 and 700 bar and its delivery to the nearest retail hydrogen refueling station (HRS).

In a small-to-medium ammonia production plant of 500 t NH_3 day^{-1}, a stream of up to 12.5 kg H_2 h^{-1} (at 99.97 %vol. H_2 and *ca.* 20 bar) can be produced on-site via PSA technology of the purge gases of the ammonia synthesis process [5,8]. This hydrogen quantity was estimated based on the recovery of 55.0 % achieved in the present work. By adjusting Eq. (2.25) - (2.26) detailed in Chapter 2 to this specific case, the levelized cost of H_2 should include the annualized capital costs (CAPEX) of the PSA unit and compressors as well as the operating costs (OPEX), due to electric energy consumption along with distribution costs in the off-site option. The detailed equations used to assess the process economics are outlined in Appendix section at the end of this chapter.

The cost of producing fuel cell grade hydrogen in situ from purge gases of ammonia plants using small-PSA units is estimated to be 0.63 € kg H_2^{-1}, which is similar to the cost of purifying H_2 by SMR. However, when considering off-site conventional SMR plants, hydrogen production costs are currently estimated to be around 2 € kg H_2^{-1} and strongly depend on the price of natural gas. In this regard, the recovered hydrogen from APG can be sold directly at the factory site as a chemical commodity with competitive prices or as fuel for FCEVs, whose market is steadily increasing. In such a scenario, compressed gas cylinders are a good alternative for low demands and short distance delivering [38,39]. The produced H_2 should be compressed from *ca.* 20 bar to 350/700 bar, according to the different current pressure levels of the tank systems between buses/trucks (350 bar) and passenger cars (700 bar) [40]. Lastly, compressed hydrogen (CH2) can be transported by tube trailers to the nearest available HRS (<20 km) [41]. The techno-economic assessment is summarized in Table 4.13, and discussed below.

Table 4.13. Cost sheet of hydrogen recovery via small-scale PSA

	H_2 at 20 bar	**H_2 at 350 bar**	**H_2 at 700 bar**
CAPEX (€)			
PSA unit	321,000	321,000	321,000
Compressor (s)	-	179,600	241,600
Sub-total	321,000	500,600	562,600
OPEX (€ $year^{-1}$)			
PSA unit	28,700	28,700	28,700
Compressor (s)	-	24,800	31,600
CH2 delivery	-	22,000	22,000
Sub-total	28,700	75,500	82,300
Levelized cost (€ kg H_2^{-1})	0.63	1.17	1.39

Based on the economic assumptions described above, the cost to purify ammonia waste hydrogen stream using small-PSA units, compress and transport is *ca.* 1.17 and 1.39 € kg H_2^{-1}, respectively, depending on the dispensing pressure of 350 or 700 bar. Moreover, these values are in the range of those obtained from economic study included in Chapter 2, where the cost of liquefied hydrogen obtained from an industrial hydrogen-containing waste stream has been estimated between 1.36 to 1.68 € kg H_2^{-1}, depending on the type of transformation technology considered. That would be equivalent to less than 0.06 € kWh^{-1}, which is cheaper than the price of electricity in many developed countries.

These values permit reducing H_2 costs by at least 40 %; this saving value was calculated based on off-site H_2 production by SMR plus compression and transportation until the refueling station [42]. Although the economic assumptions may vary both with time and location, the resultant costs are reasonable values as they entail the essential stages of the waste-to-hydrogen production route. As a distributed hydrogen production, these hydrogen sources can be crucial in the early stage of transition to the future global hydrogen-incorporated economy, pushing hydrogen down to competitive prices. These estimations strongly depend on the available volume of the waste hydrogen streams. Nevertheless, this form of distributed hydrogen production assumes that a complete hydrogen distribution and storage infrastructure is available. Meanwhile, the produced hydrogen can be used at the industrial site for fueling hydrogen-powered forklifts and other machinery, thus eliminating the need for long battery recharging.

4.4 CONCLUSIONS

Industrial hydrogen-rich waste streams hold promise in their upgrading to feed fuel cell stacks. As in the ammonia synthesis process, a gaseous stream is purged to keep the inert gases concentration below a threshold value, this stream contains large hydrogen quantities, which can be recovered. A four-bed PSA unit packed with 5A zeolite was studied to purify hydrogen from a simulated effluent gas (H_2:N_2:CH_4:Ar, 58:25:15:2 %v/v) of ammonia synthesis process.

The adsorption equilibrium isotherms of H_2, N_2, CH_4, and Ar on four pre-selected adsorbents was obtained. According to the equilibrium separation factor it was concluded that activated carbon AC is the best adsorbent for removing Ar, whereas LiX and 5A zeolites remove more effectively N_2 and CH_4, respectively. Therefore, 5A zeolite was selected as the best adsorbent for purifying H_2 from ammonia purge gas stream due to its well-balanced N_2/H_2 and CH_4/H_2 separation factors and acceptable Ar removal performance. To assess the performance of the selected adsorbent, 5A zeolite, single and multi-component breakthrough curves were experimentally carried out in a single packed column, and further simulated. The results, simulations and experimental, indicate that the first impurity to break thought the column is Ar, followed by N_2 and finally by CH_4.

Consequently, the separation performance of the four-bed PSA unit packed with zeolite 5A can be affected by the Ar adsorption for concentrations as low as 2 %. The PSA experiments were conducted in a 4-column PSA unit with 12-events cycle, comprising 9 elementary steps. The role of operating parameters in PSA performance such as P/F ratio, adsorption step time and adsorption pressure, was investigated. The overall PSA performance was evaluated in terms of purity, recovery and productivity of H_2 product. The experimental unit was optimized to maximize the responses based on RSM models for three specific final applications, in compliance with ISO 14687 standards. The PSA unit of this study can produce H_2 with 99.25 % - 99.97 % purity with 75.3 % - 55.5 % of recovery, respectively, where Ar and N_2 are the main impurities at the product stream. A significant loss of recovery and productivity happens when H_2 purity was set at +99.9 %vol. The study showed the feasibility of the PSA process packed with 5A zeolite to produce a wide purity range of H_2 product streams from a feed mixture containing as impurities N_2, CH_4 and Ar, as simulated ammonia purge gas.

In addition to the technical performance, a simplified economic analysis was carried out. Thus, the optimal conditions of the PSA unit can be changed to obtain from lower hydrogen purity for industrial use +98 % vol. by recycling it back to the feed of the ammonia plant, to

higher purity for road vehicle systems +99.97 %, at exactly the time when hydrogen demand for mobility begin to be fully felt. The cost to purify an ammonia waste hydrogen stream to + 99.97 % vol. using a small-PSA unit, compress and transport has been estimated to be 1.17 to 1.39 € kg H_2^{-1}, respectively, depending on the dispensing pressure of 350 or 700 bar; these values were estimated to be 40 % below the current commercial costs.

ABBREVIATIONS

AD	adsorption
AD/BF	providing backfill
ANOVA	analysis of variance
APG	ammonia purge gas
BD	blowdown
BF	backfill
BPR	backpressure regulator
CAPEX	capital costs
CCD	central composite design
CH2	compressed hydrogen
DoE	design of experiments
DPE	depressurization pressure equalization
DSL	dual site Langmuir model
FCEV	fuel cell electric vehicles
FPPE	first pressurization pressure equalization
HRS	hydrogen refueling station
ICE	internal combustion engine
ISO	International Standard Organization
LDF	linear driving force model
MFC	flow controller
MFM	flow meter
ODE	ordinary differential equation
OPEX	operating costs
PDE	partial differential equation
PEMFC	polymer electrolyte membrane fuel cells
PG	purge
PSA	pressure swing adsorption
RSM	response surface methodology

SMR	steam methane reforming
SPPE	second pressurization pressure equalization
TCD	thermal conductivity detector
TT	thermocouple
UDS	upwind differencing scheme

NOMENCLATURE

Parameters

L_{bed}	length of the column (cm)
$P_{\mathrm{i}}, P_{\mathrm{j}}$	partial pressure in the gas phase (bar)
R^2	determination coefficient (-)
X_{i}	dimensionless process factors
b_{∞}	affinity constant at infinite temperature (bar^{-1})
d_{p}	particle diameter (mm)
k_{i}	mass transfer coefficient (s^{-1})
m_{ads}	adsorbent mass loaded to the bed (kg)
q^*	molar concentration in the adsorbed phase ($mol\ kg^{-1}$)
q_{max}	isotherm parameter, maximum adsorbed concentration ($mol\ kg^{-1}$)
t_{cycle}	total operating time during an entire cycle (s)
$\alpha_{\mathrm{i/j}}$	separation factor between gases *i* and *j* (-)
$\hat{\mathrm{y}}$	process response (-)
HP	hydrogen purity (%)
HR	hydrogen recovery (%)
P	pressure (bar)
P/F	purge-to-feed ratio (-)
Q	volumetric flow rate ($L_N\ min^{-1}$)
R	ideal gas constant ($J\ mol^{-1}\ K^{-1}$)
$RMSE$	root-mean-square-error (-)
RSS	residual sum of squares (%)
T	temperature (°C)
b	affinity constant (bar^{-1})
d	diameter (cm)
t	time variable (s)
y	gas-phase mole fraction (-)

Greek symbols

ρ_{p}	particle density (g cm^{-3})
ΔH	heat of adsorption (J mol^{-1})
β	polynomial model coefficient (-)

Subscripts/superscripts

+1	upper level of the DoE factor
0	outside
-1	lower level of the DoE factor
1, 2	dual-site Langmuir sites
ad	adsorption
eq	equalization
exp	experimental data
F	feed stream
h	high
i, j	gas component
in	inside
k	experimental adsorption data point
l	low
mod	modeling data
N	total number of experimental adsorption data points
prod	product

REFERENCES

[1] S.C.T. J. Perrin, R. Steinberger-Wilkens, CertifHy project "Overview of the market segmentation for hydrogen across potential customer groups, based on key application areas," 2015.

[2] D. Favreau, S. Vinot, Roads2HyCom Project: Fuel cells and hydrogen in a sustainable energy economy, (2009).

[3] T. Dong, L. Wang, A. Liu, X. Guo, Q. Ma, G. Li, Q. Sun, Experimental study of separation of ammonia synthesis vent gas by hydrate formation, Pet. Sci. 6 (2009) 188–193.

[4] Fertilizer company personal communication, (2017).

[5] Z. Wu, W. Wenchuan, The recovery of ammonia from purge gas, (2017). www.cryobridge.com/Ammonia.pdf.

[6] S.H. Cho, K.T. Chue, J.N. Kim, A two stage PSA for argon and hydrogen recovery from ammonia purge gas, Chem. Eng. Commun. 163 (1998) 97–109.

[7] M.R. Rahimpour, A. Asgari, Modeling and simulation of ammonia removal from purge gases of ammonia plants using a catalytic Pd–Ag membrane reactor, J. Hazard. Mater. 153 (2008) 557–565.

[8] M.R. Rahimpour, A. Asgari, Production of hydrogen from purge gases of ammonia plants in a catalytic hydrogen-permselective membrane reactor, Int. J. Hydrogen Energy. 34 (2009) 5795–5802.

[9] F. Siavashi, M. Saidi, M.R. Rahimpour, Purge gas recovery of ammonia synthesis plant by integrated configuration of catalytic hydrogen-permselective membrane reactor and solid oxide fuel cell as a novel technology, J. Power Sources. 267 (2014) 104–116.

[10] M.R. Karami, P. Keshavarz, M. Khorram, M. Mehdipour, Analysis of ammonia separation from purge gases in microporous hollow fiber membrane contactors, J. Hazard. Mater. 260 (2013) 576–584.

[11] Q. Sun, J. Liu, A. Liu, X. Guo, L. Yang, J. Zhang, Experiment on the separation of tail gases of ammonia plant via continuous hydrates formation with TBAB, Int. J. Hydrogen Energy. 40 (2015) 6358–6364.

[12] J.C. Santos, F.D. Magalhães, A. Mendes, Contamination of zeolites used in oxygen production by PSA: Effects of water and carbon dioxide, Ind. Eng. Chem. Res. 47 (2008) 6197–6203.

[13] D.K. Moon, D.G. Lee, C.H. Lee, H2 pressure swing adsorption for high pressure syngas from an integrated gasification combined cycle with a carbon capture process, Appl. Energy. 183 (2016) 760–774.

[14] R.T. Yang, Sorbents for Applications, in: Adsorbents Fundam. Appl., Wiley-Interscience, Hoboken, New Jersey, 2003: pp. 280–381.

[15] D. Broom, Characterizing adsorbents for gas separations, Chem. Eng. Prog. 114 (2018) 30–37.

[16] M. Bastos-Neto, A. Moeller, R. Staudt, J. Böhm, R. Gläser, Dynamic bed measurements of CO adsorption on microporous adsorbents at high pressures for hydrogen purification processes, Sep. Purif. Technol. 77 (2011) 251–260.

[17] D. Ferreira, R. Magalhães, P. Taveira, A. Mendes, Effective adsorption equilibrium isotherms and breakthroughs of water vapor and carbon dioxide on different adsorbents, Ind. Eng. Chem. Res. 50 (2011) 10201–10210.

[18] A.M. Ribeiro, C.A. Grande, F.V.S. Lopes, J.M. Loureiro, A.E. Rodrigues, A parametric study of layered bed PSA for hydrogen purification, Chem. Eng. Sci. 63 (2008) 5258–5273.

[19] F. Relvas, R.D. Whitley, C. Silva, A. Mendes, Single-Stage Pressure Swing Adsorption for Producing Fuel Cell Grade Hydrogen, Ind. Eng. Chem. Res. 57 (2018) 5106–5118.

[20] C.A. Grande, Advances in Pressure Swing Adsorption for Gas Separation, ISRN Chem. Eng. 2012 (2012) 1–13.

[21] P. Cruz, J.C. Santos, F.D. Magalhaes, A. Mendes, Cyclic adsorption separation processes: Analysis strategy and optimization procedure, Chem. Eng. Sci. 58 (2003) 3143–3158.

[22] J.K. Telford, A brief introduction to design of experiments, Johns Hopkins APL Tech. Dig. (Applied Phys. Lab. 27 (2007) 224–232.

[23] M.J. Anderson, P.J. Whitcomb, RSM Simplified: Optimizing Processes Using Response Surface Methods for Design of Experiments, CRC Press Book, Boca Raton, Florida, 2017.

[24] Ž.R. Lazić, Design of Experiments in Chemical Engineering, Wiley-VCH: Weinhem, Weinheim, Germany, 2005.

[25] G.-M. Nam, B.-M. Jeong, S.-H. Kang, B.-K. Lee, D.-K. Choi, Equilibrium isotherms of CH4, C2H6, C2H4, N2, and H2 on Zeolite 5A using a static volumetic method, J. Chem. Eng. Data. 50 (2005) 72–76.

[26] M. Yavary, H. Ale Ebrahim, C. Falamaki, Competitive Adsorption Equilibrium Isotherms of CO, CO2, CH4, and H2 on Activated Carbon and Zeolite 5A for Hydrogen Purification, J. Chem. Eng. Data. 61 (2016) 3420–3427.

[27] D.A. Kennedy, M. Mujcin, E. Trudeau, F.H. Tezel, Pure and Binary Adsorption Equilibria of Methane and Nitrogen on Activated Carbons, Desiccants, and Zeolites at Different Pressures, J. Chem. Eng. Data. 61 (2016) 3163–3176.

[28] J.A.C. Silva, A. Ferreira, P.A.P. Mendes, A.F. Cunha, K. Gleichmann, A.E. Rodrigues, Adsorption Equilibrium and Dynamics of Fixed Bed Adsorption of CH4/N2 in Binderless Beads of 5A Zeolite, Ind. Eng. Chem. Res. 54 (2015) 6390–6399.

[29] J.A. Delgado, V.I. Águeda, M.A. Uguina, J.L. Sotelo, P. Brea, C.A. Grande, Adsorption and diffusion of H2, CO, CH4, and CO2 in BPL activated carbon and 13X zeolite: Evaluation of performance in pressure swing adsorption hydrogen purification by simulation, Ind. Eng. Chem. Res. (2014).

[30] S. Cavenati, C.A. Grande, A.E. Rodrigues, Adsorption Equilibrium of Methane, Carbon Dioxide, and Nitrogen on Zeolite 13X at High Pressures, J. Chem. Eng. Data. (2004).

[31] S. Auerbach, K. Carrado, P. Dutta, Handbook of Zeolite Science and Technology, 2003.

[32] Y. Park, D.K. Moon, Y.H. Kim, H. Ahn, C.H. Lee, Adsorption isotherms of CO2, CO, N2, CH4, Ar and H2 on activated carbon and zeolite LiX up to 1.0 MPa, Adsorption. (2014).

[33] T.A. Golden, Timothy Christopher; Farris, Thomas Stephen; Maliszewskyj, Robin Joyce; Cook, Use of activated carbon adsorbent in argon and/or oxygen controlling hydrogen PSA, U.S. Patent 6,261,343, 2001.

[34] ISO 14687: Hydrogen Fuel: Product Specification, Part 1: All applications except proton exchange membrane (PEM) fuel cell for road vehicles, 2009.

[35] ISO 14687: Hydrogen Fuel: Product Specification, Part 2: Proton exchange membrane (PEM) fuel cell applications for road vehicles, (2009).

[36] ISO 14687: Hydrogen Fuel: Product Specification, Part 3: Proton exchange membrane (PEM) fuel cells applications for stationary appliances, (2009).

[37] M. Yavary, H.A. Ebrahim, C. Falamaki, The effect of number of pressure equalization steps on the performance of pressure swing adsorption process, Chem. Eng. Process. Process Intensif. 87 (2015) 35–44.

[38] S. De-León Almaraz, C. Azzaro-Pantel, L. Montastruc, S. Domenech, Hydrogen supply chain optimization for deployment scenarios in the Midi-Pyrénées region, France, Int. J. Hydrogen Energy. 39 (2014) 11831–11845.

[39] C. Yang, J. Ogden, Determining the lowest-cost hydrogen delivery mode, Int. J. Hydrogen Energy. 32 (2007) 268–286.

[40] R. Berger, Fuel Cell Electric Buses - Potential for Sustainable Public. Transport in Europe, 2015.

[41] J.H. Han, J.H. Ryu, I.B. Lee, Modeling the operation of hydrogen supply networks considering facility location, Int. J. Hydrogen Energy. 37 (2012) 5328–5346.

[42] International Energy Agency (IEA), Large-Scale Hydrogen Delivery Infrastructure, 2015.

[43] K.S.K. Douglas M. Ruthven, S. Farooq, Pressure Swing Adsorption, John Wiley & Sons Inc, United States, 1993.

[44] K.R. Wood, Y.A. Liu, Y. Yu, Design, Simulation and Optimization of Adsorptive and Chromatographic Separations, Wiley-VCH, New York, 2018.

[45] J.A. Delgado, V.I. Agueda, M.A. Uguina, J.L. Sotelo, P. Brea, Hydrogen recovery from off-gases with nitrogen-rich impurity by pressure swing adsorption using CaX and 5A zeolites, Adsorption. 21 (2015) 107–123.

[46] D.D. Do, Adsorption Analysis: Equilibria and Kinetics, Imperial College Press, 1998.

[47] W. Rohsenow, J. Hartnett, Y. Cho, Handbook of Heat transfer, Third Edition., McGraw-Hill Education, New York, 1998.

[48] Greg F. Naterer, Advanced Heat Transfer, Second Edition, CRC Press Book, Boca Raton, Florida, 2018.

[49] www.engineeringtoolbox.com, Engineering ToolBox. Material Properties, Online. (2019).

[50] B. Ohs, M. Falkenberg, M. Wessling, Optimizing hybrid membrane-pressure swing adsorption processes for biogenic hydrogen recovery, Chem. Eng. J. (2019) 452–461.

[51] A. Mivechian, M. Pakizeh, Hydrogen recovery from Tehran refinery off-gas using pressure swing adsorption, gas absorption and membrane separation technologies: Simulation and economic evaluation, Korean J. Chem. Eng. 30 (2013) 937–948.

[52] U.S.D. of Energy, H2A analysis, (2019). www.hydrogen.energy.gov.

[53] T.Q. Hua, R.K. Ahluwalia, J.K. Peng, M. Kromer, S. Lasher, K. McKenney, K. Law, J. Sinha, Technical assessment of compressed hydrogen storage tank systems for automotive applications, Int. J. Hydrogen Energy. 36 (2011) 3037–3049.

[54] Eurostat, Electricity price statistics - Statistics Explained, 2018. ec.europa.eu.

APPENDIX

Simulation approach of breakthrough curves

According to these assumptions, the governing equations and input values are presented in Table A.4.1. Therefore, model parameters introduced in the program to simulate breakthrough tests are shown in Table A.4.2 to Table A.4.3. After that, the developed model was validated comparing selected simulation results with the corresponding breakthrough experiments.

Table A.4.1. Model parameters for a breakthrough process [45]

Fluid-phase mass balance for each component
$-D_{\mathrm{L}}\frac{\partial^2 c_{\mathrm{i}}}{\partial \mathrm{z}^2}+\frac{\partial}{\partial \mathrm{z}}(\mathrm{v}\cdot c_{\mathrm{i}})+\frac{\partial c_{\mathrm{i}}}{\partial \mathrm{t}}+\frac{(1-\varepsilon)}{\varepsilon}\frac{\partial \bar{q}_{\mathrm{i}}}{\partial t}=0$
Overall mass balance of the mixture
$\mathrm{C}\frac{\partial \mathrm{v}}{\partial \mathrm{z}}+\frac{\partial \mathrm{C}}{\partial \mathrm{t}}+\frac{(1-\varepsilon)}{\varepsilon}\sum_{\mathrm{i}}\frac{\partial \bar{q}_{\mathrm{i}}}{\partial t}=0$
Ideal gas law
$\mathrm{p}=\mathrm{R}T\sum_{\mathrm{i}} c_{\mathrm{i}}$
Mass transfer rate by the Linear Driving Force (LDF) model
$\frac{\partial \bar{q}_{\mathrm{i}}}{\partial t}=k_{\mathrm{i}}\left(q_{\mathrm{i}}^{*}-\bar{q}_{\mathrm{i}}\right)=\frac{15\cdot D_{\mathrm{app}}}{{r_{\mathrm{p}}}^2}\left(q_{\mathrm{i}}^{*}-\bar{q}_{\mathrm{i}}\right)$
Dual-Site Langmuir isotherm model
$q_{\mathrm{i}}^{*}=\frac{q_{\mathrm{max},1}\cdot b_1\cdot P_{\mathrm{i}}}{1+b_1\cdot P_{\mathrm{i}}}+\frac{q_{\mathrm{max},2}\cdot b_2\cdot P_{\mathrm{i}}}{1+b_2\cdot P_{\mathrm{i}}}$ $b_1=b_{\infty,1}\cdot \mathrm{e}^{\Delta H_1/\mathrm{R}T}$ $b_2=b_{\infty,2}\cdot \mathrm{e}^{\Delta H_2/\mathrm{R}T}$
Fluid-phase heat balance
$C_{\mathrm{pg}}\frac{\partial}{\partial \mathrm{z}}(v\cdot T)+\left(C_{\mathrm{pg}}+\frac{(1-\varepsilon)}{\varepsilon}C_{\mathrm{ps}}\right)\frac{\partial T}{\partial t}-\sum_{\mathrm{i}}(-\Delta H_{\mathrm{i}})\frac{(1-\varepsilon)}{\varepsilon}\frac{\partial \bar{q}_{\mathrm{i}}}{\partial t}+\frac{2h_i}{\varepsilon r_{\mathrm{i}}}(T-T_{\mathrm{w}})=0$
Energy balance equation per unit length of column wall
$\rho_{\mathrm{w}}C_{\mathrm{pw}}A_{\mathrm{w}}\frac{\partial T_{\mathrm{w}}}{\partial t}=2\pi r_{\mathrm{i}}h_{\mathrm{i}}(T-T_{\mathrm{w}})-2\pi r_{\mathrm{o}}h_{\mathrm{o}}(T_{\mathrm{w}}-T_{\mathrm{amb}})$
Momentum equation balance (Ergun equation)
$-\frac{\partial P}{\partial z}=1.5\cdot 10^{-3}\frac{(1-\varepsilon_{\mathrm{i}})^2}{\left(2r_{\mathrm{p}}\right)^2{\varepsilon_{\mathrm{i}}}^3}\mu v_g+1.75\cdot 10^{-5}\mathrm{M}\rho_{\mathrm{g}}\frac{(1-\varepsilon_{\mathrm{i}})}{2r_{\mathrm{p}}{\varepsilon_{\mathrm{i}}}^3}{v_g}^2$

Constant bed porosity is assumed in the breakthrough simulations. In this work, physical properties of the adsorbent have been measured for 5A zeolite, i.e. inter-particle porosity by mercury porosimetry, and the material density by helium pycnometry. The related material properties were calculated using the equations reported elsewhere [46].

Table A.4.2. Column characteristics, adsorbent properties and operating conditions

Parameter	Description	Value	Units
-	Number of layers	1	-
-	Bed type	Vertical	-
-	Spatial Dimensions	1-D	-
-	Thermocouple distance	2.5	cm
-	Adsorbent type	5A zeolite	-
-	Shape	Spherical beads	-
L_{bed}	Bed length	33.8	cm
d_{in}	Inside diameter	3.2	cm
d_0	Outside diameter	3.5	cm
V_{col}	Column volume	265.1	cm^3
w_t	Wall thickness	0.2	cm
m_{ads}	Mass of the adsorbent	193.1	g
r_p	Average particle radius	1.03	mm
ρ_{bulk}	Bulk solid density	728.5	kg m^{-3}
ρ_{solid}	Adsorbent density	2.36	g m^{-3}
$V_{skeleton}$	Skeleton volume	81.9	cm^3
$V_{total,\ ads}$	Total adsorbent volume	170.6	cm^3
ε_p	Intra-particle porosity	0.29	-
ε_i	Inter-particle porosity	0.57	-
ε_T	Total porosity	0.69	-
V_{gas}	Gas volume	183.2	cm^3

Table A.4.3. Mass and energy balance characteristics

Parameter	Description	Value	Units
C_{ps}	Adsorbent heat capacity	1000	J kg^{-1} K^{-1}
C_w	Wall specific heat	477	J kg^{-1} K^{-1}
K_w	Wall thermal conductivity	14.4	W m^{-1} K^{-1}
ρ_w	Wall density	7860	Kg m^{-3}
k_i	Mass transfer coefficients	-	-
	H_2	4.9	s^{-1}
	N_2	13.6	s^{-1}
	CH_4	15.3	s^{-1}
	Ar	6.1	s^{-1}
	Heat transfer coefficient	-	-
$h_{gas\text{-}solid}$	Gas-particles	See Table A.4.4	W m^{-2} K^{-1}
$h_{gas\text{-}wall}$	Gas-wall	See Table A.4.4	W m^{-2} K^{-1}
$h_{wall\text{-}env}$	Wall-Environment	6.0	W m^{-2} K^{-1}
T	Feed/Surroundings temperature	40	°C

Table A.4.4. Heat transfer coefficients at 0.5 L_N min^{-1}, 1 bar and 40 °C

Parameter	Mixture (%)	N_2:He (%)	H_2:He (%)	CH_4:He (%)	Ar:He (%)
y_{CH_4}	15	0	0	15	0
y_{CO}	0	0	0	0	0
y_{CO_2}	0	0	0	0	0
y_{He}	38	75	80	85	98
y_{H_2}	20	0	20	0	0
y_{N_2}	25	25	0	0	0
y_{Ar}	2	0	0	0	2
$h_{gas-solid}$ (W m^{-2} K^{-1})	189.9	193.7	216.3	195.7	208.3
$h_{gas-wall}$ (W m^{-2} K^{-1})	15.3	13.0	8.1	9.8	8.7

In a packed bed, there are three different phases depicted in Figure A.4.1: 1) the gas phase, 2) the solid phase, where takes place adsorption and diffusion, and 3) the wall column, where the energy may be transferred to or from the environment. Therefore, the mass and energy balance parameters are evaluated as follows: the adsorbent heat capacity of 5A zeolite is reported with a value of 1000 J kg^{-1} K^{-1} [47]. The wall properties were collected for a stainless-steel column [16]. The value of the heat transfer coefficient between the gas and the particles, $h_{gas-solid}$, is estimated using the correlation of Wakao and Kaguei (1982) [48]. The internal convective heat transfer between the gas and the wall, $h_{gas-wall}$, is calculated using the correlation proposed by Li and Finlayson [49]. Finally, the wall-environment heat transfer, $h_{wall-env}$, is calculated using empirical correlations described elsewhere [50]. General gas properties, like thermal conductivity, density, viscosity and specific heat were estimated for each inlet conditions and taken as constants along the bed [51]. The LDF method uses the mass transfer coefficients calculated for each gas, wherein these transport parameter values are related to the intra-particle diffusivity, D_{app} and to the radius of the adsorbent particle r_p.

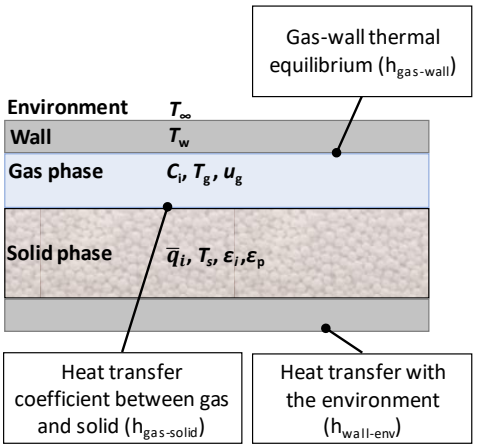

Figure A.4.1. Schematic presentation of the fixed bed

Economic benefits

The hydrogen levelized cost, $Cost_{\mathrm{H_2}}$, used to assess the process economics is calculated by dividing the equivalent annual costs, EAC, by the estimated product mass flow rate, $\dot{m}_{\mathrm{Prod}}$, and the annual operation time, t_{Ope}, and is described by the following formula [52]:

$$Cost_{\mathrm{H_2}} = \frac{EAC}{\dot{m}_{\mathrm{Prod}} \cdot t_{\mathrm{ope}}} \qquad \text{Eq. (A.4.1)}$$

The product mass flowrate $\dot{m}_{\mathrm{Prod}}$, depends upon the considered hydrogen purity and recovery. In order to estimate $\dot{m}_{\mathrm{Prod}}$, a small-to-medium ammonia production plant is supposed to be the base case scenario, in which up to 10% of the purge gases of the ammonia synthesis process could be valorized [1]. Thus, product mass flow rate is calculated by adapting Eq. (2.2) from Chapter 2 to this case study, as follow:

$$\dot{m}_{\mathrm{prod}} = \left(\dot{m}_{\mathrm{NH3}} \cdot R_{\mathrm{APG}} \cdot EF \cdot y^{F}_{\mathrm{H_2}}\right) \cdot HR \qquad \text{Eq. (A.4.2)}$$

with $\dot{m}_{\mathrm{NH3}}$ as the plant's capacity, R_{APG} as the ratio of APG produced, EF the emission factor, $y_{\mathrm{H_2,feed}}$ the hydrogen feed fraction, and HR the hydrogen recovery, which varies depending on the final application. The hydrogen quantity was estimated based on the achieved recovery value of 55.0 % at fuel-cell grade hydrogen during cyclic PSA process optimization. All process parameters for hydrogen upgrading are summarized in Table A.4.5.

Table A.4.5. Process parameters for hydrogen upgrading

Parameter	Description	Value	Units
$\dot{m}_{\mathrm{NH3}}$	Ammonia plant's capacity	500	t NH_3 day^{-1}
R_{APG}	Pre-set ratio of APG produced	180 - 240	Nm^3 APG ton NH_3^{-1}
EF	Emission factor	10	%
HR	H_2 recovery at fuel-cell grade	55.5	%
$y^{\mathrm{F}}_{\mathrm{H_2}}$	Feed fraction (H_2/N_2/CH_4/Ar)	58/25/15/2	% vol.
P_{ads}	Adsorption pressure	20	bar
$y^{\mathrm{P}}_{\mathrm{H_2}}$	Hydrogen purity	99.97	% vol.
$\dot{m}_{\mathrm{prod}}$	Product mass flow rate	12.5	kg H_2 h^{-1}

Therefore, the levelized cost of H_2 entails the total investment costs, $CAPEX$, as well as the annual operating costs, OPEX. The capital costs were annualized assuming an interest rate, ir, of 10 % and a plant lifetime of 15 years, DEP. The equivalent annual costs are given by:

$$EAC = CAPEX \cdot \frac{ir}{1-(1+ir)^{-DEP}} + \mathrm{OPEX} \qquad \text{Eq. (A.4.3)}$$

The first scenario under study, fuel-cell grade hydrogen at 20 bar, entails only the PSA stage. For this case, the PSA unit incurs in fixed capital,$CAPEX_{\mathrm{PSA}}$, and operational production costs, $OPEX_{\mathrm{PSA}}$, based upon the investment cost of a reference case [53], following six-tenths-factor rule indicated in Eq. (2.4) in Chapter 2. $CAPEX_{\mathrm{PSA}}$ includes direct costs (equipment cost, installation cost, piping, electrical system and building) and indirect costs (engineering and supervision, contractor's fee and contingency). On the other hand, $OPEX_{\mathrm{PSA}}$ includes utilities, operating labor, maintenance and repairs. For simplification, it was assumed that the operational production costs, $OPEX_{\mathrm{PSA}}$, are directly proportional to the base reference. Table A.4.6 shows all assumptions and parameters for economic analysis.

The second scenario, compressed fuel-cell grade hydrogen, requires apart from the purification step, the product compression for 350-bar and 700-bar refueling, and its delivery to the nearest refueling station. In such a scenario, capital costs of the required compressors, $CAPEX_{\mathrm{Compressor}}$, were estimated using the H2A framework [54]; whereas the compression operational costs were based on the energy consumption of the compressors, E_{CH2}, which is established at 2.9 kWh kgH_2^{-1} and 3.7 kWh kgH_2^{-1} for the 350 and 700-bar storage options, respectively [55]. In such a scenario, the total capital and operating costs are calculated as follows:

$$CAPEX = CAPEX_{\mathrm{PSA}} + CAPEX_{\mathrm{Compressor}} \quad \text{Eq. (A.4.3)}$$

$$OPEX = OPEX_{\mathrm{PSA}} + OPEX_{\mathrm{Compressor}} + OPEX_{\mathrm{Delivery}} \quad \text{Eq. (A.4.4)}$$

Hence, the energy costs for compression are the product of the product rate, $\dot{m}_{\mathrm{Prod}}$; the compressor power, E_{CH2}; and the EU-28 average electricity price,p_{energy}, for industrial consumers [56]:

$$OPEX_{\mathrm{Compressor}} = \dot{m}_{\mathrm{prod}} \cdot E_{\mathrm{CH2}} \cdot p_{\mathrm{energy}} \quad \text{Eq. (A.4.5)}$$

Besides, the total operating costs also entail the compressed hydrogen (CH2) delivery cost , $OPEX_{\mathrm{Delivery}}$, assuming the unit transportation cost by tube trailers, $p_{\mathrm{CH2,delivery}}$ for short distance exporting (< 20 km) [41]:

$$OPEX_{\mathrm{Delivery}} = \dot{m}_{\mathrm{prod}} \cdot d_{\mathrm{Delivery}} \cdot p_{\mathrm{CH2,Delivery}} \quad \text{Eq. (A.4.6)}$$

Table A.4.6. Assumptions and parameters for economic analysis

Parameter	Description	Value	Units
DEP	Plant lifetime	15	years
UF_{PSA}	Update factor for PSA unit (2011/2018)	1.03	-
ir	Interest rate	10	%
p_{energy}	Electricity price	0.078	€ kWh^{-1}
$E_{\mathrm{CH2,350}}$	Compressor power to 350 bar	2.9	kWh kgH_2^{-1}
$E_{\mathrm{CH2,700}}$	Compressor power to 700 bar	3.7	kWh kgH_2^{-1}
t_{ope}	annual operation time	8000	hours $year^{-1}$
$p_{\mathrm{CH2,delivery}}$	Tube Trailer Cost	10.04	€ km^{-1} $tonH_2^{-1}$
d_{delivery}	Delivery distance to HRS	20	km

CHAPTER 5

CONCLUSIONS AND FUTURE WORK

5.1 CONCLUSIONS

In this thesis, the most promising gas-clean up technologies to contribute to the upcycling of industrial hydrogen-containing waste gas streams, have been assessed in terms of performance. Initially, hydrogen as a unique and versatile energy carrier has been explained, focusing in its potential as a future carbon-free road transport fuel. Therefore, for completely switching over to a hydrogen economy, an environmentally clean process should produce hydrogen to have positive impact on decarbonization. In this regard, hydrogen-rich industrial waste streams that in some cases are simply vented or flared to the atmosphere, has also become attractive sources to be upgraded to power fuel cells, promoting the circular economy by upcycling the resources.

In **Chapter 1,** an extensive screening procedure has been performed to identify industrial waste gaseous streams with major potential in their upgrading to feed fuel cell stacks. This has effectively led to the identification of many industrial sectors with available surplus hydrogen as chlorine-alkali, methanol, ammonia and steel industries, but also refineries and petrochemical plants. Industrial surplus hydrogen varies in its purity, depending on the industrial process from which it comes. Whereas off-gases from chlor-alkali electrolysis are mostly at fuel-cell grade hydrogen, by-product hydrogen from coal carbonization is in the range of 55 to 66 % vol. H_2. Therefore, a purification process is needed in some cases for further use of hydrogen (other than generation of process heat). Then, established hydrogen purification techniques has been introduced. Special detail has been taken while describing polymeric membrane systems and pressure swing adsorption (PSA) technologies, since there are the ones that exhibit the best cost-effective performance. The state-of-the art of membrane-based processes and PSA technologies has been key to identify the research trends in these gas separation techniques. Furthermore, a detailed description of the fuel quality requirements for fuel cell systems has been presented to meet these targets.

In **Chapter 2,** an optimization modelling approach has been applied to address the identification of the optimal hydrogen supply chain (HSC) for the north of Spain, which integrates industrial hydrogen-rich waste gas sources and converts them into liquefied hydrogen, by maximizing the net present value (NPV) as the objective function. The mathematical modelling approach based on multi-scenario multi-period mixed-integer linear programming (MILP) contributes to satisfy the growing hydrogen demand for stationary and road transport applications over a 30-year time horizon. For the case study of the northern Spain region, 4,135 km^2 and 11,723,776 inhabitants, it has been identified a pull of 3 possible raw materials, 8 possible suppliers, 17 merchants, 3 conversion technologies, 36 customers and 1 unique

product, leading to the cost-optimal solution over the 2020 - 2050 period. Within a more sustainable framework, the results provide a basis for assessing the techno-economic feasibility of various by-product gases to embed sustainability into HSC. The available amounts of surplus hydrogen are distributed in the model according to their real geographical locations. Furthermore, centralized steam methane reforming (SMR) with carbon capture and storage (CCS) has been considered as benchmark technology in order to satisfy the expected demand for hydrogen, while renewable source infrastructures like wind and solar farms continue developing for its large scale integration. In this regard, optimal decisions to determine how and when stakeholders shall invest in developing the hydrogen infrastructure have been obtained, regarding the technology selection, facility location and sizing, and yearly production planning. The analysis has been performed over two scenarios of hydrogen demand, and the results show that as long as both scenarios of hydrogen demand apply, all generated case studies lead to a solution with positive NPVs. The main conclusion that can be drawn is that the use of inexpensive surplus hydrogen sources such as R50 (coke oven gases) and R99 (chlor-alkali off-gases) offers an economic solution to cover hydrogen demand in the very early stage of transition to the future global hydrogen-incorporated economy, especially when surplus hydrogen generation is closer to the demand markets. Collectively, our results appear consistent with other studies, which suggest the potential utility of industrial hydrogen for fueling hydrogen vehicles during the transition phase. In this regard, hydrogen production via purification systems stands out as the most profitable solution with payback periods lower than 6 years, which strongly depends on the available volume of the industrial waste streams.

Furthermore, **Chapter 3** reports new data on the performance of commercial polymeric membranes for hydrogen selective separations, which serves as the basis for the evaluation of the membrane technologies for hydrogen recovery from industrial waste gases. The permeation of pure gases and multicomponent mixtures of H_2, N_2, CH_4, CO, and CO_2 at different operation conditions through dense polymeric films has been investigated. Moreover, operating conditions that govern the practical feasibility of commercial membranes are discussed. In this way, new knowledge on membrane behavior related to real process conditions is revealed for commercially available polymeric membranes. In this chapter, mixed-gas permeation through three different non-porous polymeric membranes (polyetherimide (PEI), polyethersulfone (PES) and polybenzimidazole (PBI)) has been studied over three different synthetic waste gas streams: ammonia purge gas (APG) (H_2/ N_2/ CH_4 (% vol.): 58.6/ 25.7/ 15.7), coke oven gas (COG) (H_2/ N_2/ CO_2/ CO/ CH_4 (% vol.): 60.2/ 4.7/ 2.1/ 6.8/ 26.2) and methanol purge gas (MPG) (H_2/ N_2/ CO_2/ CO/ CH_4 (% vol.): 63.1/ 11.3/11.1/3.4/ 11.2). Also, the influence of temperature, transmembrane

pressure and feed gas composition on gas permeation was examined. Regarding the major findings of this study, it should be notice that, all gas permeabilities were increased at higher temperatures in the mixed gas system. Even so, all studied cases H_2/N_2, H_2/CH_4 and H_2/CO selectivity values decrease with temperature, while H_2/CO_2 increases. On the other hand, permeability of low-sorbing penetrants (i.e. H_2, N_2, CH_4, CO) as feed gas exhibit insignificant change with pressure, whereas the permeability tendency observed for CO_2 showed that a decreasing trend upon the transmembrane pressure increased. Moreover, strong dependency of H_2 permeability on CO_2 concentration inducing a decay of H_2/CO_2 selectivity in mixed-gas experiments for the studied membranes. Although single gas permeabilities are similar to those reported in previous research, competitive sorption effect results in a slight drop in the permeability of H_2 with respect to pure gases using PEI and PES membranes. Although the maximum hydrogen purity obtained using PEI membrane was 99.7 % vol. H_2 from APG, 98.8 % from COG and 95.4 % from MPG, it would be necessary further upgrading of the permeate stream to the required quality to comply with ISO 14687 series.

Finally, by taking advantage of the PSA technology to obtain high-purity hydrogen, a four-bed PSA unit packed with 5A zeolite was studied to purify hydrogen from a simulated effluent gas (H_2:N_2:CH_4:Ar, 58:25:15:2 %) of ammonia synthesis process in **Chapter 4**. As in the ammonia synthesis process, a gaseous stream is purged to keep the inert gases concentration below a threshold value; this stream contains large hydrogen quantities, which can be recovered. Firstly, the adsorption equilibrium isotherms of H_2, N_2, CH_4, and Ar on four pre-selected adsorbents have been obtained. According to the equilibrium separation factors, it was concluded that activated carbon AC is the best adsorbent for removing Ar, whereas LiX and 5A zeolites remove more effectively N_2 and CH_4, respectively. Nonetheless, given that, the bulk density of zeolite is higher than for AC, 728 kg m^{-3} and 600 kg m^{-3}, respectively, and that the separation factor is only 1.3 times higher, the benefit of using an additional AC layer is almost negligible. Therefore, 5A zeolite was selected as the best adsorbent for purifying H_2 from ammonia purge gas stream due to its well-balanced N_2/H_2 and CH_4/H_2 separation factors and acceptable Ar removal performance. To assess the performance of the selected adsorbent, 5A zeolite, single component and multicomponent breakthrough curves have been experimentally carried out in a single packed column, and further simulated. The results, simulations and experimental, have indicated that the first impurity to break thought the column is Ar, followed by N_2 and finally by CH_4. Consequently, the separation performance of the four-bed PSA unit packed with zeolite 5A can be affected by the Ar adsorption for concentrations as low as 2 %. The PSA experiments have been conducted in a 4-column PSA unit with 12-events cycle, comprising 9 elementary steps.

The role of operating parameters in PSA performance such as purge-to-feed (P/F) ratio, adsorption step time and adsorption pressure, has been investigated. The overall PSA performance has been evaluated in terms of purity, recovery and productivity of H_2 product. The experimental unit has been optimized to maximize the responses based on response surface methodology (RSM) models for three specific final applications, in compliance with ISO 14687 standards. The PSA unit of this study can produce H_2 with 99.25 % - 99.97 % vol. purity with 75.3 % - 55.5 % of recovery, respectively, where Ar and N_2 are the main impurities at the product stream. A significant loss of recovery and productivity happens when H_2 purity was set at + 99.9 % vol. The study showed the feasibility of the PSA process packed with 5A zeolite to produce a wide purity range of H_2 product streams from a feed mixture containing as impurities N_2, CH_4 and Ar, as simulated ammonia purge gas. In addition to the technical performance, a simplified economic analysis has been carried out. The cost to purify an ammonia waste hydrogen stream to + 99.97 % vol. using a small-PSA unit, compress and transport has been estimated to be 1.17 to 1.39 € kg H_2^{-1}, respectively, depending on the dispensing pressure of 350 or 700 bar. These values permit reducing H_2 costs by at least 40 % based on off-site H_2 production by SMR plus compression and transportation until the refueling station.

5.2 FUTURE WORK

This thesis intends to open up the possibility of upcycling industrial hydrogen-containing waste gas streams to obtain hydrogen with fuel cell specification, in terms of performance as well as profitability. Thus far, the obtained results, which for the first time analyze the economic advantages of integrating upcycled industrial hydrogen in HSC, could support future decision-making policies. Likewise, the proposed methodology could be extended over different spatial regions and timeframes. Moreover, established hydrogen purification systems, polymeric membranes and PSA processes, have been assessed by using different multicomponent gas mixtures. Nevertheless, despite the achievements that have been described through the chapters of this thesis, there are still challenges ahead and some future trends can be defined to continue with the research of this thesis.

Regarding the proposed optimization model, it could be extended to other multi-echelon problems to encompass other variables alongside factors such as: clean feedstock (i.e. renewable energy sources), technical feasibility and performance of a sustainable HSC. The presence of inherent uncertainties on significant input parameters might prove important to the optimization model. Thus, the estimation of forecast uncertainties in different parts of the chain is essential to obtain optimal solutions in a dynamic approach, instead of the steady state

proposed model. Particularly, supply uncertainty of surplus hydrogen could be reduced by assessing the variability of the hydrogen composition and available volume with real-data obtained site-by-site in each supplier company. Besides, raw material and product prices uncertainty as a result of external factors (i.e. decrease in natural gas prices or vice versa) could be analyzed with a stochastic model characterized by probability distribution of potential outcomes within a given interval. Regarding the timeframe, if an hourly time intervals were adopted, the operational problem could also include the management and utilization of the industrial surplus hydrogen taking into account other utilization alternatives (i.e. hydrogen-to-chemical or hydrogen-to-gas applications). These alternatives will depend on the purity level required for each specific end-use at the same time as avoiding supply-demand mismatches within the industry itself. Furthermore, the Geographical Information System (GIS) based approach could be included as a component of the optimization method to provide the best overview of the future hydrogen infrastructure. To identify a more sustainable design, it is necessary to include environmental concerns beyond the economic performance into a multi-objective problem, while obtaining a trade-off between both objectives.

Concerning commercial hydrogen-selective membranes based on non-porous polymeric materials tested in a lab-scale set up using multicomponent gas mixtures, future research should further developed. With the experimentally obtained mixed permeances, required membrane area for a specific separation can be calculated and optimum operational conditions can be found. Although the maximum hydrogen purity obtained using PEI membrane was up to 99.7 % vol. H_2 from APG , 98.8 % from COG and 95.4 % from MPG, it would be necessary further upgrade to the required quality in comply with ISO 14687 series. In fact, it is worth noting that although H_2 purities obtained are higher than 98 % vol. H_2 for APG and COG mixtures, which may indeed be used as a commodity chemical in many industrial processes, they are still far from fuel cell requirements. Besides, membrane processes should be tested under real feeds to ensure membrane stability for long-term operation. Issues, such as the improvement of the permeation parameters as well as the gas productivity grade still remain in the attention of the academic and industrial community, and there are several directions of such endeavor. On the one hand, synthetic and physical chemists attempt to improve selectivity, permeability or both of polymeric materials. On the other hand, hydrogen recovery could be maximized for a certain value of purity by using cascade membrane module systems or coupling it with conventional processes. Thus, a hybrid membrane-PSA system could be designed by using optimization techniques to determine the optimal integration scheme.

Finally, the assessment of a four-bed PSA unit packed with 5A zeolite to produce purified hydrogen for diverse final applications has been presented using a synthetic gas mixture, based on APG. These novel findings are of special interest for fertilizer companies worldwide that manufactures ammonia in order to produce distributed hydrogen from waste gas effluents. Thus, the optimal conditions of the PSA unit can be changed to obtain from lower hydrogen purity for industrial use (98 %) to higher purity for road vehicle systems (> 99.97 %), at exactly the time when hydrogen demand for mobility begin to be fully felt. The achieved recovery is assumed to be very conservative due to the PSA system has only 4 absorbers fed at a relatively low pressure ≤ 9 bar. However, these recoveries should be higher at real conditions by taking advantage of the significant pressure swing growth, due to the pressure of APG wasted is already high (150 – 200 bar). This is an interesting topic for in situ application. Looking forward, further attempts could be made to refine the PSA process such as the reduction of idle periods normally used to match cycle sequencing in order to maximize the productivity. In this regard, the design of the PSA cycle can be carried out by modelling different scenarios to estimate the optimal duration of each of the steps from one simple to a complex model. Moreover, the obtained data correspond to well-known adsorbents and can be considerably improved by using new high performance adsorbents to achieve higher throughputs with the same or even less volume of adsorbent. Furthermore, when argon concentration in feed gas mixture may exceed 2 % as stated in the case study, the PSA process could be improved with an additional layer of activated carbon AC as the best adsorbent for argon removal hence the optimum carbon-to-zeolite ratio should be obtained. To guarantee optimum performance in real conditions, trace components of ammonia should also be evaluated in future to avoid detrimental effects not only by the presence of competitive cations that occupy the available ion-exchange sites on the zeolites, but also on the fuel cell performance due to ammonium ions (NH_4^+) formation within membrane electrode assembly [1,2]. Also, other relevant waste gas streams should be studied by identified the best adsorbent for the presence of other impurities such as CO or CO_2. Regardless, process intensification using membrane technology offers a compact and modular solution for capital and energy savings, by taking advantage of both separation techniques presented in this thesis.

REFERENCES

[1] H. Huang, L. Yang, Q. Xue, et al., Removal of ammonium from swine wastewater by zeolite combined with chlorination for regeneration, J. Environ. Manage. 160 (2015) 333–341.

[2] J.L. Aprea, Quality specification and safety in hydrogen production, commercialization and utilization, Int. J. Hydrogen Energy. 39 (2014) 8604–8608.

CAPÍTULO 5

CONCLUSIONES Y TRABAJO FUTURO

5.1 CONCLUSIONES

En esta tesis, las tecnologías de separación de gases más prometedoras para la recuperación de hidrógeno a partir de corrientes gaseosas residuales de origen industrial han sido evaluadas en términos de rendimiento y rentabilidad. Primero, se ha introducido el hidrógeno como vector energético, enfocándose en su potencial como combustible libre de carbono para el transporte por carretera. Para poder tener un impacto medioambientalmente positivo dentro de una economía basada en hidrógeno, éste debería ser producido por un proceso sostenible libre de emisiones. Asimismo, las corrientes gaseosas residuales ricas en hidrógeno, que en algunos casos simplemente son quemadas o venteadas a la atmósfera, resultan ser una fuente de recursos muy atractiva para poder ser usadas como fuel en pilas de combustible tras mejorar su grado de pureza, promoviendo así la economía circular de los recursos.

En el **Capítulo 1**, se ha llevado a cabo un procedimiento exhaustivo de identificación de corrientes gaseosas residuales de origen industrial con mayor potencial de ser recuperadas y poder alimentar celdas de combustible. Esto ha contribuido eficazmente a la identificación de varios sectores industriales que tienen disponible excedente de hidrógeno tales como las industrias cloro-álcali, la de metanol, la del amoniaco o las acerías, pero también refinerías o la industria petroquímica. La pureza del excedente de hidrógeno industrial disponible es variable dependiendo del tipo de proceso en el que se generan. Mientras que los gases de salida procedentes de la electrólisis de salmuera son producidos con una elevada pureza de hidrógeno, el contenido de hidrógeno en el subproducto generado durante el proceso de coquización del carbón puede variar entre 55 - 66 %. Es por ello que, en algunos casos, resulta necesario un proceso de purificación de los gases para darle un uso final distinto que la generación de calor. Por consiguiente, las principales técnicas de purificación de hidrógeno han sido introducidas. Se ha puesto especial énfasis en los sistemas de membranas poliméricas, así como en las tecnologías de adsorción por cambio de presión (PSA, por sus siglas en inglés), debido a que son las que exhiben mejores rendimientos. El estado del arte de los procesos basados en membranas y de las tecnologías de PSA ha sido clave para identificar las tendencias de investigación en las técnicas de separación de gases. Además, se ha presentado una descripción en detalle de los requerimientos de calidad del hidrógeno para su aplicación en pilas de combustibles.

En el **Capítulo 2**, se ha aplicado un modelo de optimización para abordar la determinación óptima de una cadena de suministro de hidrógeno (HSC) para el norte de España, la cual integre corrientes industriales residuales ricas en hidrógeno y las convierta en hidrógeno licuado, maximizando el valor actual neto (NPV) como función objetivo. El modelo matemático propuesto basado en programación lineal entera mixta (MILP) multi-escenario y multi-periodo, contribuye a satisfacer una demanda creciente de hidrógeno para aplicaciones estacionarias y de transporte por carretera a lo largo de un horizonte temporal de 30 años. Para el caso de estudio de la región del norte de España, 4.135 km^2 y 11.723.776 habitantes, se ha identificado un total de 3 posibles materias primas, 8 compañías suministradoras, 17 empresas transformadoras, 3 tecnologías de conversión, 36 clientes, y 1 único producto, conducen a la solución más rentable para el periodo 2020 - 2050. En un marco de desarrollo más sostenible, los resultados obtenidos proporcionan una base para evaluar la viabilidad técnico-económica de integrar varios subproductos gaseosos en una HSC. Las cantidades disponibles del excedente de hidrógeno de las industrias son distribuidas en el modelo de acuerdo con su localización geográfica real. Asimismo, se ha considerado el reformado de metano con vapor de agua (SMR) con captura y secuestro de carbono (CCS) como la tecnología de referencia para satisfacer una demanda creciente de hidrógeno, mientras que la integración de la infraestructura basada en fuentes renovables como la eólica y la solar continúa en desarrollo. Como resultado se han obtenido las decisiones óptimas para determinar cómo y cuándo los diferentes agentes implicados deberán realizar sus inversiones para desarrollar una infraestructura de hidrógeno, de acuerdo con la selección, localización y capacidad de las tecnologías transformadoras, junto con un plan de producción anual. El análisis ha sido desarrollado sobre dos escenarios diferentes de demanda de hidrógeno, y los resultados muestran que, a lo largo de los escenarios empleados, todos los casos de estudio generados dan lugar a una solución con valores de NPV positivos. La principal conclusión que puede sacarse es que el uso de las fuentes de hidrógeno residuales tales como R50 (gas alto horno de coque) y R99 (gases de salida cloro-álcali) ofrecen una solución económica para cubrir la demanda de hidrógeno en una etapa inicial de la transición hacia una economía que incorpora hidrógeno, especialmente cuando el excedente generado está próximo a los nichos de mercado. En conjunto, dichos resultados son consistentes con otros estudios, en lo que se comenta la potencial utilidad de hidrógeno industrial como combustible para alimentar vehículos con hidrógeno durante una fase de transición. Es este sentido, la producción de hidrógeno mediante sistemas de purificación destaca como la solución económicamente más rentable con un periodo de retorno de menos de 6 años, a pesar de depender fuertemente del volumen de corriente de gas residual disponible.

Asimismo, el **Capítulo 3** reporta nuevos datos sobre el comportamiento de membranas poliméricas comerciales, los cuales sirven de base para la evaluación de la tecnología de membranas para recuperar hidrógeno a partir de mezclas de gases industriales. Se ha investigado la permeación de gases puros y mezclas de gases multi-componentes de H_2, N_2, CH_4, CO, y CO_2 a diferentes condiciones de operación a través de membranas densas poliméricas. Además, se ha analizado el efecto de las condiciones de operación que rigen la viabilidad práctica de las membranas comerciales. En este sentido, nuevos conocimientos sobre el comportamiento de membranas en condiciones reales son revelados para varias membranas poliméricas comerciales. Se ha estudiado la permeación de mezclas de gases a través de las siguientes tres membranas densas poliméricas: polieterimida (PEI), polietersulfona (PES) y polibenzimidazole (PBI), con tres corrientes sintéticas de gases residuales: gases de purga de amoniaco (APG) (H_2/ N_2/ CH_4: 58,6/ 25,7/ 15,7 %), gas alto horno de coque (COG) (H_2/ N_2/ CO_2/ CO/ CH_4: 60,2/ 4,7/ 2,1/ 6,8/ 26,2 %) y gases de purga de metanol (MPG) (H_2/ N_2/ CO_2/ CO/ CH_4: 63,1/ 11,3/11,1/3,4/ 11,2 %). También se ha examinado la influencia de la temperatura, la presión transmembrana y la composición de la alimentación en la permeación de los gases. Entre los mayores hallazgos de este estudio cabe destacar que, en los experimentos de mezclas de gases, las permeabilidades de todos los gases aumentan al incrementarse la temperatura. En todos los casos de estudio los valores de selectividad de H_2/N_2, H_2/CH_4 y H_2/CO decrecen con el aumento de temperatura, mientras que los de H_2/CO_2 aumentan. Por otro lado, la permeabilidad de especies penetrantes con baja adsorción (ej. H_2, N_2, CH_4, CO) prácticamente no exhibe cambios con respecto a la presión transmembrana, mientras que la tendencia de permeabilidad observada para el CO_2 muestra una tendencia decreciente a medida que la presión aumenta. Asimismo, se observa una fuerte dependencia de la permeabilidad de H_2 con la concentración de CO_2 induciendo a una caída de la selectividad H_2/CO_2 en mezclas de gases para las membranas estudiadas. Efectos competitivos de adsorción dan lugar a una caída de la permeabilidad de H_2 con respecto a los valores de gases puros usando las membranas de PEI y PES, mientras que ligeramente un efecto opuesto puede observarse en el caso de PBI. Aunque la máxima pureza de hidrógeno obtenido usando la membrana de PEI fue, 99,7 % vol. H_2 a partir de APG, 98,8 % a partir de COG y 95,4 % a partir de MPG, resulta necesario incrementar la pureza de la corriente de permeado a la calidad requerida de acuerdo con la serie de estándares ISO 14687.

En el **Capítulo 4**, se ha estudiado una unidad de cuatro columnas de PSA cargadas con zeolita tipo 5A para purificar hidrógeno a partir de una corriente de gases sintética (H_2:N_2:CH_4:Ar, 58:25:15:2 %) que se genera durante el proceso de síntesis de amoniaco. Dentro del proceso de

síntesis de amoniaco, una corriente gaseosa es purgada para mantener la concentración de gases inertes por debajo de un valor definido; dicha corriente gaseosa contiene grandes cantidades de hidrógeno que puede ser recuperado. En primer lugar, se han obtenido las isotermas de equilibrio de adsorción de H_2, N_2, CH_4, y Ar de cuatro adsorbentes preseleccionados. De acuerdo a los factores de separación, se concluye que el carbón activo es el adsorbente más selectivo al Ar, mientras que las zeolitas tipo LiX y 5A son las más efectivas para eliminar N_2 y CH_4 respectivamente. Es por ello que finalmente se ha seleccionado la zeolita tipo 5A como el mejor adsorbente para purificar H_2 a partir de una corriente de purga de amoniaco ya que posee factores equilibrados de separación N_2/H_2 y CH_4/H_2, a su vez que un valor aceptable para la eliminación del Ar. Sin embargo, dado que la densidad aparente de la zeolita es superior a la del AC, 728 kg m^{-3} y 600 kg m^{-3}, respectivamente, y el factor de separación es sólo 1.3 veces superior, el beneficio de usar una capa de AC es casi despreciable. Para continuar con la caracterización del adsorbente seleccionado, zeolita tipo 5A, se han realizado experimentalmente curvas de ruptura de cada compuesto y con mezcla de gases multi-componente en una columna empacada con dicho material, y posteriormente se han simulado. Los resultados, experimentales y simulados, indican que la primera impureza en salir de la columna es Ar, seguido de N_2 y finalmente CH_4. Consecuentemente, la capacidad de separación de una unidad de cuatro columnas de PSA cargada con zeolita tipo 5A se ve afectada por la adsorción de Ar a concentraciones bajas de un 2 %. Se han llevado a cabo una serie de experimentos en una unidad de cuatro columnas de PSA con 12 eventos de ciclo y 9 pasos elementales. Asimismo, se ha investigado el efecto de ciertos parámetros de operación, tales como el ratio purga-alimentación (P/F), el tiempo de adsorción, y la presión de operación, en el desempeño de la unidad de PSA. La capacidad global de la unidad de PSA se ha evaluado en términos de pureza, recuperación y productividad del producto hidrógeno. La unidad experimental ha sido optimizada para maximizar los factores respuesta usando la metodología de la superficie de respuesta (RSM), para tres aplicaciones finales específicas de acuerdo con los estándares ISO 14687. La unidad de PSA de estudio puede producir H_2 con una pureza de entre 99,25 % - 99,97 % vol. y una recuperación de 75,3 % - 55,5 %, respectivamente, donde Ar and N_2 constituyen las principales impurezas de la corriente de producto. Un decrecimiento significativo de la recuperación y la productividad ocurre cuando la pureza del hidrógeno se fija a un valor + 99,9 % vol. El estudio realizado muestra la viabilidad del proceso de PSA cargado con zeolita 5A para producir un amplio rango de purezas de hidrógeno a partir de una mezcla de gases de entrada que contienen impurezas de N_2, CH_4 y Ar, en base a los gases de purga de la síntesis de amoniaco.

Tras el estudio experimental, se ha llevado a cabo un análisis económico simplificado. Se ha estimado que el coste total de purificar los gases de purga de la síntesis de amoniaco hasta una pureza de + 99,97 % vol., usando una unidad pequeña de PSA, incluyendo los costes de compresión y transporte, entre 1,17 a 1,39 € kg H_2^{-1}, en función de si la presión de distribución es de 350 o 700 bar, respectivamente. Estos valores obtenidos permiten reducir los costes de producción de hidrógeno al menos un 40 %, en relación a los costes de producción de hidrógeno mediante reformado de gas natural, incluyendo costes de compresión y transporte hasta la estación de suministro.

5.2 TRABAJO FUTURO

Esta tesis trata de contribuir en la recuperación de corrientes gaseosas residuales de origen industrial con el fin de obtener hidrógeno con las especificaciones necesarias para su aplicación en pilas de combustible, en términos de rendimiento y rentabilidad. Los resultados obtenidos hasta la fecha, los cuales por primera vez analizan las ventajas de integrar hidrógeno residual industrial en una cadena de suministro de hidrógeno, podrían ser un mecanismo de apoyo en la toma de decisiones políticas. Además, la metodología propuesta podría extenderse a diferentes regiones espaciales y periodos. Asimismo, se han evaluado los principales sistemas de purificación de hidrógeno, las membranas poliméricas y la adsorción por cambio de presión (PSA) usando diferentes mezclas de gases multi-componentes. Sin embargo, a pesar de los avances descritos a lo largo de los capítulos de la tesis, todavía quedan retos por delante y algunas tendencias futuras pueden ser definidas para continuar con la investigación de la tesis.

En relación al modelo de optimización propuesto, éste puede ser extendido a otros problemas multi-eslabón con el fin de abarcar otras variables a lo largo de factores tales como otras materias primas (ej. fuentes de energía renovable), y de viabilidad técnica y desarrollo en una HSC sostenible. La presencia de incertidumbres en parámetros de entrada significativos pueden ser una observación importante a tener en cuenta en el modelo de optimización. De este modo, la valoración y pronóstico de incertidumbres en diferentes partes de la cadena resulta esencial para obtener soluciones óptimas dentro de un enfoque dinámico, en lugar del modelo estático propuesto. Particularmente, las incertidumbres relacionadas con el suministro de hidrógeno residual podrían reducirse evaluando la variabilidad de la composición de hidrógeno en dichas corrientes, así como obtener el volumen disponible usando datos reales extraídos de cada una de las empresas suministradoras. A parte, la incertidumbre de los precios de materias primas y productos como resultado de factores externos (ej. de déficit a superávit o viceversa) podría ser analizada con un modelo estocástico caracterizado por una distribución

probabilística de los posibles resultados dentro de un intervalo. En relación al periodo de estudio, si el intervalo de tiempo adoptado fuera por horas, el problema operacional podría también incluir la gestión y utilización de corrientes de hidrógeno residuales teniendo en cuenta otras alternativas de uso finales (ej. materia prima de productos químicos o su inyección a la red de gas natural). Estas alternativas dependerán a su vez del nivel de pureza requerido para cada uso final específico, al mismo tiempo que facilitarían la adaptación entre oferta y demanda dentro de la propia industria. Por otra parte, los sistemas de información geográfica (GIS) podrían ser incluidos como un componente en el método de optimización ofreciendo una mejor visualización de la implantación de la futura infraestructura de hidrógeno. Asimismo, con el fin de identificar un diseño más sostenible, es necesario incluir cuestiones medioambientales más allá del objetivo económico en un problema multi-objetivo, mientras se obtiene una solución intermedia entre ambos.

En lo que respecta a las membranas comerciales selectivas de hidrógeno basadas en materiales poliméricos no porosos testadas a escala laboratorio usando mezclas de gases multi-componentes, podrían realizarse avances en futuras investigaciones. Con las permeabilidades de mezclas obtenidas experimentalmente, se podría calcular el área de membrana requerida para una separación específica y obtener las condiciones de operación óptimas. Aunque la máxima pureza de hidrógeno obtenido usando la membrana de PEI fue, 99,7 % vol. H_2 a partir de APG, 98,8 % a partir de COG y 95,4 % a partir de MPG, resulta necesario incrementar la pureza de la corriente de permeado a la calidad requerida de acuerdo con la serie de estándares ISO 14687. Cabe observar que, aunque las purezas obtenidas son superiores al 98 % vol. H_2 para las mezclas de APG y COG, y que actualmente podrían usarse como materia prima de productos químicos en varios procesos industriales, estos valores todavía están lejos de los requerimientos de pilas de combustible. Además, los procesos de membranas deberían testarse bajo las condiciones reales de alimentación para asegurar la estabilidad de la membrana a largo plazo. Cuestiones tales como la mejora de los parámetros de permeación y del grado de productividad, reciben especial atención en la comunidad científica e industrial, y hay varias direcciones que se pueden tomar. Por un lado, polímeros químicos sintéticos intentan mejorar la selectividad, la permeabilidad o ambos parámetros en dichos materiales. Por otro lado, la recuperación de hidrógeno podría maximizarse a un valor dado de pureza usando sistemas de módulos de membranas en cascada o bien acoplándolo con otros procesos de separación convencionales. Por ello, se podría diseñar un sistema híbrido membrana-PSA usando técnicas de optimización para determinar el esquema de integración óptimo.

Finalmente, los resultados obtenidos tras la evaluación de una unidad de cuatro columnas de PSA cargado con zeolita 5A a partir de una mezcla sintética de gases de purga de amoniaco, son de especial interés para compañías de todo el mundo productoras de fertilizantes, en las cuales se manufactura amoniaco, con el fin de generar hidrógeno de forma distribuida. Asimismo, las condiciones de operación óptimas de la unidad de PSA podrían ser modificadas para obtener desde hidrógeno con una pureza apta para su uso industrial (98 %) hasta la pureza requerida por los vehículos de pasajeros (> 99.97 %), en el momento exacto en el que la demanda de hidrógeno en el sector transporte comience a ser notable. Se asume que la recuperación es moderada, debido a que el sistema de PSA tiene sólo cuatro adsorbedores y está alimentada a presiones relativamente bajas ≤ 9 bar. Sin embargo, estas recuperaciones deberían ser superiores en condiciones reales, aprovechando que la corriente de APG está disponible a elevadas presiones (150 – 200 bar). Éste es un tema de gran interés a tratar para su aplicación in situ. De cara al futuro, se podrían hacer diversos esfuerzos en mejorar el proceso de PSA tales como la reducción de los periodos de inactividad de las columnas con el fin de maximizar la productividad, y que normalmente se usan para ajustar la secuencia del ciclo. En esta línea, el diseño óptimo del ciclo de PSA podría obtenerse mediante modelado y así estimar la duración óptima de cada paso, partiendo desde un modelo más simple a uno más complejo. Asimismo, los resultados obtenidos corresponden a adsorbentes comerciales y éstos podrían ser mejorados usando adsorbentes a medida de alto rendimiento que sean capaces de aumentar la productividad para un mismo volumen dado. Además, cuando la concentración de argón en la corriente de alimentación pueda exceder el 2 % establecido en el caso de estudio, el proceso de PSA podría mejorarse añadiendo una capa adicional de carbón activo como el adsorbente más selectivo al argón, y para ello, el ratio carbón activo/zeolita óptimo debería ser obtenido. Con el fin de garantizar el rendimiento del sistema en las condiciones reales, se deberían evaluar en un futuro componentes traza de amoniaco para evitar efectos perjudiciales no solo por la presencia de cationes competitivos que ocupan sitios disponibles de intercambio iónico en las zeolitas, sino también en el rendimiento de pilas de combustible debido a la formación de iones de amonio (NH_4^+) dentro del ensamble electrodo-membrana [1,2]. Independientemente, la intensificación de procesos usando tecnología de membranas ofrece una solución compacta y modular con ahorros en costes de energía y capital. Por tanto, un sistema híbrido membrana-PSA para purificar hidrógeno podría ser óptimamente diseñado, aprovechando las ventajas de ambas técnicas de separación presentadas en esta tesis.

REFERENCIAS

[1] H. Huang, L. Yang, Q. Xue, et al., Removal of ammonium from swine wastewater by zeolite combined with chlorination for regeneration, J. Environ. Manage. 160 (2015) 333–341.

[2] J.L. Aprea, Quality specification and safety in hydrogen production, commercialization and utilization, Int. J. Hydrogen Energy. 39 (2014) 8604–8608.

APPENDIX I

SCIENTIFIC CONTRIBUTIONS

In this appendix are listed the publications as well as the contributions presented at local, national and international conferences during the predoctoral period.

- Articles published or accepted for publication in international scientific journals indexed in the Journal Citation Reports® (JCR)

1. M. Yáñez, A. Ortiz, B. Brunaud, I.E. Grossmann, I. Ortiz, Contribution of upcycling surplus hydrogen to design a sustainable supply chain: The case study of Northern Spain, Appl. Energy. 231 (2018) 777–787. DOI: 10.1016/j.apenergy.2018.09.047. (JCR impact factor 2018: 8.426, Q1 position 08 of 103 in the Energy & Fuels Category, Q1 position 05 of 138 in the Chemical Engineering Category)

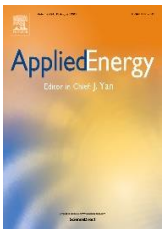

2. M. Yáñez, F. Relvas, A. Ortiz, D.Gorri, A. Mendes, I. Ortiz, PSA purification of waste hydrogen from ammonia plants to fuel cell grade, Sep. Purif. Technol. (2019) In Press. DOI: 10.1016/j.seppur.2019.116334. (JCR impact factor 2018: 5.107, Q1 position 14 of 138 in the Chemical Engineering Category)

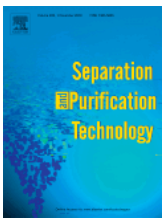

3. M. Yáñez, A. Ortiz, D.Gorri, I. Ortiz, Comparative performance of commercial polymeric membranes in the recovery of industrial hydrogen waste gas streams, Int. J. Hydrogen Energy, (2019) Under Review. (JCR impact factor 2018: 4.084, Q2 position 31 of 103 in the Energy & Fuels Category)

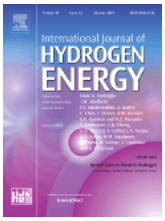

- Publications in conferences proceedings

M. Yáñez, A. Ortiz, D. Gorri, I. Ortiz., Hydrogen recovery from industrial gaseous waste streams in the SUDOE region. 6th Symposium on Hydrogen, Fuel Cells and Advanced Batteries (HYCELTEC). ISBN: 978-972-752-233-0.

M. Yáñez, A. Ortiz, D. Gorri, I. Ortiz. Supply chain optimization of hydrogen recovery from industrial gaseous waste streams at SUDOE region, 3rd Congreso Iberoamericano de Hidrógeno y Pilas de Combustible (IBERCONAPPICE). ISBN: 978-84-697-6342-1.

M. Yáñez, A. Ortiz, B. Brunaud, I. Ortiz, Surplus hydrogen reuse through decision-making techniques in northern Spain, European Hydrogen Energy Conference (EHEC). ISBN: 978-84-09-01620-4.

M. Yáñez, A. Ortiz, D. Gorri, I. Ortiz. Recovery of industrial waste hydrogen by membrane technology, 10th International Conference on Hydrogen technologies (Hydrogen Days). ISBN: 978-80-907264-2-0.

M. Yáñez, A. Ortiz, B. Brunaud, I.E. Grossmann, I. Ortiz. The use of optimization tools for the hydrogen circular economy, 29th European Symposium on Computer - Aided Process Engineering (ESCAPE-29). ISBN (Part B): 978-0-12-819940-4.

- Contributions to scientific meetings and conferences

M. Yáñez, A. Ortiz, D. Gorri, I. Ortiz., Hydrogen recovery from industrial gaseous waste streams in the SUDOE region. 6th Symposium on Hydrogen, Fuel Cells and Advanced Batteries (HYCELTEC), 19-23 June 2017, Porto (Portugal). Poster presentation.

M. Yáñez, A. Ortiz, D. Gorri, I. Ortiz. Supply chain optimization of hydrogen recovery from industrial gaseous waste streams at SUDOE region, 3rd Congreso Iberoamericano de Hidrógeno y Pilas de Combustible (IBERCONAPPICE), 17 - 20 October 2017 Huesca (Spain). Oral presentation.

M. Yáñez, A. Ortiz, B. Brunaud, I. Ortiz, Surplus hydrogen reuse through decision-making techniques in northern Spain, European Hydrogen Energy Conference (EHEC), 14 - 16 March 2018, Málaga (Spain). Oral presentation.

M. Yáñez, A. Ortiz, D. Gorri, B. Brunaud, I.E. Grossmann, I. Ortiz. Contribution of upcycling surplus hydrogen to design a sustainable supply chain: The case study of Northern Spain, World Hydrogen Energy Conference (WHEC), 17 - 22 June 2018, Rio de Janeiro (Brazil). Digital poster presentation.

M. Yáñez, A. Ortiz, D. Gorri, B. Brunaud, I.E. Grossmann, I. Ortiz. Upcycling surplus hydrogen to design a sustainable supply chain, Workshop: Challenges for the implementation of hydrogen as an energy vector, 21 November 2018, Lisboa (Portugal). Oral presentation.

M. Yáñez, A. Ortiz, D. Gorri, I. Ortiz. Recovery of industrial waste hydrogen by membrane technology, 10th International Conference on Hydrogen technologies (Hydrogen Days), 27 - 29 March 2019, Prague (Czech Republic). Poster presentation.

M. Yáñez, A. Ortiz, B. Brunaud, I.E. Grossmann, I. Ortiz. The use of optimization tools for the hydrogen circular economy, 29th European Symposium on Computer - Aided Process Engineering (ESCAPE-29), 16 - 19 June 2019, Eindhoven (The Netherlands). Oral presentation.

M. Yáñez, F. Relvas, A. Ortiz, D. Gorri, A. Mendes, I. Ortiz. High-purity hydrogen production by PSA technology from ammonia purge gas, 3rd International Congress of Chemical Engineering (ANQUE-ICCE), 19 - 21 June 2019, Santander (Spain). Poster presentation.

M. Yáñez, F. Relvas, A. Ortiz, D. Gorri, A. Mendes, I. Ortiz. Fuel cell grade hydrogen purification by PSA of purge gases from ammonia plants, 7th Symposium on Hydrogen, Fuel Cells and Advanced Batteries (HYCELTEC), 01 - 03 July 2019, Barcelona (Spain). Poster presentation.

M. Yáñez, A. Ortiz, D. Gorri, I. Ortiz. Hydrogen recovery from industrial gaseous waste streams using polymeric membranes, Fuel Cells, Electrolysers & H2 Processing Forum (EFCF 2019), 02 - 05 July 2019, Lucerne (Switzerland). Oral presentation.

M. Yáñez, F. Relvas, A. Ortiz, D. Gorri, A. Mendes, I. Ortiz. High-purity hydrogen production by PSA technology of purge gases from ammonia plants, Congreso Iberoamericano de Hidrógeno y Pilas de Combustible (IBERCONAPPICE), 23 - 25 October 2019, Madrid (Spain). Oral presentation.

M. Yáñez, A. Ortiz, D. Gorri**,** B. Brunaud, I.E. Grossmann, I. Ortiz. Contribution of upcycling surplus hydrogen to design of a sustainable supply chain: The case study of Northern Spain, AIChE Annual Meeting (AIChE), 10 - 15 November 2019, Orlando (USA). Poster presentation.

- Other contributions

A. Marcos-Madrazo, G. Díaz-Sainz, **M. Yáñez**, A. Fernández-Barquína, C. Casado-Coterillo, Some important things chemical engineering students never asked about research, IV Conference on Innovation on Chemical Engineering Education (CIDIQ), 21 - 23 January 2018, Santander (Spain). Poster presentation.